I. MOTION OF A SPHERE IN THE PRESENCE OF A PLANE INTERFACE

II. MODELING OF NON-ISOTHERMAL TURBULENT FLOWS

Thesis by

Seong Hee Lee

In Partial Fulfillment of the Requirements

for the Degree of

Doctor of Philosophy

California Institute of Technology

Pasadena, California

1980

(Submitted December 20, 1979)

Dedicated to my wife, Jae,

and to my parents

ACKNOWLEDGMENT

I wish to thank my advisor, Professor L. Gary Leal, for his guidance and encouragement throughout the course of this work. I am grateful for the opportunity to work in his group. It is a great pleasure to thank many friends, and in particular Bernd Trebitz, Masato Koda, Paul Chan, Clarke Berdan, Grant Tiefenbruck, Phil Wood, Bill Olbricht, Gerry Fuller, Paul Dunlap, Barry Bentley, Art Stelson, Bill Moonan, Greg Ryskin, Jaisam Kim, Fred Gelbard, and Don Kuehne for their much valued help in research as well as in work environment. My special thanks are due to Kathy Lewis for her excellent typing of this thesis. I wish to express my sincere gratitude to my parents and my parents-in-law for their continuous support and encouragement. Most of all, I would like to thank my wife, Jae, for her love and faith in me and her understanding.

PREFACE

This dissertation is concerned with two independent subjects: motion of a solid particle in the presence of a fluid interface and modeling of non-isothermal turbulent flows. When a small particle moves near an interface, the drag force on the particle is changed from Stokes law owing to the presence of the interface. This type of wall effect plays an important role in a wide range of interesting problems including the Brownian motion of a colloidal particle, motion of micro-organisms, and the collection of small particle via bubble or drop flotation type process. In Part I, we have solved the simplest problem of this type, the motion of a solid sphere in the presence of a flat interface, by two distinct methods; namely, solution via the reciprocal theorem of Lorentz (1907) and solution via superposition using the eigensolutions of Laplace's equation in bipolar coordinates.

In Part II, the modeling of non-isothermal turbulent flows is studied. The development of a realistic model to describe the turbulent transport of momentum, heat, and mass is basic to the study of geophysical fluid mechanics as well as many important technological flow problems. In the first section, the second-order closure technique for mean Reynolds stress is extended to the non-isothermal turbulent flows with negligible buoyancy effects using the rational closure scheme of Lumley and Khajeh-Nouri (1974). In the second section, we develop a model for triple correlations from their exact transport equations. The model for triple correlations can be easily applied to the study of meteorological flows and buoyant heat convection, since the gravitational effects can be analyzed without additional assumptions or approximations.

ABSTRACT

Part I.

The motion of a sphere in the presence of a fluid/fluid interface is studied. First, a solution is derived for a point force near a plane interface. Then the solution is extended to include the higher-order terms which are required to describe the motion of a solid sphere. Singularities of higher orders at the center of the sphere are obtained by using the method of reflections. This method yields asymptotic solutions for the general motion of a sphere in the presence of an interface.

A general solution for Stokes' equation in bipolar coordinates is also derived, and then applied to the arbitrary motion of a sphere in the presence of a plane fluid/fluid interface. The drag force and hydrodynamic torque on the sphere are then calculated for four specific motions of the sphere; namely, translation perpendicular and parallel to the interface and rotation about an axis which is perpendicular and parallel, respectively, to the interface. These numerically exact solutions are compared with the previous approximate solutions. The latter can be generalized to a variety of particle shapes, and it is thus important to assess their accuracy for this case of spherical particles where an exact solution can be obtained.

Part II.

The second-order, mean Reynolds stress turbulence closure approximation is extended to non-isothermal turbulent flows with negligible buoyancy. We apply the method of invariant modeling [Lumley and Khajeh-Nouri (1974)] to systematically model the various higher order moments in the governing equations. This approach yields a general form for each unknown correlation in the transport equations of $\overline{u_i\theta}$, $\overline{\theta^2}$ and ε_θ each containing many terms with parameters that must be determined from experimental data. For practical application, it is necessary to reduce the number of terms. In the present work, the most important terms are filtered from the general model for each unknown moment and their parameters are evaluated based on experimental data.

A semi-analytical method is used to derive models for the triple correlations of fluctuating velocity and temperature in a nonisothermal turbulent flow based upon the exact equations which govern their transport and production processes. In this study, these governing equations are transformed to a set of coupled linear algebraic equations for $\overline{u_iu_ju_k}$, $\overline{u_iu_j}$, $\overline{u_i\theta^2}$ and $\overline{\theta^3}$ by assuming: (1) a quasi-Gaussian structure for the fourth-order moments, (2) slow variations of the mean flow in the streamwise direction, (3) negligible convection of the triple correlations, and (4) certain simple models for the remaining higher-order correlations. A model for the triple correlations can thus be obtained by solving the set of linear algebraic equations.

Table of Contents

Table of Contents (continued)

PART I. MOTION OF A PARTICLE IN THE PRESENCE OF A FLUID INTERFACE.

A. MOTION OF A SPHERE IN THE PRESENCE OF A PLANE INTERFACE

Part 1. An Approximate Solution by Generalization of the Method of Lorentz.

by

S. H. Lee, R. S. Chadwick[†] and L. G. Leal

Department of Chemical Engineering
California Institute of Technology
Pasadena, California 91125

[†]Present Address: Department of Mechanics and Structures, UCLA.

ABSTRACT

The motion of a sphere in the presence of a fluid/fluid interface is studied. First, a solution is derived for a point force near a plane interface. Then the solution is extended to include the higher order terms which are required to describe the motion of a solid sphere. Singularities of higher orders at the center of the sphere are obtained by using the method of reflections. For a fluid/fluid interface with an arbitrary viscosity ratio, the drag force and the hydrodynamic torque are calculated for the special cases of motion of a sphere perpendicular and parallel to the interface. In addition, the rotational motion of a sphere is also investigated.

1. Introduction

When a small solid particle moves near an interface, the drag force on the particle is changed from Stokes law due to the presence of the interface. This type of "wall" effect plays an important role in a wide range of interesting problems including the Brownian motion of a colloidal particle, motion of micro-organisms, and the collection of small particles via bubbles or drop "flotation" type processes.

In the present paper, we study the simplest problem of this type; namely, the motion of a solid sphere in an arbitrary direction near a plane fluid/fluid interface. The Reynolds number based on particle size is assumed to be very small so that the creeping motion approximation is valid. In addition, we assume that the interface remains flat. The resulting solutions are therefore valid, as a first approximation, in any circumstances where the interface deformation remains small. Physically, this may be the case when the distance between the center of sphere and the interface is much bigger than the sphere diameter or when either the surface tension or the density difference between the two fluids is very large.

Three distinct methods have been commonly employed to study particle motions in the presence of a flat (or nearly flat) interface; namely, (1) a standard solution via superposition using the eigensolutions of Laplace's equation in bipolar coordinates, (2) solution via the reciprocal theorem of Lorentz (1907), and (3) solution via the fundamental solution of Laplace equation expressed in integral form.

The most frequently used technique, via eigensolutions of Laplace's

equation in bipolar coordinates was initiated by Jeffery (1912, 1915) who derived the general solution of Laplace's equation in bipolar coordinates, and used it to solve for the fluid motion generated by two spheres which are rotating about their line of centers. Subsequently, Stimson and Jeffery (1926) used the same method to calculate the drag force for two spheres translating along their line of centers with the same constant velocity. Much later, Dean and O'Neill (1963) utilized the general solution of Laplace's equation in bipolar coordinates to study the motion which is caused by the slow rotation of a sphere near an infinite rigid plane when the axis of rotation is parallel to the plane. O'Neill (1964) also investigated the translational motion of a sphere parallel to a plane solid wall. Finally, Bart (1968) extended the general solution for axisymmetric flow of Jeffery (1915) to the motion of a spherical drop which is moving normal to a liquid/liquid interface.

The reciprocal theorem approach was pioneered by Lorentz (1907) who derived a solution for the motion generated by a point force in the presence of a plane solid wall. Aderogba (1976) utilized the Papkovitch-Neuber solution for Stokes' equation to solve for the motion induced by a Stokeslet near a fluid/fluid interface. He superposed linear solutions with arbitrary coefficients to satisfy boundary conditions on the interface, namely the continuity of velocity and stress. However, the normal velocity at $z = 0$ is not zero in his solution, which implies that the interface is not steady. Because of this, his solution is only valid at the initial instant that the Stokeslet is imposed.

Finally, Faxen (1921) treated the motion of a sphere parallel to two external plane walls, using the fundamental solution of Laplace's

equation in an integral form. The extension of his theory to nonspherical bodies, and to shear and parabolic flows has been carried out by many investigators [cf. Happel and Brenner (1973)].

In this paper, we generalize the reciprocal theorem approach of Lorentz (1907), to derive a general lemma for obtaining solutions of Stokes' equations that satisfy continuity of velocity, continuity of shear stress and zero normal velocity on a flat interface, given only an arbitrary solution of Stokes' equations for an unbounded domain with no interface. This lemma is then used to determine the general solution of Stokes' equations for a point force near the interface [i.e. the counterpart in this two fluid system to the fundamental Stokeslet solution in a single, unbounded fluid]. Since this solution does not satisfy the continuity of normal stress, it is only valid, as indicated earlier, as a first approximation under conditions when the deformation of the interface at steady state would remain very small.

The lemma is then used to determine the motion generated by a finite size solid sphere which is translating, without rotation, either perpendicular or parallel to the interface. Provided the interface is flat, as assumed, these solutions can be superposed to obtain the solution for translation in an arbitrary direction. These solutions were obtained in the following manner. First, we put singularities at the center of the sphere which satisfy boundary conditions in an infinite fluid [i.e. the point force and the potential dipole]. Next, the lemma was used to obtain solutions for a point force and a potential dipole which satisfy boundary conditions at the interface. In general, however, these solutions do not satisfy boundary conditions at the sphere surface, and additional higher-order

singularities must then be included at the center of the sphere. The appropriate higher-order terms are determined in the asymptotic limit, $a/d \ll 1$ (i.e. a = sphere radius and d = distance between sphere center and interface.), and the resulting solutions are then valid in the same limit. Similarly, we also studied the fluid motion generated by the rotation of a stationary sphere whose axis is parallel or perpendicular to the interface. Due to the linearity of the Stokes' equation and boundary conditions, the solutions of these four problems (i.e. translation without rotation, and rotation without translation) are sufficient to determine the particle and fluid motions for any arbitrary applied force and/or torque on the particle.

The method of analysis used in this paper, and particularly the solutions for a point-force, are easily extended to the motion of slender, rod-like particles near a fluid/fluid interface. All that is required is that the distribution of singularities is known for motion of the particle in an infinite fluid.

The present paper comprises Part I of a three-part study. In the forthcoming Part II of this work, we will discuss the exact solution in bipolar coordinates for the motion of a sphere near a fluid/fluid interface. This exact solution is derived in the form of an infinite series, whose coefficients can be determined numerically. A detailed comparison between the approximate results of the present paper and the exact solution will be presented in Part II. The third part of this study, Part III, is concerned with interface deformation. We consider two cases: (1) that in which the final steady-state deformation is small and calculable using the velocity and pressure fields generated in Parts I and II, and (2)

where the interface deformation is not small. In the latter case, a numerical solution of the complete problem is required to determine the velocity and pressure fields. In Part III, we consider a novel numerical method for determining the shape of the interface in this situation. In the former case, we can use the known (i.e. calculated) shape of the interface, and the velocity fields for a flat interface to determine the first correction to the force acting on a particle due to interface deformation. This is accomplished by using the reciprocal theorem in a manner reminiscent of Ho and Leal (1974).

2. Basic Equations

We begin by considering the governing differential equations and boundary conditions for an arbitrarily shaped rigid particle which moves, with translational velocity $\underline{U}$ and angular velocity $\underline{\Omega}$, near an interface which separates two immiscible fluids that will be denoted as I and II. Apart from the disturbance flow induced by the particle, the two fluids are both assumed to be stationary. Furthermore, the undisturbed interface is assumed to be flat, and the particle to be wholly immersed in the fluid II.

The theoretical analysis which follows will be valid in the limit of small Reynolds number,

$$Re_d \equiv \frac{Ud}{\nu_2} \left(\text{or } \frac{\Omega d^2}{\nu_2} \right) \ll 1$$

where ν_2 represents the kinematic viscosity of fluid II

and d is the separation distance between the particle "center" and the undisturbed interface. This condition guarantees that the particle moves a very short distance on the time scale characteristic of vorticity diffusion over the distance d, and in this case, the equations of motion reduce to the steady Stokes' equations in both fluids,

$$\left.\begin{aligned} 0 &= -\nabla p_i + \nabla^2 \underline{u}_i \\ 0 &= \nabla \cdot \underline{u}_i \end{aligned}\right\} \quad i = 1,2 \tag{1}$$

The variables in these equations may be considered to be non-dimensionalized with respect to the characteristic variables: $u_c = U$ (or Ωa), $\ell_c = a$ (a particle length scale), and $p_c = \mu_i U/a$ (or $\mu_i \Omega$). In view of the linearity of these equations, and in anticipation of the fact that we will eventually restrict our attention to small deformations of the flat interface, we will consider the translational and rotational components of the particle motion separately. The boundary conditions for $\underline{u}_1$ and $\underline{u}_2$ in the translational problem are thus,

$$\underline{u}_1, \underline{u}_2 \to 0 \qquad \text{as} \qquad |\underline{x}| \to \infty \,, \tag{2a}$$

$$\underline{u}_2 = \underline{e} \qquad \text{on the particle surface} \tag{2b}$$

plus the conditions

$$\underline{u}_1 = \underline{u}_2 \tag{2c}$$

$$\underline{n}\cdot\underline{u}_1 = \underline{n}\cdot\underline{u}_2 = \kappa \frac{\partial f}{\partial t} \tag{2d}$$

$$\begin{aligned} [\![\underline{n}\cdot\underline{\underline{T}}]\!] &\equiv \lambda \underline{n}\cdot\underline{\underline{T}}_1 - \underline{n}\cdot\underline{\underline{T}}_2 \\ &= \left[\left(\frac{\sigma}{\mu_2 U}\right)\left(-\frac{\kappa}{r}\frac{\partial f}{\partial r} - \kappa^3 \frac{\partial^2 f}{\partial r^2}\right)\underline{n} + \frac{ga^2(\rho_1 - \rho_2)}{\mu_2 U} f\, \underline{n}\right] \end{aligned} \tag{2e}$$

at the interface, S, which is represented by

$$S: \quad H \equiv z - \ell(t) - f(r,\phi,t) = 0 \tag{3}$$

It may be noted that the dimensionless distance from the particle center to the undeformed interface, i.e. $d(t)/a$, has been denoted as $\ell(t)$. The unit normal, $\underline{n}$, and the factor κ are defined as

$$\underline{n} \equiv \frac{\nabla H}{|\nabla H|} \, , \quad \kappa \equiv \frac{1}{|\nabla H|} \, .$$

The parameters appearing in (2e) are the viscosity ratio, $\lambda \equiv \mu_1/\mu_2$ the interfacial tension σ and the density difference, $\Delta\rho \equiv \rho_1 - \rho_2$, in addition to the quantities which were defined earlier. The equations (2c) and (2e) are the conditions of continuity of velocity and stress, respectively, while (2d) is the kinematic condition which relates the time rate of change of the shape function, f, to the normal velocities at the interface. Although we will not explicitly consider the problem of particle rotation in this initial discussion of governing equations and boundary conditions, we note here that the problem is formally identical with U replaced by Ω and the condition (2b) appropriately modified to $\underline{u}_2 = \hat{\underline{e}} \wedge \underline{r}$ on the particle surface.

The problem represented by (1) - (3) is, of course, both time-dependent and highly nonlinear due to the fact that f is unknown. Thus, the solution (for example, the shape function $\underline{f}$), for any instantaneous $\underline{U}$ and particle position (or $\underline{\Omega}$ and position plus orientation if it is non-spherical) will not be a unique function of the conditions at that instant, but rather will depend on the conditions and interface shape at earlier times. The first two papers of the present series are, however, concerned with circumstances in which the interface deformation is both small and dependent solely upon the instantaneous conditions.

The assumption that the interface shape depends on the current flow conditions only is, of course, precisely equivalent to the statement that the interface shape is the equilibrium shape for a given U and a specified particle position; in particular, the interface shape at any instant will be the steady-state shape corresponding to the stress and pressure fields in the two fluids at that instant. Thus, the obvious physical requirement for this condition to be satisfied is that the particle motion be sufficiently "slow" that the (dimensionless) particle displacement, ℓ^*, in the time required for the interface to reach equilibrium for a given "applied" normal stress difference, $[\![\underline{n}\cdot\underline{n}\cdot\underline{\underline{T}}]\!]$, is small compared to the separation distance, $\ell(t)$. In addition, the time required to achieve a steady stress distribution at the interface after a change in the particle velocity (say, after an abrupt start-up of the particle motion) must be short compared to the time scale for significant displacement of the particle. The latter condition is exactly the condition $Re_d << 1$, which was already assumed in using the steady Stokes' equations. The conditions necessary in order that $\ell^* << \ell$ may be deduced by examining the equation (2e). Two distinct cases exist, depending upon whether the viscosity ratio is fixed (though perhaps large) or whether it is asymptotically large. In the latter case, the interface deformation will be small for finite times, but always unsteady and the problem is not considered in the present analysis. We consider the case in which λ is fixed. In order to insure that $\ell^* << \ell$ as assumed, we require either

$$\frac{U\mu_2}{\sigma} << 1 \qquad (4a)$$

or

$$\frac{U\mu_2}{ga^2\Delta\rho} << 1 \qquad (4b)$$

depending on which quantity is larger, or

$$\frac{a}{d} \ll 1 \ . \tag{4c}$$

When <u>any</u> of the conditions, (4), is satisfied, the interface deformation will not only be in quasi-equilibrium, but the <u>magnitude</u> of the deformation will also be asymptotically small; i.e. $O(\delta)$ in the cases (4a) or (4b) or $O(\delta^m)$ in case (4c), where ε represents whichever of the three parameters (4a - 4c) is asymptotically small and $m \geq 2$. The two conditions, (4a) and (4b) yield a <u>small</u> interface deformation by balancing the normal stress jump on the left-hand side of (2e) with a large surface tension or a large density differential. The condition (4c) yields <u>small</u> deformations because the normal-stress <u>difference</u> is small, $O(\frac{a}{d})^m$, when the particle is far from the fluid interface.

In any of these cases, the problem can be analyzed completely by means of an asymptotic expansion for small δ in which

$$f = \delta^m f_1(r,\phi) + \delta^{m+1} f_2(r,\phi) + \ldots \tag{5}$$

and

$$\begin{aligned} \underline{u}_i &= \underline{u}_i^{(0)} + \delta \underline{u}_i^{(1)} + \ldots \\ p_i &= p_i^{(0)} + \delta p_i^{(1)} + \ldots \end{aligned} \tag{6}$$

for fixed λ. Substituting (5) and (6) into (2a) - (2e) (for the translational case), we obtain

$$\underline{u}_1^{(0)}, \ \underline{u}_2^{(0)} \to 0 \ \text{ as } \quad |\underline{x}| \to \infty \tag{7a}$$

$$\underline{u}_2^{(0)} = \underline{e} \quad \text{on the particle surface} \tag{7b}$$

$$\underline{u}_1^{(0)} = \underline{u}_2^{(0)} \tag{7c}$$

$$\underline{n}\cdot\underline{u}_1^{(0)} = \underline{n}\cdot\underline{u}_2^{(0)} = 0 \tag{7d}$$

$$\left[\!\left[\underline{t}\cdot\underline{n}\cdot\underline{\underline{T}}^{(0)}\right]\!\right] = 0 \tag{7e}$$

plus one of the conditions

$$\left[\!\left[\underline{n}\cdot\underline{n}\cdot\underline{\underline{T}}^{(0)}\right]\!\right] = f_1 \qquad ; \qquad \delta \equiv \frac{\mu_2 U}{ga^2\Delta\rho} \to 0,\ \frac{\mu_2 U}{\sigma} = O(1),\ \frac{a}{d} = O(1)$$

$$= -\left(\frac{1}{r}\frac{\partial f_1}{\partial r} + \frac{\partial^2 f_1}{\partial r^2}\right) \qquad ; \qquad \delta \equiv \frac{\mu_2 U}{\sigma} \to 0,\ \frac{\mu_2 U}{ga^2\Delta\rho} = O(1),\ \frac{a}{d} = O(1)$$

$$= \left(\frac{\sigma}{\mu_2 U}\right)\left(-\frac{1}{r}\frac{\partial f_1}{\partial r} - \frac{\partial^2 f_1}{\partial r^2}\right); \qquad \delta \equiv \frac{a}{d} \to 0,\ \frac{\mu_2 U}{\sigma} = O(1),\ \frac{\mu_2 U}{ga^2\Delta\rho} = O(1)$$

$$+ \frac{ga^2\Delta\rho}{\mu_2 U} f_1 \tag{7f}$$

in the limit as $\delta \to 0$. The power m which appears in (5) and (6) equals 1 when (4a) or (4b) is satisfied with $a/d = O(1)$, but is generally ≥ 2 for the case (4c).

The zero-order approximation, which is defined by the conditions (7a) - (7e), plus the governing equations (1), thus represents the motion of a particle near a <u>flat</u> fluid interface. When the velocity and pressure fields have been determined from these equations and boundary conditions, the normal stress condition (7f) can then be used to determine a first approximation to the deviation of the interface shape from flat. Higher order terms which account for the effects of interface deformation on the velocity and pressure fields can then be obtained via a straightforward

continuation of the expansion procedure, though one must account for the interface deformation in calculating the unit normal and tangent vectors, $\underline{n}$ and $\underline{t}$, at higher-order in δ. In this paper, and the one (part II) which follows, we shall be concerned only with solutions for the zero-order problem.

3. Method of Solution

Let us then consider the solution of the equations (1), plus boundary conditions (7a) - (7e), for the specific case of a rigid, spherical particle of radius a which is immersed wholly in fluid II. As indicated in the Introduction, we shall approach this problem using a generalization of the method of Lorentz (1907), which can later be adapted to solution of the same problem with more complicated particle geometry.

Lorentz (1907) used the reciprocal theorem to determine the general solution of (1) for fluid motion in the presence of a plane solid wall. We extend his solution to the general case of a fluid/fluid interface. For creeping motion of a fluid near a flat fluid/fluid interface, we state the following lemma.

Lemma Consider two immiscible fluids, fluid I for $z > 0$ and fluid II for $z < 0$, which are contiguous to each other at $z = 0$. If $\underline{u}$ and p are a solution of Equations (1) in an infinite fluid II, then the functions

$$\underline{u}_1 = \frac{1}{1+\lambda}(\underline{u} - \hat{\underline{u}}), \quad p_1 = \frac{\lambda}{1+\lambda}(p - \hat{p}) \quad \text{for } z > 0 \tag{8}$$

$$\left.\begin{aligned} \underline{u}_2 &= (\underline{u} + \underline{u}^*) - \frac{\lambda}{1+\lambda}(\underline{u}^* - \hat{\underline{u}}^*) \\ p_2 &= (p + p^*) - \frac{\lambda}{1+\lambda}(p^* - \hat{p}^*) \end{aligned}\right\} \text{for } z < 0 \tag{9}$$

satisfy Equations (1), plus the conditions (7c - 7e) of continuity of velocity, continuity of shear stress and zero normal velocity at z = 0. Here, $(\hat{\underline{u}},\hat{p})$ is the associated solution [cf. Lorentz 1907] for $(\underline{u},p)$ defined as

$$\hat{\underline{u}} \equiv -\underline{\underline{J}}\cdot\underline{u} - 2z\nabla w + z^2\nabla p \tag{10}$$

$$\hat{p} \equiv p + 2z\frac{\partial p}{\partial z} - 4\frac{\partial w}{\partial z} \tag{11}$$

and $(\underline{u}^*,p^*)$ is the reflected image solution for $(\underline{u},p)$ defined as

$$\underline{u}^* \equiv \underline{\underline{J}}\cdot\underline{u}(x,y,-z) \tag{12}$$

$$p^* \equiv p(x,y,-z). \tag{13}$$

Finally, $(\hat{\underline{u}}^*,\hat{p}^*)$ is the associated solution for $(\underline{u}^*,p^*)$. The operator $\underline{\underline{J}}$ and the constant λ are defined as

$$\underline{\underline{J}} \equiv \{J_{ij}\} = \delta_{ij} - 2\delta_{i3}\delta_{j3}$$

$$\lambda \equiv \mu_1/\mu_2$$

and w is the z-component of $\underline{u}$.

This lemma can be easily proven by using the uniqueness of a solution for Stokes' equation (Lee 1979). $(\underline{u}_2,p_2)$ becomes identical to Lorentz' general solution for fluid motion near a solid wall when λ goes to infinity. Moreover, for the points far away from the interface, $(\underline{u}_2,p_2)$ reduces to the solution in an infinite fluid, $(\underline{u},p)$.

With the above lemma, we can easily calculate the solution of (1) for the motion of a particle in the presence of a plane interface, once the solution for particle motion in an infinite fluid is known. In the following sections, we will examine the case of a solid sphere which is translating and rotating in an arbitrary direction near an interface. Due to the linearity of Equations (1), this problem can be solved by superposing solutions for translation perpendicular and parallel to the interface and for rotation with the axis of rotation perpendicular and parallel to the interface. Prior to considering this problem, however, we briefly examine the solution for a point force located in one of the fluids near a flat fluid/fluid interface.

In order to obtain this solution using our lemma, we first require the corresponding solution for a point force in a single, unbounded fluid. This is the familiar Stokeslet solution.

$$\underline{u}_S(\underline{x},\underline{\alpha}) = \frac{\underline{\alpha}}{R} + \frac{(\underline{\alpha}\cdot\underline{x})\underline{x}}{R^3} \tag{14}$$

$$p_S(\underline{x},\underline{\alpha}) = 2\frac{\underline{\alpha}\cdot\underline{x}}{R^3} \tag{15}$$

where the strength and orientation of the point force are represented by $\underline{\alpha}$, and $R \equiv |\underline{x}|$. Let us consider a Stokeslet located at $\underline{x} = (0,0,-\ell)$. Substituting Equations (14) and (15) in Equations (8) and (9), we obtain

$$\underline{u}_{1,S}(\underline{x},\underline{\alpha}) = \frac{1}{1+\lambda}(\underline{\underline{I}} + \underline{\underline{J}})\cdot\left(\frac{\underline{\alpha}}{R_+} + \frac{(\underline{\alpha}\cdot\underline{x}_+)\underline{x}_+}{R_+^3}\right)$$

$$+ \frac{2z}{1+\lambda}\left[\frac{-\alpha_z\underline{x}_+}{R_+^3} + \frac{\ell\underline{\alpha}}{R_+^3} + \frac{(\underline{\alpha}\cdot\underline{x}_+)}{R_+^3}\underline{i}_z - \frac{3(\underline{\alpha}\cdot\underline{x}_+)\ell}{R_+^5}\underline{x}_+\right] \tag{16}$$

$$p_{1,s}(\underline{x},\underline{\alpha}) = \frac{-4\lambda}{1+\lambda}\left[\frac{z\alpha_z}{R_+^3} - \frac{\underline{\alpha}\cdot\underline{x}_+}{R_+^3} + \frac{3(\underline{\alpha}\cdot\underline{x}_+)\ell}{R_+^5} z_+\right] \tag{17}$$

$$\underline{u}_{2,s}(\underline{x},\underline{\alpha}) = \underline{u}_s(\underline{x}_+,\underline{\alpha}) + \left(\frac{1}{1+\lambda}\underline{\underline{J}} - \frac{\lambda}{1+\lambda}\underline{\underline{I}}\right)\cdot\left(\frac{\underline{\alpha}}{R_-} + \frac{(\underline{\alpha}\cdot\underline{x}_-)}{R_-^3}\underline{x}_-\right)$$
$$+ \frac{2\lambda}{1+\lambda}\frac{z}{R_-^3}\underline{\underline{J}}\cdot\left[-\alpha_z\underline{x}_- + \ell\underline{\alpha} + (\underline{\alpha}\cdot\underline{x}_-)\underline{i}_z - \frac{3\ell}{R_-^2}(\underline{\alpha}\cdot\underline{x}_-)\underline{x}_-\right] \tag{18}$$

$$p_{2,s}(\underline{x},\underline{\alpha}) = P_s(\underline{x}_+,\underline{\alpha}) + 2\frac{(\underline{\alpha}\cdot\underline{x}_-)}{R_-^3} + 4\frac{\lambda}{1+\lambda}\left[\frac{-\alpha_z z}{R_-^3} - \frac{(\underline{\alpha}\cdot\underline{x}_-)}{R_-^3}\right.$$
$$\left. + \frac{3\ell(\underline{\alpha}\cdot\underline{x}_-)z_-}{R_-^5}\right] \tag{19}$$

where

$$R_+ = \left(x^2 + y^2 + (z+\ell)^2\right)^{1/2},\quad R_- = \left(x^2 + y^2 + (-z+\ell)^2\right)^{1/2},$$
$$\underline{x}_+ = (x,y,z+\ell),\quad \underline{x}_- = (x,y,-z+\ell),\quad z_+ = z+\ell,$$
$$z_- = -z+\ell,\quad \text{and}\quad \underline{\underline{I}} = \text{identity matrix, } \delta_{ij}.$$

This solution will be used in the following sections in analyzing the velocity and pressure fields generated by a finite solid sphere which is centered at $z = -\ell$. In addition, it may also be used in the context of a slender-body approximation to determine the velocity and pressure fields for a slender particle which is near a fluid interface.

To show the fundamental characteristics of the solution, Equations (16) - (19), we will evaluate the stream function for $\underline{\alpha} = \alpha_o\underline{i}_z$ and the normal stress imbalance at $z = 0$ for $\underline{\alpha} = \alpha_o\underline{i}_z$ and $\underline{\alpha} = \alpha_o\underline{i}_x$. The latter are qualitatively indicative of the expected interface shape for translation of a particle normal and parallel to the undisturbed interface, $z = 0$.

For the axisymmetric flow with $\underline{\alpha} = \alpha_o\underline{i}_z$ at $z = -\ell$, the stream function can be easily calculated from Equations (16) and (18).

$$\phi_1 = \frac{2\alpha_o \ell z}{(1+\lambda)R_+}\left(1 - \frac{z_+^2}{R_+^2}\right) \qquad \text{for } z > 0 \tag{20}$$

$$\phi_2 = -\alpha_o R_+ \left(1 - \frac{z_+^2}{R_+^2}\right) + \alpha_o R_- \left(1 - \frac{z_-^2}{R_-^2}\right)\left(1 - \frac{2\lambda}{1+\lambda}\frac{\ell z}{R_-^2}\right)$$

$$\text{for } z < 0 \tag{21}$$

In Fig. 1, the stream functions for $\underline{\alpha} = \frac{3}{4}\,\underline{i}_z$ and $\lambda = 0.01$, 1, or 100 are compared with the stream function for an unbounded single fluid. It is clearly evident that the fluid motion in both fluids is retarded as the viscosity of the upper fluid increases.

The normal stress imbalance at $z = 0$ can also be evaluated from the general solution, Equations (16) - (19). For $\underline{\alpha} = \alpha_o \underline{i}_z$,

$$-\Delta T_{zz} = 12\,\frac{\alpha_o \ell^3}{R_o^5} \tag{22}$$

and for $\underline{\alpha} = \alpha_o \underline{i}_x$,

$$-\Delta T_{zz} = 12\,\frac{\alpha_o x \ell^2}{R_o^5} \tag{23}$$

Here, $R_o \equiv (\ell^2 + x^2 + y^2)^{1/2}$. It is noted that, for a point force located in one fluid, the normal stress imbalance on the interface is independent of viscosity ratio. In Figs. 2 and 3, the right hand sides of (22) and (23) are plotted for $\alpha_o = 3/4$. It may be seen that the normal stress imbalance becomes larger as the point force approaches more closely to the interface.

4. Motion of a Sphere Normal to a Plane Fluid/Fluid Interface

In this section, we consider the motion of a solid sphere normal to an infinite, plane interface. In an infinite fluid with no external

boundaries, an exact solution for translation of a solid sphere can be obtained by superposition of the fundamental solutions for a point force (i.e. the Stokeslet solution) and a potential dipole, both applied at the center of the sphere. The Stokeslet solution for a point force in an <u>infinite</u> fluid was presented earlier, as Equations (14) and (15), together with the general solution for a point force near a fluid/fluid interface which was obtained using the lemma [Equations (8) and (9)] of the preceding section.

The velocity and pressure fields for a potential dipole in an <u>infinite</u> fluid are

$$\underline{u}_D(\underline{x},\underline{\beta}) = -\frac{\underline{\beta}}{R^3} + \frac{3(\underline{\beta}\cdot\underline{x})\underline{x}}{R^5} \tag{24}$$

$$p_D(\underline{x},\underline{\beta}) = 0 \tag{25}$$

where $\underline{\beta}$ indicates the direction and intensity of the dipole. This solution can be generalized so that it satisfies continuity of velocity and shear stress, plus zero normal velocity, at $z = 0$, by simply substituting (24) and (25) into (8) and (9). The result for a potential dipole located at $z = -\ell$ is

$$\underline{u}_{1,D}(\underline{x},\underline{\beta}) = \frac{1}{1+\lambda}(\underline{\underline{I}} + \underline{\underline{J}})\cdot\left(-\frac{\underline{\beta}}{R_+^3} + \frac{3(\underline{\beta}\cdot\underline{x}_+)\underline{x}_+}{R_+^5}\right)$$
$$+ \frac{6z}{1+\lambda}\left\{\frac{\beta_z\underline{x}_+}{R_+^5} + \frac{1}{R_+^5}\left(z_+\underline{\beta} + (\underline{\beta}\cdot\underline{x}_+)\underline{i}_z\right) - \frac{5}{R_+^7}(\underline{\beta}\cdot\underline{x}_+)z_+\underline{x}_+\right\} \tag{26}$$

$$p_{1,D}(\underline{x},\underline{\beta}) = \frac{\lambda}{1+\lambda}\frac{12}{R_+^5}\left[2\beta_z z_+ + \underline{\beta}\cdot\underline{x}_+ - \frac{5}{R_+^2}(\underline{\beta}\cdot\underline{x}_+)z_+^2\right] \tag{27}$$

$$\underline{u}_{2,D}(\underline{x},\underline{\beta}) = u_D(\underline{x}_+,\underline{\beta}) + \left(\frac{1}{1+\lambda}\underline{\underline{J}} - \frac{\lambda}{1+\lambda}\underline{\underline{I}}\right)\cdot\left(-\frac{\underline{\beta}}{R_-^3} + \frac{3(\underline{\beta}\cdot\underline{x}_-)\underline{x}_-}{R_-^5}\right)$$

$$+ \frac{\lambda}{1+\lambda}\frac{6z}{R_-^5}\underline{J}\cdot\left\{\beta_z\underline{x}_- + z_-\underline{\beta} + (\underline{\beta}\cdot\underline{x}_-)\underline{i}_z - \frac{5}{R_-^2}(\underline{\beta}\cdot\underline{x}_-)z_-\underline{x}_-\right\} \tag{28}$$

$$p_{2,D}(\underline{x},\underline{\beta}) = -\frac{\lambda}{1+\lambda}\frac{12}{R_-^5}\left[2\beta_z z_- + \underline{\beta}\cdot\underline{x}_- - \frac{5}{R_-^2}(\underline{\beta}\cdot\underline{x}_-)z_-^2\right] \tag{29}$$

The variables appearing in these solutions were all defined previously in conjunction with either (16) - (19) or (24) and (25).

Now, let us consider a sphere located with its center at $z = -\ell$ which is moving with a constant velocity toward (or away from) the interface, which is located at $z = 0$. In this case,

$$\underline{\alpha} = \underline{\alpha}_o = \frac{3}{4}\underline{i}_z \quad \text{and} \quad \underline{\beta} = \underline{\beta}_o = -\frac{1}{4}\underline{i}_z$$

and the zero-th order (i.e. infinite fluid) solution can be written as

$$\underline{u}_1^{(0)} = 0 \quad \text{and} \quad p_1^{(0)} = 0 \tag{30}$$

$$\left.\begin{aligned}\underline{u}_2^{(0)} &= \underline{u}_s(\underline{x}_+,\tfrac{3}{4}\underline{i}_z) + \underline{u}_D(\underline{x}_+,-\tfrac{1}{4}\underline{i}_z) \quad \text{and}\\ p_2^{(0)} &= p_s(\underline{x}_+,\tfrac{3}{4}\underline{i}_z)\end{aligned}\right\} \tag{31}$$

Here, the subscripts 1 and 2 refer to fluid I and fluid II, respectively while the superscript (zero, in this case) indicates the level of approximation in the context of a normal reflections-type calculation procedure.

The first correction for the presence of the interface can be evaluated simply by substituting $\underline{\alpha} = \frac{3}{4}\underline{i}_z$ and $\underline{\beta} = -\frac{1}{4}\underline{i}_z$ into Equations (16) - (19) and (26) - (29), and subtracting the zeroth-order solution (31). We identify this first "wall correction" by the superscript (1). For

convenience, the correction corresponding to the Stokeslet solution is still denoted by the subscript s, while that from the potential dipole is denoted by the subscript D, i.e.

$$\left.\begin{aligned} \underline{u}_1^{(1)} &= \underline{u}_{1,s}^{(1)}\left(\underline{x},\tfrac{3}{4}\,\underline{i}_z\right) + \underline{u}_{1,D}^{(1)}\left(\underline{x},-\tfrac{1}{4}\,\underline{i}_z\right) \\ p_1^{(1)} &= p_{1,s}^{(1)}\left(\underline{x},\tfrac{3}{4}\,\underline{i}_z\right) + p_{1,D}^{(1)}\left(\underline{x},-\tfrac{1}{4}\,\underline{i}_z\right) \end{aligned}\right\} \tag{32}$$

$$\left.\begin{aligned} \underline{u}_2^{(1)} &= \underline{u}_{2,s}^{(1)}\left(\underline{x},\tfrac{3}{4}\,\underline{i}_z\right) + \underline{u}_{2,D}^{(1)}\left(\underline{x},-\tfrac{1}{4}\,\underline{i}_z\right) \\ p_2^{(1)} &= p_{2,s}^{(1)}\left(\underline{x},\tfrac{3}{4}\,\underline{i}_z\right) + p_{2,D}^{(1)}\left(\underline{x},-\tfrac{1}{4}\,\underline{i}_z\right) \end{aligned}\right\} \tag{33}$$

Though $\underline{u}_2^{(0)}$ exactly satisfies the no-slip boundary condition on the surface of the sphere, additional singularities are needed at the center of the sphere in order to cancel the velocity field correction $\underline{u}_2^{(1)}$ which is non-zero on the sphere surface. Since $\underline{u}_2^{(1)}$ is highly complicated, it is not possible to determine singularities at the sphere center which precisely satisfy the no-slip and zero normal velocity boundary conditions. Instead, we consider the asymptotic limit $\varepsilon \equiv 1/\ell \ll 1$, and then choose singularities to cancel only the first few terms of $\underline{u}_2^{(1)}$ at the sphere surface, with $\underline{u}_2^{(1)}$ expressed in powers of ε. Examination of $\underline{u}_2^{(1)}$ shows that $\underline{u}_{2,s}^{(1)} = O(\varepsilon)$ at the sphere surface, while $\underline{u}_{2,D}^{(1)}$ is only $O(\varepsilon^3)$. Hence, the dominant singularities at the next level of approximation will be those which are required to cancel the interface "reflection" of the point force (or Stokeslet) solution. The leading terms of $\underline{u}_2^{(1)}$ near the sphere, for small ε, are

$$w_2^{(1)} = -\varepsilon\,\frac{\alpha_o}{2}\,\frac{2+3\lambda}{1+\lambda} - \varepsilon^2\,\frac{\alpha_o}{4}\,\frac{2+3\lambda}{1+\lambda}\,(z+\ell) + O(\varepsilon^3) \tag{34}$$

$$u_2^{(1)} = \varepsilon^2 \frac{\alpha_o x}{8} \frac{2 + 3\lambda}{1 + \lambda} + O(\varepsilon^3) \tag{35}$$

$$v_2^{(1)} = \varepsilon^2 \frac{\alpha_o y}{8} \frac{2 + 3\lambda}{1 + \lambda} + O(\varepsilon^3) \tag{36}$$

with $\alpha_o = |\underline{\alpha}_o| = 3/4$.

At the first, $O(\varepsilon)$, level of approximation the velocity components $u_2^{(1)}$ and $v_2^{(1)}$ parallel to the interface are zero, while the normal velocity component is simply a constant

$$- \varepsilon \frac{\alpha_o}{2} \frac{2 + 3\lambda}{1 + \lambda} .$$

Insofar as (34) - (36) are concerned, the presence of the interface is thus equivalent to an induced steady-streaming motion in the direction opposite to that of the sphere. Obviously, to counter $w_2^{(1)}$ at $O(\varepsilon)$, we require a point force and a potential dipole at the sphere center, with intensities

$$\underline{\alpha}_1 = \varepsilon \frac{3\alpha_o}{8} \frac{2 + 3\lambda}{1 + \lambda} \underline{i}_z \tag{37}$$

$$\underline{\beta}_1 = - \varepsilon \frac{\alpha_o}{8} \frac{2 + 3\lambda}{1 + \lambda} \underline{i}_z \tag{38}$$

It is important to note that the point force velocity field of strength $O(\varepsilon)$, corresponding to $\underline{\alpha}_1$, will itself generate a vertical velocity component of $O(\varepsilon^2)$ at the sphere surface when it is "reflected" from the interface. Thus, if we are to consider any correction terms of $O(\varepsilon^2)$ from (34) - (36), we must simultaneously include this additional $O(\varepsilon^2)$ correction to the velocity field near the sphere. In order to cancel this $O(\varepsilon^2)$ term at the sphere surface we require an additional point force and potential dipole at the sphere center of strength

$$\underline{\alpha}_2 = \alpha_o \left(\frac{3}{8}\frac{2+3\lambda}{1+\lambda}\right)^2 \varepsilon^2 \underline{i}_z \tag{39}$$

$$\underline{\beta}_2 = -\frac{\alpha_o}{3}\left(\frac{3}{8}\frac{2+3\lambda}{1+\lambda}\right)^2 \varepsilon^2 \underline{i}_z \tag{40}$$

The terms of $O(\varepsilon^2)$ in the Equations (32), (33) and (34) represent an axisymmetric uniaxial extensional flow with origin at the center of the sphere, and the z-axis as the symmetry axis. Chwang and Wu (1975) have shown that an extensional flow of this general type is generated in an unbounded fluid by a stresslet and a potential quadrupole.

The basic solution for a stresslet is

$$\underline{u}_{ss}(\underline{x},\underline{\gamma},\underline{\delta}) = -\left[\frac{\underline{\gamma}\cdot\underline{\delta}}{R^3} - 3\frac{(\underline{\gamma}\cdot\underline{x})(\underline{\delta}\cdot\underline{x})}{R^5}\right]\underline{x} \tag{41}$$

$$p_{ss}(\underline{x},\underline{\gamma},\underline{\delta}) = -2\left[\frac{\underline{\gamma}:\underline{\delta}}{R^3} - 3\frac{(\underline{\gamma}\cdot\underline{x})(\underline{\delta}\cdot\underline{x})}{R^5}\right] \tag{42}$$

$$\underline{\omega}_{ss}(\underline{x},\underline{\gamma},\underline{\delta}) = \frac{3}{R^5}\left[(\underline{\delta}\cdot\underline{x})\underline{\gamma} + (\underline{\gamma}\cdot\underline{x})\underline{\delta}\right]\times\underline{x} \tag{43}$$

where $\underline{\omega}$ is the vorticity vector. The potential quadrupole is defined as the derivative of a potential dipole.

$$\underline{u}_{pq}(\underline{x},\underline{\beta},\underline{i}_\ell) = \frac{\partial \underline{u}_D(\underline{x},\underline{\beta})}{\partial x_\ell} \tag{44}$$

To cancel the terms of $O(\varepsilon^2)$ in Equations (34), (35) and (36) at the sphere surface, we thus require the superposition of a stresslet and a potential quadrupole at the sphere center. The resulting velocity field is

$$\underline{u}_{2,ex}^{(2)} = \frac{1}{2} C_1 \left[\frac{\partial}{\partial z}\underline{u}_D(\underline{x}_+,\underline{i}_z) + 5\underline{u}_{ss}(\underline{x}_+,\underline{i}_z,\underline{i}_z)\right] \tag{45}$$

where

$$C_1 = \varepsilon^2 \frac{\alpha_o}{8}\frac{2+3\lambda}{1+\lambda}$$

Substituting Equations (41) and (24) into (45), we obtain

$$\underline{u}^{(2)}_{2,ex} = \frac{C_1}{2}\left[\frac{1}{R_+^3}\left\{-5 + 3\frac{1 + (\underline{I} - \underline{J})\cdot}{R_+^2}\right\} + 15\frac{z_+^2}{R_+^5}\left(1 - \frac{1}{R_+^2}\right)\right]\underline{x}_+ \qquad (46)$$

Although there is no pressure contribution from the potential quadrupole term, the contribution from the stresslet term is

$$p^{(2)}_{2,ex} = 5C_1\left(-\frac{1}{R_+^3} + 3\frac{z_+^2}{R_+^5}\right) \qquad (47)$$

Finally, the corrections to $\underline{u}^{(2)}_{2,ex}$ and $p^{(2)}_{2,ex}$ which are necessary to satisfy boundary conditions at the interface can be easily calculated from the lemma by substituting (46) and (47) into (8) and (9), and then subtracting (46) and (47) in fluid II. The results are

$$\begin{aligned}\underline{u}^{(3)}_{1,ex} = {} & \frac{C_1}{1+\lambda}\left[-\frac{5}{2}(\underline{I} + \underline{J})\cdot\frac{1}{R_+^3}\left(1 - 3\frac{z_+^2}{R_+^2}\right)\underline{x}_+ - \frac{5z}{R_+^3}\left(1 - 9\frac{z_+^2}{R_+^2}\right)\underline{i}_z\right. \\ & + 15z\left(\frac{z_+}{R_+^5} - \frac{5z_+^3}{R_+^7}\right)\underline{x}_+ - 15z^2\left(\frac{1 + (\underline{I} - \underline{J})\cdot}{R_+^5} - \frac{5z_+^2}{R_+^7}\right)\underline{x}_+\Big] \\ & + O(\varepsilon^4) \end{aligned} \qquad (48)$$

$$\begin{aligned} p^{(3)}_{1,ex} = {} & \frac{C_1\lambda}{1+\lambda}\left(\frac{+10}{R_+^3}\right)\left[-1 + 3\frac{z_+^2}{R_+^2}\left(4 - \frac{5z_+^2}{R_+^2}\right) - 3\frac{zz_+}{R_+^2}\left(3 - 5\frac{z_+^2}{R_+^2}\right)\right] \\ & + O(\varepsilon^4) \end{aligned} \qquad (49)$$

in fluid I, and

$$\begin{aligned}\underline{u}^{(3)}_{2,ex} = {} & \frac{C_1}{1+\lambda}(\underline{J} - \lambda\underline{I})\cdot\frac{5\underline{x}_-}{2R_-^3}\left[-1 + 3\frac{z_-^2}{R_-^2}\right] + C_1\frac{2\lambda}{1+\lambda}z\underline{J}\cdot \\ & \left(\frac{5}{2}\frac{1}{R_-^3}\right)\left[\frac{3z_-}{R_-^2}\left(1 - 5\frac{z_-^2}{R_-^2}\right)\underline{x}_- + \left(-1 + 9\frac{z_-^2}{R_-^2}\right)\underline{i}_z\right] + C_1\frac{\lambda}{1+\lambda}z^2\underline{J}\cdot \\ & \left(\frac{15}{R_-^5}\right)\left[1 + (\underline{I} - \underline{J})\cdot - \frac{5z_-^2}{R_-^2}\right]\underline{x}_- + O(\varepsilon^4) \end{aligned} \qquad (50)$$

$$p_{2,ex}^{(3)} = \frac{5C_1}{R_-^3}\left(-1 + 3\frac{z_-^2}{R_-^2}\right) + \frac{C_1\lambda}{1+\lambda}\frac{10}{R_-^3}\left[\frac{zz_-}{R_-^2}\left(-9 + 15\frac{z_-^2}{R_-^2}\right)\right.$$

$$\left. - \left(\frac{12z_-^2}{R_-^2} - 15\frac{z_-^4}{R_-^4} - 1\right)\right] + O(\varepsilon^4) \qquad (51)$$

in fluid II. Since the stresslet and potential quadrupole terms, (46) and (47), are $O(\varepsilon^2)$, the "reflected" velocity and pressure fields, (48) - (51), are $O(\varepsilon^3)$ at the sphere center.

Hitherto, we have evaluated the singularities at the sphere center to $O(\varepsilon^2)$. Higher order terms can be calculated in a similar manner, but we will not consider such terms here. In summary, the singularities required for a sphere moving perpendicularly to a plane interface are:

$$\text{Stokeslet: } \underline{u}_S(\underline{x}_+, \frac{3}{4}\underline{i}_z)\left[1 + \frac{3}{8}\frac{2+3\lambda}{1+\lambda}\varepsilon + \left(\frac{3}{8}\frac{2+3\lambda}{1+\lambda}\right)^2\varepsilon^2 + O(\varepsilon^3)\right]$$

$$\text{potential dipole: } \underline{u}_D(\underline{x}_+, -\frac{1}{4}\underline{i}_z)\left[1 + \frac{3}{8}\frac{2+3\lambda}{1+\lambda}\varepsilon + \left(\frac{3}{8}\frac{2+3\lambda}{1+\lambda}\right)^2\varepsilon^2 + O(\varepsilon^3)\right]$$

$$\text{stresslet: } \varepsilon^2\frac{5\alpha_o}{16}\frac{2+3\lambda}{1+\lambda}\underline{u}_{SS}(\underline{x}_+, \underline{i}_z, \underline{i}_z)$$

$$\text{potential quadrupole: } \varepsilon^2\frac{\alpha_o}{16}\frac{2+3\lambda}{1+\lambda}\frac{\partial \underline{u}_D}{\partial z}(\underline{x}_+, \underline{i}_z)$$

As there is no contribution to the drag force from a potential dipole, stresslet or potential quadrupole, the drag ratio [the drag divided by Stokes' drag] is simply given as

$$\text{Drag ratio} = 1 + \frac{3}{8}\varepsilon\frac{2+3\lambda}{1+\lambda} + \left(\frac{3}{8}\varepsilon\frac{2+3\lambda}{1+\lambda}\right)^2 + O(\varepsilon^3) \qquad (52)$$

When $\lambda \to \infty$, Equation (52) reduces to the drag ratio for the case of solid

wall, and is identical with Wakiya's results to $O(\varepsilon^2)$(cf. Happel and Brenner 1973).

In Fig. 4, the drag ratio, Equation (52), is plotted vs. the distance between the sphere center and the interface for $\lambda = 0$, 1 and ∞. The drag ratios numerically calculated by Bart (1968) are also shown in the figure. As previously mentioned, we presume $\varepsilon << 1$ in the derivation of Equation (52). Thus, for $\varepsilon << 1$, the Equation (52) agrees with Bart's result which is the exact solution for a sphere motion near a flat interface. Even for $\ell \sim 2.5$, the approximate solution shows reasonably good agreement with the exact solution. However, the two solutions deviate from each other as the sphere approaches more closely to the interface. Since the convergence of Equation (52) is poor for $\varepsilon \approx 1$, we need more higher order terms for Equation (52)

5. Motion of a Sphere Parallel to a Plane Fluid/Fluid Interface

Let us now turn to the problem of a non-rotating sphere which is translating parallel to a plane fluid/fluid interface. The zeroth order solution for this problem can be obtained by substituting $\underline{\alpha} = \alpha_o \underline{i}_x$ and $\underline{\beta} = -\frac{1}{3}\alpha_o \underline{i}_x$ into equations (30) and (31), with $\underline{u}_S$ and $\underline{u}_D$ evaluated from (14), (15), (24) and (25). Similarly, the first correction by reflection from the interface can be obtained from Equations (32) and (33), with (16) - (19) and (26) - (29).

The no-slip boundary condition on the sphere is not satisfied since the "reflected" flow field is nonzero at the sphere surface. We may examine the leading terms of this reflected field, expressed as a power series in ε,

$$u_2^{(1)} = \varepsilon \frac{\alpha_o}{4} \frac{2 - 3\lambda}{1 + \lambda} + \varepsilon^2 \frac{\alpha_o}{8} \frac{2 - 3\lambda}{1 + \lambda} (z + \ell) + O(\varepsilon^3) \tag{53}$$

$$v_2^{(1)} = O(\varepsilon^3) \tag{54}$$

$$w_2^{(1)} = -\varepsilon^2 \frac{\alpha_o x}{8} \frac{3\lambda + 2}{1 + \lambda} + O(\varepsilon^3) \tag{55}$$

In order to satisfy the no-slip and zero normal velocity conditions at the sphere surface, we need additional singularities at the sphere center which produce the velocity field of opposite sign. For the term of $O(\varepsilon)$, a Stokeslet and a potential dipole are required, which have the intensity and orientation.

$$\underline{\alpha}_1 = -\varepsilon \frac{3\alpha_o}{16} \frac{2 - 3\lambda}{1 + \lambda} \underline{i}_x \tag{56}$$

$$\underline{\beta}_1 = \varepsilon \frac{\alpha_o}{16} \frac{2 - 3\lambda}{1 + \lambda} \underline{i}_x \tag{57}$$

By induction, we also know that the interface "reflection" of the point force and potential dipole solutions corresponding to (56) and (57) will yield a nonzero contribution of $O(\varepsilon^2)$ to the x-component of velocity at the sphere surfaces. In order to satisfy boundary conditions on the sphere surface to $O(\varepsilon^2)$, we thus require an additional point force and potential dipole at the sphere center with magnitude and orientation

$$\underline{\alpha}_2 = \varepsilon^2 \alpha_o \left(\frac{3}{16} \frac{2 - 3\lambda}{1 + \lambda} \right)^2 \underline{i}_x \tag{58}$$

$$\underline{\beta}_2 = -\varepsilon^2 \frac{\alpha_o}{3} \left(\frac{3}{16} \frac{2 - 3\lambda}{1 + \lambda} \right)^2 \underline{i}_x \tag{59}$$

Further, we require singularities to cancel the $O(\varepsilon^2)$ contributions in Equations (53) and (55). Examination shows that these terms represent a linear shear flow with origin at the sphere center. Chwang and Wu (1975) discovered that a stresslet, a rotlet and a potential quadrupole were necessary to produce such a flow in an unbounded fluid. Thus, the velocity field which cancels the terms of $O(\varepsilon^2)$ in $\underline{u}^{(1)}$ at the sphere is

$$\underline{u}^{(2)}_{2,SH} = C_2 \left\{ \frac{5}{6} \underline{u}_{ss}(\underline{x}_+, \underline{i}_x, \underline{i}_z) + \frac{1}{2} \underline{u}_R(\underline{x}_+, \underline{i}_y) + \frac{1}{6} \frac{\partial}{\partial z} \underline{u}_D(\underline{x}_+, \underline{i}_x) \right\}$$
$$+ C_3 \left\{ \frac{5}{6} \underline{u}_{ss}(\underline{x}_+, \underline{i}_z, \underline{i}_x) - \frac{1}{2} \underline{u}_R(\underline{x}_+, \underline{i}_y) + \frac{1}{6} \frac{\partial}{\partial x} \underline{u}_D(\underline{x}_+, \underline{i}_z) \right\} \quad (60)$$

Here, $C_2 = -\frac{\varepsilon^2 \alpha_0}{8} \frac{2 - 3\lambda}{1 + \lambda}$, $C_3 = \frac{\varepsilon^2 \alpha_0}{8} \frac{3\lambda + 2}{1 + \lambda}$, and $\underline{u}_R$ is the velocity field due to a rotlet defined as

$$\underline{u}_R(\underline{x}, \underline{\gamma}) = \frac{\underline{\gamma} \times \underline{x}}{R^3} \quad (61)$$

Substituting Equations (24), (41) and (61) into Equation (60) yields

$$\underline{u}^{(2)}_{2,SH} = C_2 \left[\frac{z_+}{2} \left(\frac{1}{R_+^5} + \frac{1}{R_+^3} \right) \underline{i}_x + \frac{1}{2} x \left(\frac{1}{R_+^5} - \frac{1}{R_+^3} \right) \underline{i}_z + \frac{5}{2} x z_+ \left(\frac{1}{R_+^5} - \frac{1}{R_+^7} \right) \underline{x}_+ \right]$$
$$+ C_3 \left[\frac{z_+}{2} \left(\frac{1}{R_+^5} - \frac{1}{R_+^3} \right) \underline{i}_x + \frac{1}{2} x \left(\frac{1}{R_+^5} + \frac{1}{R_+^3} \right) \underline{i}_z + \frac{5}{2} x z_+ \left(\frac{1}{R_+^5} - \frac{1}{R_+^7} \right) \underline{x}_+ \right] \quad (62)$$

The pressure becomes

$$p^{(2)}_{2,SH} = 5(C_2 + C_3) \frac{x z_+}{R_+^5} \quad (63)$$

The corrections (i.e. reflections) to $(\underline{u}^{(2)}_{2,SH}, p^{(2)}_{2,SH})$ which are necessary to satisfy boundary conditions at the interface can be calculated easily from the lemma. The results are

$$\underline{u}^{(3)}_{1,SH} = \frac{1}{1 + \lambda} (\underline{\underline{I}} + \underline{\underline{J}}) \cdot \frac{1}{2R_+^3} \left[C_4 (z_+ \underline{i}_x - x \underline{i}_z) + 5C_5 \frac{x z_+}{R_+^2} \underline{x}_+ \right]$$
$$+ \frac{z}{R_+^3} \left[-C_4 + 5C_5 \frac{z_+^2}{R_+^2} \right] \underline{i}_x - 5z^2 C_5 \frac{1}{R_+^5} \left(-5 \frac{x z_+}{R_+^2} \underline{x}_+ + z_+ \underline{i}_x + x \underline{i}_z \right)$$
$$+ \frac{xz}{R_+^5} \left[\left(3C_4 - 25C_5 \frac{z_+^2}{R_+^2} \right) \underline{x}_+ + 10C_5 z_+ \underline{i}_z \right] + O(\varepsilon^4) \quad (64)$$

$$p^{(3)}_{1,SH} = \frac{\lambda}{1+\lambda}\frac{x}{R_+^5}\left[10C_5 z\left(\frac{5z_+^2}{R_+^2} - 1\right) + 20C_5 z_+ + 6C_4 z_+ - 50C_5\frac{z_+^3}{R_+^2}\right] + O(\varepsilon^5) \quad (65)$$

$$u^{(3)}_{2,SH} = \left(\frac{1}{1+\lambda}\underline{\underline{J}} - \frac{\lambda}{1+\lambda}\underline{\underline{I}}\right)\cdot\left[\frac{1}{2R_-^3}C_4(z_-\underline{i}_x - x\underline{i}_z) + \frac{5}{2}C_5\frac{xz_-}{R_-^5}\underline{x}_-\right] + \frac{\lambda z}{1+\lambda}\frac{\underline{J}\cdot}{R_-^3}\left[C_4\left(-\underline{i}_x + \frac{3x\underline{x}_-}{R_-^2}\right) + \frac{5C_5 z_-}{R_-^2}\left(z_-\underline{i}_x + 2x\underline{i}_z - \frac{5xz_-\underline{x}_-}{R_-^2}\right)\right] + \frac{5\lambda}{1+\lambda}z^2\underline{\underline{J}}\cdot C_5\left[-\frac{5}{R_-^7}xz_-\underline{x}_- + \frac{1}{R_-^5}(z_-\underline{i}_x + x\underline{i}_z)\right] + O(\varepsilon^4) \quad (66)$$

$$p^{(3)}_{2,SH} = 5C_5\frac{xz_-}{R_-^5} - \frac{2\lambda}{1+\lambda}\left[5zC_5\left(\frac{-5xz_-^2}{R_-^7} + \frac{x}{R_-^5}\right) + 3C_4\frac{xz_-}{R_-^5} - 25C_5\frac{xz_-^3}{R_-^7} + 10C_5\frac{xz_-}{R_-^5}\right] + O(\varepsilon^5) \quad (67)$$

Here, $C_4 = C_2 - C_3 = -\varepsilon^2\frac{\alpha_o}{2}\frac{1}{1+\lambda}$

and $C_5 = C_2 + C_3 = \varepsilon^2\frac{3\alpha_o}{4}\frac{\lambda}{1+\lambda}$.

Thus, for a sphere moving parallel to an interface, the singularities required at the center of sphere through $O(\varepsilon^2)$ are

Stokeslet: $\underline{u}_s(\underline{x}_+, \frac{3}{4}\underline{i}_x)\left\{1 - \varepsilon\frac{3}{16}\frac{2-3\lambda}{1+\lambda} + \left(\varepsilon\frac{3}{16}\frac{2-3\lambda}{1+\lambda}\right)^2 + O\left(\varepsilon^3\right)\right\}$

potential dipole: $\underline{u}_D(\underline{x}_+, -\frac{1}{4}\underline{i}_x)\left\{1 - \varepsilon\frac{3}{16}\frac{2-3\lambda}{1+\lambda} + \left(\varepsilon\frac{3}{16}\frac{2-3\lambda}{1+\lambda}\right)^2 + O\left(\varepsilon^3\right)\right\}$

stresslet: $\frac{5}{6}C_5\underline{\underline{u}}_{ss}(\underline{x}_+, \underline{i}_x, \underline{i}_z)$

rotlet: $\frac{1}{2} C_4 \underline{u}_R(\underline{x}_+, \underline{i}_y)$

potential quadrupole: $\frac{1}{6}\left(C_2 \frac{\partial}{\partial z} \underline{u}_D(\underline{x}_+, \underline{i}_x) + C_3 \frac{\partial}{\partial x} \underline{u}_D(\underline{x}_+, \underline{i}_z)\right)$

We can evaluate the drag ratio easily from the Stokeslet strength

$$\text{Drag ratio} = 1 - \varepsilon \frac{3}{16} \frac{2 - 3\lambda}{1 + \lambda} + \varepsilon^2 \left(\frac{3}{16} \frac{2 - 3\lambda}{1 + \lambda}\right)^2 + O(\varepsilon^3) \qquad (68)$$

It can be seen that there exists a critical viscosity ratio equal to 2/3, above which the drag force on the sphere in the presence of an interface is larger than that in an infinite fluid. For $\lambda < \frac{2}{3}$, the drag is less than it would be in an infinite fluid. Further, Equation (68) becomes identical to Faxen's (1921) results to $O(\varepsilon^2)$ when λ goes to infinity.

From the rotlet strength, the hydrodynamic torque on the particle can be obtained and is equal to

$$\underline{T} = -8\pi \underline{i}_y \frac{1}{2} (C_2 - C_3) + O(\varepsilon^3)$$

$$= \frac{3\pi}{2} \varepsilon^2 \frac{1}{1 + \lambda} \underline{i}_y + O(\varepsilon^3) \qquad (69)$$

This is the negative of the torque which is required to keep the particle from rotating. It will be noted that, when $\lambda \to \infty$, there is no term of $O(\varepsilon^2)$ in $\underline{T}$. Indeed, Faxen's (1921) solution for sphere motion near a solid wall yields $\underline{T} \sim O(\varepsilon^4)$. It is also noteworthy that for any finite λ the sense of the applied torque for a sphere which is far from the interface is <u>opposite</u> in direction to that which might be expected intuitively, and opposite to that which is required for a sphere near a solid wall (see part II of this paper).

In Fig. 5, the drag ratio, Equation (68), is plotted vs. ℓ, the distance between the sphere center and the interface, for $\lambda = 0$, 1, and ∞. O'Neill (1964) calculated the drag ratio for the motion of a sphere parallel to a plane <u>solid</u> wall by using bipolar coordinates. His results

are also shown in Fig. 5. There is a good agreement between the two solutions in the region of $\varepsilon << 1$. When a sphere approaches the interface, we need more higher order terms in Equation (68) due to the poor convergence of Equation (68) in ε power series. As expected, the difference between Equation (68) and O'Neill's solution becomes larger as $\varepsilon \to 1$.

6. Rotation of a Sphere in the Presence of an Interface

Finally, we turn to the case of a stationary sphere rotating with a constant angular velocity $\underline{\gamma}$ in the presence of a plane interface. $\underline{\gamma}$ is nondimensionalized w.r.t. u_c/ℓ_c. The solution in an infinite fluid can be simply represented by a rotlet at the center of sphere, and the velocity field generated by a rotlet is given by Equation (61). Thus the zero-th order solution for a rotating sphere in the presence of a plane interface is

$$\underline{u}_1^{(0)} = 0 \tag{70}$$

$$\underline{u}_2^{(0)} = \underline{u}_R(\underline{x}_+, \underline{\gamma}) \tag{71}$$

The first correction by reflection from the interface can be easily obtained from the lemma.

$$\underline{u}_1^{(1)} = \frac{(\underline{\underline{I}} + \underline{\underline{J}})}{1+\lambda} \cdot \left(\frac{\underline{\gamma} \times \underline{x}_+}{R_+^3} \right) + \frac{2z}{1+\lambda} \left[\frac{(\gamma_x \underline{i}_y - \gamma_y \underline{i}_x)}{R_+^3} - 3\underline{x}_+ \frac{(\gamma_x y - \gamma_y x)}{R_+^5} \right] \tag{72}$$

$$\underline{u}_2^{(1)} = \left(\frac{1}{1+\lambda} \underline{\underline{J}} - \frac{\lambda}{1+\lambda} \underline{\underline{I}} \right) \cdot \frac{(\underline{\gamma} \times \underline{x}_-)}{R_-^3} + \frac{2\lambda}{1+\lambda} z \left[\frac{(\gamma_x \underline{i}_y - \gamma_y \underline{i}_x)}{R_-^3} - 3\underline{\underline{J}} \cdot \underline{x}_- \frac{(\gamma_x y - \gamma_y x)}{R_-^5} \right] \tag{73}$$

Here, γ_x, γ_y and γ_z are the components of $\underline{\gamma}$ in $\underline{i}_x$, $\underline{i}_y$ and $\underline{i}_z$ directions, respectively.

Since the problem is linear, the solution for rotation with an arbitrary axis of rotation can be obtained by superposition of the solutions for rotation when this axis is parallel and normal, respectively, to the interface. Therefore, without loss of generality, we will solve only these two problems for rotation of a sphere.

First, let us consider a rotating sphere when the axis of rotation is perpendicular to the interface (i.e. $\gamma_z \neq 0$, $\gamma_x = \gamma_y = 0$). As discussed in the previous sections, the first correction (73) to the solution due to the presence of the interface does not satisfy no-slip boundary conditions at the sphere surface. Hence, we analyze the leading terms of (73) at the sphere surface as a power series in ε,

$$u_2^{(1)} = -\frac{1-\lambda}{1+\lambda}\frac{\gamma_z}{8}\varepsilon^3 y + O(\varepsilon^4) \tag{74}$$

$$v_2^{(1)} = \frac{1-\lambda}{1+\lambda}\frac{\gamma_z}{8}\varepsilon^3 x + O(\varepsilon^4) \tag{75}$$

$$w_2^{(1)} = 0 \tag{76}$$

To cancel this additional velocity field at the sphere surface, a rotlet is needed at the center of sphere. The velocity field generated by this rotlet is given by

$$\underline{u}_2^{(2)} = -\frac{1}{8}\frac{1-\lambda}{1+\lambda}\varepsilon^3\, \underline{u}_R(\underline{x}_+, \gamma_z \underline{i}_z) \tag{77}$$

Consequently, for the rotation of a sphere whose axis is normal to the interface, only a rotlet is required at the center of sphere through terms of $O(\varepsilon^3)$ and its strength is as follows,

$$\text{rotlet: } \underline{u}_R(\underline{x}_+, \gamma_z \underline{i}_z)\left(1 - \frac{1-\lambda}{8(1+\lambda)}\varepsilon^3 + O(\varepsilon^4)\right)$$

The torque required to maintain angular velocity, $\underline{\gamma} = \gamma_z \underline{i}_z$, can be easily calculated from the strength of rotlet,

$$\underline{T} = 8\pi\gamma_z \left(1 - \frac{1-\lambda}{8(1+\lambda)}\varepsilon^3 + O(\varepsilon^4)\right)\underline{i}_z \tag{78}$$

For $\lambda > 1$, the required torque on the sphere in the presence of an interface is larger than that in an infinite fluid while for $\lambda < 1$, it is smaller. It may be noted in this case that there is no contribution to the drag force up to $O(\varepsilon^3)$. As expected, rotation about the z axis induces no translational motion of the particle.

Now, let us consider a rotating sphere whose rotation axis is parallel to a plane interface. Substituting $\gamma_x \neq 0$ and $\gamma_y = \gamma_z = 0$ into Equation (73) and expanding each term in the power series of ε, we can evaluate the leading terms of Equation (73) at the sphere surface.

$$u_2^{(1)} = O(\varepsilon^4) \tag{79}$$

$$v_2^{(1)} = -\frac{1}{4}\frac{\gamma_x}{1+\lambda}\varepsilon^2 - \frac{2-\lambda}{8(1+\lambda)}\gamma_x(\ell + z)\varepsilon^3 + O(\varepsilon^4) \tag{80}$$

$$w_2^{(1)} = -\frac{1+4\lambda}{8(1+\lambda)}\gamma_x y\varepsilon^3 + O(\varepsilon^4) \tag{81}$$

In order to counter the term of $O(\varepsilon^2)$ in $v_2^{(1)}$, we need a Stokeslet and a potential dipole at the center of sphere with strength and orientation

$$\underline{\alpha}_1 = \varepsilon^2 \frac{3}{16}\frac{\gamma_x}{1+\lambda}\underline{i}_y \tag{82}$$

$$\underline{\beta}_1 = -\varepsilon^2 \frac{1}{16}\frac{\gamma_x}{1+\lambda}\underline{i}_y \tag{83}$$

In addition, for the shear flows of $O(\varepsilon^3)$ in Equations (80) and (81), a stresslet, a rotlet and a potential quadrupole are required at the center of sphere. They yield the following velocity field.

$$\underline{u}^{(2)}_{2,SH} = \frac{3}{8}\gamma_x\varepsilon^3\left[\frac{5}{6}\underline{u}_{ss}(\underline{x}_+,\underline{i}_y,\underline{i}_z) + \frac{1}{6}\frac{\partial}{\partial y}\underline{u}_D(x_+,\underline{i}_z)\right]$$
$$+ \frac{1}{16}\frac{-1+5\lambda}{1+\lambda}\gamma_x\varepsilon^3\underline{u}_R(\underline{x}_+,\underline{i}_x) \qquad (84)$$

Hence, the rotational motion of a sphere whose rotation axis is parallel to an interface requires the following singularities at the center of sphere.

rotlet: $\underline{u}_R(x_+,\gamma_x\underline{i}_x)\left[1 + \frac{-1+5\lambda}{1+\lambda}\frac{\varepsilon^3}{16} + O(\varepsilon^4)\right]$

Stokeslet: $\underline{u}_s(\underline{x}_+,\underline{i}_y)\left[\frac{3}{16}\frac{\gamma_x}{1+\lambda}\varepsilon^2 + O(\varepsilon^3)\right]$

potential dipole: $\underline{u}_D(\underline{x}_+,\underline{i}_y)\left[-\frac{1}{16}\frac{\gamma_x}{1+\lambda}\varepsilon^2 + O(\varepsilon^3)\right]$

stresslet: $\underline{u}_{ss}(\underline{x}_+,\underline{i}_y,\underline{i}_z)\frac{5}{16}\gamma_x\varepsilon^3$

potential quadrupole: $\frac{\partial}{\partial y}\underline{u}_D(\underline{x}_+,\underline{i}_z)\frac{1}{16}\gamma_x\varepsilon^3$

The torque on the sphere required to achieve angular velocity, $\underline{\gamma} = \gamma_x\underline{i}_x$, can be readily evaluated from the strength of rotlet.

$$\underline{T} = 8\pi\gamma_x\left[1 + \frac{-1+5\lambda}{1+\lambda}\frac{\varepsilon^3}{16} + O(\varepsilon^4)\right]\underline{i}_y \qquad (85)$$

It can be seen that, for $\lambda > \frac{1}{5}$, the required torque on the sphere increases due to the presence of an interface. For $\lambda < \frac{1}{5}$, the torque is less than it would be in an infinite fluid. In addition, there will be a drag force on the sphere which can be obtained from the strength of the Stokeslet as

$$\underline{F} = -\frac{3\pi}{2}\frac{\gamma_x}{1+\lambda}\varepsilon^2\underline{i}_y + O(\varepsilon^3) \qquad (86)$$

In this case, rotation will lead to translation of the sphere parallel to the interface unless a body force of equal magnitude and opposite sign is applied to the sphere. For a solid wall, $\lambda \to \infty$, there is no contribution to the drag force up to $O(\varepsilon^2)$ from the rotational motion of a sphere.

7. Discussion

In the previous sections, we have studied the translational and rotational motions of a sphere in the presence of a fluid/fluid interface. Due to the linearity of Stokes' equation, we can analyze the arbitrary motion of a sphere in the presence of an interface by superposing the translation of a sphere parallel and perpendicular to the interface and the rotation of a sphere with the axis of rotation parallel or perpendicular to the interface. Hence, an arbitrary motion of a sphere can be expressed in more general terms; namely, in terms of a translation tensor, a rotation tensor and a coupling tensor.

At sufficiently small Reynolds numbers, the motion of a rigid particle can be generally described by [cf. Happel and Brenner 1973]:

$$\underline{F} = \underline{\underline{K}}_T \cdot \underline{U} + \underline{\underline{K}}_C^{+} \cdot \underline{\Omega} \tag{87}$$

$$\underline{T} = \underline{\underline{K}}_C \cdot \underline{U} + \underline{\underline{K}}_R \cdot \underline{\Omega} \tag{88}$$

Here, $\underline{F}$ and $\underline{T}$ are the force and the torque exerted on the particle, $\underline{\underline{K}}_T$, $\underline{\underline{K}}_R$ and $\underline{\underline{K}}_C$ are the translation tensor, the rotation tensor, and the coupling tensor, respectively. $\underline{U}$ is the translational velocity of a particle and $\underline{\Omega}$ is the angular velocity.

Using the results in section 3, 4 and 5, the elements of the tensors, $\underline{\underline{K}}_T$, $\underline{\underline{K}}_R$ and $\underline{\underline{K}}_C$, can be determined for motion of a sphere near a plane fluid/fluid interface, i.e.

$$\underline{\underline{K}}_T = 6\pi \begin{bmatrix} K_{\parallel}^T & 0 & \\ & K_{\parallel}^T & \\ 0 & & K_{\perp}^T \end{bmatrix}, \qquad \underline{\underline{K}}_R = 8\pi \begin{bmatrix} K_{\parallel}^R & 0 & \\ & K_{\parallel}^R & \\ 0 & & K_{\perp}^R \end{bmatrix}$$

$$\underline{\underline{K}}_C = 6\pi \begin{bmatrix} 0 & K_C & 0 \\ -K_C & 0 & 0 \\ 0 & 0 & 0 \end{bmatrix}$$

where

$$K_{\parallel}^{T} = 1 - \frac{3}{16}\varepsilon\frac{2 - 3\lambda}{1 + \lambda} + \left(\frac{3}{16}\varepsilon\frac{2 - 3\lambda}{1 + \lambda}\right)^2 + O(\varepsilon^3)$$

$$K_{\perp}^{T} = 1 + \frac{3}{8}\varepsilon\frac{2 + 3\lambda}{1 + \lambda} + \left(\frac{3}{8}\varepsilon\frac{2 + 3\lambda}{1 + \lambda}\right)^2 + O(\varepsilon^3)$$

$$K_{\parallel}^{R} = 1 + \frac{\varepsilon^3}{16}\frac{- 1 + 5\lambda}{1 + \lambda} + O(\varepsilon^4)$$

$$K_{\perp}^{R} = 1 - \frac{\varepsilon^3}{8}\frac{1 - \lambda}{1 + \lambda} + O(\varepsilon^4)$$

$$K_{C} = \frac{\varepsilon^2}{4}\frac{1}{1 + \lambda} + O(\varepsilon^3)$$

Since we have completed the evaluation of the resistance tensors in Equations (87) and (88), we can easily solve other interesting problems. As one example, the motion of a freely suspended sphere under the action of an applied $\underline{F}$ can be obtained by substituting $\underline{T} = \underline{0}$ in Equation (88). The translational and angular velocities for this case are

$$\underline{U} = [\underline{\underline{K}}_T - \underline{\underline{K}}_C^{+} \cdot \underline{\underline{K}}_R^{-1} \cdot \underline{\underline{K}}_C]^{-1} \cdot \underline{F} \tag{89}$$

$$\underline{\Omega} = - \underline{\underline{K}}_R^{-1} \cdot \underline{\underline{K}}_C \cdot \underline{U} \tag{90}$$

8. Conclusion

We have derived the creeping flow solution for a point force in the presence of an interface with an arbitrary viscosity ratio. In addition, we have generalized this solution to the case of a finite-size sphere moving near a fluid/fluid interface. In the limit of an infinite viscosity ratio, these results are in accord with known solutions for motion of a sphere near a plane solid wall.

When a sphere moves normal to a plane interface, we have shown that it is necessary to modify the strength of the Stokeslet and potential dipole singularities at the sphere center, as well as add a stresslet and a potential quadrupole through terms of $O(\varepsilon^2)$. The drag ratio is $\left(1 + \frac{3}{8}\varepsilon\frac{2 + 3\lambda}{1 + \lambda}\right)$.

For the case of a sphere moving parallel to the interface, on the other hand, it is necessary to include a rotlet, as well as the Stokeslet, potential dipole, potential quadrupole and stresslet. In this case, the drag ratio is $\left(1 - \frac{3}{16}\varepsilon\frac{2 - 3\lambda}{1 + \lambda}\right)$. In addition, we have shown that a torque $\frac{3\pi}{2}\varepsilon^2\frac{1}{1 + \lambda}$ is required to keep the particle from rotating. It can be seen that the drag on a sphere moving normal to the interface is increased relative to Stokes' drag for all values of ε and λ. This is a reflection of the presence of a flat interface. Even when the upper fluid becomes essentially inviscid relative to the lower fluid, (i.e. $\lambda \to 0$), the drag on the particle is increased. The additional dissipation in fluid II which is associated with the interface is obviously greater than the <u>decrease</u> in dissipation in fluid I as $\lambda \to 0$. For parallel motion and $\varepsilon << 1$, on the other hand, there is a critical viscosity ratio $\lambda = 2/3$ which separates the regions of increased and decreased drag.

We have also studied the rotation of a sphere with a constant angular velocity near an interface. When the rotation axis is normal to the interface, only a rotlet is needed at the center of sphere through terms of $O(\varepsilon^3)$ and the hydrodynamic torque on the sphere surface is proportional to $\left(1 - \frac{1 - \lambda}{8(1 + \lambda)}\varepsilon^3\right)$. There is no drag force for this case.

When a sphere is rotating with axis of rotation parallel to the interface, a rotlet as well as a Stokeslet, a potential dipole, a potential quadrupole and a stresslet is required at the center of sphere. The required hydrodynamic torque is proportional to $\left(1 - \frac{1 - 5\lambda}{1 + \lambda} \frac{\varepsilon^3}{16}\right)$. Further, a force, $\frac{3\pi}{2} \frac{\gamma_x}{1 + \lambda} \varepsilon^2$, is required to keep the sphere from translating from its original position. The critical viscosity ratio which separates the regions of increased and decreased torque due to the presence of an interface is 1 for the rotation with a normal axis and 1/5 for the rotation with a parallel axis.

In conclusion, we can solve for arbitrary motions of a sphere in the presence of a plane interface by linearly superposing the approximate solutions for translational and rotational motions of a sphere.

The solution scheme which we have developed can be applied, in principle, for the motion of an arbitrary body near a flat interface, provided only that we know the singularity distribution in an infinite fluid. However, it should be mentioned that the higher order terms are valid only when $\varepsilon << 1$.

Acknowledgments

This work was supported by a grant, ENG78-10317, from the National Science Foundation. The authors also wish to thank Professor Howard Brenner for many helpful discussions during the initial stages of this work.

References

Aderogba, K. 1976 On Stokeslets in a two-fluid space. J. Eng. Math. 10, 143.

Bart, E. 1968 The slow unsteady settling of a fluid sphere toward a flat fluid interface. Chem. Eng. Sci. 23, 193.

Chwang, A. T. and Wu, T. Y. 1975 Hydromechanics of low-Reynolds number flow. Part 2. Singularity method for Stokes flow. J. Fluid Mech. 67, 787.

Dean, W. R. and O'Neill, M. E. 1963 A slow motion of viscous liquid caused by the rotation of a solid sphere. Mathematika 10, 13.

Faxen, H. 1921 Dissertation, Uppsala Univ.

Happel, J. and Brenner, H. 1973 *Low Reynolds Number Hydrodynamics*, Noordhoff International Pub., Leyden, The Netherlands.

Ho, B. P. and Leal, L. G. 1974 Inertial migration of rigid spheres in two-dimensional unidirectional flows. J. Fluid Mech. 65, 365.

Jeffery, G. B. 1915 On the steady rotation of a solid of revolution in a viscous fluid. London Math. Soc. 14, 327.

Jeffery, G. B. 1912 On a form of the solution of Laplace's equation suitable for problems relating to two spheres. Proc. Roy. Soc. A87, 109.

Lee, S. H. 1979 Ph.D. Dissertation, California Institute of Technology.

Lorentz, H. A. 1907 A general theorem concerning the motion of a viscous fluid and a few consequences derived from it. Abhandl. Theoret. Phys. 1, 23.

O'Neill, M. E. 1964 A slow motion of viscous liquid caused by a slowly moving solid sphere. Mathematika 11, 67.

Stimson, M. and Jeffery, G. B. 1926 The motion of two spheres in a viscous fluid. Proc. Roy. Soc. A 111, 110.

Figure Captions

Fig. 1. The stream lines due to a Stokeslet, $\underline{\alpha} = \frac{3}{4}\,\underline{i}_z(U_C\ell_C)$, located at $z = -5[\ell_C]$. $A = -2.5$, $B = -2.0$, $C = -1.5$, $D = -1.0$, $E = -0.5$, $F = -0.25$, $G = 0.005$, $H = 0.1$, $I = 0.2$, $J = 0.4$ and $K = 0.6$ $[U_C\ell_C^2]$.
(a) unbounded, (b) $\lambda = 0.01$, (c) $\lambda = 1.0$ (d) $\lambda = 100$.

Fig. 2. Normal stress imbalance on the interface, $z = 0$; $\underline{\alpha} = \frac{3}{4}\,\underline{i}_z$, $r = (x^2 + y^2)^{\frac{1}{2}}$.

Fig. 3. Normal stress imbalance on the line, $y = z = 0$; $\underline{\alpha} = \frac{3}{4}\,\underline{i}_x$.

Fig. 4. The drag ratio vs. the distance between the sphere center and the interface; $\underline{U} = \underline{i}_z$.

Fig. 5. The drag ratio vs. the distance between the sphere center and the interface; $\underline{U} = \underline{i}_x$.

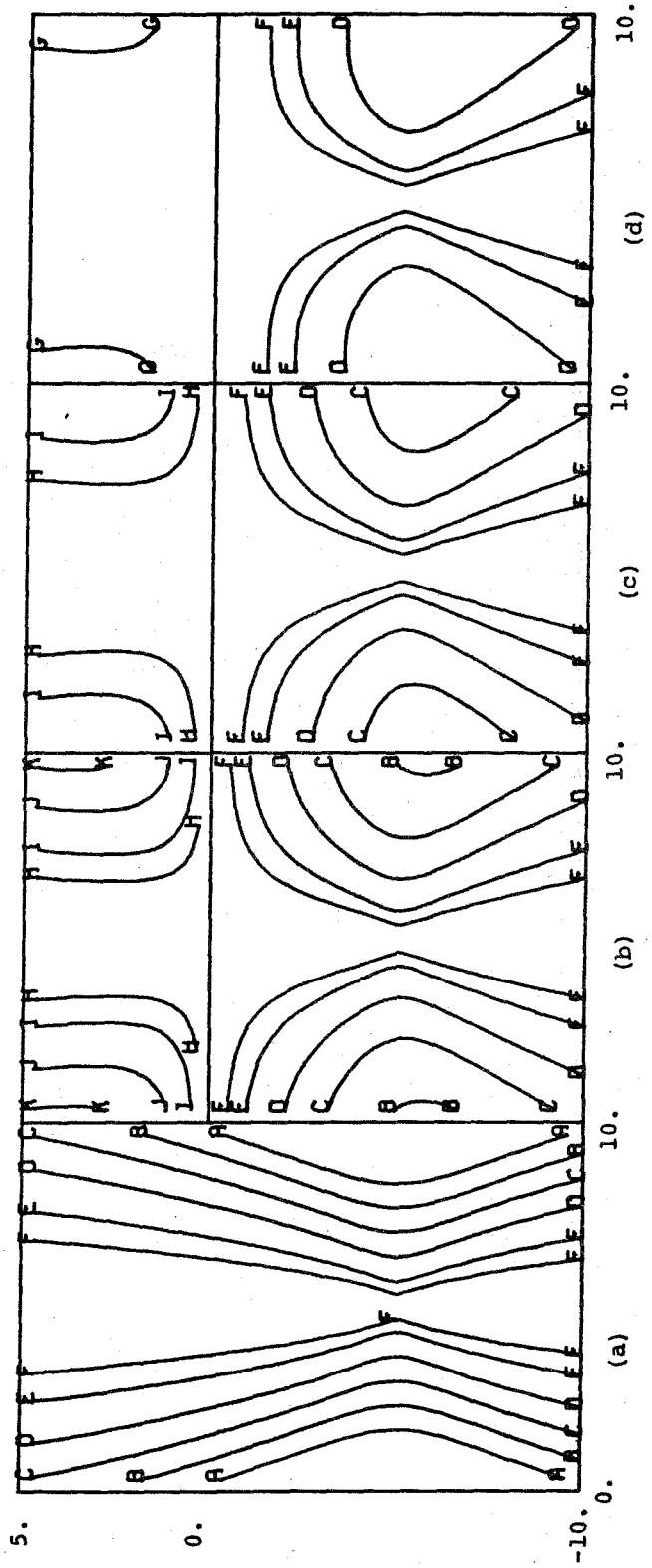

Fig. 1

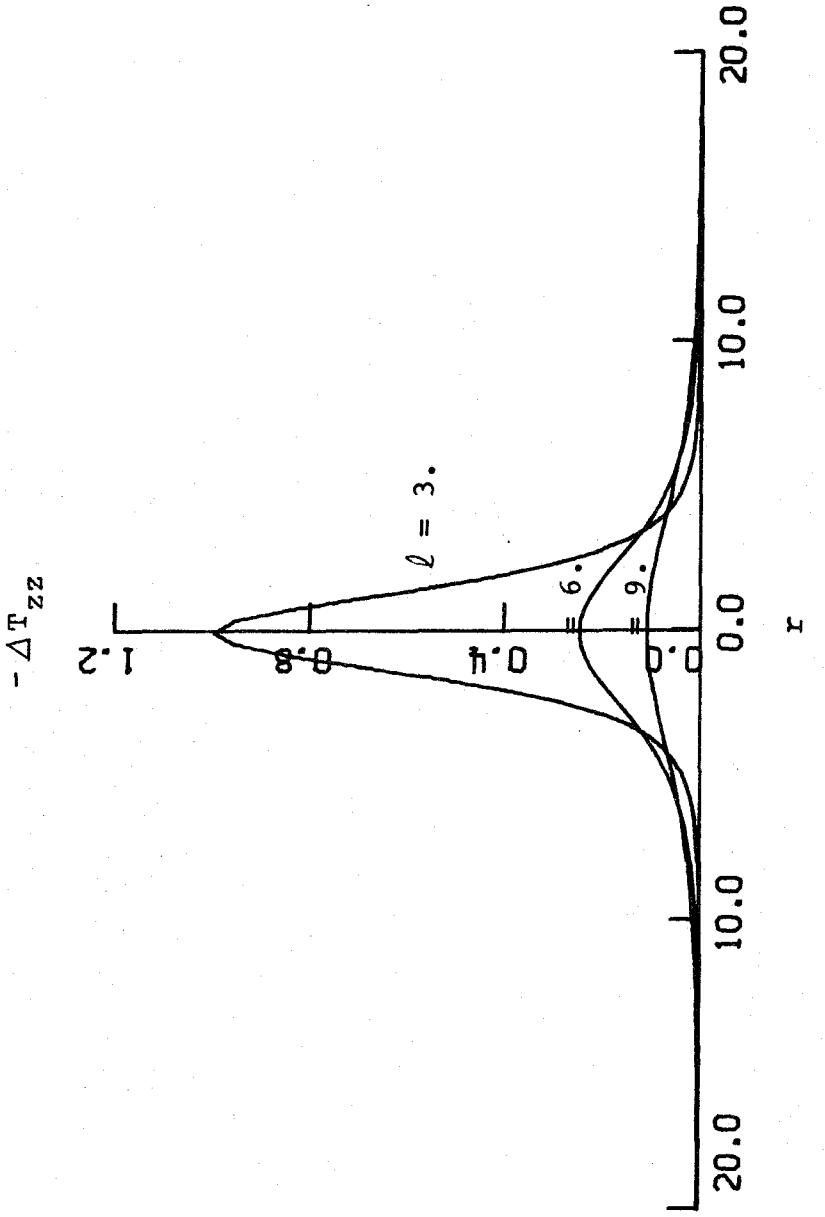

Fig. 2

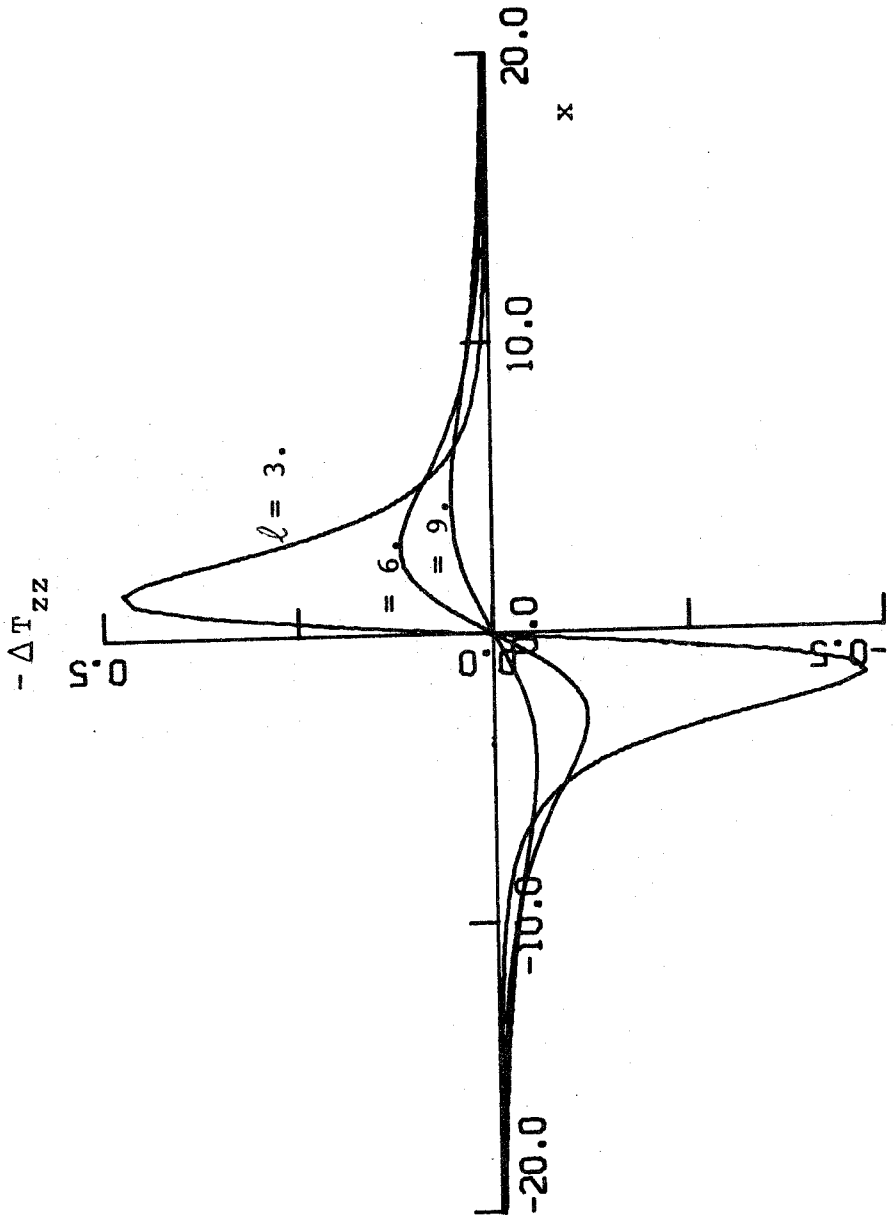

Fig. 3

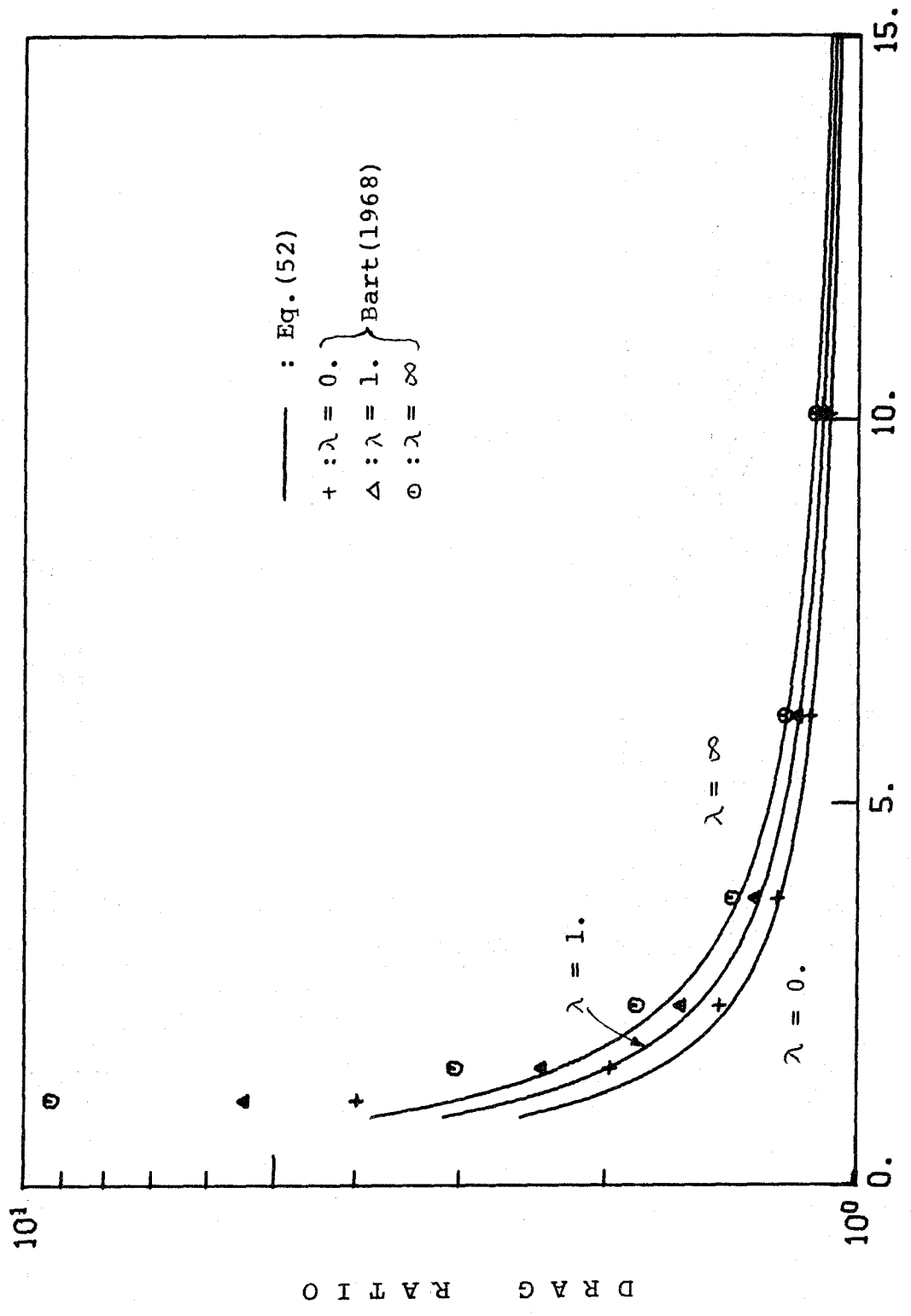
DRAG RATIO
10^1
10^0
0.
5.
10.
15.
ℓ
$\lambda = 0.$
$\lambda = 1.$
$\lambda = \infty$
+ : $\lambda = 0.$
△ : $\lambda = 1.$
⊙ : $\lambda = \infty$
Bart(1968)
: Eq.(52)

Fig. 4

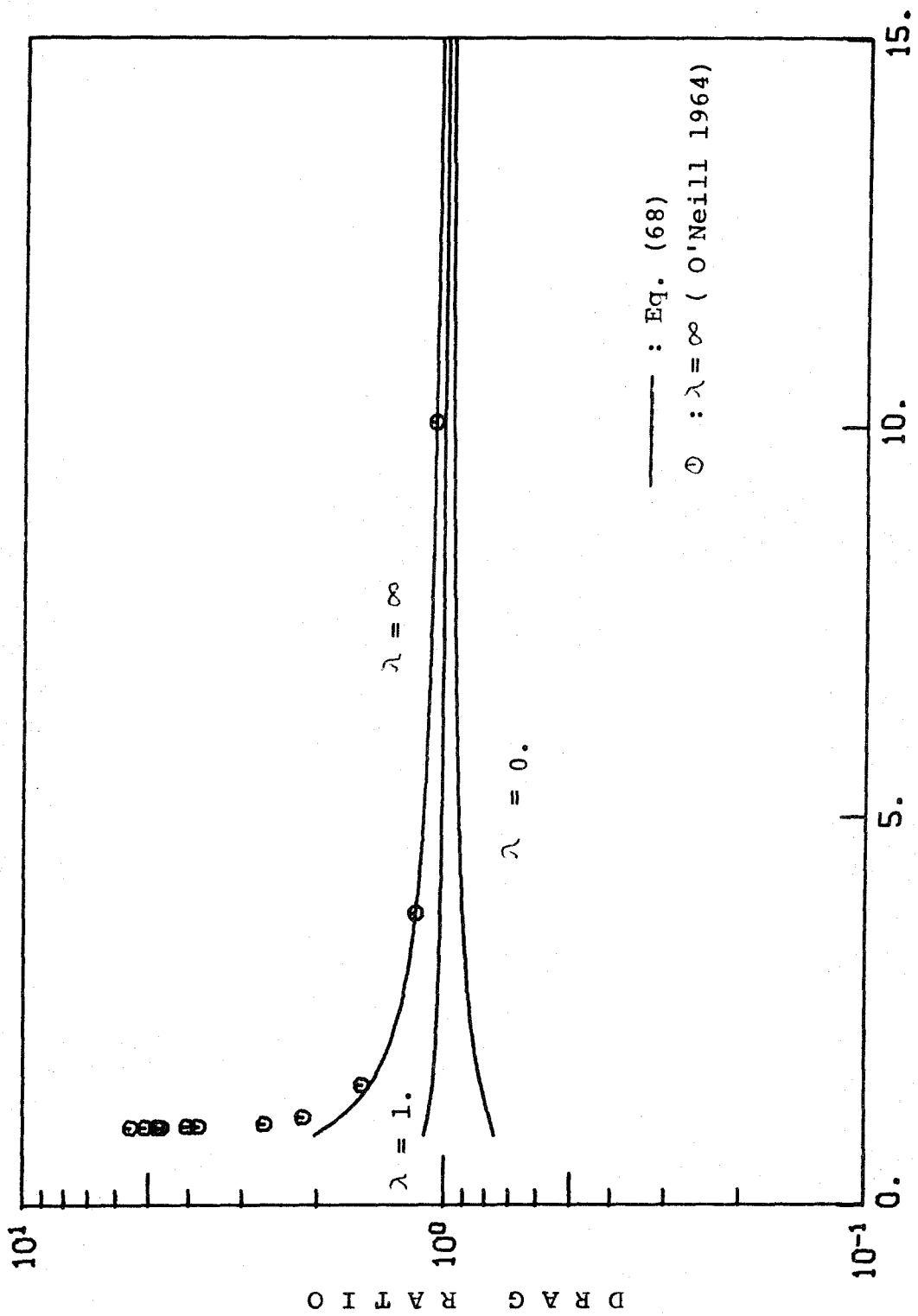
DRAG RATIO
10^1
10^0
10^{-1}
0.
5.
10.
15.
ℓ
$\lambda = \infty$
$\lambda = 1.$
$\lambda = 0.$
——— : Eq. (68)
⊖ : $\lambda = \infty$ (O'Neill 1964)

Fig. 5

APPENDIX: Derivation of the lemma on page 14.

If $\underline{u}$ is a solution of Stokes' equation giving the velocity (u_I, v_I, w_I) at the interface, the associated velocity field, the reflected velocity field, and the associated reflected velocity field yield the following velocity at the interface.

$$\hat{\underline{u}}_{z=0} = (-u_I, -v_I, w_I)$$

$$\underline{u}^*_{z=0} = (u_I, v_I, -w_I)$$

$$\hat{\underline{u}}^*_{z=0} = (-u_I, -v_I, -w_I)$$

In addition, the velocity gradient in z-direction at the interface becomes

$$\frac{\partial \underline{u}}{\partial z} = \left(\frac{\partial u}{\partial z}, \frac{\partial v}{\partial z}, \frac{\partial w}{\partial z} \right)_{z=0}$$

$$\frac{\partial \hat{\underline{u}}}{\partial z} = \left(-\frac{\partial u}{\partial z} - 2\frac{\partial w}{\partial x}, -\frac{\partial v}{\partial z} - 2\frac{\partial w}{\partial y}, -\frac{\partial w}{\partial z} \right)_{z=0}$$

$$\frac{\partial \underline{u}^*}{\partial z} = \left(-\frac{\partial u}{\partial z}, -\frac{\partial v}{\partial z}, -\frac{\partial w}{\partial z} \right)_{z=0}$$

$$\frac{\partial \hat{\underline{u}}^*}{\partial z} = \left(\frac{\partial u}{\partial z} + 2\frac{\partial w}{\partial x}, \frac{\partial v}{\partial z} + 2\frac{\partial w}{\partial y}, -\frac{\partial w}{\partial z} \right)_{z=0}$$

When the interface remains flat, the normal velocity should be identically zero. We thus consider the combined velocity fields which always give zero normal velocity of the interface: $(\underline{u}-\hat{\underline{u}})$, $(\underline{u}+\underline{u}^*)$, $(\underline{u}+\hat{\underline{u}}^*)$, $(\hat{\underline{u}}+\underline{u}^*)$, $(\hat{\underline{u}}+\hat{\underline{u}}^*)$, and $(\underline{u}^*-\hat{\underline{u}}^*)$.
It is noted that $\underline{u}$ and $\hat{\underline{u}}$ have a singularity in the lower fluid while $\underline{u}^*$ and $\hat{\underline{u}}^*$ have a singularity in the upper fluid. In the upper fluid, the velocity field should be analytical everywhere. Thus the only combined velocity field for the upper fluid is

$$\underline{u}^{(1)} = a (\underline{u} - \hat{\underline{u}}) \qquad \text{(A1)}$$

For the lower fluid, the velocity field can be expressed as

$$\underline{u}^{(2)} = b(\underline{u}-\hat{\underline{u}}) + c(\underline{u}+\underline{u}^*) + d(\underline{u}+\hat{\underline{u}}^*) + e(\hat{\underline{u}}+\underline{u}^*) + f(\hat{\underline{u}}+\hat{\underline{u}}^*) + g(\underline{u}^*-\hat{\underline{u}}^*) \tag{A2}$$

First, $\underline{u}^{(2)}$ should become $\underline{u}$ when $\underline{x}$ is far from the interface.

$$b+c+d = 1 \quad \text{and} \quad -b+e+f = 0 \tag{A3}$$

Then the equation (A2) can be written as

$$\underline{u}^{(2)} = \underline{u} + (b+c-f+g)\underline{u}^* + (1-b-c-g)\hat{\underline{u}}^* \tag{A4}$$

When we define $h = b+c+g$, $\underline{u}^{(2)}$ can be rewritten as

$$\underline{u}^{(2)} = \underline{u} + (h-f)\underline{u}^* + (1-h)\hat{\underline{u}}^* \tag{A5}$$

The velocity u and v should be continuous at the interface. From equations (A1) and (A5), we obtain

$$2a = 2h - f \tag{A6}$$

The shear stress is also continuous at the interface.

$$\frac{\partial u^{(2)}}{\partial z} + \frac{\partial w^{(2)}}{\partial x} = \lambda\left(\frac{\partial u^{(1)}}{\partial z} + \frac{\partial w^{(1)}}{\partial x}\right)$$

$$\frac{\partial v^{(2)}}{\partial z} + \frac{\partial w^{(2)}}{\partial y} = \lambda\left(\frac{\partial v^{(1)}}{\partial z} + \frac{\partial w^{(1)}}{\partial y}\right) \tag{A7}$$

Obviously,

$$\frac{\partial w^{(2)}}{\partial x} = \frac{\partial w^{(1)}}{\partial x} = \frac{\partial w^{(2)}}{\partial y} = \frac{\partial w^{(1)}}{\partial y} = 0 \quad \text{at the interface.}$$

Therefore, from equations (A1), (A5), and (A7), the continuity of T_{xz} requires

$$2\lambda a\left(\frac{\partial u}{\partial z} + \frac{\partial w}{\partial x}\right) = \frac{\partial u}{\partial z} + (h-f)\left(-\frac{\partial u}{\partial z}\right) + (1-h)\left(\frac{\partial u}{\partial z} + 2\frac{\partial w}{\partial x}\right) \tag{A8}$$

To satisfy equation (A8),

$$2\lambda a = 2 - 2h + f \tag{A9}$$

$$2\lambda a = 2 - 2h \tag{A10}$$

The continuity of T_{yz} requires the identical conditions with (A9) and (A10). From equations (A6), (A9), and (A10),

$$a = \frac{1}{1+\lambda}, \quad h = \frac{1}{1+\lambda}, \quad \text{and} \quad f = 0. \tag{A11}$$

Hence,

$$\underline{u}^{(1)} = \frac{1}{1+\lambda}\left(\underline{u} - \hat{\underline{u}}\right) \tag{A12}$$

$$\underline{u}^{(2)} = \underline{u} + \frac{1}{1+\lambda}\underline{u}^{*} + \frac{\lambda}{1+\lambda}\hat{\underline{u}}^{*} \tag{A13}$$

Since the system is linear, the pressure field can be readily obtained.

$$p^{(1)} = \frac{\lambda}{1+\lambda}\left(p - \hat{p}\right) \tag{A14}$$

$$p^{(2)} = p + \frac{1}{1+\lambda}p^{*} + \frac{\lambda}{1+\lambda}\hat{p}^{*} \tag{A15}$$

B. "Motion of a Sphere in the Presence of a Plane Interface"

Part II. An Exact Solution in Bipolar Coordinates

by

S. H. Lee and L. G. Leal

Department of Chemical Engineering
California Institute of Technology
Pasadena, California 91125

ABSTRACT

A general solution for Stokes' equation in bipolar coordinates is derived, and then applied to the arbitrary motion of a sphere in the presence of a plane fluid/fluid interface. The drag force and hydrodynamic torque on the sphere are then calculated for four specific motions of the sphere; namely, translation perpendicular and parallel to the interface and rotation about an axis which is perpendicular and parallel, respectively, to the interface. The most significant result of the present work is the comparison between these numerically exact solutions and the approximate solutions from Part I. The latter can be generalized to a variety of particle shapes, and it is thus important to assess their accuracy for this case of spherical particles where an exact solution can be obtained. In addition to comparisons with the approximate solutions, we also examine the predicted changes in the velocity, pressure and vorticity fields due to the presence of the plane interface. One particularly interesting feature of the solutions is the fact that the direction of rotation of a freely suspended sphere moving parallel to the interface can either be the same as for a sphere rolling along the interface (as might be intuitively expected), or opposite depending upon the location of the sphere center and the ratio of viscosities for the two fluids.

1. INTRODUCTION

When a small particle is translating or rotating near a fluid/fluid interface, the hydrodynamic force and torque on the particle are changed relative to their values in an unbounded fluid. In this paper, which is the second of a three-part series, we consider the simplest problem of this type; namely, the creeping motion of a rigid spherical particle of radius a whose center is instantaneously at a distance $d(> a)$ from a flat, horizontal fluid interface. This problem represents a first, asymptotic approximation for the limit of either large interfacial tension, σ, or large density difference between the two fluids, i.e.

$$\frac{\mu U}{\sigma} \ll 1 \quad \text{or} \quad \frac{\mu U}{ga^2\Delta\rho} \ll 1 \qquad \text{(translational motion)}$$

or (1)

$$\frac{\mu a\Omega}{\sigma} \ll 1 \quad \text{or} \quad \frac{\mu\Omega}{ga\Delta\rho} \ll 1 \qquad \text{(rotational motion)}$$

where a real fluid interface will remain only slightly deformed and in quasi-static equilibrium with the flow-induced stress fields in the two fluids. In part I of this series (Lee, Chadwick and Leal 1979), we obtained approximate solutions for the same problem when the sphere is far from the interface

$$\ell \equiv \frac{d}{a} \gg 1 \tag{2}$$

using a generalization of the method of Lorentz (1907). Although the condition (2) is independently sufficient for small interface deformation, the solutions in part I still require the conditions (1) to be satisfied since the interface was assumed to be flat at <u>all</u> orders of approximation in ℓ^{-1}. In the present paper, we obtain <u>exact</u> solutions for the motion of

a sphere near a flat fluid interface using a series expansion of eigensolutions in bipolar (spherical) coordinates. These exact solutions extend the domain of allowable ℓ relative to the condition (2) and thus serve to clarify some physical features of the motion of spherical particles near a fluid interface. More importantly, however, these exact solutions provide a basis for evaluating the accuracy of the asymptotic solutions as a function of ℓ. We have noted in part I that the approximate solution technique can be applied in a straightforward fashion to other particle shapes unlike the exact eigensolution expansion of the present paper which is strictly limited to spherical particles. Such generalizations could be of considerable significance in a number of applications, but only if the approximate solutions exhibit reasonable accuracy for most of the range of possible values of ℓ — certainly a big "if" in view of the condition (2). Comparison of the exact solutions obtained here with the approximate solutions of part I is particularly significant since the case of a spherical particle is the only one where exact solutions are possible for arbitrary particle motions and arbitrary values of the viscosity ratio, λ.

The use of bipolar (spherical) coordinates in low Reynolds number hydrodynamics was initiated by Jeffery (1912, 1915) who first derived eigensolutions of Laplace's equation and then used these eigensolutions to analyze the fluid motion generated by two spheres which rotate about their line of centers. Later, Stimson and Jeffery (1926) used a stream-function expansion in bipolar coordinates to solve the problem of two spheres translating along their line of centers with the same constant velocity. This work was extended by Bart (1968) to calculate the drag

force on a spherical drop which is translating normal to a flat fluid/fluid interface. A more difficult extension to the non-axisymmetric problem of a sphere rotating or translating parallel to a plane solid wall was accomplished by Dean and O'Neill (1963) and O'Neill (1964), respectively.

In this paper, we generalize the solutions of Jeffery (1912) and Dean and O'Neill (1963) to consider arbitrary translational or rotational motions of a rigid sphere in the presence of a plane fluid/fluid interface. We begin, in section 2a, by deriving a general, infinite series solution for Stokes' equation in terms of eigensolutions for bipolar (spherical) coordinates. When this solution is applied to the present class of problems, it is shown in section 2b that a complete numerical specification of the velocity and pressure fields requires the solution of an infinite set of algebraic equations for the coefficients of this series. Fortunately, in general, the magnitude of the various terms in the infinite series decreases exponentially with increasing order, and any desired degree of numerical accuracy can thus be achieved by retaining only a finite number of terms. Since the rate of convergence does decrease as ℓ decreases, it is necessary to retain a larger number of terms to yield the same numerical accuracy in the results as the sphere moves closer to the interface. This is not a serious limitation, however, since the numerical evaluation of coefficients in the truncated series reduces to the solutions of a band matrix and there is relatively little cost in computation time including a large number of terms. After generating the general solution, as described above, it is applied in section 4a to the four fundamental problems of particle translation and rotation

perpendicular and parallel to the fluid interface. As discussed in part I, the linearity of the Stokes' equations and boundary conditions allows any arbitrary motion to be described in terms of a set of three hydrodynamic resistance tensors, and these tensors can be specified completely from the solutions for the four fundamental particle motions. The only significant deviation from the solution scheme described above occurs for rotation of the sphere with the axis of rotation normal to the fluid interface. In this case, there is only one non-zero velocity component, v_ϕ, and the coefficients of the solution can be obtained analytically. The axisymmetric problem of translation normal to the interface can, of course, also be solved using a stream function as in Bart (1968). This alternative scheme for axisymmetric flows is discussed briefly in section 3, and is shown to give identical results for axisymmetric flows to the general solution derived here. It may be noted that Bart's solution for translation normal to the interface is incomplete since it is limited to the drag force on the sphere, without explicit determination of the velocity and pressure fields. Finally, the general formulae for the force and torque on the sphere are evaluated numerically in section 4b, for viscosity ratios λ = 0, 0.1, 1, 10 and ∞ and $1.1 \leq \ell \leq 10$, and compared with the approximate results of part I. Certain general features of the solutions, notably the rotation direction for a freely suspended sphere in parallel translation, are also discussed in section 4b.

2. GOVERNING EQUATIONS - THE METHOD OF SOLUTION

a. A General Solution of Stokes' Equation in Bipolar Coordinates

We begin by deriving a general solution of Stokes' equation, plus the

continuity equation

$$\nabla^2 \underline{u} = \nabla p \tag{3}$$

$$\nabla \cdot \underline{u} = 0 \tag{4}$$

in terms of the fundamental eigensolutions for bipolar coordinates. For convenience, all variables are considered to be non-dimensionalized with respect to arbitrary characteristic variables; L_c, U_c and $p_c (\equiv \mu U_c / L_c)$. A description of the bipolar coordinate system (ξ,η,ϕ) is given by Happel and Brenner (1973). In the application of our general solution to the motion of a spherical particle near a plane interface, we shall identify the interface with the coordinate surface $\eta = 0$ and the sphere with the coordinate surface $\eta = \eta_o = -\cosh^{-1}(\ell)$. Although we could solve for the velocity components in this bipolar system directly, it is more convenient for our purposes to use the bipolar eigensolutions to evaluate the velocity components in the related cylindrical coordinates, (r,z,ϕ), which are sketched together with (ξ,η,ϕ) in figure 1. The bipolar and cylindrical coordinates are related via the transformation laws

$$z = c \frac{\sinh \eta}{\cosh \eta - \cos \xi} \quad \text{and} \quad r = c \frac{\sin \xi}{\cosh \eta - \cos \xi} \tag{5}$$

in which c is a constant which can be determined by the relative location of the boundaries $\eta = 0$ and $\eta = \eta_o$ (see section 4).

It is convenient to consider the velocity field $\underline{u}$ as the sum of a homogeneous and particular solution of (3) and (4). In order to determine $\underline{u}$, we thus require a general expression for the pressure field p. According to (3) and (4), p is a harmonic function, i.e.

$$\nabla^2 p = 0 \tag{6}$$

and can therefore be expressed in terms of Jeffery's (1912) general solution of Laplace's equation in bipolar coordinates

$$p = \sum_{m=0}^{\infty} p_m(\eta,\xi) \cos(m\phi + \alpha_m) \tag{7}$$

in which

$$p_m(\eta,\xi) = (\cosh\eta - \zeta)^{\frac{1}{2}} \sum_{n=m}^{\infty} \left[A_n^m \sinh(n+\tfrac{1}{2})\eta + B_n^m \cosh(n+\tfrac{1}{2})\eta\right] \cdot \left[a_n^m P_n^m(\zeta) + b_n^m Q_n^m(\zeta)\right].$$

Here, $P_n^m(\zeta)$ and $Q_n^m(\zeta)$ are associated Legendre functions of the first and second kind, with argument $\zeta \equiv \cos\xi$. Since $Q_n^m(\zeta)$ increases to <u>infinity</u> on the z-axis, we require

$$b_n^m \equiv 0$$

in $p_m(\eta,\xi)$, thus yielding

$$p_m(\eta,\xi) = \frac{1}{c}(\cosh\eta - \zeta)^{\frac{1}{2}} \sum_{n=m}^{\infty} \left[A_n^m \sinh(n+\tfrac{1}{2})\eta + B_n^m \cosh(n+\tfrac{1}{2})\eta\right] P_n^m(\zeta) \tag{8}$$

Let us now consider the solution of (3) and (4) with p given by (7) and (8). With the components of $\underline{u}$ in the (r,ϕ,z) directions denoted, respectively, as u, v and w, the equations (3) and (4) can be written as

$$\frac{\partial p}{\partial r} = \left(\nabla^2 - \frac{1}{r^2}\right) u - \frac{2}{r^2}\frac{\partial v}{\partial \phi} \tag{9}$$

$$\frac{1}{r}\frac{\partial p}{\partial \phi} = \left(\nabla^2 - \frac{1}{r^2}\right) v + \frac{2}{r^2}\frac{\partial u}{\partial \phi} \tag{10}$$

$$\frac{\partial p}{\partial z} = \nabla^2 w \tag{11}$$

and

$$\frac{1}{r}\frac{\partial}{\partial r}(ru) + \frac{1}{r}\frac{\partial v}{\partial \phi} + \frac{\partial w}{\partial z} = 0 \tag{12}$$

with

$$\nabla^2 \equiv \left(\frac{\partial^2}{\partial r^2} + \frac{1}{r}\frac{\partial}{\partial r} + \frac{1}{r^2}\frac{\partial^2}{\partial \phi^2} + \frac{\partial^2}{\partial z^2}\right) .$$

Now, a particular solution of (9) - (11) is simply

$$\underline{u}^p = \frac{1}{2} p\, \underline{x} \tag{13}$$

where $\underline{x} = (r\underline{i}_r + z\underline{i}_z)$.

Thus, it is necessary to solve only the homogeneous equations, (9) - (11)

$$0 = \left(\nabla^2 - \frac{1}{r^2}\right) u^h - \frac{2}{r^2}\frac{\partial v^h}{\partial \phi} \tag{14}$$

$$0 = \left(\nabla^2 - \frac{1}{r^2}\right) v^h + \frac{2}{r^2}\frac{\partial u^h}{\partial \phi} \tag{15}$$

$$0 = \nabla^2 w^h \tag{16}$$

subject to (12).

The solution for w^h, which is bounded on the z-axis, can be readily obtained from the solution for p.

$$\begin{aligned} w^h &= \sum_m w_m(\eta,\xi)\cos(m\phi + \alpha_m) \\ &= (\cosh\eta - \zeta)^{\frac{1}{2}} \sum_{m=0}^{\infty}\sum_{n=m}^{\infty}\left[C_n^m \sinh(n+\tfrac{1}{2})\eta + D_n^m \cosh(n+\tfrac{1}{2})\eta\right] \\ &\quad \cdot P_n^m(\zeta)\cos(m\phi + \alpha_m) \end{aligned} \tag{17}$$

To obtain corresponding solutions for u^h and v^h, let us introduce the series expansion

$$u^h = \sum_m u_m(\eta,\xi)\cos(m\phi + \alpha_m) \tag{18}$$

$$v^h = \sum_m v_m(\eta,\xi)\sin(m\phi + \alpha_m) \tag{19}$$

Substituting (18) and (19) into the equations (14) and (15), we obtain

$$\left[\left(\frac{\partial^2}{\partial r^2} + \frac{1}{r}\frac{\partial}{\partial r} + \frac{\partial^2}{\partial z^2}\right) - \frac{m^2+1}{r^2}\right] u_m - \frac{2}{r^2} m v_m = 0 \qquad (20)$$

$$\left[\left(\frac{\partial^2}{\partial r^2} + \frac{1}{r}\frac{\partial}{\partial r} + \frac{\partial^2}{\partial z^2}\right) - \frac{m^2+1}{r^2}\right] v_m - \frac{2}{r^2} m u_m = 0 \qquad (21)$$

When $m = 0$, these equations are easily solved using Jeffery's (1912) solution,

$$u_o = (\cosh \eta - \zeta)^{\frac{1}{2}} \sum_{n=1}^{\infty} \left[E_n^o \sinh(n+\tfrac{1}{2})\eta + F_n^o \cosh(n+\tfrac{1}{2})\eta\right] P_n^1(\zeta) \qquad (22)$$

$$v_o = (\cosh \eta - \zeta)^{\frac{1}{2}} \sum_{n=1}^{\infty} \left[G_n^o \sinh(n+\tfrac{1}{2})\eta + H_n^o \cosh(n+\tfrac{1}{2})\eta\right] P_n^1(\zeta) \qquad (23)$$

For $m \geq 1$, the addition and subtraction of equations (20) and (21) yields (cf. Dean and O'Neill 1963 , and Lin 1968).

$$\left[\frac{\partial^2}{\partial r^2} + \frac{1}{r}\frac{\partial}{\partial r} + \frac{\partial^2}{\partial z^2} - \frac{1}{r^2}(m+1)^2\right]\gamma_m = 0 \qquad (24)$$

$$\left[\frac{\partial^2}{\partial r^2} + \frac{1}{r}\frac{\partial}{\partial r} + \frac{\partial^2}{\partial z^2} - \frac{1}{r^2}(m-1)^2\right]\chi_m = 0 \qquad (25)$$

where $\gamma_m \equiv u_m + v_m$ and $\chi_m \equiv u_m - v_m$. The solutions of equations (24) and (25) can again be seen from Jeffery's (1912) results to be

$$\gamma_m = (\cosh \eta - \zeta)^{\frac{1}{2}} \sum_{n=m+1}^{\infty} \left[E_n^m \sinh(n+\tfrac{1}{2})\eta + F_n^m \cosh(n+\tfrac{1}{2})\eta\right] P_n^{m+1}(\zeta) \qquad (26)$$

$$\chi_m = (\cosh \eta - \zeta)^{\frac{1}{2}} \sum_{n=m-1}^{\infty} \left[G_n^m \sinh(n+\tfrac{1}{2})\eta + H_n^m \cosh(n+\tfrac{1}{2})\eta\right] P_n^{m-1}(\zeta) \qquad (27)$$

Hence, a general solution of Stokes' equation for the velocity components (u,v,w) of the circular cylindrical coordinate system shown in figure 1 is simply

$$u = \frac{rp}{2} + u_o \cos\alpha_o + \frac{1}{2} \sum_{m=1}^{\infty} (\gamma_m + \chi_m) \cos(m\phi + \alpha_m) \tag{28}$$

$$v = v_o \sin\alpha_o + \frac{1}{2} \sum_{m=1}^{\infty} (\gamma_m - \chi_m) \sin(m\phi + \alpha_m) \tag{29}$$

$$w = \frac{zp}{2} + \sum_{m=0}^{\infty} w_m \cos(m\phi + \alpha_m) \tag{30}$$

in which p, u_o, v_o, w_m, γ_m and χ_m are conveniently expressed for present purposes in terms of the eigensolutions for bipolar coordinates which are defined in terms of the cylindrical coordinates by the equation (5). Furthermore, the velocity components (u,v,w) should satisfy the equation of continuity. Thus, substituting the equations (28), (29) and (30) into equation (12), this condition can be expressed in the form

$$\left(3 + r\frac{\partial}{\partial r} + z\frac{\partial}{\partial z}\right) p_o + 2\left(\frac{\partial}{\partial r} + \frac{1}{r}\right) u_o + 2\frac{\partial w_o}{\partial z} = 0, \text{ for } m = 0 \tag{31a}$$

and

$$\left(3 + r\frac{\partial}{\partial r} + z\frac{\partial}{\partial z}\right) p_m + \left(\frac{\partial}{\partial r} + \frac{m+1}{r}\right) \gamma_m + \left(\frac{\partial}{\partial r} - \frac{m-1}{r}\right) \chi_m + 2\frac{\partial w_m}{\partial z} = 0$$

$$\text{for } m \geq 1 \tag{31b}$$

Hence, we have derived a general solution of Stokes' equation, (28), (29) and (30), which is subject to the condition of mass continuity, (31a) and (31b).

b. Application of the General Solution to the Motion of a Sphere Near a Plane Interface

In this section, we apply the general, bipolar coordinate solution which was derived in the last section to determine the velocity and pressure fields for an arbitrary translational or rotational motion of a sphere near a plane fluid/fluid interface. The characteristic scales,

which are inherent in (3), (4) and the subsequent solution, can be defined in this case as L_c = a (sphere radius), U_c = V (translational velocity of the sphere) or Ωa (Ω = angular velocity of the sphere) and $p_c = \mu U_c/L_c$ or $\hat{\mu}U_c/L_c$ (μ is the viscosity of the lower fluid and $\hat{\mu}$ is that of the upper fluid). In order to complete the specification of the problem, we consider that the sphere is located in the lower fluid and denote the viscosity ratio between the upper and lower fluids as λ.

The general solution of the preceding section, which applies separately in the upper and lower fluids, contains eight unknown coefficients, namely A_n^m, B_n^m, ..., H_n^m, for each set of n and m, as may be seen from equations (8), (17), (22), (23), (26) and (27). Thus, including the solution constants for both fluids, we have 16 sets of unknowns to be determined in order to completely specify the velocity and pressure fields. Hereafter, the constants in the lower fluid will be denoted as A_n^m, B_n^m, ..., H_n^m, while those for the upper fluid are $\hat{A}_n^m$, $\hat{B}_n^m$, ..., $\hat{H}_n^m$. Two types of conditions remain to determine these constants. First are the boundary conditions at the sphere surface and the interface, and second, the general conditions of mass continuity, equation (31a,b), and boundedness of the velocities and pressure, which apply independent of the details of the boundary conditions. We may begin by examining the last two conditions first.

Let us start with the conditions which are required of the unknown constants to insure that the velocity and pressure fields are everywhere bounded. The necessity for such a condition arises from the fact that $\eta \to \pm \infty$ as $z \to \pm c$ on the z-axis. In the lower fluid, this causes no difficulty since the point z = - c, r = 0 lies inside the particle. In

the upper fluid, however, we must require

$$\hat{A}_n^m = -\hat{B}_n^m,\ \hat{C}_n^m = -\hat{D}_n^m,\ \hat{E}_n^m = -\hat{F}_n^m \text{ and } \hat{G}_n^m = -\hat{H}_n^m \tag{32}$$

for all n, m in order to insure that the velocities remain bounded as $z \to c$ on the z-axis.

The second general condition on the solution constants arises from the continuity equation (31a,b) which must be satisfied in both fluids. Thus, substituting equations (8), (22), (23), (26) and (27) into (31a) and (31b), we obtain two algebraic relationships among the constants which must be satisfied for arbitrary η and ξ (cf. Dean and O'Neill 1963 and Lin 1968). For m = 0, we obtain for the lower fluid

$$-\tfrac{1}{2} n A_{n-1}^o + \tfrac{5}{2} A_n^o + \tfrac{1}{2}(n+1)A_{n+1}^o - n D_{n-1}^o + (2n+1)D_n^o - (n+1)D_{n+1}^o$$

$$+ n(n-1)E_{n-1}^o - 2n(n+1)E_n^o + (n+1)(n+2)E_{n+1}^o = 0 \tag{33a}$$

$$-\tfrac{1}{2} n B_{n-1}^o + \tfrac{5}{2} B_n^o + \tfrac{1}{2}(n+1)B_{n+1}^o - n C_{n-1}^o + (2n+1)C_n^o - (n+1)C_{n+1}^o$$

$$+ n(n-1)F_{n-1}^o - 2n(n+1)F_n^o + (n+1)(n+2)F_{n+1}^o = 0 \tag{34a}$$

while for $m \geq 1$, we find

$$-\tfrac{1}{2}(n-m)A_{n-1}^m + \tfrac{5}{2} A_n^m + \tfrac{1}{2}(n+m+1)A_{n+1}^m - (n-m)D_{n-1}^m + (2n+1)D_n^m$$

$$-(n+m+1)D_{n+1}^m + \tfrac{1}{2}(n-m)(n-m-1)E_{n-1}^m - (n-m)(n+m+1)E_n^m$$

$$+\tfrac{1}{2}(n+m+1)(n+m+2)E_{n+1}^m - \tfrac{1}{2} G_{n-1}^m + G_n^m - \tfrac{1}{2} G_{n+1}^m = 0 \tag{33b}$$

$$-\frac{1}{2}(n-m)B^m_{n-1}+\frac{5}{2}B^m_n+\frac{1}{2}(n+m+1)B^m_{n+1}-(n-m)C^m_{n-1}+(2n+1)C^m_n$$

$$-(n+m+1)C^m_{n+1}+\frac{1}{2}(n-m)(n-m-1)F^m_{n-1}-(n-m)(n+m+1)F^m_n$$

$$+\frac{1}{2}(n+m+1)(n+m+2)F^m_{n+1}-\frac{1}{2}H^m_{n-1}+H^m_n-\frac{1}{2}H^m_{n+1}=0 \qquad (34b)$$

Similarly, in the upper fluid, we obtain

$$-\frac{1}{2}n\hat{A}^o_{n-1}+\frac{5}{2}\hat{A}^o_n+\frac{1}{2}(n+1)\hat{A}^o_{n+1}-n\hat{D}^o_{n-1}+(2n+1)\hat{D}^o_n$$

$$-(n+1)\hat{D}^o_{n+1}+n(n-1)\hat{E}^o_{n-1}-2n(n+1)\hat{E}^o_n+(n+1)(n+2)\hat{E}^o_{n+1}=0,$$

for $m = 0$ (35a)

and

$$-\frac{1}{2}(n-m)\hat{A}^m_{n-1}+\frac{5}{2}\hat{A}^m_n+\frac{1}{2}(n+m+1)\hat{A}^m_{n+1}-(n-m)\hat{D}^m_{n-1}+(2n+1)\hat{D}^m_n$$

$$-(n+m+1)\hat{D}^m_{n+1}+\frac{1}{2}(n-m)(n-m-1)\hat{E}^m_{n-1}-(n-m)(n+m+1)\hat{E}^m_n$$

$$+\frac{1}{2}(n+m+1)(n+m+2)\hat{E}^m_{n+1}-\frac{1}{2}\hat{G}^m_{n-1}+\hat{G}^m_n-\frac{1}{2}\hat{G}^m_{n+1}=0,$$

for $m \geq 1$ (35b)

It may be noted that the two equations, corresponding to (34a) and (34b) for the lower fluid, are not listed since they are not independent of (35a) and (35b) due to the conditions (32).

The conditions (32) and (33) - (35) apply for any regular motion of an incompressible fluid. The remaining conditions, however, depend upon the boundary conditions at the sphere surface and at the interface. Let us first consider the boundary conditions at the interface. For a plane interface, these conditions are zero normal velocity

$$w = \hat{w} = 0 \qquad \text{on} \qquad \eta = 0 \qquad (36)$$

plus continuity of the tangential components of velocity and stress. Continuity of normal stress does not enter explicity due to the assumption of a flat interface at this level of approximation, but would yield the first correction to the assumed interface shape due to the motion of the two contiguous fluids.[†] The condition (36) is satisfied trivially if

$$D_n^m = \hat{D}_n^m = 0, \text{ for all } n,m \tag{37}$$

The conditions for continuity of the tangential velocity components

$$u = \hat{u}, \quad \text{and} \quad v = \hat{v} \quad \text{on} \quad \eta = 0 \tag{38}$$

can be reduced by substituting (28) and (29) into (38). This yields

$$u_o - \hat{u}_o = -\frac{r}{2}(p_o - \hat{p}_o) \quad \text{and} \quad v_o = \hat{v}_o \quad \text{for } m = 0 \tag{39a}$$

$$\gamma_m - \hat{\gamma}_m = \chi_m - \hat{\chi}_m = -\frac{r}{2}(p_m - \hat{p}_m) \qquad \text{for } m \geq 1 . \tag{39b}$$

To satisfy equations (39a) and (39b) for all η and ξ, we require

$$-\frac{(n-m-1)}{2n-1}\left(F_{n-1}^m - \hat{F}_{n-1}^m\right) + \left(F_n^m - \hat{F}_n^m\right) - \frac{n+m+2}{2n+3}\left(F_{n+1}^m - \hat{F}_{n+1}^m\right)$$

$$= -\frac{1}{2}\left[\frac{1}{2n-1}\left(B_{n-1}^m - \hat{B}_{n-1}^m\right) - \frac{1}{2n+3}\left(B_{n+1}^m - \hat{B}_{n+1}^m\right)\right] \quad \text{for all } m \tag{40}$$

$$H_n^o = \hat{H}_n^o \qquad \text{for } m = 0 \tag{41a}$$

$$-\frac{(n-m+1)}{2n-1}\left(H_{n-1}^m - \hat{H}_{n-1}^m\right) + \left(H_n^m - \hat{H}_n^m\right) - \frac{n+m}{2n+3}\left(H_{n+1}^m - \hat{H}_{n+1}^m\right)$$

$$= -\frac{1}{2}\left[-\frac{(n-m)(n-m+1)}{2n-1}\left(B_{n-1}^m - \hat{B}_{n-1}^m\right)\right.$$

$$\left. + \frac{(n+m)(n+m+1)}{2n+3}\left(B_{n+1}^m - \hat{B}_{n+1}^m\right)\right] \quad \text{for } m \geq 1 \tag{41b}$$

[†] cf. section 2 of part I, where conditions are given which must be satisfied in order that the flat interface problem be a valid first approximation to the exact problem in which the interface is deformed.

Finally, the condition of continuity of shear stress at the interface can be expressed in the form

$$\frac{\partial u}{\partial z} = \lambda \frac{\partial \hat{u}}{\partial z} \qquad \text{and} \qquad \frac{\partial v}{\partial z} = \lambda \frac{\partial \hat{v}}{\partial z} \qquad \text{on} \quad \eta = 0 \tag{42}$$

Hence, using the general expressions for u, $\hat{u}$, v and $\hat{v}$, equation (42) becomes

$$\left.\begin{aligned} \frac{\partial}{\partial z}(u_o - \lambda \hat{u}_o) &= -\frac{r}{2}\frac{\partial}{\partial z}(p_o - \lambda \hat{p}_o) \\ \frac{\partial v_o}{\partial z} &= -\lambda \frac{\partial \hat{v}_o}{\partial z} \end{aligned}\right\} \quad \text{for } m = 0 \tag{43a}$$

$$\frac{\partial}{\partial z}(\gamma_m - \lambda \hat{\gamma}_m) = \frac{\partial}{\partial z}(\chi_m - \lambda \hat{\chi}_m) = -\frac{r}{2}\frac{\partial}{\partial z}(p_m - \lambda \hat{p}_m), \quad \text{for } m \geq 1 \tag{43b}$$

From equations (43a) and (43b), we can readily derive the following additional relationships among coefficients.

$$-(n - m - 1)\left(E^m_{n-1} - \lambda \hat{E}^m_{n-1}\right) + (2n + 1)\left(E^m_n - \lambda \hat{E}^m_n\right) - (n + m + 2)\left(E^m_{n+1} - \lambda \hat{E}^m_{n+1}\right)$$

$$= -\left(A^m_{n-1} - \lambda \hat{A}^m_{n-1}\right) + \left(A^m_{n+1} - \lambda \hat{A}^m_{n+1}\right), \quad \text{for all } m. \tag{44}$$

$$G^o_n = \lambda \hat{G}^o_n \qquad \text{for } m = 0 \tag{45a}$$

$$-(n - m + 1)\left(G^m_{n-1} - \lambda \hat{G}^m_{n-1}\right) + (2n + 1)\left(G^m_n - \lambda \hat{G}^m_n\right) - (n + m)\left(G^m_{n+1} - \lambda \hat{G}^m_{n+1}\right)$$

$$= (n - m)(n - m + 1)\left(A^m_{n-1} - \lambda \hat{A}^m_{n-1}\right) - (n + m)(n + m + 1)\left(A^m_{n+1} - \lambda \hat{A}^m_{n+1}\right)$$

$$\text{for } m \geq 1 \tag{45b}$$

The final step in obtaining a solution is to apply the "no-slip" and kinematic boundary conditions at the sphere surface, i.e.

$$\underline{u} = \underline{u}_s \qquad \text{at} \qquad \eta = \eta_o \,. \tag{46}$$

The most convenient method for doing this is to express $\underline{u}_s$ in terms of the bipolar eigenfunctions. Thus, we first expand the three components of $\underline{u}_s$ as

$$u_s = \sum_m u_s^m(\eta,\xi)\cos(m\phi + \alpha_m) \tag{47a}$$

$$v_s = \sum_m v_s^m(\eta,\xi)\sin(m\phi + \alpha_m) \tag{47b}$$

$$w_s = \sum_m w_s^m(\eta,\xi)\cos(m\phi + \alpha_m) \tag{47c}$$

Then, for $m = 0$, we may further expand the functions u_s^o and v_s^o as

$$u_s^o = (\cosh \eta_o - \zeta)^{\frac{1}{2}} \Sigma X_n^o(\eta)P_n^1(\zeta) \tag{48a}$$

$$v_s^o = (\cosh \eta_o - \zeta)^{\frac{1}{2}} \Sigma Y_n^o(\eta)P_n^1(\zeta) \tag{49a}$$

while for $m \geq 1$,

$$u_s^m + v_s^m = (\cosh \eta_o - \zeta)^{\frac{1}{2}} \Sigma X_n^m(\eta)P_n^{m+1}(\zeta) \tag{48b}$$

$$u_s^m - v_s^m = (\cosh \eta_o - \zeta)^{\frac{1}{2}} \Sigma Y_n^m(\eta)P_n^{m-1}(\zeta) \tag{49b}$$

In addition, for all m,

$$w_s^m = (\cosh \eta_o - \zeta)^{\frac{1}{2}} \Sigma Z_n^m(\eta)P_n^m(\zeta) \tag{50}$$

Now, using the general solution for the velocity components, (28) - (30), and the condition (46), we obtain, for $m = 0$,

$$u_o = u_s^o - \frac{r}{z}(w_s^o - w_o) \tag{51a}$$

$$v_o = v_s^o \tag{52a}$$

and for $m \geq 1$,

$$\gamma_m = u_s^m + v_s^m - \frac{r}{z}(w_s^m - w_m) \tag{51b}$$

$$\chi_m = u_s^m - v_s^m - \frac{r}{z}\,(w_s^m - w_m) \tag{52b}$$

In addition, for all m,

$$p_m = \frac{2}{z}\,(w_s^m - w_m) \tag{53}$$

Combining (51) - (53) with the previously derived expansions of $\underline{u}_s$, (48) - (50), we thus obtain the following additional relationships among the unknown coefficients,

$$E_n^m \sinh(n + \tfrac{1}{2})\eta_o + F_n^m \cosh(n + \tfrac{1}{2})\eta_o = \chi_n^m(\eta_o)$$

$$- \frac{1}{(2n + 3)\sinh \eta_o}\left[- Z_{n+1}^m(\eta_o) + C_{n+1}^m \sinh(n + \tfrac{3}{2})\eta_o\right]$$

$$+ \frac{1}{(2n - 1)\sinh \eta_o}\left[- Z_{n-1}^m(\eta_o) + C_{n-1}^m \sinh(n - \tfrac{1}{2})\eta_o\right], \text{ for all m} \tag{54}$$

$$G_n^o \sinh(n + \tfrac{1}{2})\eta_o + H_n^o \cosh(n + \tfrac{1}{2})\eta_o = Y_n^o(\eta_o), \text{ for } m = 0 \tag{55a}$$

$$G_n^m \sinh(n + \tfrac{1}{2})\eta_o + H_n^m \cosh(n + \tfrac{1}{2})\eta_o = Y_n^m(\eta_o)$$

$$+ \frac{(n + m)(n + m + 1)}{(2n + 3)\sinh \eta_o}\left[- Z_{n+1}^m(\eta_o) + C_{n+1}^m \sinh(n + \tfrac{3}{2})\eta_o\right]$$

$$- \frac{(n - m)(n - m + 1)}{(2n - 1)\sinh \eta_o}\left[- Z_{n-1}^m(\eta_o) + C_{n-1}^m \sinh(n - \tfrac{1}{2})\eta_o\right] \quad \text{for} \quad m \geq 1 \tag{55b}$$

$$A_n^m \sinh(n + \tfrac{1}{2})\eta_o + B_n^m \cosh(n + \tfrac{1}{2})\eta_o = \frac{-2}{\sinh \eta_o}\left[\frac{(n - m)}{2n - 1}\left\{Z_{n-1}^m(\eta_o)\right.\right.$$

$$\left. - C_{n-1}^m \sinh(n - \tfrac{1}{2})\eta_o\right\} - \cosh \eta_o\left\{Z_n^m(\eta_o) - C_n^m \sinh(n + \tfrac{1}{2})\eta_o\right\}$$

$$\left. + \frac{n + m + 1}{2n + 3}\left\{Z_{n+1}^m(\eta_o) - C_{n+1}^m \sinh(n + \tfrac{3}{2})\eta_o\right\}\right], \text{ for all m} \tag{56}$$

We have thus derived sixteen independent algebraic relations, namely (32a - d), (33) - (35), (37a,b), (40), (41), (44), (45), (54) - (56), which

may be used to evaluate all of the unknown coefficients of the general solutions in the upper and lower fluids. It should be noted that these algebraic equations are all linear. Moreover, equations (44), (45a,b) and (35a,b) suggest that

$$A_n^m = \lambda \hat{A}_n^m, \; E_n^m = \lambda \hat{E}_n^m \qquad \text{and} \qquad G_n^m = \lambda \hat{G}_n^m \tag{57}$$

The relationships (57) automatically satisfy equations (44) and (45a,b), and also satisfy (35a,b) due to equations (33a,b). It will also be noted that D_n^m, $\hat{D}_n^m$ and $\hat{C}_n^m$ are all equal to zero according to (32) and (37). Thus, it is only necessary to solve the equations (33a,b), (34a,b), (40), (41a,b), (54), (55a,b) and (56) for the seven unknown coefficients: A_n^m, B_n^m, C_n^m, E_n^m, F_n^m, G_n^m and H_n^m. This system of algebraic equations yields a band matrix and is readily solved using standard numerical methods for specified values of η_o (i.e. of particle position relative to the interface). Once the coefficients have been determined for the lower fluid, the coefficients for the upper fluid can be obtained trivially from equations (57) and (32).

3. AN ALTERNATIVE METHOD FOR AXISYMMETRIC FLOW

When the sphere is translating normal to the (plane) interface, the flow field can also be obtained using a stream function representation of the governing equations. Stimson and Jeffery (1926) derived a solution for the stream function in bipolar coordinates in order to solve for the motion generated by two spheres which are translating with equal constant velocities parallel to their line of centers. Bart (1968) later utilized the same stream function solution to evaluate the drag force for

a spherical drop which is moving normal to a flat fluid/fluid interface. However, Bart (1968) only reported the sum of the coefficients in the stream function solution which yield the drag. Therefore, for completeness, we will briefly discuss the use of the stream function solution for axisymmetric flow and present the values of all the coefficients in the stream function solution for translation of a solid sphere perpendicular to a plane fluid/fluid interface.

The stream function for any axisymmetric Stokes' flow is well known to satisfy the general equation,

$$E^4\psi = 0 \tag{58}$$

When expressed in terms of a cylindrical coordinate system, with the z-axis being the axis of symmetry,

$$E^2 \equiv r \frac{\partial}{\partial r}\left(\frac{1}{r}\frac{\partial}{\partial r}\right) + \frac{\partial^2}{\partial z^2}$$

and

$$u = \frac{1}{r}\frac{\partial \psi}{\partial z} \qquad \text{and} \qquad w = -\frac{1}{r}\frac{\partial \psi}{\partial r} \tag{59}$$

Stimson and Jeffery's (1926) general solution of equation (58) may be expressed in the form

$$\psi = (\cosh \eta - \zeta)^{-3/2} \sum_n U_n V_n \tag{60}$$

where

$$U_n = K_n \cosh(n - \tfrac{1}{2})\eta + L_n \sinh(n - \tfrac{1}{2})\eta + M_n \cosh(n + \tfrac{3}{2})\eta + N_n \sinh(n + \tfrac{3}{2})\eta$$

$$V_n = P_{n-1}(\zeta) - P_{n+1}(\zeta)$$

Now, let us suppose that ψ represents the stream function for the lower fluid. Then the stream function for the upper fluid, $\hat{\psi}$, can be

in the same functional form with coefficients, $\hat{K}_n$, $\hat{L}_n$, $\hat{M}_n$ and $\hat{N}_n$. Applying the boundary conditions that were discussed in the previous section, we can evaluate the coefficients K_n, ..., N_n, $\hat{K}_n$, ..., $\hat{N}_n$ for translation of a sphere normal to a plane fluid/fluid interface. The viscosity ratio between two fluids is again denoted by λ and the sphere is located at $\eta = \eta_o$. The results are

$$K_n = - M_n = \lambda \hat{K}_n \tag{61}$$

$$\hat{K}_n = - \hat{L}_n = - \hat{M}_n = \hat{N}_n \tag{62}$$

$$K_n = \frac{\lambda}{2} \left[(n - \tfrac{1}{2}) L_n + (n + \tfrac{3}{2}) N_n \right] \tag{63}$$

$$L_n = (2n + 3) k_n \left[\frac{- (a_n + b_n) + (c_n + d_n)\lambda + (2n - 1)(2n + 1)\sinh^2 \eta_o}{b_n - \lambda d_n} \right] \tag{64}$$

$$N_n = (2n - 1) k_n \left[\frac{(a_n + b_n) - (c_n + d_n)\lambda - (2n + 1)(2n + 3)\sinh^2 \eta_o}{b_n - \lambda d_n} \right] \tag{65}$$

Here,

$$k_n = \frac{n(n + 1)\sinh^2 \eta_o}{\sqrt{2}\,(2n - 1)(2n + 1)(2n + 3)}$$

$$a_n = (2n + 1)^2 \sinh^2 \eta_o + 4 \cosh^2 (n + \tfrac{1}{2}) \eta_o$$

$$b_n = 2 \sinh (2n + 1) \eta_o - (2n + 1) \sinh 2\eta_o$$

$$c_n = 2 \sinh (2n + 1) \eta_o + (2n + 1) \sinh 2\eta_o$$

$$d_n = 4 \sinh^2 (n + \tfrac{1}{2}) \eta_o - (2n + 1)^2 \sinh \eta_o$$

The drag force on the sphere can be easily derived (cf. Stimson and Jeffery 1926).

$$F_z = \frac{\sqrt{2}}{3} \operatorname{cosech} \eta_o \sum_n (K_n + L_n + M_n + N_n)$$

$$= \frac{4\sqrt{2}}{3} \operatorname{cosech} \eta_o \sum_n k_n \left[\frac{-a_n + \lambda c_n}{b_n - \lambda d_n} - 1 \right] \qquad (66)$$

Equation (66) is given by Bart (1968).

4. TRANSLATION AND/OR ROTATION OF A RIGID SPHERE IN A QUIESCENT FLUID NEAR A PLANE FLUID INTERFACE

Let us now consider the specific problem of a rigid sphere which is translating or rotating in a quiescent fluid near a plane fluid/fluid interface. This problem may be solved directly, for an arbitrary direction of translation or rotation, using the methods outlined in section 2. All that is required is a specification of the surface velocity of the sphere in terms of bipolar eigensolutions; namely, the coefficients X_n^m, Y_n^m and Z_n^m in (48) - (50), and solution of the resulting algebraic relationships. Due to the linearity of Stokes' equation and boundary conditions in the case of a flat interface, however, the velocity and pressure fields generated by any arbitrary motion of the sphere can be obtained by superposing the fields associated with only four fundamental modes of sphere motion; namely, translation perpendicular and parallel to the interface, and rotation (with the axis of rotation) perpendicular and parallel to the interface. Indeed, we have shown in part I how the force and torque on the particle can be related to the translational and angular velocities of the particle via three independent second-order resistance tensors whose components can be determined completely by considering the same set of flows. In the present section,

we therefore consider the application of general techniques and solution of section 2 to obtain exact solutions for the four fundamental problems mentioned above. We will consider both the detailed pressure and velocity fields, and the hydrodynamic force and torque on the sphere. As indicated in the introduction to this paper, we shall be particularly concerned with the comparison between the exact results obtained here, and the asymptotic results of part I.

We assume, in the following, that the sphere is centered at $z = -\ell$ (note that $\ell = 1$ corresponds to the sphere just touching the interface). Thus, the sphere surface is represented by $\eta = \eta_0 = -\cosh^{-1}\ell$, and the constant c in the coordinate transformation, equation (5), is given as $c = (\ell^2 - 1)^{\frac{1}{2}}$. The hydrodynamic force and torque on the particle can be calculated directly from the stress at the particle surface

$$\underline{F} = \iint d\underline{s}\cdot\underline{\underline{t}} \tag{67}$$

$$\underline{T} = \iint \underline{r} \times (d\underline{s}\cdot\underline{\underline{t}}) \tag{68}$$

Here, $\underline{\underline{t}}$ is the stress tensor, and $\underline{r}$ is the position vector of a surface element relative to the sphere center. The drag force and hydrodynamic torque may be non-dimensionalized with respect to $F_c = 6\pi\mu aV$ (or $6\pi\mu a^2\Omega$) and $T_c = 8\pi\mu a^2V$ (or $8\pi\mu a^3\Omega$), where V and Ω represent the magnitudes of the translational and rotational velocity, respectively. In the following discussion, we shall refer to the force for translation and the torque for rotation, non-dimensionalized in this fashion, as the drag ratio and the torque ratio, respectively, since they are scaled with the force and torque which would act on the sphere in an infinite fluid.

a. Boundary Conditions for the Four Fundamental Problems

Let us now turn to the specific boundary conditions, as well as formulae for the (non-dimensionalized) hydrodynamic force and/or torque on the sphere for the four fundamental modes of particle motion.

case i) Translation of a non-rotating sphere perpendicular to a plane interface.

First, we consider the translation of a non-rotating rigid sphere perpendicular to the plane fluid interface. In view of the axisymmetric nature of the problem, it is clear that the solution must be independent of the azimuthal angle, ϕ, so that the only non-zero coefficients in the general solution of section 2 are those with $m = 0$. In addition, $\alpha_o = 0$.

The remaining constants can be determined from the prescribed velocity of the sphere

$$u_s = v_s = 0, \quad w_s = 1 \qquad \text{on} \qquad \eta = \eta_o. \tag{69}$$

Expanding $w_s = 1$ in the form (50), the constants X_n^o, Y_n^o and Z_n^o, which appear in (54) - (56), are easily seen to be

$$\begin{aligned} X_n^o &= Y_n^o = 0 \\ Z_n^o &= \sqrt{2}\, e^{(n+\frac{1}{2})\eta_o} \end{aligned} \tag{70}$$

The constants A_n^o, B_n^o, ..., $\hat{H}_n^o$ can thus be evaluated in the manner outlined in section 2b.

It can be shown, after a tedious algebraic manipulation (cf. Dean and O'Neill 1963) starting from equation (67), that

$$F_x = F_y = 0$$

$$F_z = -\frac{\sqrt{2}}{3} \sinh \eta_o \sum_n \left[C_n^o - (n + \tfrac{1}{2})(A_n^o - B_n^o)\right] , \tag{71}$$

while the torque is identically zero

$$\underline{T} = \underline{0} \tag{72}$$

as expected.

case ii) Translation of a non-rotating sphere parallel to a plane interface.

We now turn to the problem of a sphere translating in the $\underline{i}_x$ direction. In this case, all terms in the general solution of section 2 vanish except for those with m = 1, and $\alpha_1 \equiv 0$. On the sphere surface,

$$u_s = \cos \phi, \quad v_s = - \sin \phi, \quad \text{and} \quad w_s = 0 \tag{73}$$

In consequence, X_n^1, Y_n^1 and Z_n^1 are

$$\left.\begin{aligned} X_n^1 = Z_n^1 = 0 \\ Y_n^1 = 2\sqrt{2}\, e^{(n+\frac{1}{2})\eta_o} \end{aligned}\right\} \tag{74}$$

and the unknown coefficients can be determined as described above.

The drag force and hydrodynamic torque, in this case, are related to these constant coefficients by means of the formulae (cf. O'Neill 1964)

$$F_y = F_z = 0$$

$$F_x = \frac{-\sqrt{2}}{6} \sinh \eta_o \sum_n \left[G_n^1 - H_n^1 + n(n + 1)(A_n^1 - B_n^1)\right] \tag{75}$$

and

$$
\left.
\begin{aligned}
T_x &= T_z = 0 \\
T_y &= \frac{\sinh^2 \eta_o}{12\sqrt{2}} \sum_n \Big[\Big(2 + e^{(2n+1)\eta_o}\Big) \Big\{ n(n+1) \Big(-2C_n^1 - A_n^1 \coth \eta_o \Big) \\
&\quad - (2n + 1 + \coth \eta_o) G_n^1 \Big\} + \Big(2 - e^{(2n+1)\eta_o}\Big) \Big\{ n(n+1) B_n^1 \coth \eta_o \\
&\quad + (2n + 1 + \coth \eta_o) H_n^1 \Big\} \Big] .
\end{aligned}
\right\} \quad (76)
$$

case iii) Rotation of a sphere normal to a plane interface.

The third problem which we consider is the rotation of a sphere with the axis of rotation normal to a plane interface. In the general solution of Stokes' equation, the non-zero terms in this case are for m = 0 and $\alpha_o = \pi/2$. Moreover, p, u and w are identically zero, as is obvious from the symmetry of the problem. We can thus calculate the coefficients for v analytically, rather than numerically. From equations (32), (41a) and (57),

$$\hat{G}_n^o = - \hat{H}_n^o , \quad H_n^o = \hat{H}_n^o , \quad \text{and} \quad G_n^o = \lambda \hat{G}_n^o \qquad (77)$$

The boundary condition on the sphere surface is

$$v_s = r \qquad \text{on} \qquad \eta = \eta_o \qquad (78)$$

Therefore, from equations (47b) and (49a), it can be shown that Y_n^o takes the value

$$Y_n^o = 2\sqrt{2}\, c\, e^{(n+\frac{1}{2})\eta_o} . \qquad (79)$$

The constants G_n^o and H_n^o can then be obtained from equations (55a), (77) and (79)

$$G_n^o = \frac{2\sqrt{2}\, c\, \lambda\, e^{(n+\frac{1}{2})\eta_o}}{\lambda \sinh(n+\frac{1}{2})\eta_o - \cosh(n+\frac{1}{2})\eta_o} \tag{80}$$

$$H_n^o = -\frac{1}{\lambda} G_n^o \quad . \tag{81}$$

The remaining non-zero constants follow from (77). It may be seen from (67) that the drag force is identically zero.

$$\underline{F} = \underline{0} \tag{82}$$

while the hydrodynamic torque (cf. Jeffery 1915) is

$$\left.\begin{aligned} T_x &= T_y = 0 \\ T_z &= \frac{\sinh^2 \eta_o}{\sqrt{2}} \sum_n n(n+1)(-G_n^o + H_n^o) \end{aligned}\right\} \tag{83}$$

case iv) Rotation of a sphere parallel to a plane interface.

Finally, let us consider a rotating sphere whose rotation axis is parallel to the y-axis. The boundary conditions on the sphere surface in this case are

$$u_s = (z+\ell)\cos\phi, \quad v_s = -(z+\ell)\sin\phi, \text{ and } w_s = -r\cos\phi \tag{84}$$

Thus, the non-zero terms in the general solution are only those for m = 1 and $\alpha_1 = 0$. X_n^1, Y_n^1 and Z_n^1 can be evaluated from the equations (84), (48b), (49b) and (50).

$$\left.\begin{aligned} X_n^1 &= 0 \\ Y_n^1 &= -2\sqrt{2}\, c(2n+1+\coth\eta_o) e^{(n+\frac{1}{2})\eta_o} \\ Z_n^1 &= -2\sqrt{2}\, c\, e^{(n+\frac{1}{2})\eta_o} \end{aligned}\right\} \tag{85}$$

The drag force and hydrodynamic torque are calculated from the equations (67) and (68) (cf. Dean and O'Neill 1963).

$$\left.\begin{aligned} F_x &= \frac{-\sqrt{2}}{6} \sinh \eta_o \sum_n \left[G_n^1 - H_n^1 + n(n+1)(A_n^1 - B_n^1)\right] \\ F_y &= F_z = 0 \end{aligned}\right\} \tag{86}$$

$$\left.\begin{aligned} T_x &= T_z = 0 \\ T_y &= -\frac{1}{3} - \frac{\sinh^2 \eta_o}{12\sqrt{2}} \sum_n \left[\left(2 + e^{(2n+1)\eta_o}\right)\left\{n(n+1)\left(-2C_n^1 - A_n^1 \coth \eta_o\right)\right.\right. \\ &\quad \left.\left. - (2n + 1 + \coth \eta_o)G_n^1\right\} + \left(2 - e^{(2n+1)\eta_o}\right) \right. \\ &\quad \left. \cdot \left\{n(n+1)B_n^1 \coth \eta_o + (2n + 1 + \coth \eta_o)H_n^1\right\}\right] \end{aligned}\right\} \tag{87}$$

b. Numerical Results and Discussion

In the preceding part of this section, we have derived formulae from which the velocity fields, and the hydrodynamic force and torque on the sphere, can be calculated for the four fundamental modes of motion of a sphere near a flat fluid interface; namely, translation perpendicular and parallel to the interface, and rotation with the axis of rotation parallel and perpendicular to the interface. With the exception of the last problem, which was solved analytically, the unknown coefficients in the general solution for the two fluids must be obtained, in principle, via a numerical solution of the infinite set of governing algebraic equations that were outlined earlier. From equations (70), (74), (79) and (85), however, it is evident that the coefficients for large n will decrease in magnitude as $e^{(n+\frac{1}{2})\eta_o}$, where $\eta_o = -\cosh^{-1} \ell$. Thus, when $\ell >> 1$, the coefficients decrease quickly (exponentially) in magnitude as the index n is increased. In this case, a very good approximation can be obtained by truncating the

solution series for "large" n. The resulting set of equations is finite and banded, and can be solved very efficiently using standard Gaussian elimination schemes for band matrices. However, as $\ell \to 1$, the rate of decrease of the coefficients with increasing n becomes slower, and it is necessary to include increasing numbers of terms (i.e. larger values of n) in order to give the same numerical accuracy in the results. Since the coefficients decrease monotonically with increase of n (for any fixed value of ℓ) after the first few terms, it is relatively easy to estimate the numerical magnitude of the error which is caused by truncation. The numerical error in the calculation of coefficients due to the truncation of terms with $n > n_{max}$ is analyzed in the appendix. Once we calculate the coefficients, we can evaluate the contribution to the drag force and hydrodynamic torque from the terms in the series for each n. The magnitude of these terms becomes approximately a geomtrical series for large n. Thus, we can easily estimate the numerical magnitude of error in the calculated values of drag force and hydrodynamic torque due to truncation. To limit the maximum relative error in the computed results for the drag force and hydrodynamic torque to values less than 5×10^{-7}. we used $n_{max} = 10$ for $\ell \geq 3.0$, $n_{max} = 15$ for $3.0 > \ell \geq 1.8$, $n_{max} = 25$ for $1.8 > \ell \geq 1.2$ and $n_{max} = 30$ for $1.2 > \ell \geq 1.1$.

In the remainder of this section, we will present and discuss the results calculated for the velocity and pressure fields, as well as for the drag and torque ratios for the four problems listed above. Particularly significant is the resulting comparison of the present "exact" solutions with the approximate solutions for $\ell >> 1$ which were obtained in part I of this work (Lee, Chadwick and Leal 1979). When the sphere

is very close to the interface, on the other hand, so that $\ell - 1 \ll 1$, lubrication theory can be applied, in principle, to obtain asymptotic solutions. Indeed, Goldman, Cox and Brenner (1967) used this technique to study the translation and rotation of a sphere near a plane solid wall. However, they found that the lubrication-theory results for force and/or torque were quite poor when compared with the numerically exact results of Dean and O'Neill (1963) and O'Neill (1964). An explanation for this discrepancy was given by O'Neill and Stewartson (1967), who independently investigated the translation of a sphere parallel to a plane solid wall, using lubrication theory. These authors showed that lubrication theory does provide an accurate description of local flow properties, but that it cannot be used (without extension) for prediction of properties of the overall flow, such as force or torque, with any degree of reliability if the flow domain includes substantial regions of weakly sheared flow away from the lubrication gap. Although O'Neill and Stewartson were eventually able to obtain successful asymptotic results for $(\ell - 1) \ll 1$, the analysis required an elaborate matching procedure to generate a solution in the "outer" region away from the gap. No such study has yet been completed for analyzing the motion of a particle which is very close to a fluid/fluid interface. Therefore, at the present time, the only results available for $(\ell - 1) \ll 1$ which could be compared with the exact solutions of this paper are for the case of solid wall, i.e. $\lambda = \infty$. Such a comparison has already been reported by O'Neill and Stewartson (1967) using the results of O'Neill (1964), and will thus not be repeated here.

We begin, in table 1, with the drag ratio for translation perpendicular to the plane interface calculated by means of our general solution technique. This same quantity was previously calculated by Bart (1968) using the stream function formulation which was discussed in section 3, and was also recalculated by us using this latter approach. Our calculations using the stream function expansion agreed exactly with the results of Bart (1968) when compared at the same value of ℓ (it may be noted here that Bart used incremental values of η_0 and thus obtained different values of ℓ from those listed in table 1). Further, the results calculated via the general solution were found to agree exactly with the values obtained by the stream function expansion. In figure 2, the "exact" drag ratios obtained in the present work are compared, for $\lambda = 0$, 1 and ∞, with these obtained using the approximate method of part I. Both results show that the drag ratio increases rapidly as the sphere approaches the interface, for all λ, due to the assumption of a flat interface. However, the drag ratio obtained in part I does not increase as fast as the exact result in the limit as ℓ approaches unity; i.e. as the sphere approaches the plane interface. The drag ratio from the "exact" solution is, in fact, unbounded as $\ell \to 1$. The approximate expansion, on the other hand, has ℓ^{-1} as the "small" parameter and is, therefore, strictly valid only when the sphere is far from the interface. In fact, the approximate solution including terms through $O(\ell^{-2})$ is seen, from figure 2, to represent the drag ratio to within 10% for ℓ as small as 2. It cannot under any circumstances exhibit the singular behavior of the exact solution for $\ell \to 1$. Nevertheless, the approximate solution does give a remarkably accurate representation of the <u>exact</u> result, over almost the whole range

of possible sphere positions. This is important, as suggested in the Introduction, because it is the approximate solution scheme which can be generalized to other particle shapes which may be important in applications. The eigensolution expansion is useful for general motions only for the case of a sphere which is considered here.

For the case of a sphere translating, without rotation, parallel to the interface, we have numerically evaluated the drag ratio, as well as the hydrodynamic torque on the sphere. The latter is equal in magnitude but opposite in sense to the torque which must be applied to the particle by external means to keep it from rotating. The drag ratio is given as a function of the position of the sphere in table 2. Examination shows that the drag actually decreases relative to Stokes' drag for an unbounded fluid for $\lambda = 0$ and 0.1. On the other hand, for the larger values of $\lambda = 1$, 10 and ∞, the drag increases relative to that in unbounded fluid as the sphere comes closer to the interface, at a rate which increases with increasing λ. These results are in qualitative accord with the asymptotic solution, as may be seen in figure 3. Indeed, in this case, the asymptotic and "exact" predictions for the drag ratio agree within 5% up to $\ell = 1.1$ for $\lambda = 0$ and $\lambda = 1$, and to $\ell \sim 1.8$ for $\lambda = \infty$. The somewhat poorer performance of the asymptotic solution in the latter case is again a reflection of the fact that the exact result for the drag ratio is unbounded in the limit $\ell \to 1$. The hydrodynamic torque which acts on the translating particle was also calculated as a function of λ and ℓ, and the detailed numerical results are shown in table 3. In addition, the numerical results for $\lambda = 0$, 1 and ∞ are compared with the approximate solution in figure 4. There is reasonable qualitative agreement between

$\ell > 1.1$ for $\lambda = 0$ and $\lambda = 1$. For $\lambda = \infty$, on the other hand, the asymptotic prediction, to $O(\ell^{-2})$, is that the torque is identically equal to zero, while the exact numerical result shows a rapid increase in the magnitude of the torque as the sphere approaches the interface. The asymptotic result is consistent with the analysis of Faxen (1921) who found that the leading contribution to the torque for a plane solid wall is $O(\ell^{-4})$. The exact solution shows that the torque for $\lambda = \infty$ only becomes significant for $\ell < \sim 2.5$, whereas the torque for the smaller values of λ is noticeable for $\ell \sim 6 - 7$, and these observations are again consistent with the wall effect being a higher order contribution in the asymptotic framework of part I. The fact that this wall contribution becomes large as $\ell \to 1$ serves as a reminder that higher order terms in the asymptotic expansion of part I do not necessarily remain small when the expansion is pushed beyond its natural range of applicability.

It will be noted, either from table 3 or figure 4, that the torque has a different sign in the limit of a solid wall ($\lambda = \infty$), than it does for a free interface ($\lambda = 0$). In the former case, the sphere would rotate, in the absence of an applied torque, in a direction consistent with "rolling" along the wall. For the free surface, on the other hand, the sphere is predicted to rotate in the opposite direction. Moreover, it may be seen from table 3 that the torque actually changes sign for intermediate λ as the sphere comes from a large distance inward toward the interface. The sense of the induced (hydrodynamic) torque in the "rolling" mode is established primarily as a consequence of the fact that a much more viscous fluid above the interface yields a small slip

velocity on the interface and thus higher velocity gradients above the sphere than below it. The "reversal" in the induced torque when the upper fluid is much less viscous than the lower fluid results primarily from the existence of a substantial slip velocity on the interface, and a resultant velocity gradient above the sphere which is smaller than below. The fact that the interface remains flat in the present theory, does not play a critical role in this aspect of the parallel translation problem. A more detailed examination of the sense of the induced torque, or, equivalently, of the direction of the rotation which would occur in the absence of an applied torque, is presented in figure 5. Here, we have plotted the position of the sphere center where the induced hydrodynamic torque is identically zero, as a function of the viscosity ratio, λ. As λ increases, we see that the location of this point moves further from the interface. The fact that $\lambda_{crit} \to \sim 6$, as $\ell \to 1$ is somewhat surprising, and not easily explainable.

The problem of a rotating sphere whose rotation axis is normal to the interface is, as previously mentioned, easy to analyze because there is only one non-zero velocity component, v, which is parallel to the flat interface. Since the condition of zero normal velocity at the interface is satisfied identically in this case, the velocity field and the torque required to rotate the sphere will only differ from the case of rotation in a single unbounded fluid if the viscosities of the two fluids are not equal, i.e. if $\lambda \neq 1$. Furthermore, it is evident that the torque ratio must be larger than 1 if $\lambda > 1$, and smaller than 1 if $\lambda < 1$. In table 4, the torque ratios are tabulated for various values of λ and, in figure 6, they are compared with the results which were obtained via the approximate

solution in part I. The approximate solution agrees extremely well with the exact solution for the whole range of ℓ down to $\ell \sim 1.1$. Apparently, the higher-order terms in the approximate solution are insignificant insofar as the torque on the sphere is concerned.

Finally, we consider the results for rotation when the axis of rotation is parallel to the interface. The hydrodynamic torque ratio for this case is given in table 5. According to the asymptotic theory from part I, which was carried out to terms of $O(\ell^{-3})$, the torque ratio should exceed one when $\lambda > 1/5$ and fall below one for $\lambda < 1/5$. This result is, of course, based on only the first term of the asymptotic expansion and the latter is only valid for large ℓ. Indeed, the torque ratio calculated numerically was found to be 1.00000 when $\ell = 10$ and $\lambda = 1/5$. As the particle is placed closer to the interface, however, the torque ratio is found to eventually exceed unity even for $\lambda = 0$, although the critical value of ℓ where this occurs is seen to <u>decrease</u> as λ is decreased (i.e. to occur when the sphere is closer to the interface). In figure 7, the numerically evaluated torque ratio from this study is plotted together with the approximate (asymptotic) solution of part I. For $\ell >> 1$, the two solutions are in excellent agreement. However, at $\ell \sim 2$, the two solutions diverge, especially for the case $\lambda = 0$ where the asymptotic result continues to decrease below unity while the exact solution first decreases for large ℓ, but then increases sharply as $\ell \to 1$. As before, this latter behavior may correspond to higher-order terms in the asymptotic solution, but there is no <u>guarantee</u> that it should necessarily appear at all in an expansion which is only valid for $\ell >> 1$. There is also a non-zero drag force generated in this problem, which is equal in magnitude

but opposite in direction to the force that would have to be applied to the sphere to keep it from translating parallel to the interface (cf. Brenner 1964). However, the details of this force need not be reported here as it can be calculated directly from the torque which acts on a sphere that is translating parallel to the interface (table 3). Indeed, we have noted in equations (82) and (83) of part I that the coupling tensor which relates the force on a rotating sphere to its angular velocity should be anti-symmetric and the transpose of the coupling tensor relates the torque on a translating sphere to its translational velocity. This reciprocal relationship between the translational and rotational problems was satisfied by the numerical results for the two problems in our present study. It should be mentioned here that the calculation of Dean and O'Neill (1963) was numerically erroneous (cf. Goldman, Cox and Brenner 1967) and, thus, does not agree with our results for $\lambda = \infty$.

The fact that exact results are available for the force and/or torque provides an opportunity to see whether the asymptotic results of part I can be improved at all. Specifically, the force and torque were found in part I to be related solely to the Stokeslet and rotlet strengths, and these appear to be geometric series to the level of approximation which was analyzed in part I. Since these geometric series are easily summed, it is possible that improved results for the force and torque could be obtained for $\ell \sim O(1)$. Obviously, there is no guarantee that additional contributions may not occur at higher orders in ℓ^{-1} which would invalidate the simple geometric form which is assumed for the series in this summing process. However, we believe that it is of interest to investigate the

comparison between the exact results obtained above, and the "summed" approximate results from part I. For the four fundamental motions of a sphere, we have compared this newly suggested approximate solution, as well as the original solution of part I with the exact solutions in figures 2, 3, 6 and 7. There is no difference in the numerical accuracy of the two approximate results in the region of $\ell \gg 1$. However, for $\ell \sim 1$, the "summed" series shows somewhat improved comparison with the exact solution for most cases relative to the original solution of part I, though the results are still not quantitatively accurate. When the sphere is translating normal to the interface, for $\lambda = 1$, 10 and ∞, the "summed" series reveals a more rapid increase in the drag force than occurs in the exact solution as $\ell \to 1$. Since the summed series is of the form $(1 - \alpha/\ell)^{-1}$, there is a singularity indicated for $\ell = \alpha$ rather than $\ell = 1$, as expected. This is, of course, both a consequence and an indication of the existence of higher-order terms in the exact solution which do not fit the geometric form which is suggested by the first few terms of the asymptotic series. The case $\lambda = 0$ of parallel rotation, which is poorly predicted by the original asymptotic series, is <u>not</u> significantly improved for the same reason. The same limit, $\lambda = 0$, for perpendicular translation, on the other hand, shows excellent agreement with the exact solution, suggesting the absence of higher-order terms of a fundamentally different nature for this particular limiting case.

Finally, in order to achieve a more complete understanding of the motion of a sphere in the presence of a plane interface, we have plotted pressure, velocity and vorticity fields for the translational motion of a sphere with $\lambda = 0.1$ and $\ell = 5$. When the sphere is moving normal to the interface, the flow field is axisymmetric. Thus, we show the stream

function in figure 8. The streamlines are obviously deflected due to the presence of the "impermeable" plane interface. The pressure field for this problem is illustrated in figure 9. Although the dynamic pressure is positive above the sphere and negative below the sphere as would also be true in an unbounded fluid, the plane interface clearly disrupts the fore-aft anti-symmetry of the pressure field about $z = -\ell$. The dynamic pressure in the upper fluid is negative, and there is a pressure jump across the interface due in part to the fact that it is specified as flat. In figures 10 and 11, the velocity components, u and w, are plotted, respectively. In addition, the vorticity, ω_ϕ, is plotted in figure 12. In these figures, it can be clearly seen that the presence of the impermeable interface suppresses the velocity component in the z-direction while it enhances the velocity component in the r-direction due to the small viscosity of the upper fluid. Thus, negative vorticity ω_ϕ is generated at the interface. However, as expected, strong positive vorticity ω_ϕ is generated at the sphere surface. Hence, in the lower fluid, there exists only a small region of negative vorticity ω_ϕ near the interface. Since the shear stress is continuous across the interface with $\lambda \neq 1$, there naturally occurs a vorticity jump across the interface.

We have also examined the flow field generated by a sphere which is moving parallel to a plane interface. We consider that the sphere is moving in x-direction. The pressure field is shown in figure 13. It is noted that in the lower fluid, positive dynamic pressure builds up in front of the sphere while negative dynamic pressure builds up behind the sphere. However, in the upper fluid, the pressure is negative for $x > 0$

and positive for $x < 0$. In figures 14 and 15, u_x on $y = 0$ and u_x on $x = 0$ are respectively plotted. These figures ostensibly show that the velocity gradient in the upper side of the sphere is smaller than that in the lower side of the sphere for this case of = 0.1. The velocity component w on $y = 0$ is depicted in figure 16. Although w is still anti-symmetric relative to $x = 0$, the anti-symmetry of w relative to $z = -\ell$ is disrupted due to the presence of the interface. Finally, ω_y is plotted in figure 17. For this case, the vorticity generated by the interface has the same sign as the vorticity generated by the upper side of the sphere. The anti-symmetry of ω_y with respect to $z = -\ell$ is distorted, and there is a jump in ω_y across the interface as expected.

References

Bart, E. 1968 The slow unsteady settling of a fluid sphere toward a flat fluid interface. Chem. Eng. Sci. 23, 193.

Brenner, H. 1964 The Stokes resistance of an arbitrary particle - II. An extension. Chem. Eng. Sci. 19, 599.

Dean, W. R. and O'Neill, M. E. 1963 A slow motion of viscous liquid caused by the rotation of a solid sphere. Mathematika 10, 13.

Faxen, H. 1921 Dissertation, Uppsala Univ.

Goldman, A. J., Cox, R. G. and Brenner, H. 1967 Slow viscous motion of a sphere parallel to a plane wall - I. Motion through a quiescent fluid. Chem. Eng. Sci. 22, 637.

Happel, J. and Brenner H. 1973 Low Reynolds Number Hydrodynamics. Noordhoff International Pub., Leyden, The Netherlands.

Jeffery , G. B. 1912 On a form of the solution of Laplace's equation suitable for problems relating to two spheres. Proc. Roy. Soc. A 87, 109.

Jeffery , G. B. 1915 On the steady rotation of a solid of revolution in a viscous fluid. London Math. Soc. 14, 327.

Lee, S. H., Chadwick, R. S. and Leal, L. G. 1979 Motion of a sphere in the presence of a plane interface. Part I. An approximate solution by generalization of the method of Lorentz. J. Fluid Mechanics 93, 705.

Lin, C. 1968 PhD Dissertation, Univ. of Washington.

Lorentz, H. A. 1907 A general theorem concerning the motion of a viscous fluid and a few consequences derived from it. Abhandl. Theoret. Phys. 1, 23.

O'Neill, M. E. 1964 A slow motion of viscous liquid caused by a slowly moving solid sphere. Mathematika 11, 67.

O'Neill, M. E. and Stewartson, K. 1967 On the slow motion of a sphere parallel to a nearby plane wall. J. Fluid Mech. 27, 705.

Stimson, M. and Jeffery, G. B. 1926 The motion of two spheres in a viscous fluid. Proc. Roy. Soc. A111, 110.

APPENDIX: Estimation of Numerical Errors in the Calculated Coefficients Due to the Truncation of Terms of Large n.

Let us express the linear equations for the system as

$$\underline{\underline{a}}_n \cdot \underline{x}_{n-1} + \underline{\underline{b}}_n \cdot \underline{x}_n + \underline{\underline{c}}_n \cdot \underline{x}_{n+1} = \underline{d}_n \qquad \text{for } n = 1, 2, \ldots \tag{A1}$$

We define the ratio tensor for $\underline{x}_n$, $\underline{\underline{\alpha}}_n$ (a diagonal tensor), as

$$\underline{x}_{n+1} = \underline{\underline{\alpha}}_n \cdot \underline{x}_n \tag{A2}$$

Then the equation (A1) can be written as

$$\underline{x}_n = \left[\underline{\underline{a}}_n \cdot \underline{\underline{\alpha}}_{n-1}^{-1} + \underline{\underline{b}}_n + \underline{\underline{c}}_n \cdot \underline{\underline{\alpha}}_n \right]^{-1} \cdot \underline{d}_n \tag{A3}$$

When we truncate $\underline{x}_n$ for $n > N$, the equation (A1) becomes

$$\underline{\underline{a}}_n \cdot \hat{\underline{x}}_{n-1} + \underline{\underline{b}}_n \cdot \hat{\underline{x}}_n + \underline{\underline{c}}_n \cdot \hat{\underline{x}}_{n+1} = \underline{d}_n \quad \text{for} \quad n=1,2\ldots,N-1 \tag{A4}$$

and

$$\underline{\underline{a}}_N \cdot \hat{\underline{x}}_{N-1} + \underline{\underline{b}}_N \cdot \hat{\underline{x}}_N = \underline{d}_N \quad \text{for} \quad n=N \tag{A5}$$

Here, $\hat{\underline{x}}_i$ is the calculated $\underline{x}_i$ after truncating $\underline{x}_n$ for $n > N$. Subtracting (A1) from (A4) and (A5) yields

$$\underline{\underline{a}}_N \cdot \underline{E}_{n-1} + \underline{\underline{b}}_n \cdot \underline{E}_n + \underline{\underline{c}}_n \cdot \underline{E}_{n+1} = \underline{0} \quad \text{for} \quad n=1,2,\ldots,N-1 \tag{A6}$$

$$\underline{\underline{a}}_N \cdot \underline{E}_{N-1} + \underline{\underline{b}}_N \cdot \underline{E}_N = \underline{\underline{c}}_N \cdot \left[\underline{\underline{a}}_{N+i} \underline{\underline{\alpha}}_N^{-1} + \underline{\underline{b}}_{N+1} + \underline{\underline{c}}_{N+1} \cdot \underline{\underline{\alpha}}_{N+1} \right]^{-1} \cdot \underline{d}_{N+1}$$

$$\text{for} \quad n=N \tag{A7}$$

where $\underline{E}_n \equiv \hat{\underline{x}}_n - \underline{x}_n$.

Let us define the ratio tensor for $\underline{E}_n$ as

$$\underline{E}_{n+1} = \underline{\underline{\beta}}_n \cdot \underline{E}_n \tag{A8}$$

Then the error in $\hat{\underline{x}}_n$ can be simply written as

$$\underline{E}_n = \hat{\underline{x}}_n - \underline{x}_n = \left\{ \prod_{i=N-1}^{n} - \left[\underline{\underline{a}}_i \cdot \underline{\underline{\beta}}_{i-1}^{-1} + \underline{\underline{b}}_i \right]^{-1} \cdot \underline{\underline{c}}_i \cdot \right\} \left[\underline{\underline{a}}_N \cdot \underline{\underline{\beta}}_{N-1}^{-1} + \underline{\underline{b}}_N \right]^{-1} \cdot$$

$$\underline{\underline{c}}_N \cdot \left[\underline{\underline{a}}_{N+1} \cdot \underline{\underline{\alpha}}_N^{-1} + \underline{\underline{b}}_{N+1} + \underline{\underline{c}}_{N+1} \cdot \underline{\underline{\alpha}}_{N+1} \right]^{-1} \cdot \underline{d}_{N+1} \tag{A9}$$

For simplicity, let us assume $\underline{\underline{\alpha}}_i \sim \alpha_i \underline{\underline{I}}$ and $\underline{\underline{\beta}}_i \sim \beta_i \underline{\underline{I}}$. Then, since $|\underline{\underline{a}}_i|$, $|\underline{\underline{c}}_i| \sim \frac{1}{2} |\underline{\underline{b}}_i| \sim O(1)$ for large i, the maximum component of $\underline{E}_n$ is

$$|\underline{E}_n|_\infty \sim \left[\prod_{i=N-1}^{n} \frac{1}{\frac{1}{\beta_{i-1}} + 2} \right] \frac{|\underline{d}_{N+1}|_\infty}{\left(2 + \frac{1}{\beta_{N-1}}\right)\left(2 + \frac{1}{\alpha_N} + \alpha_{N+1}\right)} \tag{A10}$$

Equation (A10) clearly shows that the truncation error in $\hat{\underline{x}}_n$ which is proportional to $|\underline{d}_{N+1}|_\infty$ becomes smaller as n decreases.

Table 1. Drag Ratio for a Sphere Translating Perpendicular to a Plane Interface.

ℓ/λ	0.	0.1	1.	10.	∞
10.	1.08096	1.08492	1.10311	1.12193	1.12619
5.	1.17560	1.18477	1.22788	1.27429	1.28509
3.	1.33015	1.34875	1.43954	1.54387	1.56921
2.	1.59668	1.63314	1.82163	2.06257	2.12554
1.8	1.71575	1.76053	1.99726	2.31347	2.39877
1.6	1.90031	1.95812	2.27341	2.72202	2.84891
1.4	2.23492	2.31625	2.78090	3.51180	3.73562
1.2	3.10459	3.24343	4.10294	5.74513	6.34089
1.1	4.62554	4.85033	6.34941	9.88127	11.45916

Table 2. Drag Ratio for a Sphere Translating Parallel to a Plane Interface.

ℓ/λ	0.	0.1	1.	10.	∞
10.	0.963802	0.971778	1.00937	1.05000	1.05948
5.	0.929866	0.944792	1.01843	1.10466	1.12586
3.	0.887536	0.910258	1.02935	1.18558	1.22716
2.	0.838826	0.869082	1.04038	1.30374	1.38275
1.8	0.823629	0.855875	1.04331	1.34899	1.44521
1.6	0.805414	0.839792	1.04641	1.41140	1.53438
1.4	0.783367	0.819922	1.04946	1.50476	1.67553
1.2	0.756617	0.795140	1.05172	1.66838	1.95271
1.1	0.741287	0.780568	1.05191	1.82067	2.26430

Table 3. Hydrodynamic Torque, T_y $[8\pi\mu Va^2]$ on a Sphere Translating Parallel to a Plane Interface.

ℓ/λ	0.	0.1	1.	10.	∞
10.	1.80701×10^{-3}	1.65564×10^{-3}	9.42116×10^{-4}	1.70909×10^{-4}	-9.01197×10^{-6}
5.	6.97030×10^{-3}	6.42965×10^{-3}	3.76051×10^{-3}	6.31416×10^{-4}	-1.38502×10^{-4}
3.	1.84409×10^{-2}	1.71498×10^{-2}	1.03518×10^{-2}	1.37629×10^{-3}	-1.02023×10^{-3}
2.	3.89104×10^{-2}	3.65666×10^{-2}	2.29995×10^{-2}	1.51380×10^{-3}	-5.02471×10^{-3}
1.8	4.69457×10^{-2}	4.42916×10^{-2}	2.83220×10^{-2}	1.07144×10^{-3}	-7.68745×10^{-3}
1.6	5.76360×10^{-2}	5.46761×10^{-2}	3.58197×10^{-2}	-5.26852×10^{-3}	-1.25431×10^{-2}
1.4	7.21370×10^{-2}	6.90015×10^{-2}	4.70316×10^{-2}	-2.83454×10^{-3}	-2.26136×10^{-2}
1.2	9.20012×10^{-2}	8.92500×10^{-2}	6.56741×10^{-2}	-1.04024×10^{-2}	-4.96377×10^{-2}
1.1	1.04431×10^{-1}	1.02479×10^{-1}	8.11697×10^{-2}	-1.92084×10^{-2}	-8.87633×10^{-2}

Table 4. Torque Ratio for a Rotating Sphere When the Axis of Rotation is Normal to a Plane Interface.

ℓ/λ	0.	0.1	1.	10.	∞
10.	0.999875	0.999898	1.00000	1.00010	1.00013
5.	0.999001	0.999183	1.00000	1.00082	1.00100
3.	0.995394	0.996228	1.00000	1.00380	1.00465
2.	0.984666	0.987411	1.00000	1.01299	1.01593
1.8	0.979135	0.982846	1.00000	1.01794	1.02203
1.6	0.970698	0.975851	1.00000	1.02585	1.03184
1.4	0.957358	0.964702	1.00000	1.03950	1.04893
1.2	0.935753	0.946358	1.00000	1.06624	1.08322
1.1	0.920464	0.933118	1.00000	1.09149	1.11707

Table 5. Torque Ratio for a Rotating Sphere When the Axis of Rotation is Parallel to a Plane Interface.

ℓ/λ	0.	0.1	1.	10.	∞
10.	0.999942	0.999975	1.00013	1.00028	1.00031
5.	0.999574	0.999835	1.00102	1.00224	1.00251
3.	0.998289	0.999466	1.00487	1.01051	1.01180
2.	0.995768	0.999598	1.01758	1.03714	1.04178
1.8	0.995174	1.00036	1.02495	1.05230	1.05892
1.6	0.995321	1.00256	1.03751	1.07781	1.08785
1.4	0.998923	1.00942	1.06174	1.12603	1.14295
1.2	1.02046	1.03643	1.12127	1.24091	1.27664
1.1	1.06555	1.08590	1.20075	1.38898	1.45485

Figure Captions

Figure 1 Bipolar Coordinates (η,ξ,ϕ).

Figure 2 Drag ratio for the translation of a sphere perpendicular to a plane interface; ——: exact solution, --- : approximate solution, ■■■ : summed series.

Figure 3 Drag ratio for the translation of a sphere parallel to a plane interface; —— : exact solution, --- : approximate solution, ■■■ : summed series.

Figure 4 Hydrodynamic torque $[8\pi\mu Va^2]$ on a sphere translating parallel to a plane interface; —— : exact solution, --- : approximate solution.

Figure 5 The location of sphere center where $T_y = 0$ for translation of a sphere parallel to a plane interface.

Figure 6 Torque ratio for the rotation of a sphere when the axis of rotation is perpendicular to a plane interface; —— : exact solution, --- : approximate solution, ■■■ : summed series.

Figure 7 Torque ratio for the rotation of a sphere when the axis of rotation is parallel to a plane interface; —— : exact solution, --- : approximate solution, ■■■ : summed series.

Figure 8 Stream function $[U_c L_c]$ for the translation of a sphere perpendicular to a plane interface ($\lambda = 0.1$, $\ell = 5$ and $\underline{u}_s = \underline{i}_z$); A = 0.6, B = 0.4, C = 0.2, D = 0.0, E = -0.2, F = -0.4, G = -0.6, H = -0.8, I = -1.0, J = -1.4, K = -1.8, L = -2.2

Figure 9 Pressure [$\mu U_c/L_c$ for $z < 0$, $\hat{\mu} U_c/L_c$ for $z > 0$] for the translation of a sphere perpendicular to a plane interface ($\lambda = 0.1$, $\ell = 5$ and $\underline{u}_s = \underline{i}_z$);
A = 1.0, B = 0.6, C = 0.4, D = 0.2, E = 0.1, F = 0.05,
G = 0.0, H = -0.05, I = -0.1, J = -0.2, K = -0.4, L = -0.6

Figure 10 $u_r[U_c]$ for the translation of a sphere perpendicular to a plane interface ($\lambda = 0.1$, $\ell = 5$ and $\underline{u}_s = \underline{i}_z$);
A = 0.15, B = 0.12, C = 0.09, D = 0.06, E = 0.03, F = 0.0,
G = -0.03, H = -0.06, I = -0.09, J = -0.12

Figure 11 $u_z[U_c]$ for the translation of a sphere perpendicular to a plane interface ($\lambda = 0.1$, $\ell = 5$ and $\underline{u}_s = \underline{i}_z$);
A = 0.8, B = 0.6, C = 0.4, D = 0.3, E = 0.2, F = 0.1, G = 0.0,
H = -0.03, I = -0.06, J = -0.09

Figure 12 $\omega_\phi[U_c/L_c]$ for the translation of a sphere perpendicular to a plane interface ($\lambda = 0.1$, $\ell = 5$ and $\underline{u}_s = \underline{i}_z$);
A = 0.8, B = 0.4, C = 0.2, D = 0.1, E = 0.05, F = 0.025,
G = 0.0, H = -0.01, I = -0.03, J = -0.05

Figure 13 Pressure [$\mu U_c/L_c$ for $z < 0$, $\hat{\mu} U_c/L_c$ for $z > 0$] on $y = 0$ for the translation of a sphere parallel to a plane interface ($\lambda = 0.1$, $\ell = 5$ and $\underline{u}_s = \underline{i}_x$);
A = 3.0, B = -3.0, C = 2.0, D = -2.0, E = 1.0, F = -1.0,
G = 0.5, H = -0.5, I = 0.25, J = -0.25, K = 0.1, L = -0.1,
M = 0.05, N = -0.05, O = 0.01, P = -0.01

Figure 14 $u_x[U_c]$ on $y = 0$ for the translation of a sphere parallel to a plane interface ($\lambda = 0.1$, $\ell = 5$ and $\underline{u}_s = \underline{i}_x$);
$A = 0.8$, $B = 0.7$, $C = 0.6$, $D = 0.5$, $E = 0.4$, $F = 0.35$,
$G = 0.3$, $H = 0.25$, $I = 0.20$.

Figure 15 $u_x[U_c]$ on $x = 0$ for the translation of a sphere parallel to a plane interface ($\lambda = 0.1$, $\ell = 5$ and $\underline{u}_s = \underline{i}_x$);
$A = 0.8$, $B = 0.7$, $C = 0.6$, $D = 0.5$, $E = 0.4$, $F = 0.35$,
$G = 0.3$, $H = 0.25$, $I = 0.2$

Figure 16 $u_z[U_c]$ on $y = 0$ for the translation of a sphere parallel to a plane interface ($\lambda = 0.1$, $\ell = 5$ and $\underline{u}_s = \underline{i}_x$);
$A = 0.11$, $B = -0.11$, $C = 0.08$, $D = -0.08$, $E = 0.05$, $F = -0.05$,
$G = 0.02$, $H = -0.02$, $I = 0.012$, $J = -0.012$, $K = 0.008$,
$L = -0.008$, $M = 0.004$, $N = -0.004$, $O = 0.0$

Figure 17 $\omega_y[U_c/L_c]$ on $y = 0$ for the translation of a sphere parallel to a plane interface ($\lambda = 0.1$, $\ell = 5$ and $\underline{u}_s = \underline{i}_x$);
$A = 2.0$, $B = 1.0$, $C = 0.3$, $D = 0.1$, $E = 0.0$, $F = -0.025$,
$G = -0.1$, $H = -0.15$, $I = -0.3$, $J = -1.0$, $K = -2.0$

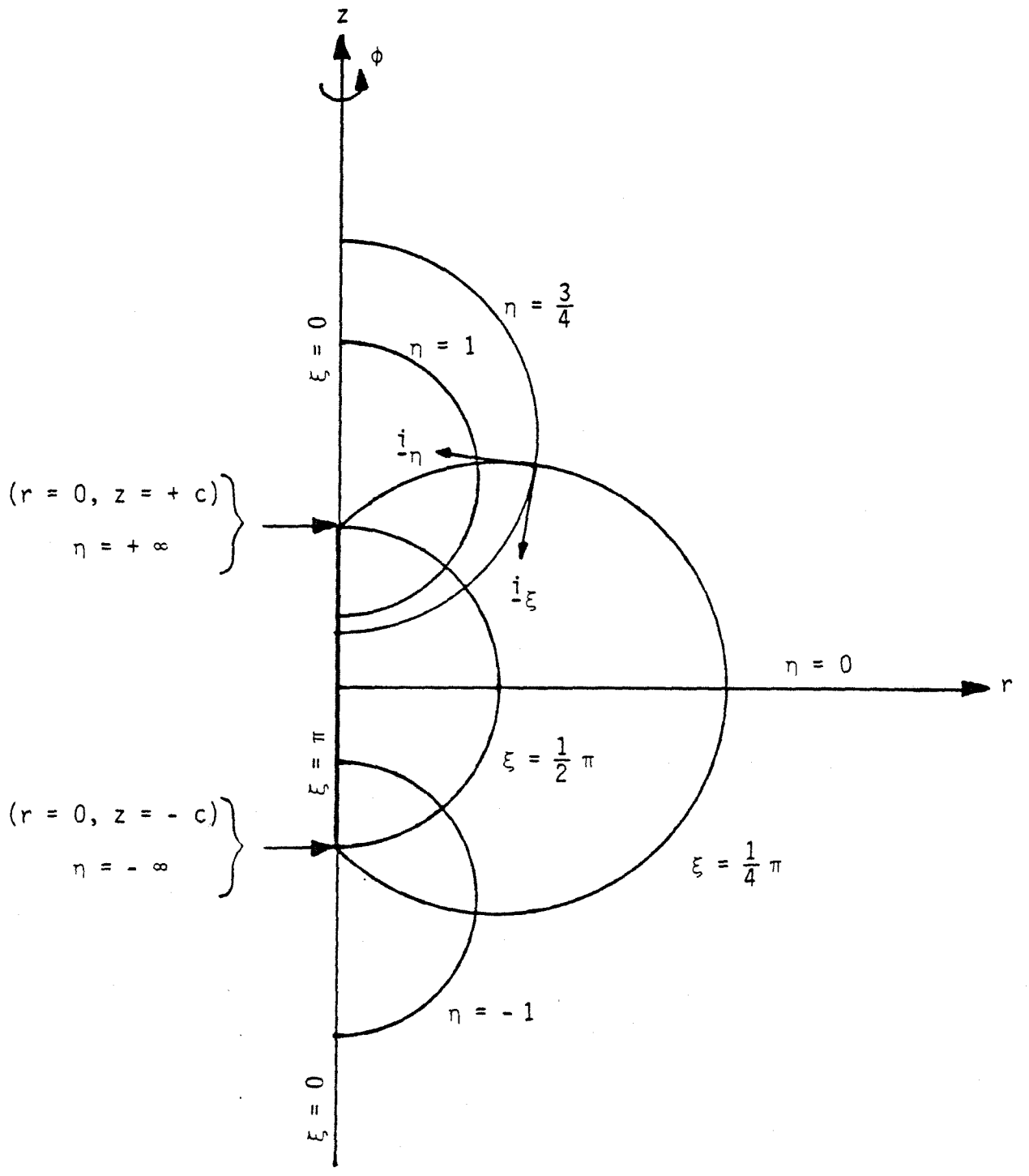

Figure 1

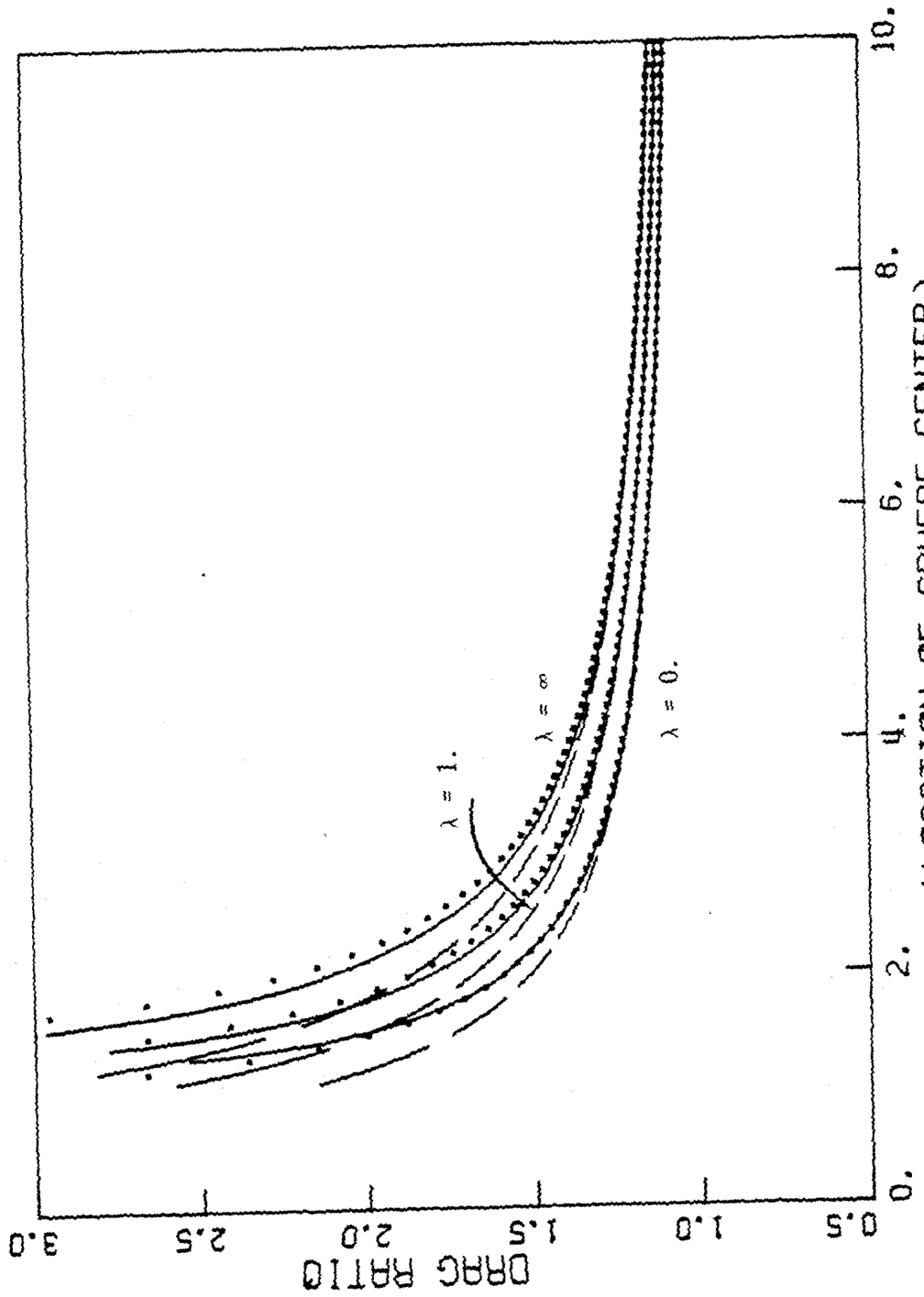
10.
8.
6.
4.
2.
ℓ (LOCATION OF SPHERE CENTER)
λ = 1.
λ = ∞
λ = 0.
0.5
1.0
1.5
2.0
2.5
3.0
DRAG RATIO
0.

Figure 2

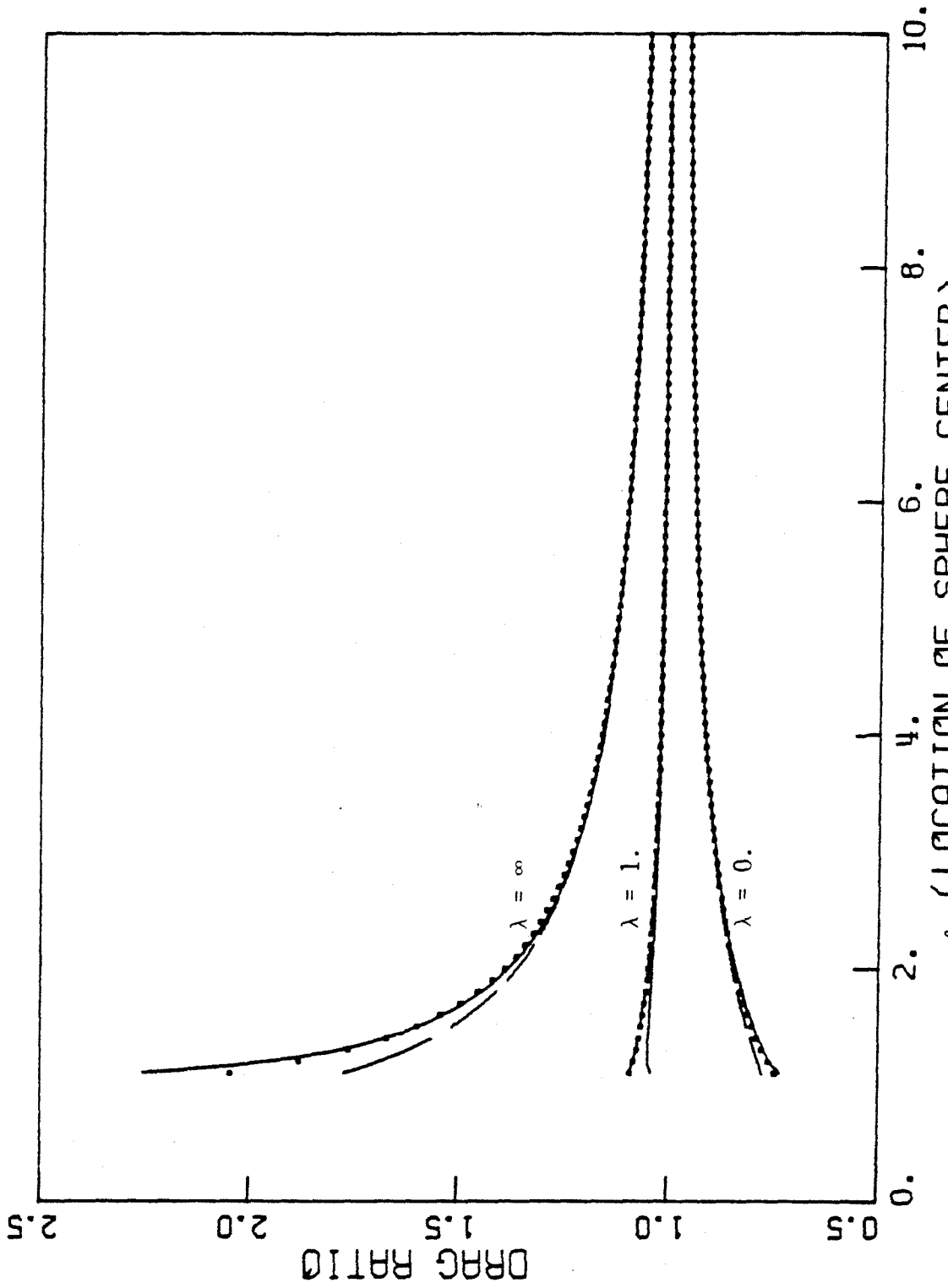
DRAG RATIO
0.5
1.0
1.5
2.0
2.5
0.
2.
4.
6.
8.
10.
ℓ (LOCATION OF SPHERE CENTER)
λ = ∞
λ = 1.
λ = 0.

Figure 3

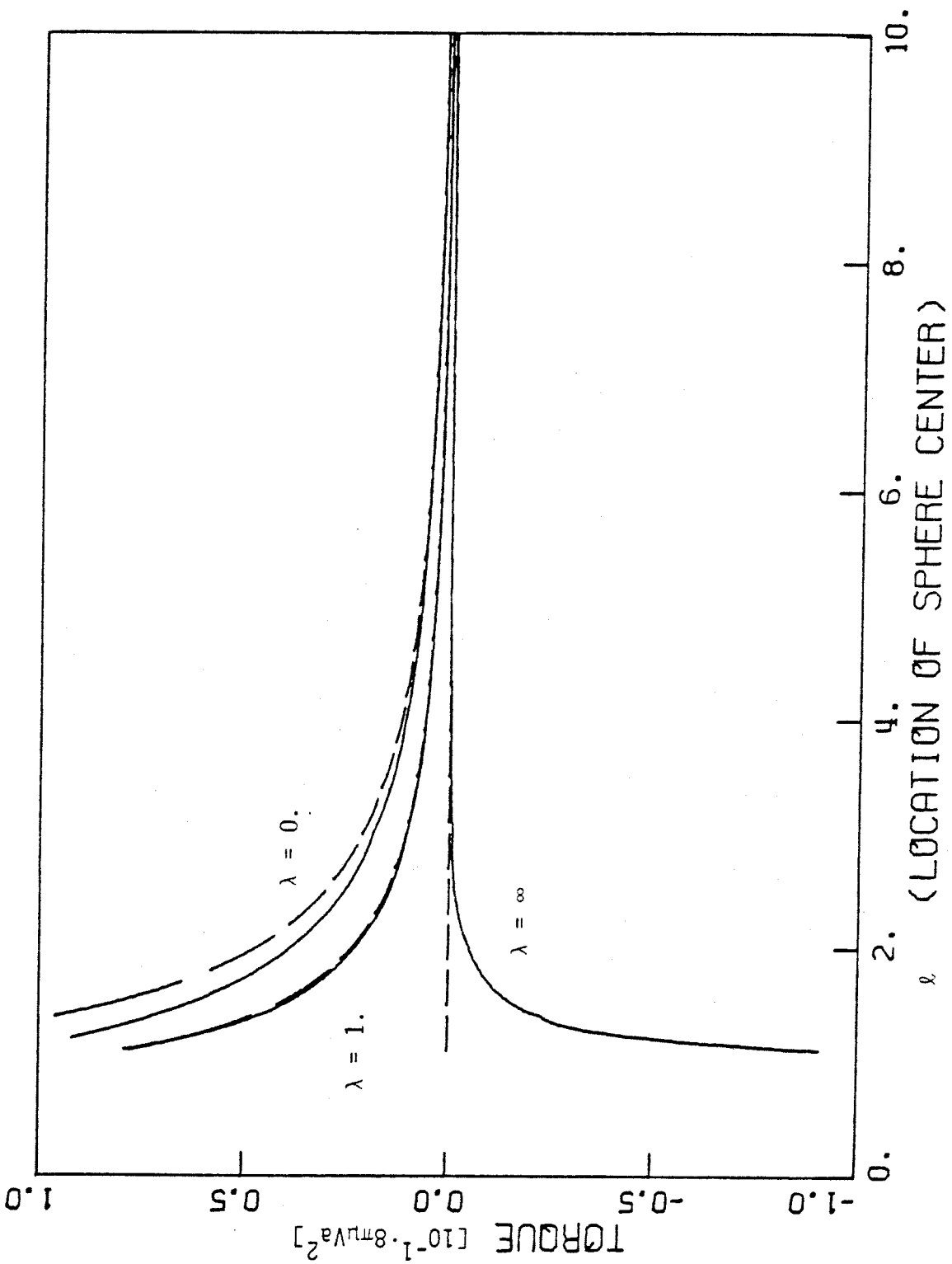
TORQUE [$10^{-1.8}\pi\mu Va^2$]
1.0
0.5
0.0
-0.5
-1.0
0.
2.
4.
6.
8.
10.
ℓ (LOCATION OF SPHERE CENTER)
λ = 0.
λ = 1.
λ = ∞

Figure 4

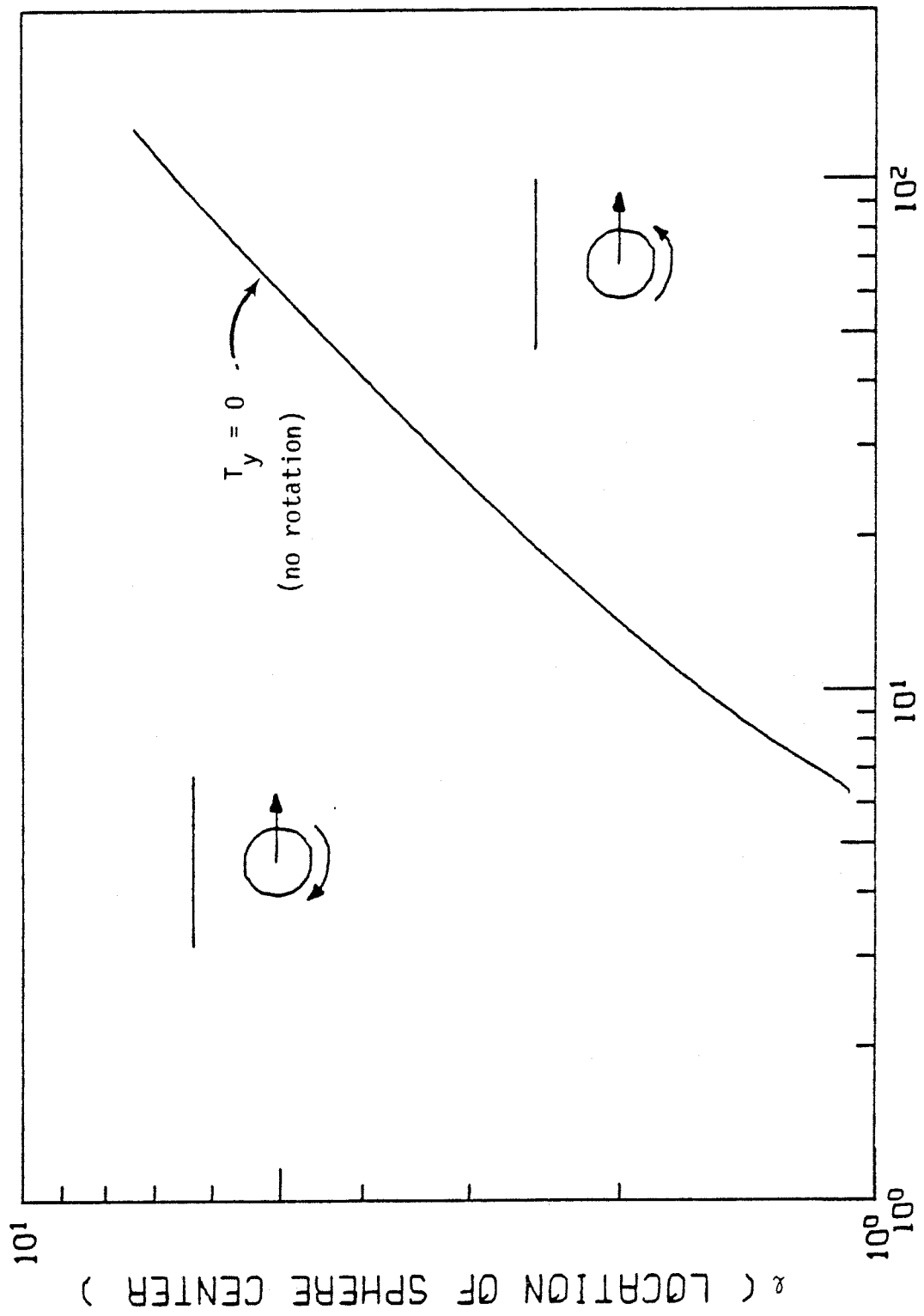
10^1
10^0
10^0
10^1
10^2
α (LOCATION OF SPHERE CENTER)
λ (VISCOSITY RATIO)
$T_y = 0$
(no rotation)

Figure 5

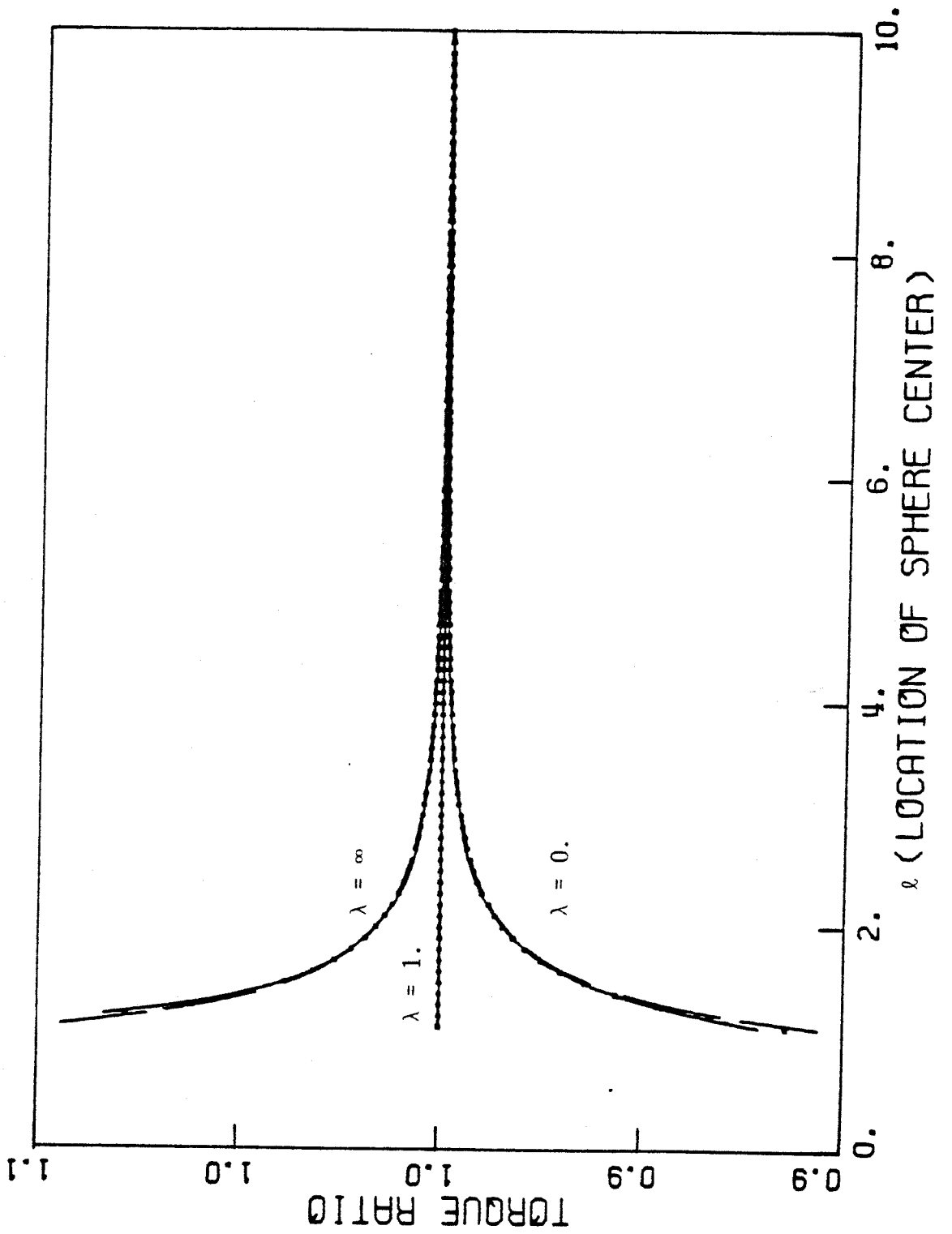
TORQUE RATIO
0.9
1.0
1.0
1.1
0.
2.
4.
6.
8.
10.
ℓ (LOCATION OF SPHERE CENTER)
λ = ∞
λ = 1.
λ = 0.

Figure 6

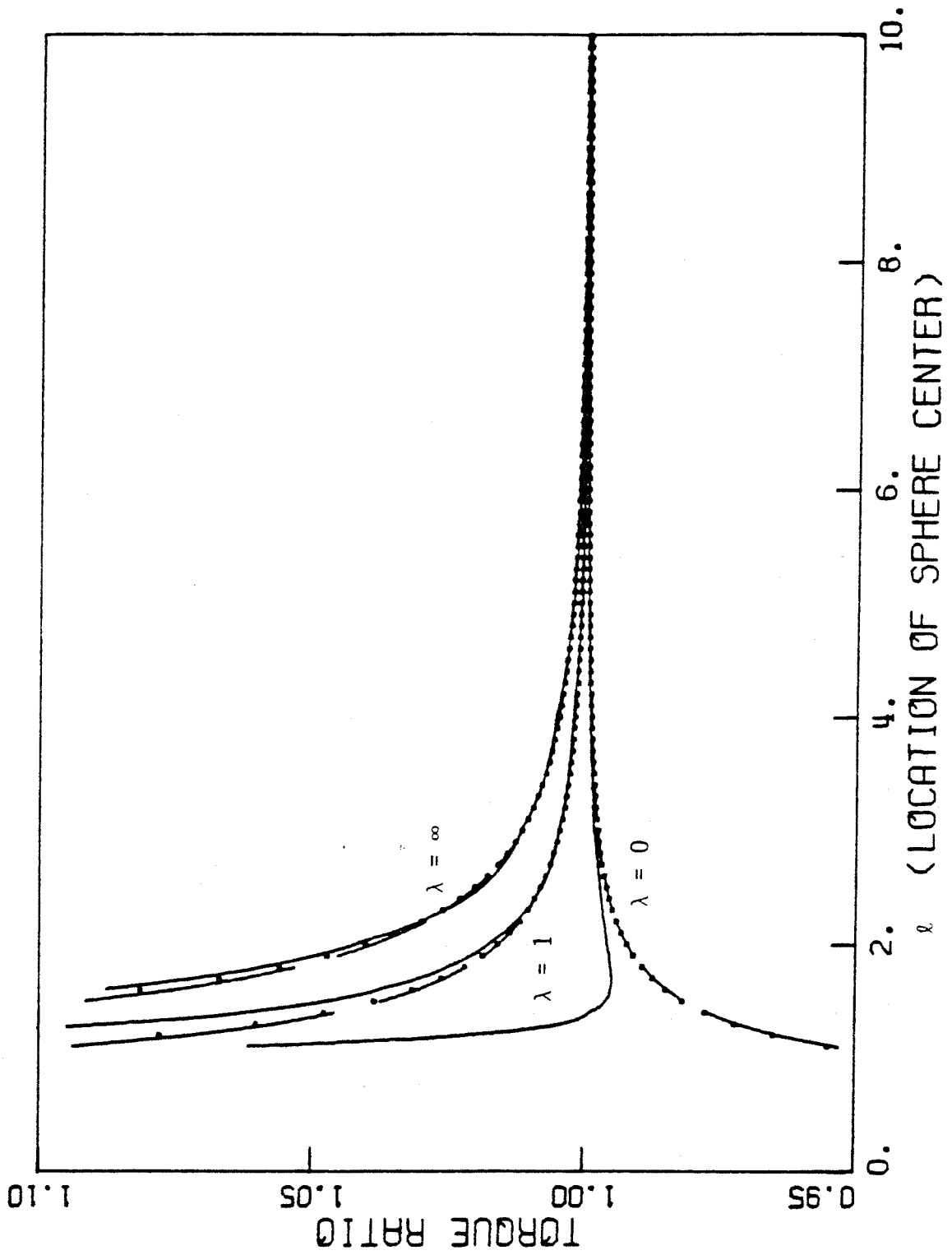
TORQUE RATIO
0.95
1.00
1.05
1.10
0.
2.
4.
6.
8.
10.
α (LOCATION OF SPHERE CENTER)
λ = ∞
λ = 1
λ = 0

Figure 7

Figure 8

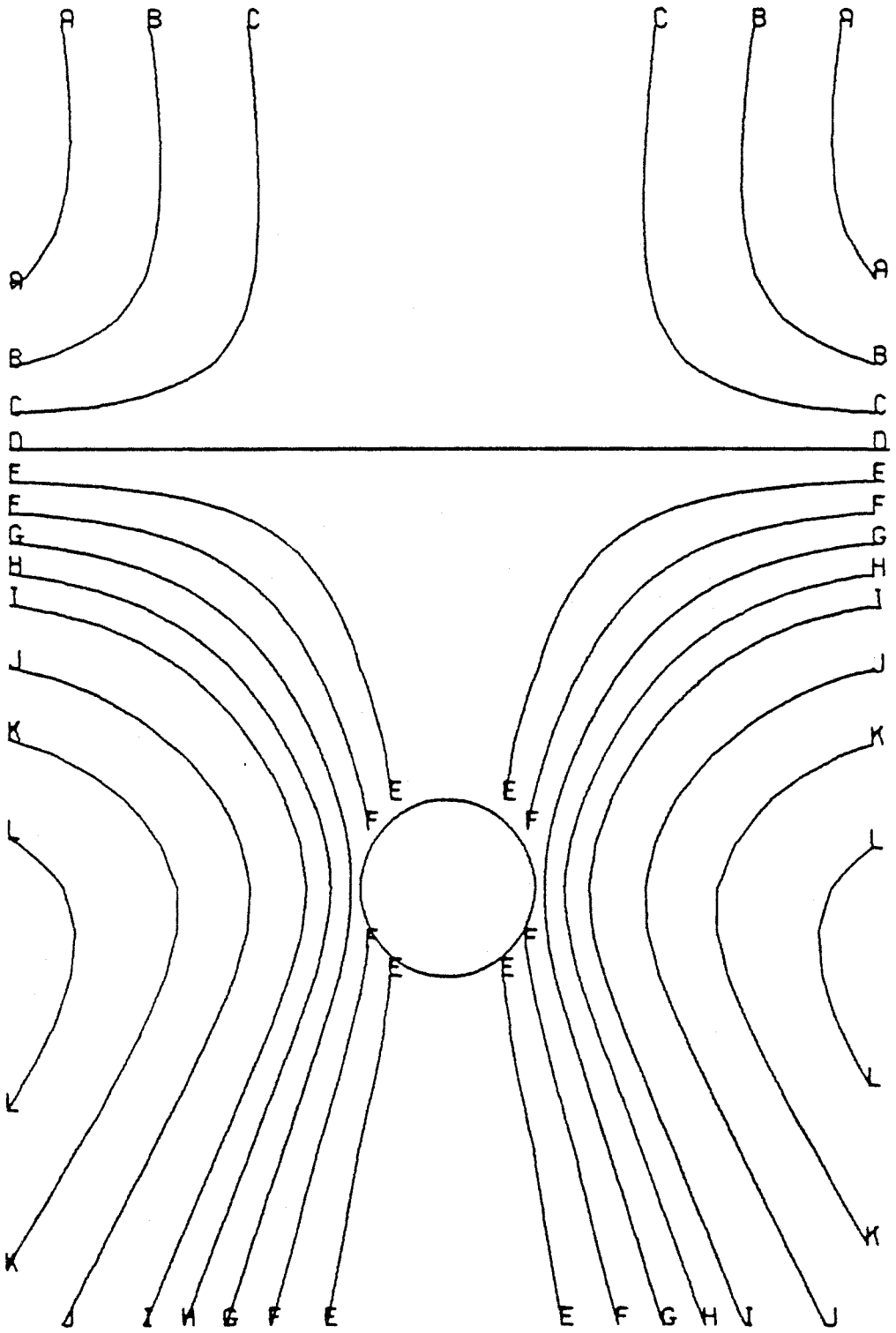

Figure 9

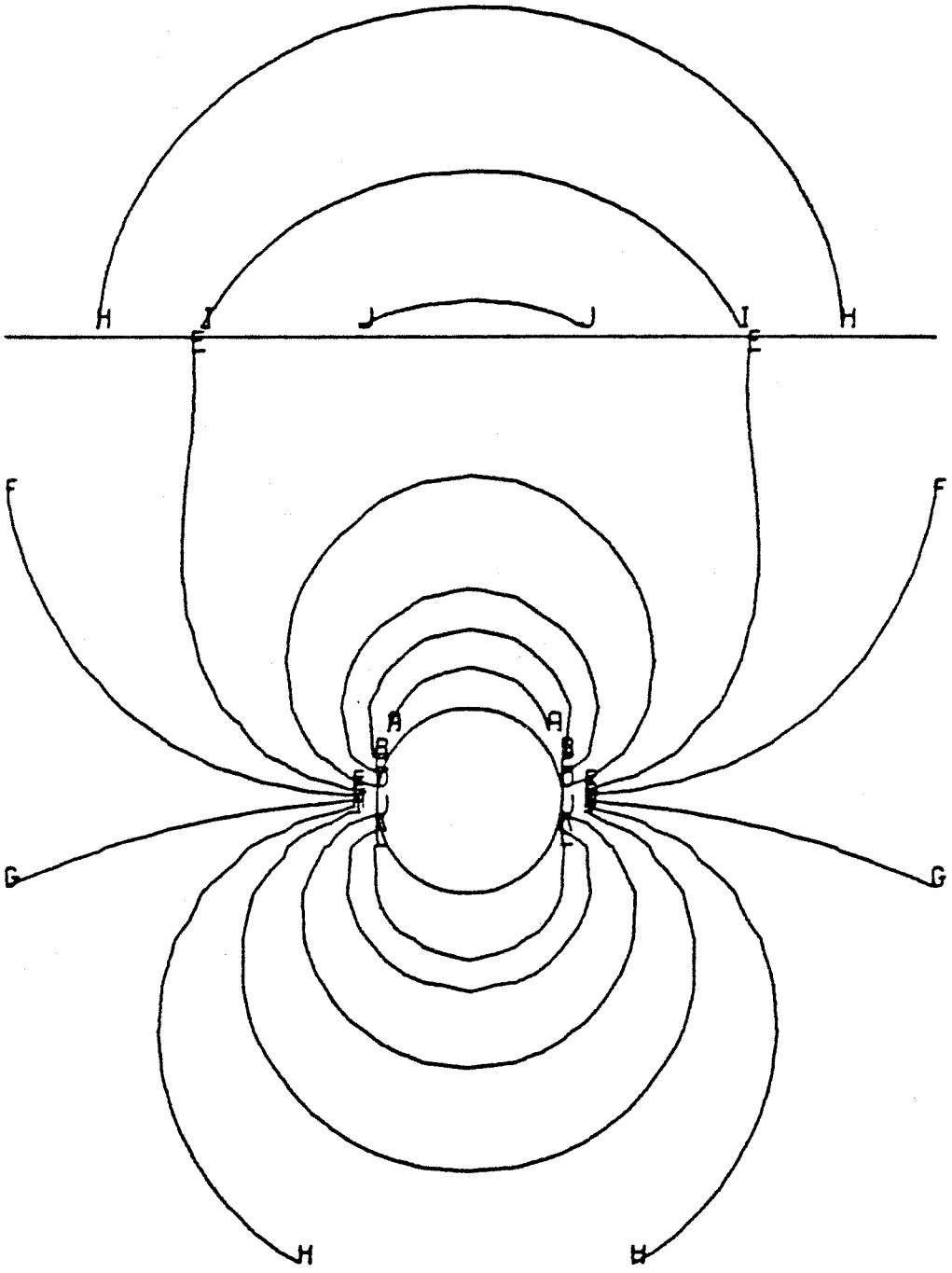

Figure 10

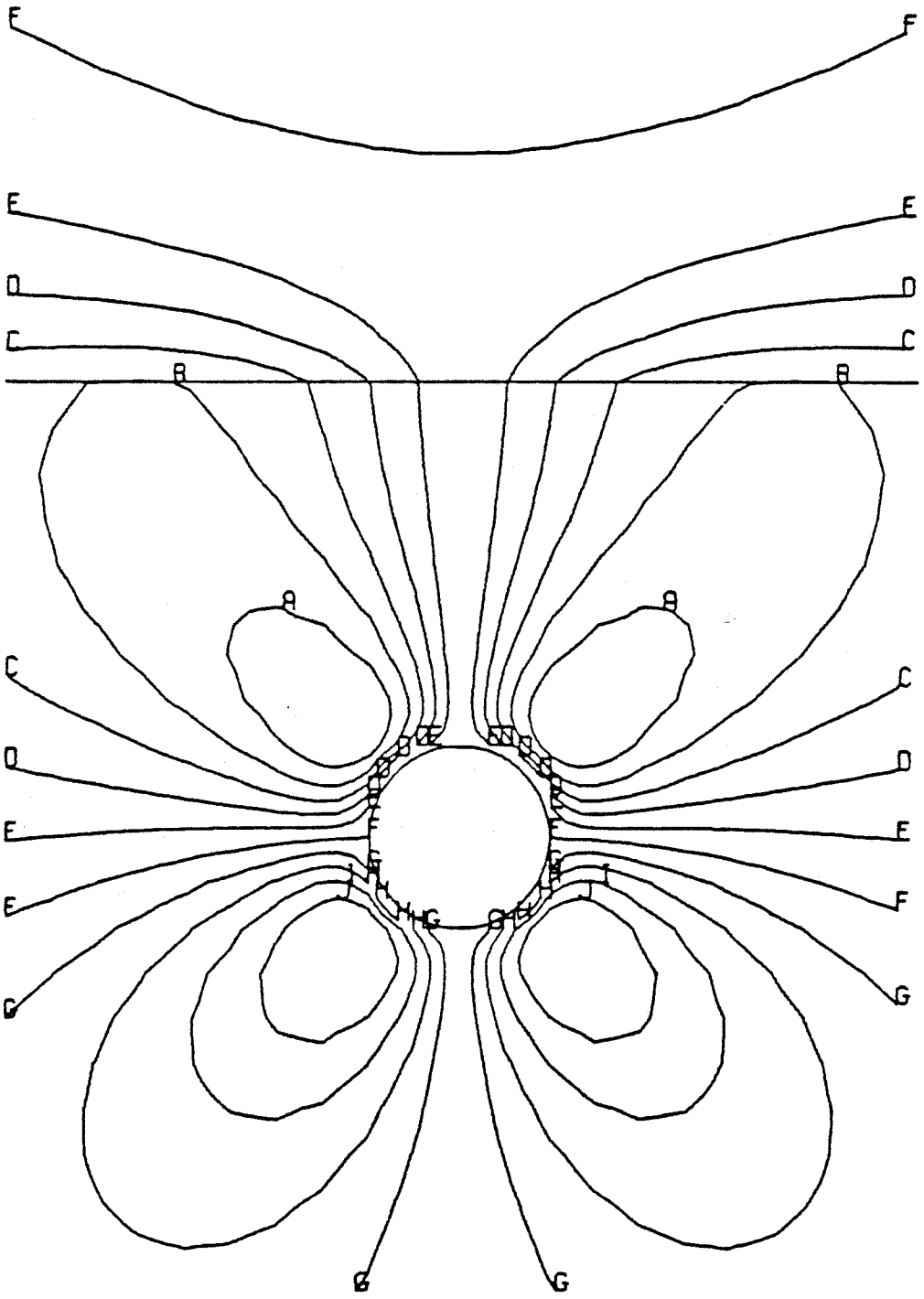

Figure 11

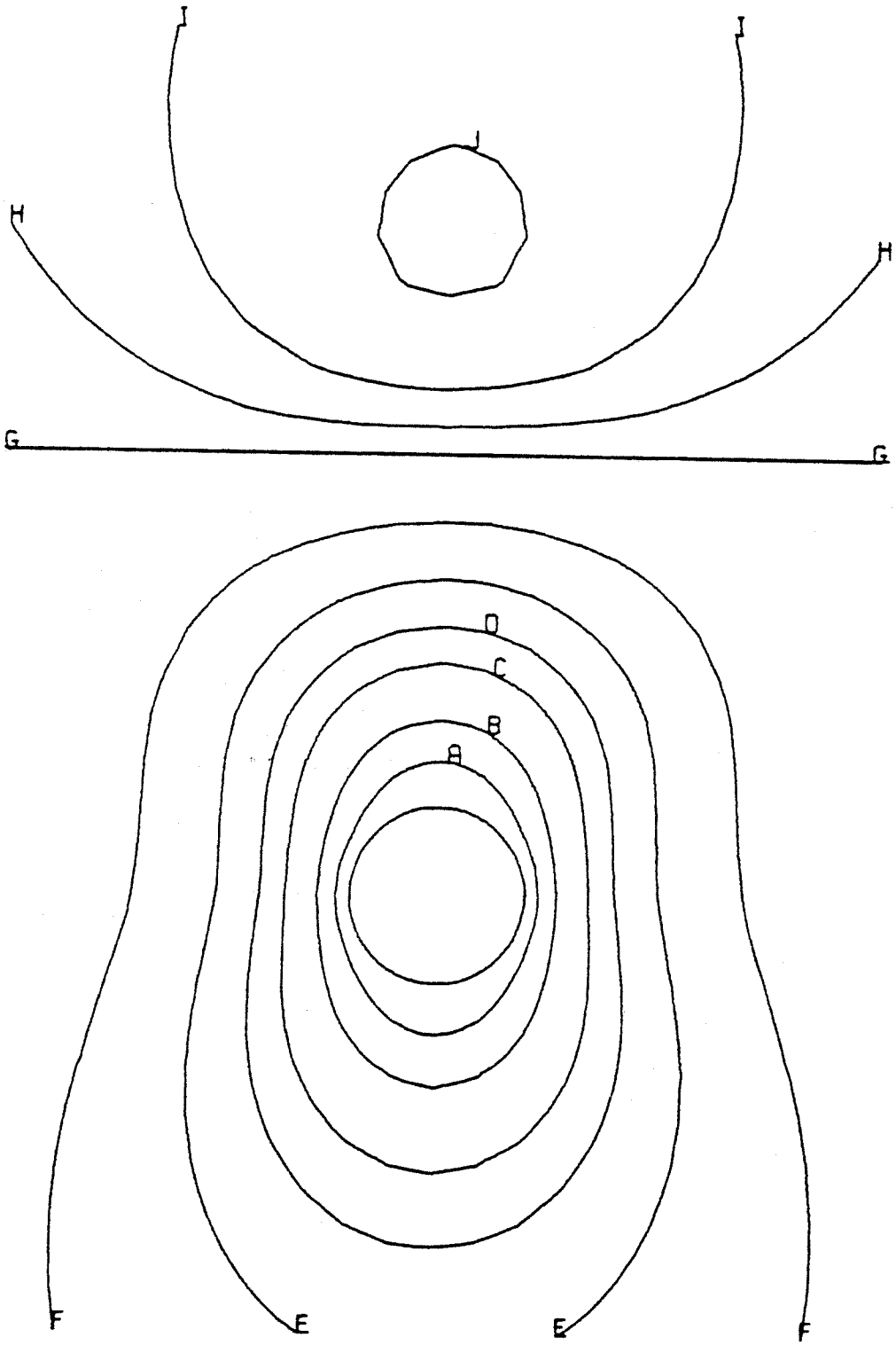

Figure 12

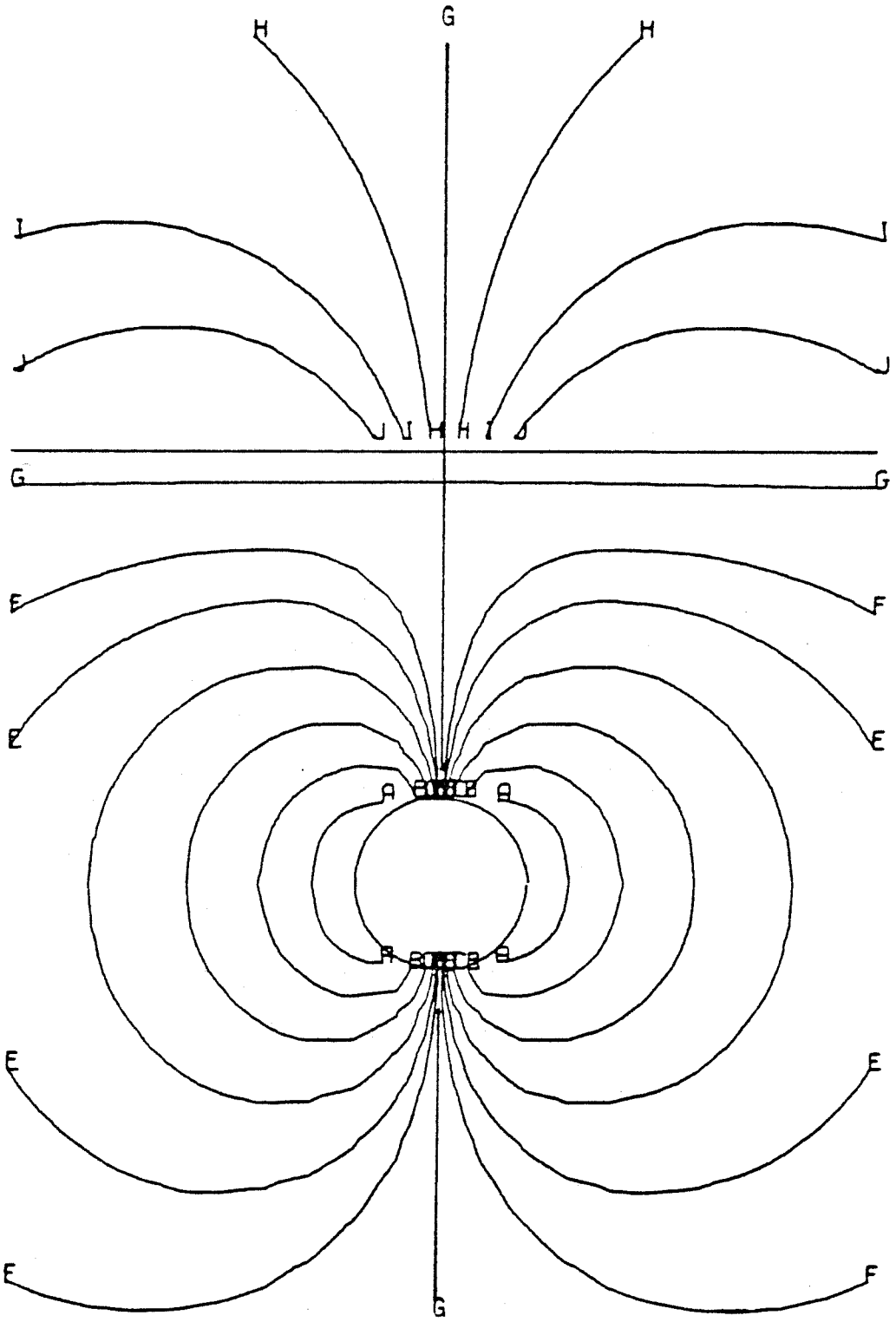

Figure 13

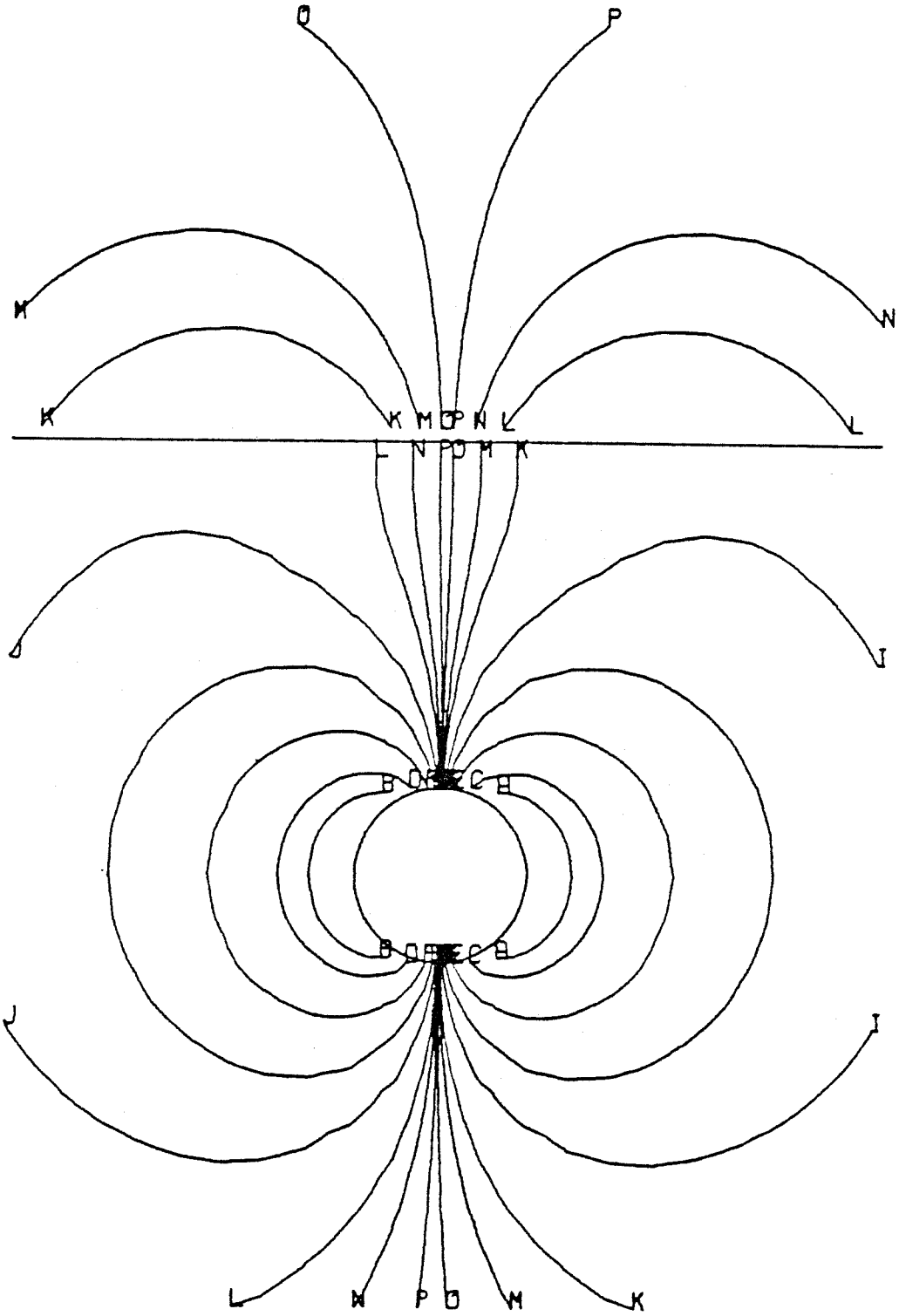

Figure 14

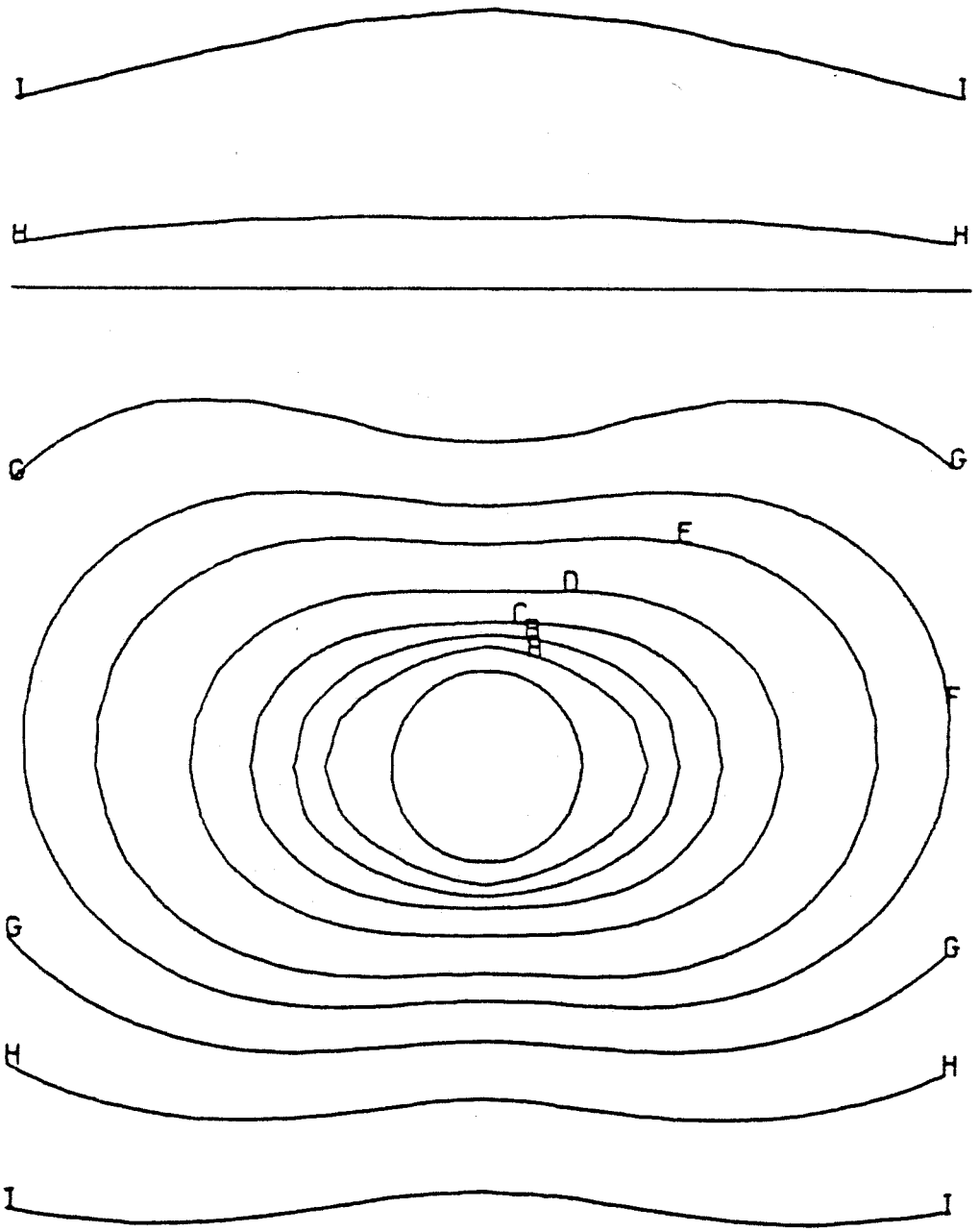

Figure 15

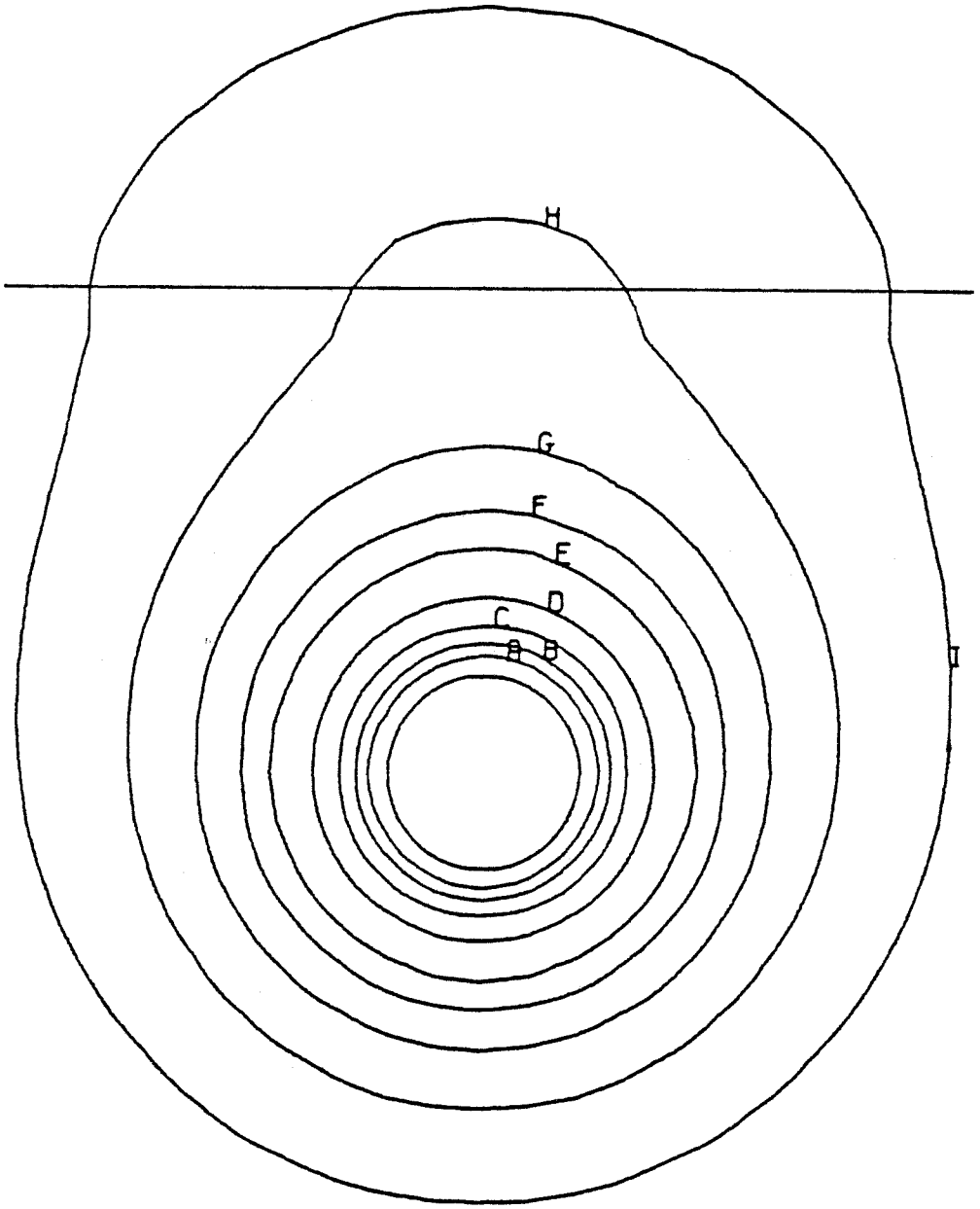

Figure 16

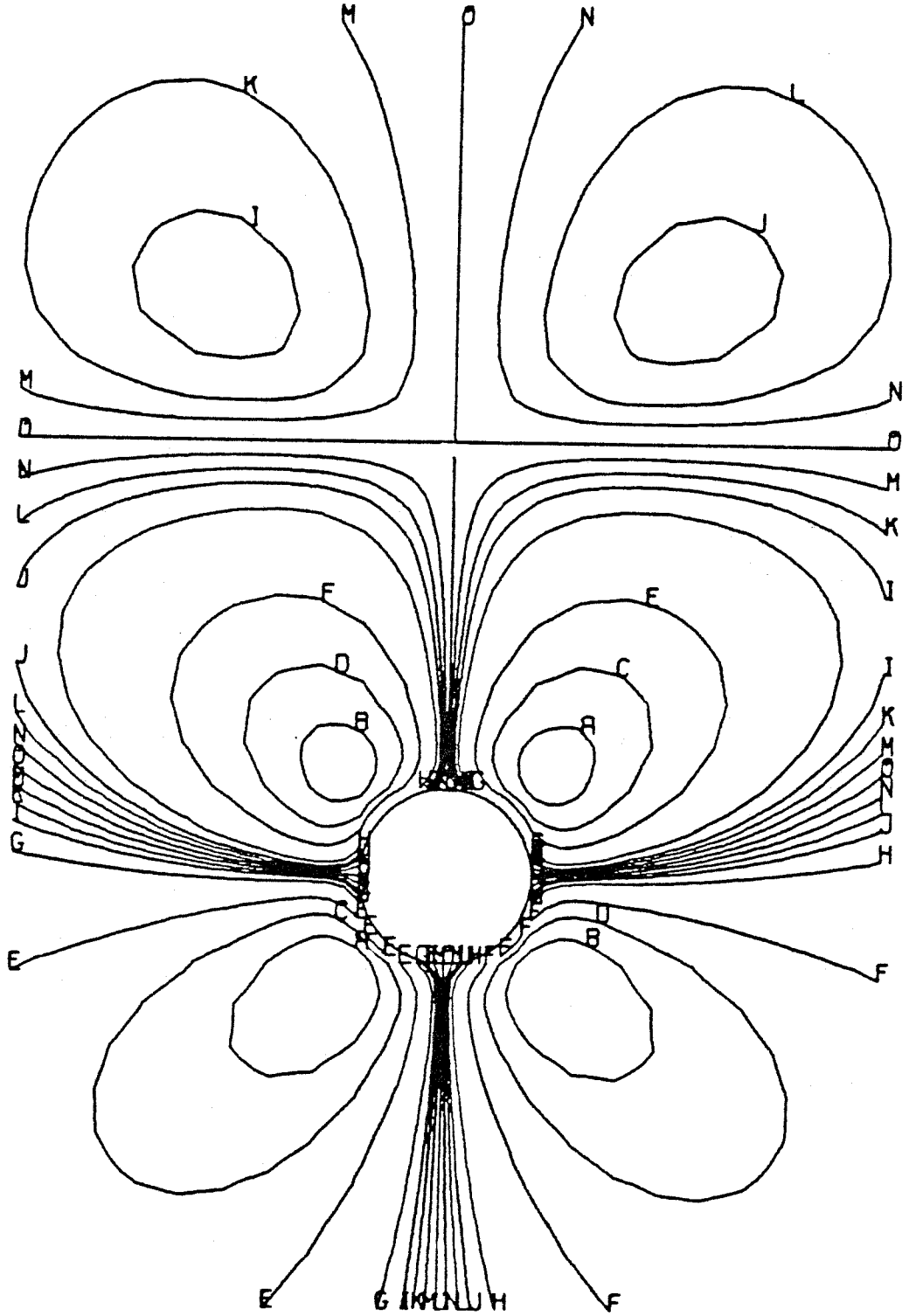

Figure 17

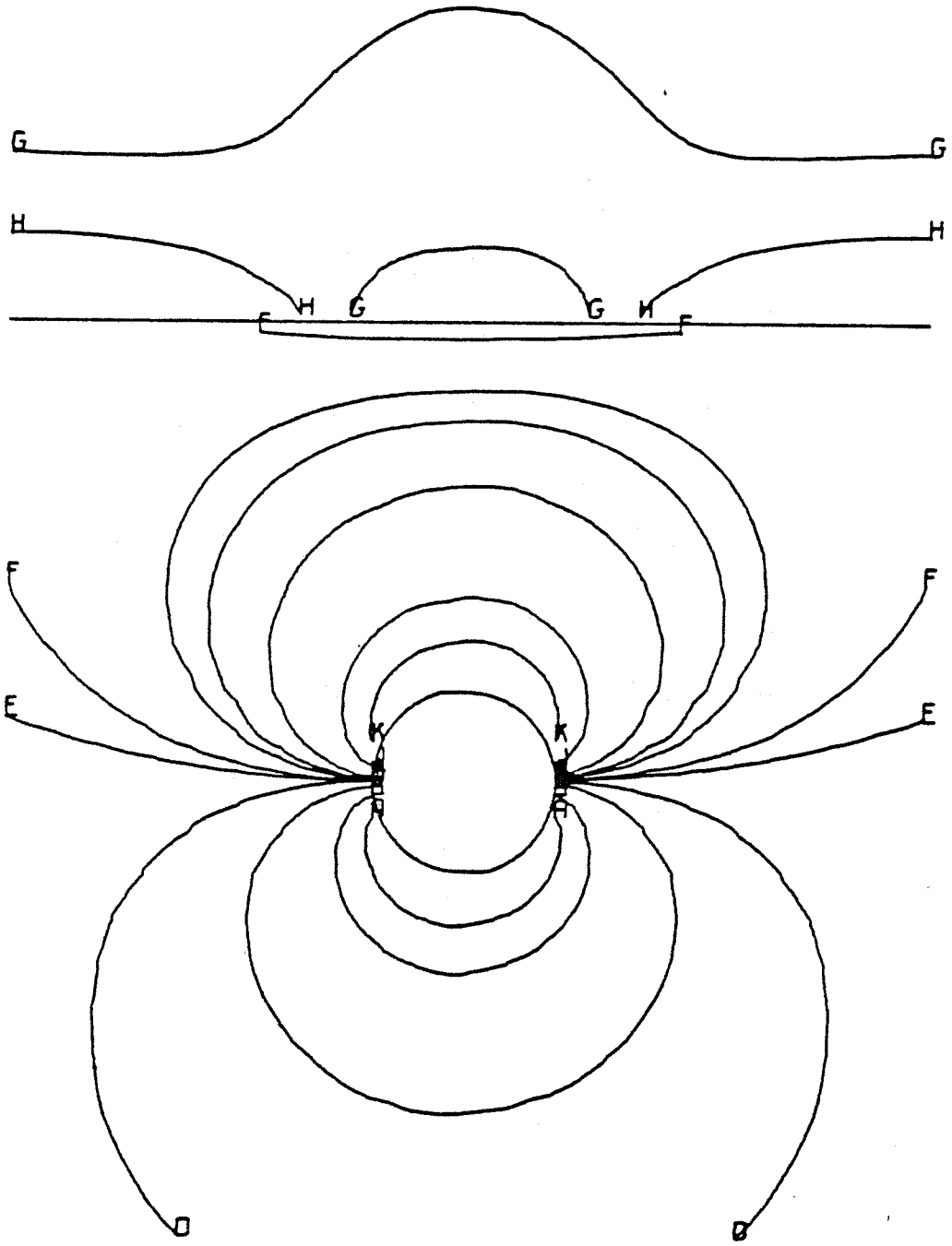

PART II. MODELING OF NON-ISOTHERMAL TURBULENT FLOWS.

A. A Second-Order Model for Non-Isothermal Turbulent Flows with Negligible Buoyancy Effects

by

S. H. Lee and L. G. Leal

Department of Chemical Engineering
California Institute of Technology
Pasadena, California 91125

Abstract

The second-order, mean Reynolds stress turbulence closure approximation is extended to non-isothermal turbulent flows with negligible buoyancy. We apply the method of invariant modeling [Lumley and Khajeh-Nouri (1974)] to systematically model the various higher order moments in the governing equations. This approach yields a general form for each unknown correlation in the transport equations of $\overline{u_i\theta}$, $\overline{\theta^2}$ and ε_θ each containing many terms with parameters that must be determined from experimental data. For practical application, it is necessary to reduce the number of terms. In the present work, the most important terms are filtered from the general model for each unknown moment and their parameters are evaluated based on experimental data for the turbulent boundary layer, Johnson (1955), the plane jet, Bashir and Uberoi (1975), the wake behind a sphere, Freymuth and Uberoi (1973), the wake behind a cylinder, Freymuth and Uberoi (1971), and the round jet, Antonia et al. (1975).

I. INTRODUCTION

The development of a realistic model to describe the turbulent transport of momentum, heat and mass is basic to the study of geophysical fluid mechanics, as well as many important technological flow problems. Recently, a great deal of research has been reported pertaining to the development and application of mean Reynolds stress models in an effort to analyze more general and complex flows.[1,2]

In many important problems, determination of the mean velocity distribution is just a first step towards predicting heat and/or mass transfer rates. However, much less effort has been given to closing the turbulent energy or mass flux equations than to closing the Reynolds stress equations. This paper is concerned with the development of a general closure model for nonisothermal turbulent flows without chemical reaction.

In spirit, the methods available for development of closure models for scalar fields in a turbulent flow are not much different from those used to develop closure models for the velocity field. In this paper, the second order, mean Reynolds stress closure technique, is extended to the case of nonisothermal flows. The method was first proposed by Chou[3] and Rotta,[4,5] who suggested a number of closure schemes. They modelled the third-order terms and the dissipation term in the Reynolds stress equation by various hypothesis. Current research along similar lines is being carried out by numerous investigators (i.e. Lumley and Khajeh-Nouri,[6] Lumley,[7] Launder et al.,[8,9] Hanjalic and Launder,[10] Daly and Harlow,[11] Shir,[12] Donaldson,[13] Wyngaard et al.,[14,15,16] etc.).

Recently, Lumley and Khajeh-Nouri[6] proposed a rational closure scheme which can generate models for the various higher order moments in a systematic manner. It allows the development of a general form for each of these unknown moments with a minimum of the ad hoc approximations which underlay most of the earlier models. Unfortunately, this general approach also generates a model for each term which contains many undetermined constants and these must be evaluated by comparison, on a term-by-term basis, with experimental data from flows of various kinds. Cormack[17] and Wood[18] have both used this procedure to develop models for the various unknown correlations for isothermal turbulent flows. Cormack evaluated the coefficients in his models by means of a systematic, term-by-term least squares fit to several sets of laboratory data.

In the present study, Cormack's general approach is extended to the development of a model for the dispersion of a passive scalar field in turbulent flow. The scalar may represent either temperature or concentration of contaminants, provided only that the gradients in these quantities are sufficiently small that neither buoyancy effects nor inhomogeneities of physical properties (viscosity, density and conductivity) are significant.

The present effort to develop functional forms for the various correlations that are required in a general model of turbulent dispersion should be considered only as a first step, based as it is on a simple term-by-term curve fit to experimental data. The second and final step, as always in this type of approach, must be to carefully evaluate the complete model (i.e. the full governing equations including <u>all</u> of the

various models for the higher-order correlations) by comparison of full dynamical computations with available experimental results. Such computations and comparisons will be reported in a future communication.

II. DERIVATION OF THE MODEL EQUATIONS

A. Transport Equations

We consider a flow accompanied by changes of density and viscosity of the fluid which are so small that the Boussinesq approximation[19] is valid. In addition, we neglect buoyancy effects and Coriolis forces. Although the model equations and related discussion will focus on the transport of heat, we can trivially change from temperature as the dependent variable to concentration of a chemical contaminant.

Decomposing the instantaneous velocity and scalar fields into a mean and a fluctuating part, and then ensemble averaging the Navier-Stokes equation yields

$$\frac{\partial U_i}{\partial t} + U_j \frac{\partial U_i}{\partial x_j} = -\frac{1}{\rho}\frac{\partial P}{\partial x_i} + \nu \frac{\partial^2 U_i}{\partial x_j \partial x_j} - \frac{\partial}{\partial x_j}\left(\overline{u_i u_j}\right) \tag{1}$$

in which U_i is the mean velocity and u_i is the fluctuation relative to this mean. The second moment $\overline{u_i u_j}$ is known as the Reynolds stress tensor. When the same procedure is applied to the continuity equation and the thermal energy equation, these become

$$\frac{\partial U_i}{\partial x_i} = 0 \quad \text{and} \quad \frac{\partial u_i}{\partial x_i} = 0 \tag{2}$$

and

$$\frac{\partial \Theta}{\partial t} + U_j \frac{\partial \Theta}{\partial x_j} = \gamma \frac{\partial^2 \Theta}{\partial x_j \partial x_j} - \frac{\partial}{\partial x_j}\left(\overline{u_j \theta}\right) \tag{3}$$

In equation (3), Θ is the mean temperature while θ represents the temperature fluctuation about this mean. The fluid density, kinematic viscosity and thermal diffusivity are denoted, respectively, as ρ, ν and γ.

The unknown terms $\overline{u_i u_j}$ and $\overline{u_i \theta}$ are the source of the well-known closure problem of the statistical theory of turbulence. Transport equations for these quantities can be derived from the Navier-Stokes and thermal energy equations for the full velocity and temperature fields, following Chou.[3] After neglecting terms which are of $O(Re^{-m})$ (cf. Ref. 20), these transport equations are

$$\frac{\partial}{\partial t}\overline{u_i u_j} + U_k \frac{\partial}{\partial x_k}\overline{u_i u_j} = - \overline{u_i u_k}\frac{\partial U_j}{\partial x_k} - \overline{u_j u_k}\frac{\partial U_i}{\partial x_k}$$
$$- \frac{\partial}{\partial x_k}\left(\overline{u_i u_j u_k} + \frac{2}{3}\frac{1}{\rho}\overline{u_k p}\,\delta_{ij}\right)$$
$$+ \frac{1}{\rho}\left(\overline{u_j \frac{\partial p}{\partial x_i}} + \overline{u_i \frac{\partial p}{\partial x_j}} - \frac{2}{3}\delta_{ij}\frac{\partial \overline{u_k p}}{\partial x_k}\right) - \frac{2}{3}\varepsilon\delta_{ij} \qquad (4)$$

$$\frac{\partial}{\partial t}\overline{u_i \theta} + U_j \frac{\partial \overline{u_i \theta}}{\partial x_j} = - \frac{\partial \Theta}{\partial x_j}\overline{u_i u_j} - \frac{\partial U_i}{\partial x_j}\overline{u_j \theta} - \frac{1}{\rho}\overline{\theta \frac{\partial p}{\partial x_i}}$$
$$- \frac{\partial}{\partial x_j}\overline{u_i u_j \theta} \qquad (5)$$

where $\varepsilon \equiv \nu \overline{\frac{\partial u_i}{\partial x_\ell}\frac{\partial u_i}{\partial x_\ell}}$. Although the temperature auto correlation, $\overline{\theta^2}$, does not appear in these equations, we anticipate its importance in equation (5) when buoyancy is included, and also as the measure of the mean square deviation of temperature from Θ in any realization of the flow system. Thus, we include the similar equation for its transport in

our present study.

$$\frac{\partial}{\partial t}\overline{\theta^2} + U_j \frac{\partial}{\partial x_j}\overline{\theta^2} = -\frac{\partial}{\partial x_j}\overline{\theta^2 u_j} - 2\overline{\theta u_j}\frac{\partial \Theta}{\partial x_j} - 2\varepsilon_\theta \qquad (6)$$

Here

$$\varepsilon_\theta \equiv \gamma \overline{\frac{\partial \theta}{\partial x_\ell}\frac{\partial \theta}{\partial x_\ell}}$$

The terms on the right hand side of equation (4) are denoted as production, diffusion, pressure strain, and dissipation, respectively. The terms in equation (5) and (6) have similar physical interpretations to those in equation (4).

The equations (4) - (6) describe the transport of the second-order quantities $\overline{u_i u_j}$, $\overline{u_i \theta}$ and $\overline{\theta^2}$ in a turbulent flow at high Reynolds number. However, each contains higher order correlations which are themselves unknown, and a closure at this second-order level thus requires additional relationships between these higher-order correlations and either the second-order correlations or the mean flow variables. The "model" which we shall discuss in this paper is really an attempt to provide reasonable approximations for these "missing" relationships. Explicit equations must also be derived for the dissipation rates ε and ε_θ. The transport equations for ε and ε_θ can be obtained by algebraic manipulation of the transport equations for u_i and θ,

$$\frac{\partial \varepsilon}{\partial t} + U_j \frac{\partial \varepsilon}{\partial x_j} = -2\nu \overline{\frac{\partial u_i}{\partial x_\ell}\frac{\partial u_j}{\partial x_\ell}\frac{\partial u_i}{\partial x_j}} - 2\nu^2 \overline{\left(\frac{\partial^2 u_i}{\partial x_j \partial x_\ell}\right)^2}$$
$$- \frac{\partial}{\partial x_j}\left[\overline{\nu u_j \left(\frac{\partial u_i}{\partial x_\ell}\right)^2} + \frac{2\nu}{\rho}\overline{\frac{\partial u_j}{\partial x_\ell}\frac{\partial p}{\partial x_\ell}}\right] \qquad (7)$$

$$\frac{\partial \varepsilon_\theta}{\partial t} + U_j \frac{\partial \varepsilon_\theta}{\partial x_j} = -\gamma \overline{\frac{\partial}{\partial x_j}\left(u_j \frac{\partial \theta}{\partial x_\ell}\frac{\partial \theta}{\partial x_\ell}\right)} - \left[2\gamma \overline{\frac{\partial u_j}{\partial x_\ell}\frac{\partial \theta}{\partial x_\ell}\frac{\partial \theta}{\partial x_j}} + 2\gamma^2 \overline{\frac{\partial^2 \theta}{\partial x_j \partial x_\ell}\frac{\partial^2 \theta}{\partial x_j \partial x_\ell}}\right] \tag{8}$$

and these contain further unknown, higher order terms which must be modelled.

Chou[3] and Lumley[7] proceeded still further to derive exact transport equations for the triple velocity correlations, but these equations contain even more unknown quantities. In the present work, only the equations (5), (6) and (8) will be considered explicitly and the unknown high order terms in those equations will be modelled. A number of models for isothermal flow [i.e. equations (4) and (7)] are already available,[1,2] including a recent model due to Wood.[18]

B. Correlations which Involve the Fluctuating Pressure

An exact equation of the Poisson form can be derived for the fluctuating pressure by simply taking the divergence of the Navier-Stokes equation using (2). By solving this equation, it is possible to obtain a physically-based estimate for the unknown correlation in equation (5) which involves the fluctuating pressure, without need to resort to the more cumbersome machinery of invariant modelling. We examine this term in the present section.

Using the method described above, Chou[3] has obtained an explicit solution for the pressure fluctuation, p, in terms of mean and fluctuating velocity components,

$$\frac{1}{\rho}p = \underbrace{\frac{1}{2\pi}\iiint \frac{\partial U_m'}{\partial \xi_n}\frac{\partial u_n'}{\partial \xi_m}\frac{1}{r}\,dV}_{(I)} - \underbrace{\frac{1}{4\pi}\iiint \frac{\partial^2}{\partial \xi_m \partial \xi_n}\left(\overline{u_m'u_n'} - u_m'u_n'\right)\frac{1}{r}\,dV}_{(II)}$$

$$+ \frac{1}{4\pi}\frac{1}{\rho}\iint \underbrace{\left\{\frac{1}{r}\frac{\partial p'}{\partial n} - p'\frac{\partial}{\partial n}\left(\frac{1}{r}\right)\right\}}_{(III)} dS \qquad (9)$$

The term (III) is negligible for flow which is far from any boundary, and we restrict our attention to this case. The character of the remaining terms (I) and (II) is quite different from one another. In particular, the former is linear in fluctuating velocity, while the latter is bilinear. For convenience, we denote the term (I) as $\frac{p^{(1)}}{\rho}$ and the term (II) as $\frac{p^{(2)}}{\rho}$. Utilizing equation (9), an expression for the temperature-pressure gradient correlation, $-\frac{1}{\rho}\overline{\theta\frac{\partial p}{\partial x_i}}$ in equation (5), may be derived as follows.

$$-\frac{1}{\rho}\overline{\theta\frac{\partial p}{\partial x_i}} = -\frac{1}{\rho}\left(\overline{\theta\frac{\partial p^{(1)}}{\partial x_i}} + \overline{\theta\frac{\partial p^{(2)}}{\partial x_i}}\right)$$

$$= -\frac{1}{2\pi}\iiint \frac{\partial}{\partial \xi_i}\left[\frac{\partial U_m'}{\partial \xi_n}\frac{\partial}{\partial \xi_m}\overline{u_n'\theta}\right]\frac{1}{r}\,dV$$

$$+ \frac{1}{4\pi}\iiint \frac{\partial^3 \overline{u_m'u_n'\theta}}{\partial \xi_m \partial \xi_n \partial \xi_i}\frac{1}{r}\,dV \qquad (10)$$

Launder[8] and Lumley[7] derived a leading order approximation for $-\frac{1}{\rho}\overline{\theta\frac{\partial p^{(1)}}{\partial x_i}}$ by assuming that the mean velocity gradient is constant over the domain of integration, i.e.

$$-\frac{1}{\rho}\overline{\theta\frac{\partial p^{(1)}}{\partial x_i}} = \frac{2}{10}\frac{\partial U_\ell}{\partial x_m}\left(4\delta_{i\ell}\overline{\theta u_m} - \delta_{im}\overline{\theta u_\ell}\right) \qquad (11)$$

The same authors have also speculated on an appropriate form for $\overline{\theta \frac{\partial p^{(2)}}{\partial x_i}}$, but the resultant model is on much less satisfactory ground than (11).

Because of the uncertainty of the "derived" forms for $\overline{\theta \frac{\partial p^{(2)}}{\partial x_i}}$, we have elected to develop a model for this term (next section) using the apparatus of invariant modelling. Since this model must simultaneously include all of the terms which are possible for $-\overline{\theta \frac{\partial p^{(1)}}{\partial x_i}}$, there is no advantage in distinguishing between $p^{(1)}$ and $p^{(2)}$ for purposes of determining the model coefficients from the experimental data for $-\overline{\theta \frac{\partial p}{\partial x_i}}$, and we will thus consider the model which we derive as representing the complete temperature/pressure gradient correlation. Of course, one possibility is that the optimal coefficient for the term $\frac{\partial U_\ell}{\partial x_m}(4\delta_{i\ell}\overline{\theta u_m} - \delta_{im}\overline{\theta u_\ell})$ in this model will be $\frac{2}{10}$ as suggested by equation (11). However, this presumes a negligible contribution of the same form from $p^{(2)}$, as well as the validity of Launder[8] and Lumley's[7] assumptions in deriving (11), and thus needs to be examined by comparison with experimental data.

C. Models for Higher Order Correlations - Invariant Modelling

The theory of invariant modelling was first adopted to analyze isotropic turbulence by Robertson.[21] However, the theory has also been extensively used in the derivation of constitutive relations for viscoelastic fluids.[22] In applying the method of invariant modelling to the unknown correlation functions in the Reynolds equations for turbulent flow, Lumley[23,24] assumed that turbulence exhibits two of the properties of Coleman and Noll's 'simple' fluid, namely: (1) a fading memory for prior states and (2) a limited awareness of the turbulent structure at nearby points. These assumptions allow the unknown third-order moments at a space and time point to be expressed as a function of the second-order moments or their first few spatial derivatives at the same point. The underlying justification for this assumption is incomplete, but we follow all previous modellers and adopt it here as a plausible assumption which is necessary to make any progress toward a "turbulence model."

For nonisothermal flows with negligible buoyancy effects, we require models for the terms $\overline{u_i\theta^2}$, $-\overline{u_iu_j\theta}$, $-\frac{1}{\rho}\overline{\theta\frac{\partial p}{\partial x_i}}$, $-\gamma\frac{\partial}{\partial x_j}\left(\overline{u_j\frac{\partial\theta}{\partial x_\ell}\frac{\partial\theta}{\partial x_\ell}}\right)$, and $-2\gamma\left[\overline{\frac{\partial u_j}{\partial x_\ell}\frac{\partial\theta}{\partial x_\ell}\frac{\partial\theta}{\partial x_j}}+\gamma\left(\overline{\frac{\partial^2\theta}{\partial x_j\partial x_\ell}}\right)^2\right]$ which appear on the right hand sides of equations (5), (6) and (8). The higher-order terms which appear in (4) and (7) have been modelled in the earlier studies of Wood.[18] In order to apply the method of invariant modelling, we must first hypothesize a

functional form to specify the independent functional variables. In the first three of the third-order terms listed above, we assume that the unknown correlation may depend on all of the available second-order and mean flow variables.

$$\overline{u_i\theta^2} = F_i^1\left\{a_{\ell m},\ q^2,\ \overline{u_\ell\theta},\ \overline{\theta^2},\ \varepsilon,\ \varepsilon_\theta,\ \frac{\partial U_\ell}{\partial x_m},\ \frac{\partial \Theta}{\partial x_\ell}\right\} \tag{12}$$

$$\overline{u_iu_j\theta} = F_{ij}^2\left\{a_{\ell m},\ q^2,\ \overline{u_\ell\theta},\ \overline{\theta^2},\ \varepsilon,\ \varepsilon_\theta,\ \frac{\partial U_\ell}{\partial x_m},\ \frac{\partial \Theta}{\partial x_\ell}\right\} \tag{13}$$

$$-\frac{1}{\rho}\,\overline{\theta\,\frac{\partial p}{\partial x_i}} = F_i^3\left\{a_{\ell m},\ q^2,\ \overline{u_\ell\theta},\ \overline{\theta^2},\ \varepsilon,\ \varepsilon_\theta,\ \frac{\partial U_\ell}{\partial x_m},\ \frac{\partial \Theta}{\partial x_\ell}\right\} \tag{14}$$

Here, $q^2 = \overline{u_\ell u_\ell}$ and $a_{\ell m} \equiv \overline{u_\ell u_m} - \frac{1}{3}\,\delta_{\ell m} q^2$. In the case of the unknown correlations in the equation for ε_θ, however, we include all possible turbulence quantities but neither $\frac{\partial U_\ell}{\partial x_m}$ nor $\frac{\partial \Theta}{\partial x_\ell}$, i.e.

$$-\gamma\left(\overline{u_i\,\frac{\partial\theta}{\partial x_\ell}\,\frac{\partial\theta}{\partial x_\ell}}\right) = F_i^4\left\{a_{\ell m},\ q^2,\ \overline{u_\ell\theta},\ \overline{\theta^2},\ \varepsilon,\ \varepsilon_\theta\right\} \tag{15}$$

$$-2\gamma\left(\overline{\frac{\partial u_\ell}{\partial x_m}\,\frac{\partial\theta}{\partial x_m}\,\frac{\partial\theta}{\partial x_\ell}} + \gamma\left(\overline{\frac{\partial^2\theta}{\partial x_\ell\partial x_m}}\right)^2\right) = F^5\left\{a_{\ell m},\ q^2,\ \overline{u_\ell\theta},\ \overline{\theta^2},\varepsilon,\ \varepsilon_\theta\right\} \tag{16}$$

The terms in equations (15) and (16) represent the turbulent flux of ε_θ and the production and dissipation of ε_θ by vortex stretching and thermal conduction, respectively. Therefore, we presume that these terms depend primarily on the small scale turbulence structure, rather than mean velocity or temperature gradients.

In Lumley and Khajeh-Nouri's previous work,[6] <u>all</u> of the necessary functionals were assumed to be independent of mean flow gradients. Moreover, on the basis of a direct examination of equations (5) and (6), they

did not include ε in equation (12), or ε_θ in equations (13) and (14). In non-isothermal turbulent flow, however, there may be two representative turbulent length scales determined respectively by the velocity and temperature fields. Thus, the functional forms proposed here include the possibility of spatial derivatives of q^2, a_{ij}, ε, ε_θ, $\overline{\theta^2}$ and $\overline{u_i\theta}$. The proper length scale for the spatial derivatives of q^2, a_{ij} and ε is q^2/ε, while that for $\overline{\theta^2}$ and ε_θ is $\overline{\theta^2}q/\varepsilon_\theta$ ($\overline{u_i\theta}$ may be intermediate as regards the length scale appropriate to its spatial derivatives). Thus, even though the transport equations (5) and (6) do not explicitly contain ε or ε_θ, it is necessary to include ε and ε_θ as independent variables in the functionals (12) - (16).

We formally expand these functionals in increasing orders of anisotropy and inhomogeneity (See Ref. 17 for a discussion of the definition for orders of anisotropy and inhomogeneity. It may be noted that $\overline{u_i\theta}$ is considered first-order in anisotropy for present purposes.). Due to the generality of the forms (12) - (16), the functional expansions will generate many more terms than are possible to simultaneously curve fit with limited experimental data. Therefore, instead of attempting to eliminate terms one-by-one from the complete model via a sensitivity test as suggested by Cormack,[17] we develop and apply a filtering process to systematically add terms of increasing significance as measured by their influence on the accuracy of least squares fit to experimental data.

For simplicity in the following presentation, we define the following vectors and tensors.

$$\underline{\underline{A}} \equiv \{a_{ij}\},\ \underline{\underline{A}}_x \equiv \left\{\frac{\partial a_{ij}}{\partial x_k}\right\},\ \underline{\underline{A}}_x{}^2 \equiv \left\{\frac{\partial^2 a_{ij}}{\partial x_k \partial x_\ell}\right\},$$

$$\underline{Q}_x \equiv \left\{\frac{\partial q^2}{\partial x_i}\right\},\ \underline{\underline{Q}}_x{}^2 \equiv \left\{\frac{\partial^2 q^2}{\partial x_i \partial x_j}\right\},\ \underline{\Theta}_x \equiv \left\{\frac{\partial \Theta}{\partial x_i}\right\}$$

$$\underline{\underline{B}} \equiv \{\overline{u_i\theta}\},\ \underline{\underline{B}}_x \equiv \left\{\frac{\partial \overline{u_i\theta}}{\partial x_j}\right\},\ \underline{\underline{B}}_x{}^2 \equiv \left\{\frac{\partial^2 \overline{u_i\theta}}{\partial x_j \partial x_k}\right\}, \tag{17}$$

$$\underline{\Phi}_x \equiv \left\{\frac{\partial \overline{\theta^2}}{\partial x_i}\right\},\ \underline{\underline{\Phi}}_x{}^2 \equiv \left\{\frac{\partial^2 \overline{\theta^2}}{\partial x_i \partial x_j}\right\},\ \underline{E}_x \equiv \left\{\frac{\partial \varepsilon}{\partial x_i}\right\},$$

$$\underline{\underline{E}}_x{}^2 \equiv \left\{\frac{\partial^2 \varepsilon}{\partial x_i \partial x_j}\right\},\ \underline{E}_x^\theta \equiv \left\{\frac{\partial \varepsilon_\theta}{\partial x_i}\right\},\ \underline{\underline{E}}_x^\theta{}^2 \equiv \left\{\frac{\partial^2 \varepsilon_\theta}{\partial x_i \partial x_j}\right\}$$

The trace operators for third-order tensors are defined as follows.

$$Tr_1(\underline{\underline{\underline{C}}}) \equiv C_{i\ell\ell},\ Tr_2(\underline{\underline{\underline{C}}}) \equiv C_{\ell i\ell} \text{ and } Tr_3(\underline{\underline{\underline{C}}}) \equiv C_{\ell\ell i} \tag{18}$$

Let us now turn to the derivation of general forms for the models of $\overline{u_i\theta^2}$, and the unknown correlations in the ε_θ and $\overline{u_i\theta}$ equations.

a) General Form for the Model of $\overline{u_i\theta^2}$

We begin with the general form for the model of $\overline{u_i\theta^2}$. Some restrictions on this general form follow from the fact that $\overline{u_i\theta^2}$ should remain invariant when the gradient of the mean temperature field is reversed without changing the velocity field. Specifically, all homogeneous terms which could be generated from equation (12) must vanish, and, in addition, many inhomogeneous terms must be excluded from the model.

The mean velocity gradient tensor, $\frac{\partial U_i}{\partial x_j}$, can be decomposed into its symmetric and anti-symmetric parts, these representing mean strain rate, S_{ij}, and the mean vorticity Ω_{ij}, respectively. The principle of material indifference cannot be imposed in turbulence modeling because rigid rotation

has significant effects on Reynolds stress and other high-order terms.[24] Thus, it cannot be supposed that the expressions (12) - (14) should be independent of Ω_{ij} when expressed in a reference frame which translates and rotates with the local mean translational and angular velocities, as is true of constitutive relations in non-Newtonian continuum mechanics. If we retain all possible terms, it does not therefore make any difference whether $\frac{\partial U_i}{\partial x_j}$ or the decomposed form $(S_{ij} + \Omega_{ij})$ is used for a model. However, when we choose only a few terms as a simplified model, the performance of this reduced model may depend on which form of the mean velocity gradient is adopted. In our opinion, the decomposition into mean strain rate and mean vorticity is preferred as it allows separate evaluation of the dependence of the model on S_{ij} and Ω_{ij}. To minimize the total number of terms, we consider only those terms which are linear in S_{ij} or Ω_{ij}.

The model terms for $\overline{u_i\theta^2}$ can then be classified into four groups: $\{V_1\}$, which have no dependence on mean flow or temperature variables; $\{V_2\}$, which involve S_{ij}; $\{V_3\}$, which involve Ω_{ij}; and $\{V_4\}$, which are dependent on $\partial\Theta/\partial x_i$.

From equation (12), model terms of these various types can be easily generated up to order (2,2) [here, order (a,b) means ath order in anisotropy and bth order in inhomogeneity].

The model terms without mean flow variables are

$$\{V_1\} = \alpha_2 \underline{\Phi}_x \frac{\overline{\theta^2 q^2}}{\varepsilon_\theta} + \alpha_9 \underline{A}\cdot\underline{E}_x^\theta \frac{(\overline{\theta^2})^2}{\varepsilon_\theta^2} + \alpha_{14} \underline{B}(\underline{B}\cdot\underline{\Phi}_x) \frac{1}{\varepsilon_\theta} + \alpha_{16} \underline{B}(\underline{B}\cdot\underline{E}_x^\theta) \frac{\overline{\theta^2}}{\varepsilon_\theta}$$

$$+ \alpha_{20}(\underline{\underline{B}}_x\cdot\underline{B}) \frac{\overline{\theta^2}}{\varepsilon_\theta} + \alpha_{23}(\underline{\underline{B}}_x\cdot\underline{B}) \frac{q^2}{\varepsilon} + \alpha_{33}(\underline{\underline{A}}_x:\underline{\underline{A}}) \frac{\overline{\theta^2}}{\varepsilon} + (27 \text{ terms}) \quad (19)$$

The model terms involving S_{ij} are

$$\{V_2\} = \alpha_{38}\, \underline{\underline{S}}\cdot\underline{E}_x^{\theta}\, \frac{(\overline{\theta^2})^2 q^4}{\varepsilon\, \varepsilon_\theta^2} + \alpha_{54}(\underline{\underline{B}}\underline{Q}_x):\underline{\underline{S}}\underline{\underline{B}}\, \frac{q^2}{\varepsilon^2} + \alpha_{57}(\underline{B}\cdot\underline{Q}_x)(\underline{B}\cdot\underline{\underline{S}})\, \frac{q^2}{\varepsilon^2}$$

$$+ \alpha_{61}(\underline{B}\cdot\underline{E}_x)(\underline{B}\cdot\underline{\underline{S}})\, \frac{q^4}{\varepsilon^3} + \alpha_{62}(\underline{\underline{B}}\underline{\Phi}_x):\underline{\underline{S}}\underline{\underline{B}}\, \frac{q^2}{\varepsilon\, \varepsilon_\theta} + \alpha_{70}\underline{\underline{B}}_x:\underline{\underline{S}}\underline{\underline{B}}\, \frac{\overline{\theta^2} q^2}{\varepsilon\, \varepsilon_\theta}$$

$$+ \alpha_{77}\, \underline{B}\cdot\underline{\underline{S}}\cdot\underline{\underline{B}}_x^T\, \frac{q^4}{\varepsilon^2} + (28 \text{ terms}), \tag{20}$$

while the model terms with Ω_{ij} are

$$\{V_3\} = \alpha_{80}\underline{Q}_x\cdot\underline{\underline{\Omega}}\, \frac{\overline{\theta^2} q^4}{\varepsilon^2} + \alpha_{81}\, \underline{E}_x\cdot\underline{\underline{\Omega}}\, \frac{\overline{\theta^2} q^6}{\varepsilon^3} + \alpha_{82}\, \underline{\Phi}_x\cdot\underline{\underline{\Omega}}\, \frac{\overline{\theta^2} q^4}{\varepsilon\, \varepsilon_\theta} + (33 \text{ terms}) \tag{21}$$

Finally, the model terms which depend linearly on $\partial\Theta/\partial x_i$ can be expressed in the form

$$\{V_4\} = \alpha_{119}\, \underline{\Theta}_x\cdot\underline{Q}_x\underline{\underline{B}}\, \frac{\overline{\theta^2} q^2}{\varepsilon\, \varepsilon_\theta} + \alpha_{132}\, \underline{B}\cdot Tr_1(\underline{\underline{A}}_x)\underline{\Theta}_x + \alpha_{133}(\underline{\underline{B}}\underline{\Theta}_x):\underline{\underline{A}}_x + (17 \text{ terms}) \tag{22}$$

The model for $\overline{u_i\theta^2}$ is then the sum of all terms in (19) - (22).

b) General Forms for Modeled Terms in the ε_θ Advection Equation

Let us now consider the general forms of models for the unknown, higher-order correlations in the advection/diffusion equation for ε_θ, beginning with $-\gamma\overline{u_i \frac{\partial\theta}{\partial x_\ell}\frac{\partial\theta}{\partial x_\ell}}$.

i) $-\gamma\overline{u_i \frac{\partial\theta}{\partial x_\ell}\frac{\partial\theta}{\partial x_\ell}}$

Model terms for $-\gamma\overline{u_i \frac{\partial\theta}{\partial x_\ell}\frac{\partial\theta}{\partial x_\ell}}$ can be generated with relative ease from equation (15). As this term is differentiated in the ε_θ advection equation, its model generates results in the dynamical calculation which are one order higher in inhomgeneity than the model itself. Furthermore, since

the independent variables of functionals (15) and (16) are identical, the differentiation of one model term for $-\gamma\overline{u_i \frac{\partial\theta}{\partial x_\ell}\frac{\partial\theta}{\partial x_\ell}}$ yields terms with the same form as the model terms for $-2\gamma\left[\overline{\frac{\partial u_i}{\partial x_\ell}\frac{\partial\theta}{\partial x_\ell}\frac{\partial\theta}{\partial x_j}} + \gamma\overline{\left(\frac{\partial^2\theta}{\partial x_j\partial x_\ell}\right)^2}\right]$. Thus, for simplicity, we only consider terms up to order (1,1), with the exception of $\underline{B}$ where we include terms of order (2,1) [no model terms contain $\underline{B}$ at the (1,1) level]. As there are multiple length scales in the equation (15), we can generate many terms just by combining scalars such as ε, ε_θ, q^2 and $\overline{\theta^2}$ without increasing the order in inhomogeneity and anisotropy. However, by inference from the form of $-\gamma\overline{u_i \frac{\partial\theta}{\partial x_\ell}\frac{\partial\theta}{\partial x_\ell}}$, we assume that the appropriate length scale for scaling purpose is that characteristic of temperature field, $\frac{\overline{\theta^2}q}{\varepsilon_\theta}$. In addition, as $-\gamma\overline{u_i \frac{\partial\theta}{\partial x_\ell}\frac{\partial\theta}{\partial x_\ell}}$ is second-order in θ, it can be primarily represented with model terms of first-order in $\overline{\theta^2}$ or ε_θ. The resulting model is

$$-\gamma\overline{u_i \frac{\partial\theta}{\partial x_\ell}\frac{\partial\theta}{\partial x_\ell}} = \gamma_1 \underline{Q}_x \frac{\varepsilon_\theta q^2}{\varepsilon} + \gamma_{18}\,\underline{B}\,\mathrm{Tr}(\underline{\underline{B}}_x) + \gamma_{19}\,\underline{B}\cdot\underline{\underline{B}}_x + \gamma_{20}\,\underline{B}\cdot\underline{\underline{B}}_x^T + (16\text{ terms}). \tag{23}$$

ii) $-2\gamma\left[\overline{\frac{\partial u_j}{\partial x_\ell}\frac{\partial\theta}{\partial x_\ell}\frac{\partial\theta}{\partial x_\ell}} + \gamma\overline{\left(\frac{\partial^2\theta}{\partial x_j\partial x_\ell}\right)^2}\right]$

Direct examination of the form of $-2\gamma\left[\overline{\frac{\partial u_j}{\partial x_\ell}\frac{\partial\theta}{\partial x_\ell}\frac{\partial\theta}{\partial x_\ell}} + \gamma\overline{\left(\frac{\partial^2\theta}{\partial x_j\partial x_\ell}\right)^2}\right]$

shows that it is second-order in θ. Thus the model terms of first-order in $\overline{\theta^2}$ or ε_θ might be expected to primarily represent the term.

In addition, since the dissipation term, $-2\gamma^2\overline{\left(\frac{\partial^2\theta}{\partial x_j\partial x_\ell}\right)^2}$,

can be also considered to be of second-order in the thermal conductivity, γ, it may be approximately proportional to ε_θ^2. However, to reduce the total size of the model, terms involving ε_θ^2 are retained only in the homogeneous model. The functional, equation (16), is expanded up to order (2,2).

The homogeneous model, $\{D_H\}$, is

$$\{D_H\} = \left(\beta_1 + \beta_2 \frac{II}{q^4}\right) \frac{\varepsilon_\theta \varepsilon}{q^2} + \left(\beta_3 + \beta_4 \frac{II}{q^4}\right) \frac{\varepsilon_\theta^2}{\overline{\theta^2}} + \underline{B}\cdot\underline{B} \left(\beta_5 \frac{\varepsilon_\theta \varepsilon}{\overline{\theta^2} q^4} + \beta_6 \frac{\varepsilon_\theta^2}{\overline{\theta^2} q^2} + \beta_7 \frac{\varepsilon^2}{q^6}\right). \tag{24}$$

Here, $II \equiv a_{ij} a_{ij}$

The corresponding inhomogeneous model, $\{D_I\}$, is

$$\{D_I\} = \mathrm{Tr}(\underline{\underline{\Phi}}_x 2)\left(\beta_{33} q^2 + \beta_{34} \frac{\varepsilon_\theta}{\varepsilon} \frac{q^4}{\overline{\theta^2}}\right) + \beta_{37} \underline{\underline{A}} : (\underline{E}_x \underline{E}_x) \frac{\overline{\theta^2}}{\varepsilon^2} + \beta_{48} \underline{\underline{A}} : \underline{\underline{\Phi}}_x 2 \frac{\varepsilon_\theta q^2}{\varepsilon \overline{\theta^2}} + \mathrm{Tr}(\underline{\Phi}_x \cdot \underline{\underline{A}}_x)\left(\beta_{69} + \beta_{70} \frac{\varepsilon_\theta}{\varepsilon} \frac{q^2}{\overline{\theta^2}}\right) + \beta_{100} \underline{\underline{B}}_x : \underline{\underline{B}}_x^T + (108 \text{ terms}). \tag{25}$$

c) General Forms for the Modeled Terms in the $\overline{u_i \theta}$ Advection Equation

We now turn to the allowable forms for the modeled terms in the $\overline{u_i \theta}$ equation, beginning with the velocity/temperature correlation - $\overline{u_i u_j \theta}$.

i) $-\overline{u_i u_j \theta}$

Due to the fact that $-\overline{u_i u_j \theta}$ is differentiated in equation (5), a model term which involves $\frac{\partial U_i}{\partial x_j}$ or $\frac{\partial \Theta}{\partial x_i}$ will produce higher order terms like $\frac{\partial^2 U_i}{\partial x_j \partial x_k}$ or $\frac{\partial^2 \Theta}{\partial x_i \partial x_j}$.

Thus, for simplicity of the model, the functional equation (13) is expanded up to order (2,1), excluding terms which involve $\frac{\partial U_i}{\partial x_j}$ and $\frac{\partial \Theta}{\partial x_i}$, to yield

$$
\begin{aligned}
-\overline{u_i u_j \theta} \;=\; & \{\zeta_1(\underline{\underline{B}}_x + \underline{\underline{B}}_x^T) + \zeta_2\, \mathrm{Tr}(\underline{\underline{B}}_x)\underline{\underline{I}}\}\, \frac{q^4}{\varepsilon} \\
& + \{\zeta_3(\underline{\underline{B}}_x + \underline{\underline{B}}_x^T) + \zeta_4\, \mathrm{Tr}(\underline{\underline{B}}_x)\underline{\underline{I}}\}\, \frac{q^2\overline{\theta^2}}{\varepsilon_\theta} \\
& + \zeta_{15}(\underline{\underline{B}}_x \cdot \underline{\underline{A}} + \underline{\underline{A}} \cdot \underline{\underline{B}}_x^T)\, \frac{q^2}{\varepsilon} + \zeta_{20}\, \mathrm{Tr}(\underline{\underline{A}} : \underline{\underline{B}}_x)\underline{\underline{I}}\, \frac{\overline{\theta^2}}{\varepsilon_\theta} \\
& + \zeta_{21}\left(\underline{B}\, \mathrm{Tr}_1(\underline{\underline{A}}_x) + \mathrm{Tr}_1(\underline{\underline{A}}_x)\underline{B}\right) \frac{q^2}{\varepsilon} + (29 \text{ terms}). \qquad (26)
\end{aligned}
$$

Note that $-\overline{u_i u_j \theta}$ changes its sign when the gradient of mean temperature field is reversed. Hence, there are obviously no homogeneous terms in the allowable form for $-\overline{u_i u_j \theta}$.

ii) $-\frac{1}{\rho}\overline{\theta \frac{\partial p}{\partial x_i}}$

Finally, we turn to the allowable form for a model of the temperature-pressure gradient correllation. Again, it is necessary to identify an appropriate characteristic length scale for scaling purposes. It may be anticipated that this scale is more likely to be associated with spatial structure of the velocity field than the temperature field. Nevertheless, the choice is not altogether obvious, and we thus choose to include several terms which are scaled with the characteristic thermal scale in our homogeneous model in order to examine this speculation. Terms with mean velocity gradients are included only in the homogeneous model because the model can represent experimental data well even without inhomogeneous terms involving $\frac{\partial U_i}{\partial x_j}$ (cf. Section IV E). Moreover, there are already many

terms to be considered. Terms with $\frac{\partial\Theta}{\partial x_i}$ are excluded from the same reason. Further, considering that $-\frac{1}{\rho}\overline{\theta\frac{\partial}{\partial x_i}p}$ is first-order in the fluctuating temperature θ, we omit the terms of higher order in θ, for instance, $\underline{B}(\underline{\Phi}_x\cdot\underline{\Phi}_x)$, $\underline{B}(\underline{E}_x^{\theta}\cdot\underline{E}_x^{\theta})$, $\underline{B}(\underline{\Phi}_x\cdot\underline{E}_x^{\theta})$ etc. Allowable homogeneous terms, $\{P_H\}$, in the model for $-\frac{1}{\rho}\overline{\theta\frac{\partial p}{\partial x_i}}$ are then as follows

$$\{P_H\} = \left(\eta_1 + \eta_2\frac{II}{q^4}\right)\frac{\varepsilon}{q^2}\underline{B} + \left(\eta_3 + \eta_4\frac{II}{q^4}\right)\frac{\varepsilon_\theta}{\theta^2}\underline{B} + \left(\eta_5\frac{\varepsilon}{q^4} + \eta_6\frac{\varepsilon_\theta}{\theta^2q^2}\right)\underline{\underline{A}}\cdot\underline{B}$$
$$+ \left(\eta_7\frac{\varepsilon}{q^6} + \eta_8\frac{\varepsilon_\theta}{\theta^2q^4}\right)\underline{\underline{A}}\cdot\underline{\underline{A}}\cdot\underline{B} + \eta_9\underline{B}\cdot\underline{\underline{S}} + \eta_{10}\underline{B}\cdot\underline{\underline{\Omega}} + \{\eta_{11}\underline{\underline{A}}\cdot\underline{\underline{S}}\cdot\underline{B}$$
$$+ \eta_{12}\underline{B}(\underline{\underline{A}}:\underline{\underline{S}}) + \eta_{13}\underline{\underline{S}}\cdot\underline{\underline{A}}\cdot\underline{B} + \eta_{14}\underline{\underline{A}}\cdot\underline{\underline{\Omega}}\cdot\underline{B} + \eta_{15}\underline{\underline{\Omega}}\cdot\underline{\underline{A}}\cdot\underline{B}\}\frac{1}{q^2}. \qquad (27)$$

Inhomogeneous terms, $\{P_I\}$, subject to the restrictions listed above are

$$\{P_I\} = \eta_{19}\underline{E}_x(\underline{B}\cdot\underline{E}_x)\frac{q^4}{\varepsilon^3} + \eta_{40}\underline{\underline{\Phi}}_x{}^2\cdot\underline{B}\frac{q^2}{\varepsilon_\theta} + \eta_{44}\underline{Q}_x\cdot\underline{\underline{B}}_x\frac{q^2}{\varepsilon}$$
$$+ \eta_{45}\underline{Q}_x\,\mathrm{Tr}(\underline{\underline{B}}_x)\frac{q^2}{\varepsilon} + \eta_{47}\underline{E}_x\cdot\underline{\underline{B}}_x\frac{q^4}{\varepsilon^2} + \eta_{51}\underline{\Phi}_x\mathrm{Tr}(\underline{\underline{B}}_x)\frac{q^2}{\varepsilon_\theta} + \eta_{55}\underline{\underline{B}}_x:\underline{\underline{A}}_x\frac{q^2}{\varepsilon}$$
$$+ \eta_{57}\underline{\underline{B}}_x^T\,\mathrm{Tr}_1(\underline{\underline{A}}_x)\frac{q^2}{\varepsilon} + \eta_{62}\,\mathrm{Tr}_2(\underline{\underline{B}}_x{}^2)\frac{q^4}{\varepsilon} + (42\text{ terms}). \qquad (28)$$

A model derived for $-\frac{1}{\rho}\overline{\theta\frac{\partial p^{(1)}}{\partial x_i}}$ by Launder[8] and Lumley[7] was discussed briefly in section IIB. Here, we model $-\frac{1}{\rho}\overline{\theta\frac{\partial p}{\partial x_i}}$ rather than its "component" parts since $p^{(1)}$ and $p^{(2)}$ cannot be distinguished in the general expansion of the functional (14). However, if $p^{(2)}$ is assumed to be independent of the mean flow variables, the equation (11) suggests $\eta_9 = \frac{3}{10}$ and $\eta_{10} = \frac{1}{2}$ and these values may comprise a useful approximation. Their appropriateness will be examined in section IVE using experimental data.

III. PARAMETER EVALUATION FOR HOMOGENEOUS FLOWS

The best way to evaluate the coefficients in the models for each of the higher-order moments is to apply the model first to simple flows, and then proceed systematically to more complicated flows. The general forms generated in the previous section by the invariant modelling approach contain far too many terms to be effectively evaluated with only one type of flow. Unfortunately, there are only a few well documented experimental studies for nonisothermal flows, and our ability to apply this approach is somewhat restricted. In the case of a homogeneous flow, however, there are only two modelled correlations to be considered, namely those given in equations (24) and (27), and the procedure can be applied more efficiently. In the present section, we therefore restrict our attention to homogeneous flows. Following this, in section IV, we shall consider non-homogeneous flows.

Our starting point in evaluating a model for homogeneous flows [i.e. for determining the constants in equations (24) and (27)] is to consider the rate of decay of temperature fluctuations behind a heated grid in a wind tunnel. The most extensive set of data is that of Lin and Lin,[25] who also compared their results with the earlier works of Yeh,[26] Gibson and Schwarz,[27] and Mills et al.[28] The previous studies had obtained decay rates proportional to x^{-n} with n ranging from 0.87 to 1.50 and x representing distance downstream from the grid. However, Lin and Lin's data show clearly that the decay power is a function of the initial intensity of the temperature fluctuations (i.e. the power supplied in heating the

grid).† Thus, it may be surmised that a high initial intensity in the temperature fluctuations provides an initial inhomogeneity or anisotropy, which would have to be considered in interpreting the experimental results. When the initial fluctuations are limited to lower intensities where the homogeneous model may be expected to apply, Hinze's theoretical derivation[29] and Gibson and Schwarz' experiment[27] reveal coincidently that the intensity of a scalar fluctuation will decay as the $-\frac{3}{2}$ power of distance from the grid. If this value is taken as a standard decay power in homogeneous isotropic flow, the relationship between β_1 and β_3 in equation (24) may be calculated as explained below.

Let us assume that $\overline{\theta^2}$ and q^2 decay in a homogeneous isotropic flow as follows

$$\overline{\theta^2} = a_1 x^{-m} \tag{29}$$

$$q^2 = b_1 x^{-n} \tag{30}$$

One may then calculate the dissipation rates by using the relationship between Eulerian spatial derivatives and Langrangian time derivatives following a fluid element

$$\varepsilon_\theta = -\frac{1}{2}\frac{\overline{d\theta^2}}{dt} = -\frac{1}{2} U \frac{\overline{d\theta^2}}{dx} = \frac{a_1}{2} Umx^{-m-1} \tag{31}$$

$$\varepsilon = -\frac{1}{2}\frac{dq^2}{dt} = -\frac{1}{2} U \frac{dq^2}{dx} = \frac{b_1}{2} Unx^{-n-1} \tag{32}$$

For a homogeneous isotropic flow, $\beta_1 \frac{\varepsilon_\theta \varepsilon}{q^2}$ and $\beta_3 \frac{\varepsilon_\theta^2}{\overline{\theta^2}}$ are the only terms that do not vanish in the equations (23), (24) and (25). Thus, equation (8) can be written as

†It may also be anticipated that the decay power will be sensitive to the "drag" characteristics of the grid, or the intensity of the turbulent velocity fluctuations.

$$U \frac{\partial \varepsilon_\theta}{\partial x} = \beta_1 \frac{\varepsilon_\theta \varepsilon}{q^2} + \beta_3 \frac{\varepsilon_\theta^2}{\overline{\theta^2}} \quad . \tag{33}$$

Substituting equations (30), (31) and (32) into equation (33), we find

$$-2(m+1) = n\beta_1 + m\beta_3 \; . \tag{34}$$

Here, $m = 3/2$ as discussed earlier and $n = 1$ from the theoretical derivation for isotropic turbulence (cf. Ref. 29). From careful examination of various experimental data, Cormack also suggested $n = 1$ at large Reynolds number.[17] From equation (34), we thus obtain

$$\beta_1 = -5, \quad \text{if} \quad \beta_3 = 0 \tag{35}$$

and

$$\beta_3 = -10/3, \quad \text{if} \quad \beta_1 = 0 \; . \tag{36}$$

We may of course retain both of the terms involving β_1 and β_3, provided the coefficients β_1 and β_3 satisfy equation (34). However, it is possible that the two terms together will give no better results than either one of them individually, with constants given either by (35) or (36). It is prudent to withhold judgment on this matter in view of the need for simplicity in the resulting model. This will be discussed again in section IV.D.

One other term of the homogeneous model which may be evaluated relatively easily is that associated with $\overline{\theta u_i}\,(q^2/\overline{\theta^2})^{1/2}$. Lumley et al.[6] suggested that in the limit of small anisotropy, i.e., late in the decay, $\overline{\theta u_i}\,(q^2/\overline{\theta^2})^{1/2}$ should decay at the same rate as a_{ij}. Now it is known that the return-to-isotropy term,

$$\Delta_{ij} \equiv \frac{1}{\rho}\left\{ \overline{u_j \frac{\partial p}{\partial x_i}} + \overline{u_i \frac{\partial p}{\partial x_j}} - \frac{2}{3}\delta_{ij} \frac{\partial \overline{u_k p}}{\partial x_k} \right\} ,$$

in a weakly anisotropic flow behaves asymptotically as

$$\Delta_{ij} \sim \frac{\varepsilon}{cq^2} a_{ij} \cdot \tag{37}$$

The constant c was shown by Cormack[17] to be approximately 0.162. Thus, applying Lumley's hypothesis, the coefficient of the leading term $\eta_1 \frac{\varepsilon}{q^2} b_i$ in equation (27) is calculated from equation (4) and (5) to be

$$\eta_1 = -\frac{1}{c} - \frac{1}{2} = -6.67$$

In Fig. 1, the modeled equation (5) with $\eta_1 = -6.67$ is compared with Yeh and Van Atta's experimental results,[30] where the velocity field is nearly homogeneous and isotropic but $\overline{u\theta}$ is slightly anisotropic. The model with $\eta_1 = -6.67$ shows good agreement with the experimental results.

Due to the lack of well documented experimental data for homogeneous flows, we cannot proceed to determine the other coefficients of the homogeneous model. Thus, these coefficients will be evaluated simultaneously with coefficients of the inhomogeneous terms in section IV.

IV. PARAMETER EVALUATION FOR INHOMOGENEOUS FLOWS

A. Available Experimental Data

Five flows with inhomogeneity have been found which may be used to initialize the present model. These are the turbulent boundary layer of Johnson,[31,32,33] the plane jet of Bashir and Uberoi,[34,35] the wake behind a sphere due to Freymuth and Uberoi,[36] the wake behind a cylinder of Freymuth and Uberoi,[37] and the round jet of Antonia et al.[38,39] Besides these, Aihara, Koyama and Morishita[40] studied a round jet of helium and Davies, Keffer and Baines[41] studied a heated plane jet. Unfortunately,

these latter two experimental studies cannot be used directly to determine the coefficients in a model of the type considered here because they lack some of the needed data, for example $\overline{v\theta^2}$ or $\overline{v\theta}$. Though $\overline{v\theta^2}$ and $\overline{v\theta}$ could have been estimated from equations (5) and (6), these flows were not used for the initialization of the present model, in order to maximize the uniformity and consistency of the applied experimental data.

Each of the five chosen flows asymptotically approaches a self-preserving region where the governing equations reduce to ordinary differential equations. The similarity functions and characteristic variables are shown in Table 1.

We have fitted, by a least squares method, the ten similarity functions for each of the four flows with polynomial equations which are smooth up to the second derivative. Since the data are available in discrete form, the most straightforward approach is to approximate derivatives by their finite-difference representations. However, Cormack[17] noted that although this leads to adequate estimates of first derivatives, second derivatives estimated in this manner display an unacceptable random error. Hence, we have used the representation of data points with polynomial equations. When a single polynomial equation cannot properly represent the whole range of flow conditions, a composite form of two equations was used which gave good representation of the function and continuous first and second derivatives over the complete domain. Before describing the use of these polynomial data fits to evaluate model parameters, some additional comments about the various experimental results are necessary.

First, we may note that accurate experiments for wakes and jets with

no appreciable buoyancy should show measured curves for second-order moments which are symmetric or antisymmetric with respect to $\eta = 0$ [where η is a similarity variable (cf. Table 1)]. However, most experimental measurements for wakes and jets do not exactly satisfy this symmetry or antisymmetry. Thus, in these cases, only the half plane, $\eta \geq 0$, was explicitly considered in constructing models. Nevertheless, the polynomial representation of data was fitted to the complete data base after shifting the data for $\eta < 0$ to the plane $\eta > 0$.

Second, we note in the case of the turbulent boundary layer that Johnson[32] measured the dissipation rate ε with an assumption of isotropy which does not exist in the near wall region. A more sophisticated method to determine ε is to measure some (up to five) of the nine contributions to this sum and to assume that isotropy relations may be used to derive the remainder.[42,43,44] Another more recent method is to use the inertial subrange in the spectra.[45,46] Fitting the spectra with a $-\frac{5}{3}$ power law provides a simple relation to calculate ε. Unfortunately, however, Johnson did not measure the spectra, so his experimental data for the turbulent boundary layer in the near wall region cannot be improved. Klebanoff[43] has found that the approximation of local isotropy can be applied for $y/\delta > 0.7$. Thus, only the turbulent boundary layer data in this region have been used in constructing our model.

In the case of the wake behind a circular cylinder, Freymuth and Uberoi[37] did not measure all of the kinematic variables, but the missing data were obtained earlier by Townsend.[47,48] We thus use a composite of the data of Freymouth and Uberoi[37] and Townsend[47,48] in the parameter evaluation for our model. It is disappointing, however, that the measured

values of $\overline{u^2}$ from Freymuth and Uberoi are not in good agreement with those from Townsend. Because of this, it is possible that there will exist a discrepancy between model predictions and experimental data for the cylindrical wake.

It should also be noted that we did not use the turbulent boundary layer data of Johnson[31] for the modeling of $\overline{u_i\theta^2}$ or high-order terms in the ε_θ advection equation. The measured values of $\overline{u_i\theta^2}$ are so small away from the boundary that they are not credible on account of anticipated large relative errors. In addition, since ε_θ becomes very small and changes little along the vertical axis in the region which is far from the boundary, it is difficult to accurately compute the spatial derivative of ε_θ in equation (8).

Finally, we should mention that the correlation $\overline{u_i\theta^2}$ is evaluated directly from measured experimental data. However, since no direct measurements of the higher-order terms in equations (5) and (8) are available, we estimate $\left\{-\frac{1}{\rho}\,\overline{\theta\,\frac{\partial p}{\partial x_i}} - \frac{\partial}{\partial x_j}\,\overline{u_i u_j \theta}\right\}$ in equation (5) and

$$\left\{-\gamma\,\frac{\partial}{\partial x_j}\,\overline{u_j\,\frac{\partial\theta}{\partial x_\ell}\,\frac{\partial\theta}{\partial x_\ell}} - 2\gamma\left[\overline{\frac{\partial u_j}{\partial x_\ell}\,\frac{\partial\theta}{\partial x_\ell}\,\frac{\partial\theta}{\partial x_j}} + \gamma\left(\overline{\frac{\partial^2\theta}{\partial x_j \partial x_\ell}}\right)^2\right]\right\}$$

in equation (8) by evaluating the remaining terms in the equations.

B. Parameter Estimation Scheme

As shown in the section IIC, there are many terms in the present general forms for each higher-order correlation. It is thus imperative to systematically choose the most significant terms (hopefully few in number) and evaluate their parameters. Given a possible combination of terms, we evaluate the optimal parameters of the model in a least squares

sense by minimizing the standard deviation from experimental data. The appropriateness of the model is then judged based on the magnitude of the standard deviation. We focus our attention in the present work on the self-similar domains in each of the five test flows.

To give equal weight to each flow measurement, the total range of the similarity variable was discretized into 20 grid intervals, and all variables were then evaluated at each node point by using interpolation or smooth curve representation of the original experimental data.

Optimal parameters for each modeled term are determined by a least-squares analysis in which we minimize the sum of the deviations between model predictions and experimental data. It is implicitly assumed that every data point of a flow has equal standard deviation and that the standard deviations of different flows are proportional to the root mean square magnitude of the experimental data.

The most direct method of determining the best model for each "unknown" correlation may be to calculate standard deviations for all possible combinations of terms and then choose the model with minimum standard deviation. However, a substantial amount of computation time is required even to evaluate the standard deviations for all possible combinations of three terms, and thus the "direct" scheme suggested above would require a prohibitive amount of computation. For isothermal flow, Cormack[17] generated models for the various unknown correlations by systematically eliminating terms (one by one) which did not significantly increase the standard deviation between experimental data and the best-fit model. For non-isothermal flows, there are too many terms in each model to yield a distinct deviation difference by the elimination of

single terms. Moreover, we are obviously interested in models with a minimum number of terms. Thus we apply a direct filtering method which is based on the assumption that any term which gives consistently good representation of experimental results in an m-term model should be retained in a model with n > m terms. In effect, we assume that the model is gradually improved by adding terms, rather than replacing terms. This assumption reduces the amount of computation required for model initialization to a practical level. It should be noted that cylindrical coordinates were used to derive the basic equations and models for axi-symmetric flow.

C. Parameter Evaluation for $\overline{u_i\theta^2}$

Zeman and Lumley[49] modeled $\overline{u_i\theta^2}$, for zero mean motion, starting from the advection equation for triple correlations. However, a more common model for $\overline{u_i\theta^2}$ is the model of eddy diffusivity.[50,51] To date, the eddy diffusivity model

$$\overline{u_i\theta^2} = -\alpha'\ell q \frac{\overline{\partial\theta^2}}{\partial x_i} \tag{38}$$

is the only one which is sufficiently documented to be compared with our new model. The length scale ℓ in this eddy diffusivity model can be determined from the eddy viscosity model for Reynolds stress.

$$\ell = -\frac{1}{q}\frac{a_{ij}}{S_{ij}} \tag{39}$$

The well-known drawback of this eddy diffusivity model is that it does not work well for flows with multiple velocity and length scales. If a_{ij} does not become zero fast enough where S_{ij} vanishes, the length scale

ℓ increases to infinity. Thus the model is not applicable for a wide range of flow fields. In the following, we describe the procedure to construct a new model from equations (19) - (22) and its comparison with the eddy diffusivity model, equation (38).

First, the standard deviations from experimental data were calculated for each term in equations (19) - (22) using the optimal, least-squares value of the associated parameter. The terms 23, 20, 16 or 14 were found to give the best representations of the data. We then evaluated the standard deviations for all possible combinations of two terms from equations (19) - (22). Not surprisingly, the models with one of terms 23, 20, 16 and 14 were found to give consistently the best results. Hence, to reduce the amount of computation, it was assumed that any model with three or more terms should include at least one of these four terms. Among three-term models, the model with terms 16, 70 and 61 yielded the smallest standard deviation relative to the data. Moreover, models with term 16 show consistently better representation of experimental data than those with terms 23, 20 or 14. Since the best two-term and three-term models with term 16 were always found to include one of 70, 119, 54 or 57, we then examined all possible four-term models with term 16 and at least one of these four terms. In this case, four-term models which include terms 16 and 70 show much less deviation from experimental data than the other combinations. Finally, to propose an optimal five-term model, we investigated the performance of all five-term models with four terms that constituted one of the best ten four-term models.

In consequence, we propose a series of terms 16, 70, 61, 2 and 133 from which one- to five-term models can be constructed sequentially by

adding terms. The optimal parameters and standard deviation for each model are shown in Table 2. Even the three-term model represents experimental data fairly well except for the plane jet. Since the improvement between the four- and five-term models is small, we use the four-term model for comparison with experimental data in Figs. 2.1 - 2.5. One weakness of this model is that, compared with the experimental data, the predicted value of $\overline{u_i\theta^2}$ develops slowly around the center line of wakes and jets and vanishes quickly near the edges. Nevertheless, in general, the model displays a quite good representation of experimental results with relatively few terms.

To compare the eddy diffusivity model with our new model, the coefficient α' in equation (38) was optimized for each flow and for all flows. The results are shown in Table 3. The optimal coefficient varies widely from 0.24 to 1.72, depending on the flow type. In Figs. 2.1 - 2.5, the comparison of our new four-term model and the eddy diffusivity model is also depicted for each flow. Obviously, the four-term model displays a much better representation of experimental data than the eddy diffusivity model. When the gradient of mean velocity disappears more rapidly than Reynolds stress, the eddy diffusivity model increases unreasonably as shown in Fig. 2.3. In the prediction of $\overline{u\theta^2}$, where u is the fluctuating velocity in the downstream direction, $\frac{\partial\theta^2}{\partial x_1}$ is simply incapable of mirroring the characteristics of $\overline{u\theta^2}$. Therefore, the prediction of the eddy diffusivity model is very poor as shown in Fig. 2.5.

D. Parameter Evaluation for the Thermal Fluctuation Dissipation Equation

Many researchers have directly modeled the dissipation rate of fluctuating temperature, ε_θ. For example, by analogy with the eddy diffusivity model for $\overline{u_i\theta}$, Monin and Yaglom[51] proposed a model for ε_θ.

$$\varepsilon_\theta = \frac{1}{2\alpha''}\frac{\overline{\theta^2}q}{\ell} \tag{40}$$

where the length scale, ℓ, can be determined from equation (39). However, in the construction of a second-order model, we implicitly assume that all second-order terms will be obtained by solution of the appropriate transport equations, with third- or higher-order terms in these equations modeled in terms of second- or lower-order terms. Thus, to construct a self-consistent second-order model, it is necessary to model the unknown higher-order terms in the ε_θ transport equation. Lumley[7] suggested a model for the right-hand side of equation (8) in the form

$$\text{R.H.S. of eq. (8)} = -3.73\frac{\varepsilon_\theta^2}{\overline{\theta^2}} + 20.7\frac{\varepsilon^2}{q^6}\,\overline{\theta u_i}\,\overline{\theta u_i} + 1.9\,\varepsilon_\theta\frac{a_{ij}a_{ij}\varepsilon}{q^6} + K\,a_{ij}\frac{\partial U_i}{\partial x_j}\frac{\varepsilon_\theta}{q^2} \tag{41}$$

Here, we construct a second-order model for the right-hand side of ε_θ transport equation from equations (23) - (25) and compare both the new model and Lumley's model with experimental data. As it is very difficult to actually measure the terms on the right-hand side of equation (8), we can only estimate their sum by evaluating the terms on the left-hand side of equation (8). Hence, we model all terms on the right-hand side of equation (8) together.

To begin, we investigate the role of terms 1 and 3 in equation (24) for the overall representation of experimental data, because the relationship between the parameters of these two terms can be obtained from the decay law of $\overline{\theta^2}$ as discussed in section III. The standard deviations from experimental data were computed for all possible two-term models which involved either term 1 with $\beta_1 = -5$ or term 3 with $\beta_3 = \frac{-10}{3}$ [see equations (35) and (36)]. In addition, we calculated the standard deviations of three-term models which included both term 1 and term 3 with parameters β_1 and β_3 satisfying equation (34). It was found that the two-term models with term 3 were always better than those which included term 1. Furthermore, three-term models with term 1 and term 3 together do not significantly improve the representation of experimental data compared with two-term models involving term 3. Therefore, in the interest of simplicity, we included only term 3 with a fixed parameter $\frac{-10}{3}$ in constructing a model for the right-hand side of equation (8).

We next examined all possible two- and three-term models from equations (23) - (25) that include term 3. For two-term models, those with term 3 and one of the terms 5, 6 or 7 in equation (24) showed the best results. Moreover, three-term models involving term 3 and one of the above three terms yielded consistently better representation of experimental data than those with other terms. Apparently term 5, 6 and 7 in equation (24) have similar properties as regards model behavior. However, the models with terms 3 and 5 always give slightly better results than those with term 3 and one of terms 6 and 7 in three- and four-term models. Therefore, it is suggested that term 3 and 5 in equation (24) should be included in any model with two or more terms. Following the

procedural outline of section IV.C, an optimal five-term model was chosen from all possible combinations of five terms which had four terms that were one of the best ten four-term models. From these calculations, we obtain an optimal model with the sequence of terms 3, 5, 33, 48 and 69 in equations (24) and (25). This model does not contain any term in equation (23). However, a model with terms 3, 5, 34 and 48 in equations (24) and (25) and term 8 in equation (23) has a comparable standard deviation. Nevertheless, we chose the former model because a model term in equation (23) must be differentiated in equation (8) and this makes a dynamic computation slightly more complicated. It should be cautioned, however, that this choice does not necessarily mean that $-\gamma \overline{u_i \frac{\partial\theta}{\partial x_\ell} \frac{\partial\theta}{\partial x_\ell}}$ is unimportant. As we do not have experimental data which can distinguish each term in equation (8), we choose a simple overall model for the right-hand side of equation (8).

The optimal parameters and standard deviation of the new model are sequentially tabulated for each level in Table 4. Even the four-term model with terms 3, 5, 33 and 48 in equations (24) and (25) shows relatively good agreement with experimental data except for the case of the plane jet. Predictions for the five-term model are depicted for each flow in Figs. 3.1 - 3.4. For the plane jet, the model decreases more quickly near the edge than the experimental data. One probable explanation is that experimental errors are relatively large near the edge due to the small values of dynamic variables. For the wake behind a cylinder, the model displays a physically improbable deflection in Fig. 3.3. However, this might occur because of the discrepancy between the two experiments by

Freymuth and Uberoi[37] and Townsend,[47,48] which were used by us to generate a "complete" data set. In spite of these deviations between data and predictions, the model proposed seems to be generally satisfactory.

The five-term model was also compared with Lumley's model in Figs. 3.1 - 3.4 and Table 5. Lumley's model with his suggested parameters shows reasonably good prediction for the wake behind a sphere, but is relatively poor for the other flows. By optimizing the parameters using the present collection of experimental data, Lumley's model is improved with regard to the deviation from experiment. However, Lumley's model is still very poor in predicting the right-hand side of ε_θ transport equation for the round jet as shown in Fig. 3.4. This is perhaps not surprising in view of the fact that Lumley's model is essentially a homogeneous one.

E. Parameter Evaluation for $\left\{ - \frac{1}{\rho} \overline{\theta \frac{\partial p}{\partial x_i}} - \frac{\partial}{\partial x_j} \overline{u_i u_j \theta} \right\}$

Although the term, $- \frac{1}{\rho} \overline{\theta \frac{\partial p}{\partial x_i}}$, is very difficult to measure experimentally and well documented data for $\overline{u_i u_j \theta}$ are not available at present, $\left\{ - \frac{1}{\rho} \overline{\theta \frac{\partial p}{\partial x_i}} - \frac{\partial}{\partial x_j} \overline{u_i u_j \theta} \right\}$ can be estimated by difference in equation (5). $- \frac{1}{\rho} \overline{\theta \frac{\partial p}{\partial x_i}}$ and $- \frac{\partial}{\partial x_j} \overline{u_i u_j \theta}$ have, in appearance, different characteristics in the sense that the former is a second-order correlation of fluctuating temperature and fluctuating pressure, while the latter is a third-order correlation of fluctuating velocity and fluctuating temperature. Of course, the pressure field is associated with the velocity field. Indeed, as shown in equation (9), p can be directly related not only to the

fluctuating velocity component but also to the mean velocity gradient. Using this result, several leading terms of a model for $-\frac{1}{\rho}\,\theta\,\overline{\frac{\partial p}{\partial x_i}}$ were evaluated in section II.B.

The only model available in the literature is that of Launder[8] who suggested the following form for $-\frac{1}{\rho}\,\theta\,\overline{\frac{\partial p}{\partial x_i}}$

$$-\frac{1}{\rho}\,\theta\,\overline{\frac{\partial p}{\partial x_i}} = \frac{4}{5}\,\overline{\theta u_\ell}\,\frac{\partial U_i}{\partial x_\ell} - \frac{1}{5}\,\overline{\theta u_\ell}\,\frac{\partial U_\ell}{\partial x_i} - 8.0\,\frac{\varepsilon}{q^2}\,\overline{u_i\theta} + 6.0\,a_{i\ell}\,\overline{u_\ell\theta}\,\frac{\varepsilon}{q^4} \qquad (42)$$

In addition, by ad hoc assumption, he proposed a model for $-\overline{u_i u_j \theta}$.

$$-\overline{u_i u_j \theta} = \frac{0.11}{2}\,\frac{q^2}{\varepsilon}\left(\overline{u_j u_\ell}\,\frac{\partial \overline{u_i\theta}}{\partial x_\ell} + \overline{u_i u_\ell}\,\frac{\partial \overline{u_j\theta}}{\partial x_\ell}\right) \qquad (43)$$

In the present sub-section, we develop a new model for $\left\{-\frac{1}{\rho}\,\theta\,\overline{\frac{\partial p}{\partial x_i}} - \frac{\partial}{\partial x_\ell}\,\overline{u_i u_\ell \theta}\right\}$ from equations (26) - (28). As previously mentioned, several parameters of the model were determined in section II and III, namely $\eta_1 = -6.67$, $\eta_9 = \frac{3}{10}$, and $\eta_{10} = \frac{1}{2}$ in equation (27). Hereafter, reference to a term number with parenthesis is for equation (26), while that without parenthesis is for equations (27) and (28). As an initial step, we investigated the suitability of the homogeneous terms and parameters for inhomogeneous flows. We found that term 1 is very important and the parameter $\eta_1 = -6.67$ is very close to the optimal value with regard to the data for inhomogeneous flows. On the other hand, terms 9 and 10 do not improve the model much in comparison with the experimental data and the optimal values of parameters are different from the values derived in section II.B. The best <u>five</u>-term model with $\eta_1 = 6.67$, $\eta_9 = 3/10$ and $\eta_{10} = 1/2$ is compared in Table 7 with the best <u>three</u>-term model with

η_1 = - 6.67 and the other parameters freely chosen. The deviation of the five-term model relative to experimental data is slightly higher than that of the three-term model, and the two added terms are the same with nearly equal optimal parameters in the two models. The obvious implication is that 9 and 10 are not significant in the model especially for inhomogeneous flow. Since experimental data for homogeneous flows are not available to examine the significance of these terms in that case, the homogeneous terms 9 and 10 were not included in the construction of a new model.

To propose a model which can be improved sequentially by adding terms, we first evaluated the standard deviation from data for all possible two-term models which included term 1 with η_1 = - 6.67. The best two-term model is a model with terms 1 and 13. Furthermore, we examined all three-term models with η_1 = - 6.67. Three-term models which involve terms 1 and 13 consistently yielded the best representations of experimental data. A three-term model with terms 1, 13 and 62 is good enough to be applied to dynamic computation (see Table 6). However, to investigate the performance of four-term models, we evaluated the standard deviations for all possible four-term models with terms 1 and 13. Additionally, we also calculated the standard deviations for all five-term models which had four terms that constituted one of the best ten four-term models. From these results, we obtained two five-term models which can be improved starting from one-term by sequentially adding terms. Those are the series of terms 1, 13, 62, 40 and 51 and that of terms 1, 13, (4), 45 and 57. Although the latter is slightly better for four- or five-term models than the former, the former is recommended for initial computational purposes because it can represent

experimental data satisfactorily even with terms 1, 13 and 62.

The optimal parameters for the two-term to five-term models from terms 1, 13, 62, 40 and 51 are shown in Table 6, and the three-term model with terms 1, 13 and 62 is compared with experimental data in Figs. 4.1 - 4.7. The overall prediction is very good except for the plane jet. Bashir and Uberoi[34] calculated $\overline{v\theta}$ from the mean heat transfer equation (3) and noticed a big disagreement between the calculated and measured values of $\overline{v\theta}$. Bashir[35] suspected that it might be attributed to a departure of the experiment from two-dimensionality. We calculated $\left\{ -\frac{1}{\rho}\,\overline{\theta\,\frac{\partial p}{\partial x_i}} - \frac{\partial}{\partial x_\ell}\,\overline{u_i u_\ell \theta} \right\}$ from the $\overline{u_i\theta}$ transport equation. Therefore, if two-dimensionality is not satisfied in the experiment, some discrepancy would naturally occur between the model and experimental data. We thus recalculated the model parameters, using $\overline{v\theta}$ for the plane jet calculated from equation (3) and the experimental data for the other variables. The results are shown in Table 6 and Fig. 4.3. As hypothesized, the model improves substantially for "prediction" of the plane jet. For the other flows, there is no difference in the representation of the model because the optimal parameters remain almost the same.

Finally, the three-term model with terms 1, 13 and 62 was compared with Launder's model, equations (42) and (46) in Figs. 4.1 - 4.7 and Table 7. We used his model with suggested parameters and with optimized parameters to minimize the deviation from the present experimental data. In general, even though his model consists of 5 terms, the present three-term model provides a much better representation of the experimental data. Launder's model is especially poor for $\left(-\frac{1}{\rho}\,\overline{\theta\,\frac{\partial p}{\partial x_2}} - \frac{\partial}{\partial x_\ell}\,\overline{u_\ell u_2 \theta} \right)$ in the

turbulent boundary layer, where the difference between data and the model is almost one order of magnitude (see Fig. 4.1).

V. CONCLUSIONS

A second-order model for nonisothermal flow with negligible buoyancy effects has been extensively studied using the invariant modelling method. Unfortunately, this approach generates so many model terms that there are uncertainties in filtering a few significant terms. Nevertheless, the objective of constructing practical models with minimal ad hoc assumptions was fulfilled by careful examination of model terms on the basis of experimental data from flows of various kinds. For the estimation of model parameters, we used the experimental data of the turbulent boundary layer due to Johnson,[31] the plane jet due to Bashir and Uberoi,[34] the wake behind a sphere due to Freymuth and Uberoi,[36] the wake behind a cylinder due to Freymuth and Uberoi[37] and the round jet due to Antonia et al.[38,39]

The results are

$$\overline{u_i\theta^2} = -1.73\, b_i b_\ell \frac{\partial \varepsilon_\theta}{\partial x_\ell} \frac{\overline{\theta^2}}{\varepsilon_\theta^2} - 0.109\, b_i \frac{\partial b_\ell}{\partial x_m} S_{\ell m} \frac{\overline{\theta^2 q^2}}{\varepsilon \varepsilon_\theta} - 0.0230\, b_\ell b_m \frac{\partial \varepsilon}{\partial x_\ell} S_{mi} \frac{q^4}{\varepsilon^3} - 0.0152 \frac{\partial \overline{\theta^2}}{\partial x_i} \frac{\overline{\theta^2 q^2}}{\varepsilon_\theta}$$

$$\text{R.H.S. of } \varepsilon_\theta \text{ transport eq.} = \frac{-10}{3} \frac{\varepsilon_\theta^2}{\overline{\theta^2}} + 36.3\, b_\ell b_\ell \frac{\varepsilon_\theta \varepsilon}{\overline{\theta^2} q^4} + 0.0309 \frac{\partial^2 \overline{\theta^2}}{\partial x_\ell \partial x_\ell} q^2 + 0.480\, a_{\ell m} \frac{\partial \overline{\theta^2}}{\partial x_\ell \partial x_m} \frac{\varepsilon_\theta q^2}{\varepsilon \overline{\theta^2}} - 0.544 \frac{\partial \overline{\theta^2}}{\partial x_\ell} \frac{\partial a_{\ell m}}{\partial x_m}$$

$$\left\{ -\frac{1}{\rho}\,\overline{\theta\,\frac{\partial p}{\partial x_i}} - \frac{\partial}{\partial x_\ell}\,\overline{u_\ell u_i \theta} \right\} = -6.67\, b_i \frac{\varepsilon}{q^2} + 9.71\, S_{i\ell} a_{\ell m} b_m + 0.179 \frac{\partial^2 b_\ell}{\partial x_i \partial x_\ell} \frac{q^4}{\varepsilon}$$

where $b_i = \overline{u_i \theta}$.

As suggested earlier, these recommended models should now be tested and further refined by application in a full dynamical calculation.

Bibliography

1. W. C. Reynolds, Adv. in Chem. Eng. 9, 193 (1974).
2. W. C. Reynolds, Annual Rev. of Fluid Mech., 183 (1976).
3. P. Y. Chou, Q. Appl. Math. 3, 31 (1945).
4. J. Rotta, Z. für Physik 129, 547 (1951).
5. J. Rotta, Z. für Physik 132, 51 (1951).
6. J. L. Lumley and B. Khajeh-Nouri, Adv. in Geophysics 18A, 169 (1974).
7. J. L. Lumley, 'Prediction Methods for Turbulent Flows,' Lecture Series 76, von Karman Inst. of Fluid Mech. (1975).
8. B. E. Launder, 'Progress in the Modelling of Turbulent Transport,' Lecture Series 76, von Karman Inst. of Fluid Mech. (1975).
9. B. E. Launder, G. J. Reece and W. Rodi, J. Fluid Mech. 68, 537 (1975).
10. K. Hanjalic and B. E. Launder, J. Fluid Mech. 52, 609 (1972).
11. B. J. Daly and F. H. Harlow, Phys. Fluids 13. 2634 (1970).
12. C. C. Shir, J. Atmos. Sci. 30, 1327 (1973).
13. C. du P. Donaldson, AIAA J. 10, 4 (1972).
14. J. C. Wyngaard, O. R. Cote and K. S. Rao, Adv. in Geophysics 18A, 193 (1974).
15. J. C. Wyngaard, S. P. S. Arya and O. R. Cote, J. Atm. Sci. 31, 747 (1974).
16. J. C. Wyngaard and O. R. Cote, Boundary Layer Meteorology 7, 289 (1974).
17. D. Cormack, Ph.D. Thesis, Calif. Inst. of Tech. (1975).
18. P. E. Wood, Ph.D. Thesis, Calif. Inst. of Tech. (1978).
19. H. Schlichting, Boundary Layer Theory, McGraw Hill, New York (1968).
20. H. Tennekes and J. L. Lumley, A First Course in Turbulence, M.I.T. Press, Cambridge, Massachusetts (1972).

21. H. P. Robertson, Proc. Camb. Phil. Soc. 36, 209 (1940).

22. B. D. Coleman and W. Noll, Ann. N.Y. Acad. Sci. 89, 672 (1961).

23. J. L. Lumley, Phys. Fluids 10, 1405 (1967).

24. J. L. Lumley, J. Fluid Mech. 41, 413 (1970).

25. S-C. Lin and S-C. Lin, Phys. Fluids 16, 1587 (1973).

26. T. T. Yeh, Ph.D. Thesis, Univ. of Calif., San Diego (1971).

27. C. H. Gibson and W. H. Schwartz, J. Fluid Mech. 16, 365 (1963).

28. R. R. Mills, Jr., A. L. Kistler, V. O. O'Brien and S. Corrsin, NACA TN-4288 (1959).

29. J. O. Hinze, Turbulence, McGraw Hill, New York (1975).

30. T. T. Yeh and C. W. Van Atta, J. Fluid Mech. 58, 233 (1973).

31. D. S. Johnson, OSR Technical Note 55-289, Johns Hopkins University (1955).

32. D. S. Johnson, J. Appl. Mech. 26, 325 (1959).

33. D. S. Johnson and N. J. Whippany, J. Appl. Mech. 24, 2 (1957).

34. J. Bashir and M. S. Uberoi, Phys. Fluids 18, 405 (1975).

35. J. Bashir, Ph.D. Thesis, Univ. of Colorado (1973).

36. P. Freymuth and M. S. Uberoi, Phys. Fluids 16, 161 (1973).

37. P. Freymuth and M. S. Uberoi, Phys. Fluids 14, 2574 (1971).

38. R. A. Antonia, A. Prabhu and S. E. Stephenson, J. Fluid Mech. 72, 455 (1975).

39. R. A. Antonia and A. Prabhu, AIAA Journal 14, 221 (1976).

40. Y. Aihara, H. Koyama and E. Morishita, Phys. Fluids 17, 665 (1974).

41. A. E. Davies, J. F. Keffer and W. D. Baines, Phys. Fluids 18, 770 (1975).

42. J. Lauffer, NACA Report 1174 (1954).

43. P. S. Klebanoff, NACA Report 1247 (1955).

44. I. Wygnaski and H. E. Fiedler, J. Fluid Mech. 41, 237 (1970).

45. P. Bradshaw, NPL Aero, Rep. 1220 (1967).

46. P. Bradshaw, Aero. Res. Counc. R. & M. 3603 (1967).

47. A. A. Townsend, The Structure of Turbulent Shear Flow, Cambridge Univ. Press, Cambridge, England (1956).

48. A. A. Townsend, J. Sci. Res. 2 (ser. A), 451 (1949).

49. O. Zeman and J. L. Lumley, J. Atm. Sci. 33, 1974 (1976).

50. P. A. Libby, Phys. Fluids 19, 494 (1976).

51. A. S. Monin and A. M. Yaglom, Statistical Fluid Mechanics, Vols. 1 and 2, M.I.T. Press, Cambridge (1971).

52. M. S. Uberoi and P. Freymuth, Phys. Fluids 13, 2205 (1970).

53. M. S. Uberoi and P. Freymuth, Phys. Fluids 12, 1359 (1969).

Table 1. Characteristic Variables and Similarity Functions.

Similarity Functions:

$$U = U_c f_1(\eta), \quad \Theta = \Theta_c f_2(\eta), \quad (\overline{u^2})^{1/2} = U_c f_3(\eta)$$

$$(\overline{v^2})^{1/2} = U_c f_4(\eta), \quad (\overline{\omega^2})^{1/2} = U_c f_5(\eta), \quad \overline{uv} = U_c^2 f_c(\eta)$$

$$\overline{v\theta} = U_c \Theta_c f_7(\eta), \quad (\overline{\theta^2})^{1/2} = \Theta_c f_8(\eta), \quad \varepsilon = (U_c^3/L_c) f_g(\eta)$$

$$\varepsilon_\theta = (U_c \Theta_c^2 / L_c) f_{10}(\eta) \qquad \text{where } \eta = y/Lc$$

Characteristic Variables:

	Flow	L_c	U_c	Θ_c	Reference
1.	Turbulent Boundary Layer	$\delta(x)$: boundary layer thickness	U_o = Const.	$T_w - T_o$ = Const.	Johnson[31,32]
2.	Plane Jet	$x - x_o$	$U_o \left(\frac{x - x_o}{d}\right)^{-1/2}$	$\Theta_o \left(\frac{x - x_o}{d}\right)^{-1/2}$	Bashir & Uberoi[34] Bashir[35]
3.	Wake Behind a Sphere	$d \left(\frac{x - x_o}{d}\right)^{1/3}$	$U_o \left(\frac{x - x_o}{d}\right)^{-2/3}$	$\Theta_o \left(\frac{x - x_o}{d}\right)^{-2/3}$	Freymuth & Uberoi[36] Uberoi & Freymuth[52]
4.	Wake behind a Cylinder	$\{d(x - x_o)\}^{1/2}$	$U_o \left(\frac{x - x_o}{d}\right)^{-1/2}$	$\Theta_o \left(\frac{x - x_o}{d}\right)^{-1/2}$	Freymuth & Uberoi[37] Uberoi & Freymuth[53]
5.	Round Jet	$x - x_o$	$U_o \left(\frac{x - x_o}{d}\right)^{-1}$	$\Theta_o \left(\frac{x - x_o}{d}\right)^{-1}$	Antonia et al.[38,39]

Table 2. Model for $\overline{u_i\theta^2}$.

Parameters in Eqs. (19) - (22)	α_{16}	α_{70}	α_{61}	α_{2}	α_{133}	Standard Deviation
one-term model	-0.437					0.723
two-term model	-1.01	-0.0805				0.649
three-term model	-2.04	-0.134	-0.0270			0.369
four-term model	-1.73	-0.109	-0.0230	-0.0152		0.313
five-term model	-1.78	-0.115	-0.0245	-0.0164	0.0229	0.281

Table 3. Parameter of eddy diffusivity model for $\overline{u_i\theta^2}$.

Flows Included in Parameter Estimation	Optimal Parameter in Eq. (38)	Standard Deviation
Plane jet	1.35	0.624
Wake behind a sphere	1.09	0.641
Wake behind a cylinder	0.291	0.880
Round jet - $\overline{v\theta^2}$	1.72	0.669
$\overline{u\theta^2}$	0.239	0.999
All flows	0.564	0.773

Table 4. Model for R.H.S. of ε_θ transport equation.

Parameters in Eqs. (24) & (25)	β_3	β_5	β_{33}	β_{48}	β_{69}	Standard Deviation
two-term model	$\frac{-10}{3}$	47.4				0.662
three-term model	$\frac{-10}{3}$	46.7	0.0161			0.602
four-term model	$\frac{-10}{3}$	40.5	0.0334	0.522		0.382
five-term model	$\frac{-10}{3}$	36.3	0.0309	0.480	-0.544	0.264

Table 5. Comparison of Models for R.H.S. of ε_θ Transport Equation.

Parameters in Equations (24) & (25)	β_3	β_2	β_5	β_7	β_{33}	β_{48}	β_{69}	$a_{ij}\frac{\partial U_i}{\partial x_j}\frac{\varepsilon_\theta}{q^2}$ †	Standard Deviation
Lumley's (1975) Model with suggested parameter	-3.73	1.9		20.7				-256.*	1.38
Lumley's (1975) Model with optimized parameter	-3.73**	13.8		82.2				118.	0.623
Five-term Model	$\frac{-10}{3}$		36.3		0.0309	0.480	-0.544		0.264

†This term was not included in equation (24)

*This term was optimized with present experimental data since it was not reported by the author.

**Term 3 is determined from the decay law of fluctuating sealer therefore, it was not optimized.

Table 6. Model for $-\frac{1}{\rho}\theta\overline{\frac{\partial p}{\partial x_i}} + \frac{\partial}{\partial x_\ell}\overline{u_\ell u_i \theta}$.

Parameters in Eq. (27) & (28)	η_1	η_{13}	η_{62}	η_{40}	η_{51}	Standard Deviation
two-term model	-6.67	11.7				0.444
		(11.8)*				(0.382)
three-term model	-6.67	9.71	0.179			0.291
		(9.69	0.157)			(0.225)
four-term model	-6.67	10.3	0.148	0.166		0.281
		(10.2	0.125	0.176)		(0.204)
five-term model	-6.67	10.7	0.0873	0.328	-0.397	0.259
		(10.4	0.0816	0.273	-0.299)	(0.183)

*Model parameters with parenthesis were determined with calculated data of $\overline{u_i\theta}$ for the plane jet and experimental data for the others.

Table 7. Comparison of Models for $\left\{ -\frac{1}{\rho}\ \overline{\theta \frac{\partial p}{\partial x_i}} + \frac{\partial}{\partial x_\ell}\ \overline{u_\ell u_i \theta} \right\}$.

Term N_o in Eqs. (27) & (28)	η_9	η_{10}	η_1	η_5	η_{13}	η_{62}	*	Standard Deviation
Launder's (1975) Model with Suggested Parameters	$\frac{3}{10}$	$\frac{1}{2}$	- 8.0	6.0			0.055	0.697
Launder's (1975) Model with optimized parameters	$\frac{3}{10}$	$\frac{1}{2}$	-19.0	23.2			0.140	0.514
Three-Term Model			- 6.67		9.71	0.179		0.291
Five-Term Model with Fixed Parameters of terms 1, 9 and 10.	$\frac{3}{10}$	$\frac{1}{2}$	- 6.67		8.02	0.192		0.329

*$\frac{\partial}{\partial x_m}\left[\frac{q^2}{\varepsilon}\left(\overline{u_m u_\ell}\ \frac{\partial \overline{u_i \theta}}{\partial x_\ell} + \overline{u_i u_\ell}\ \frac{\partial \overline{u_m \theta}}{\partial x_\ell}\right)\right] \equiv \frac{\partial}{\partial x_m}\left[\left\{\text{term 15} + \frac{1}{3}\ (\text{term 1})\right\}\ \text{in equation (26)}\right]$.

Figure Captions

Fig. 1 Comparison of model with Yeh and Van Atta's experimental results.[30]

Fig. 2 Comparison of $\overline{v\theta^2}$ models for a plane jet.

□ : experimental data by Bashir and Uberoi.[34]

-Δ- : four term model.

-+- : eddy diffusivity model with coeff. optimized for all flows.

-x- : eddy diffusivity model with coeff. optimized only for a plane jet.

Fig. 2.2 Comparison of $\overline{v\theta^2}$ models for a wake behind a sphere.

□ : experimental data by Freymuth and Uberoi.[36]

-Δ- : four term model.

-+- : eddy diffusivity model with coeff. optimized for all flows.

-x- : eddy diffusivity model with coeff. optimized only for a wake behind a sphere.

Fig. 2.3 Comparison of $\overline{v\theta^2}$ models for a wake behind a cylinder.

□ : experimental data by Freymuth and Uberoi.[37]

-Δ- : four term model

-+- : eddy diffusivity model with coeff. optimized for all flows.

-x- : eddy diffusivity model with coeff. optimized only for a wake behind a cylinder.

Fig. 2.4 Comparison of $\overline{v\theta^2}$ models for a round jet.

□ : experimental data by Antonia et al.[38]

-Δ- : four term model.

-+- : eddy diffusivity model with coeff. optimized for all flows.

-x- : eddy diffusivity model with coeff. optimized only for a round jet.

Fig. 2.5 Comparison of $\overline{u\theta^2}$ models for a round jet.

□ : experimental data by Antonia et al.[38]

-△- : four-term model.

-+- : eddy diffusivity model with coeff. optimized for all flows.

-x- : eddy diffusivity model with coeff. optimized only for a round jet.

Fig. 3.1 Comparison of models for R.H.S. of ε_θ transport equation for a plane jet.

□ : experimental data by Bashir and Uberoi.[34]

-◇- : five-term model.

-+- : Lumley's model with suggested parameters.

-x- : Lumley's model with modified parameters.

Fig. 3.2 Comparison of models for R.H.S. of ε_θ transport equation for a wake behind a sphere.

□ : experimental data by Freymuth and Uberoi.[36]

-◇- : five-term model.

-+- : Lumley's model with suggested parameters.

-x- : Lumley's model with modified parameters.

Fig. 3.3 Comparison of models for R.H.S. of ε_θ transport equation for a wake behind a cylinder.

□ : experimental data by Freymuth and Uberoi.[37]

-◇- : five-term model.

-+- : Lumley's model with suggested parameters.

-x- : Lumley's model with modified parameters.

Fig. 3.4 Comparison of models for R.H.S. of ε_θ transport equation for a round jet.

□ : experimental data by Antonia et al.[38]

-◇- : five-term model.

-+- : Lumley's model with suggested parameters.

-x- : Lumely's model with modified parameters.

Fig. 4.1 Comparison of $\left\{ -\frac{1}{\rho}\,\theta\,\overline{\frac{\partial p}{\partial x_i}} - \frac{\partial}{\partial x_\ell}\,\overline{u_i u_\ell \theta} \right\}$ models for a turbulent boundary layer (i = 2).

□ : experimental data by Johnson.[31]

-Δ- : three-term model.

-x- : Launder's model with suggested parameters.

-+- : Launder's model with modified parameters.

Fig. 4.2 Comparison of $\left\{ -\frac{1}{\rho}\,\theta\,\overline{\frac{\partial p}{\partial x_i}} - \frac{\partial}{\partial x_\ell}\,\overline{u_i u_\ell \theta} \right\}$ models for a turbulent boundary layer (i = 1).

□ : experimental data by Johnson.[31]

-Δ- : three-term model.

-x- : Launder's model with suggested parameters.

-+- : Launder's model with modified parameters.

Fig. 4.3 Comparison of $\left\{ -\frac{1}{\rho}\,\overline{\theta\,\frac{\partial p}{\partial x_i}} - \frac{\partial}{\partial x_\ell}\,\overline{u_i u_\ell \theta} \right\}$ models for a plane jet ($i = 2$).

⊡ : experimental data by Bashir and Uberoi.[34]

-Δ- : three-term model.

-x- : Launder's model with suggested parameters.

-+- : Launder's model with modified parameters.

--- : three-term model based on calculated values of parameters for a plane jet.

Fig. 4.4 Comparison of $\left\{ -\frac{1}{\rho}\,\overline{\theta\,\frac{\partial p}{\partial x_i}} - \frac{\partial}{\partial x_\ell}\,\overline{u_i u_\ell \theta} - \frac{1}{r}\,(\overline{u_r^2 \theta} - \overline{u_\theta^2 \theta}) \right\}$ models for a wake behind a sphere ($i = r$).

⊡ : experimental data by Freymuth and Uberoi.[36]

-Δ- : three-term model.

-x- : Launder's model with suggested parameters.

-+- : Launder's model with modified parameters.

Fig. 4.5 Comparison of $\left\{ -\frac{1}{\rho}\,\overline{\theta\,\frac{\partial p}{\partial x_i}} - \frac{\partial}{\partial x_\ell}\,\overline{u_i u_\ell \theta} \right\}$ models for a wake behind a cylinder ($i = 2$).

⊡ : experimental data by Freymuth and Uberoi.[37]

-Δ- : three-term model.

-x- : Launder's model with suggested parameters.

-+- : Launder's model with modified parameters.

Fig. 4.6 Comparison of $\left\{ -\frac{1}{\rho}\,\theta\,\frac{\partial p}{\partial x_i} - \frac{\partial}{\partial x_\ell}\,\overline{u_\ell u_i \theta} - \frac{1}{r}\,(\overline{u_r^2 \theta} - \overline{u_\theta^2 \theta}) \right\}$ models for a round jet (i = 2).

⊡ : experimental data by Antonia et al.[38]

-Δ- : three-term model.

-x- : Launder's model with suggested parameters.

-+- : Launder's model with modified parameters.

Fig. 4.7 Comparison of $\left\{ -\frac{1}{\rho}\,\theta\,\frac{\partial p}{\partial x_i} - \frac{\partial}{\partial x_\ell}\,\overline{u_i u_\ell \theta} - \frac{1}{r}\,\overline{u_x u_r \theta} \right\}$ models for a round jet (i = 1).

⊡ : experimental data by Antonia et al.[38]

-Δ- : three-term model.

-x- : Launder's model with suggested parameters.

-+- : Launder's model with modified parameters.

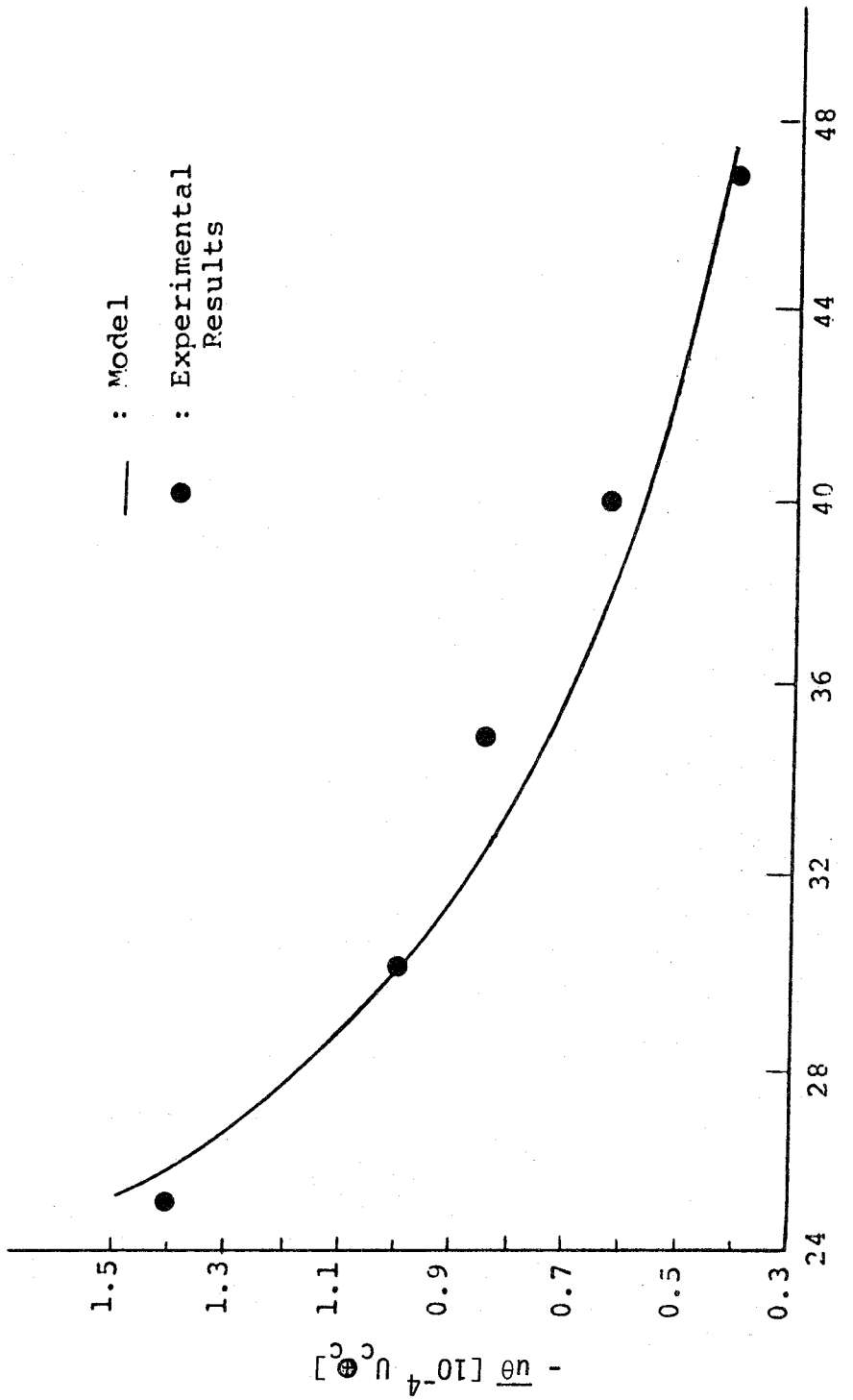
: Model
: Experimental Results
$-\overline{u\theta}\ [10^{-4}\ U_c\theta_c]$
1.5
1.3
1.1
0.9
0.7
0.5
0.3
24
28
32
36
40
44
48
x/ℓ_c

Fig. 1

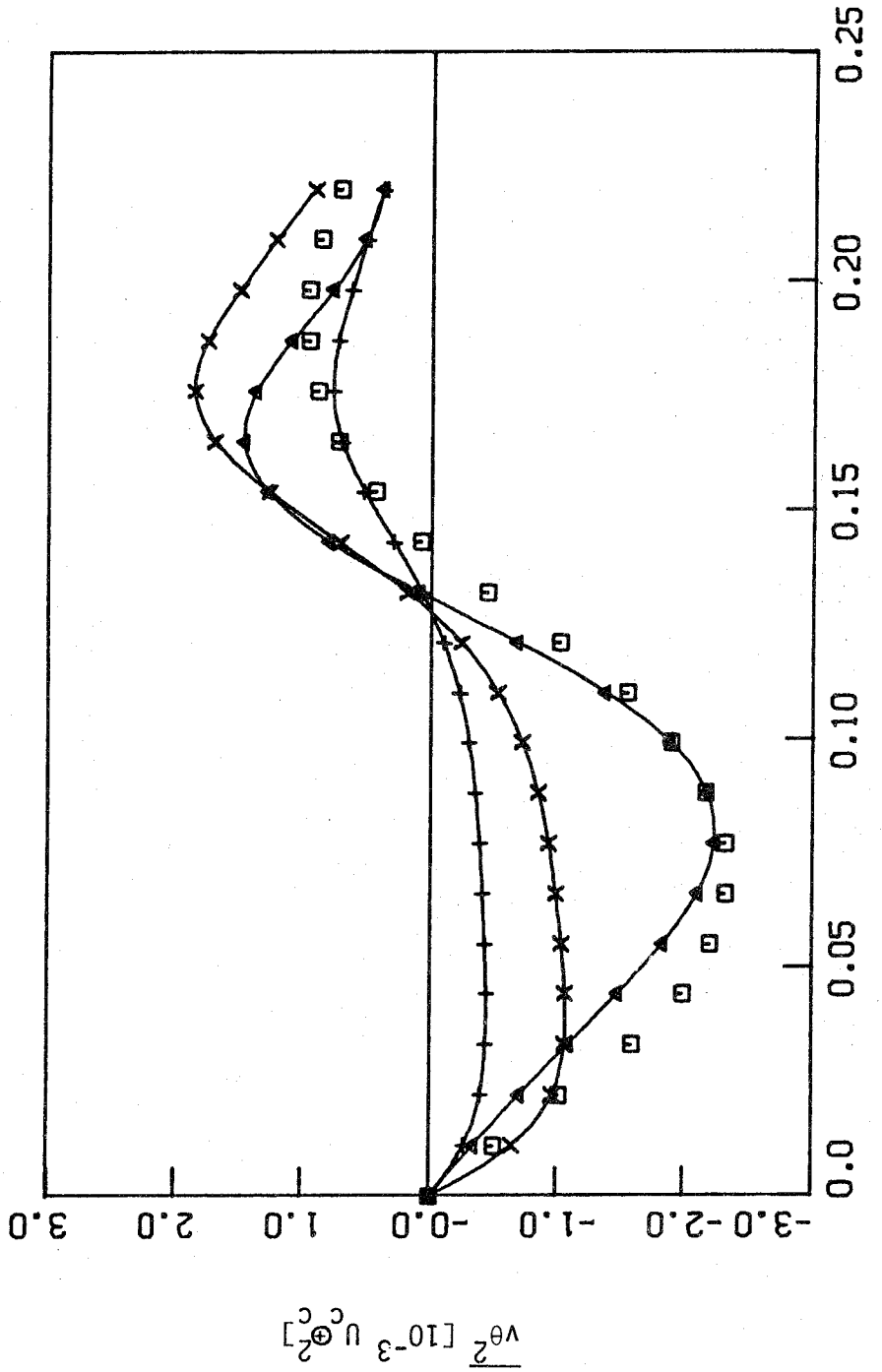
-3.0
-2.0
-1.0
-0.0
1.0
2.0
3.0
0.0
0.05
0.10
0.15
0.20
0.25
η
$\overline{v\theta^2}$ [10^{-3} $u_c\Theta_c^2$]

Fig. 2.1

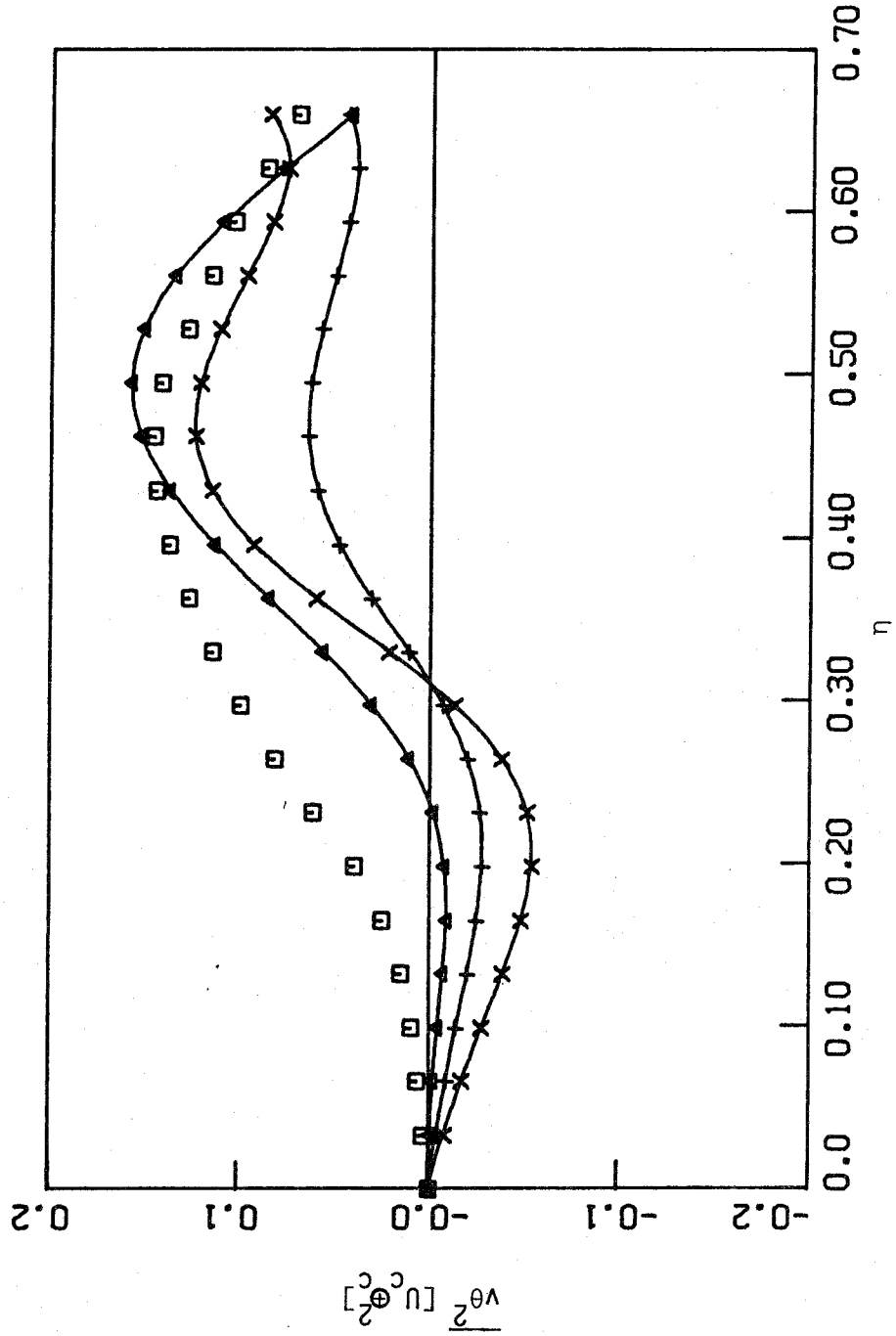
0.70
0.60
0.50
0.40
0.30
0.20
0.10
0.0
η
-0.2
-0.1
-0.0
0.1
0.2
$\overline{v\theta^2}$ [$U_c\theta_c^2$]

Fig. 2.2

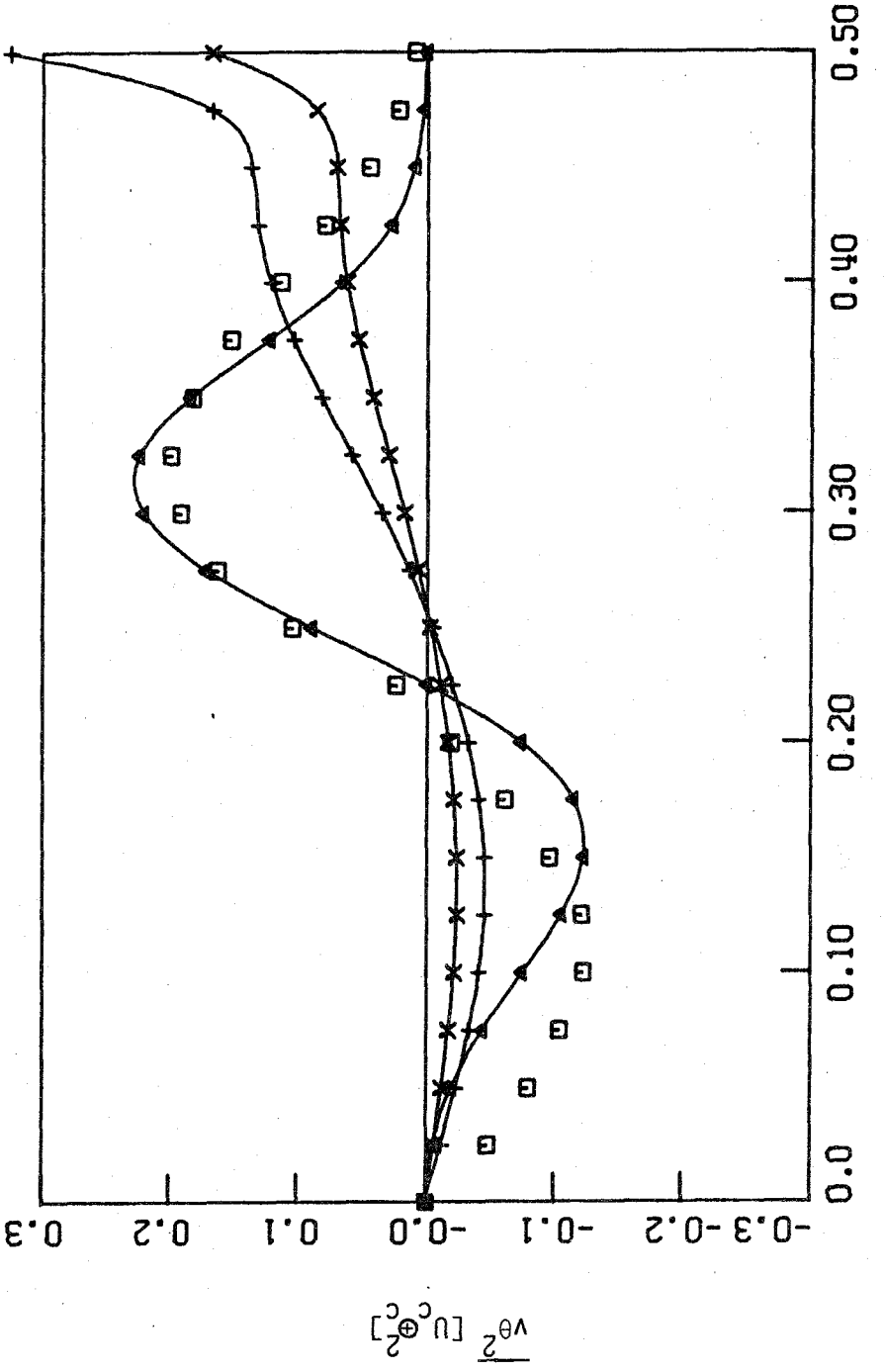
0.0
0.10
0.20
0.30
0.40
0.50
η
-0.3
-0.2
-0.1
-0.0
0.1
0.2
0.3
$\overline{v\theta^2}$ [$U_c\Phi_c^2$]

Fig. 2.3

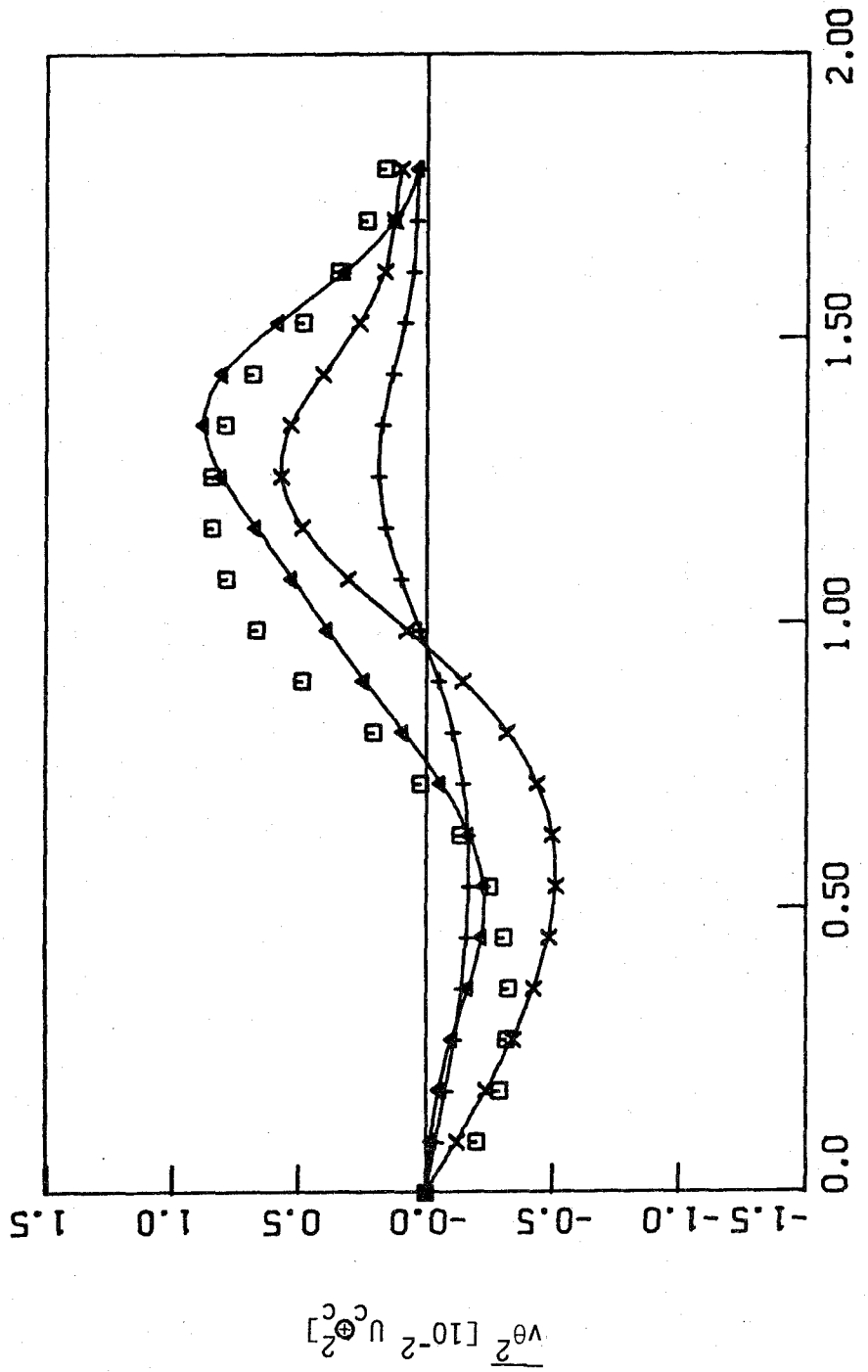

Fig. 2.4

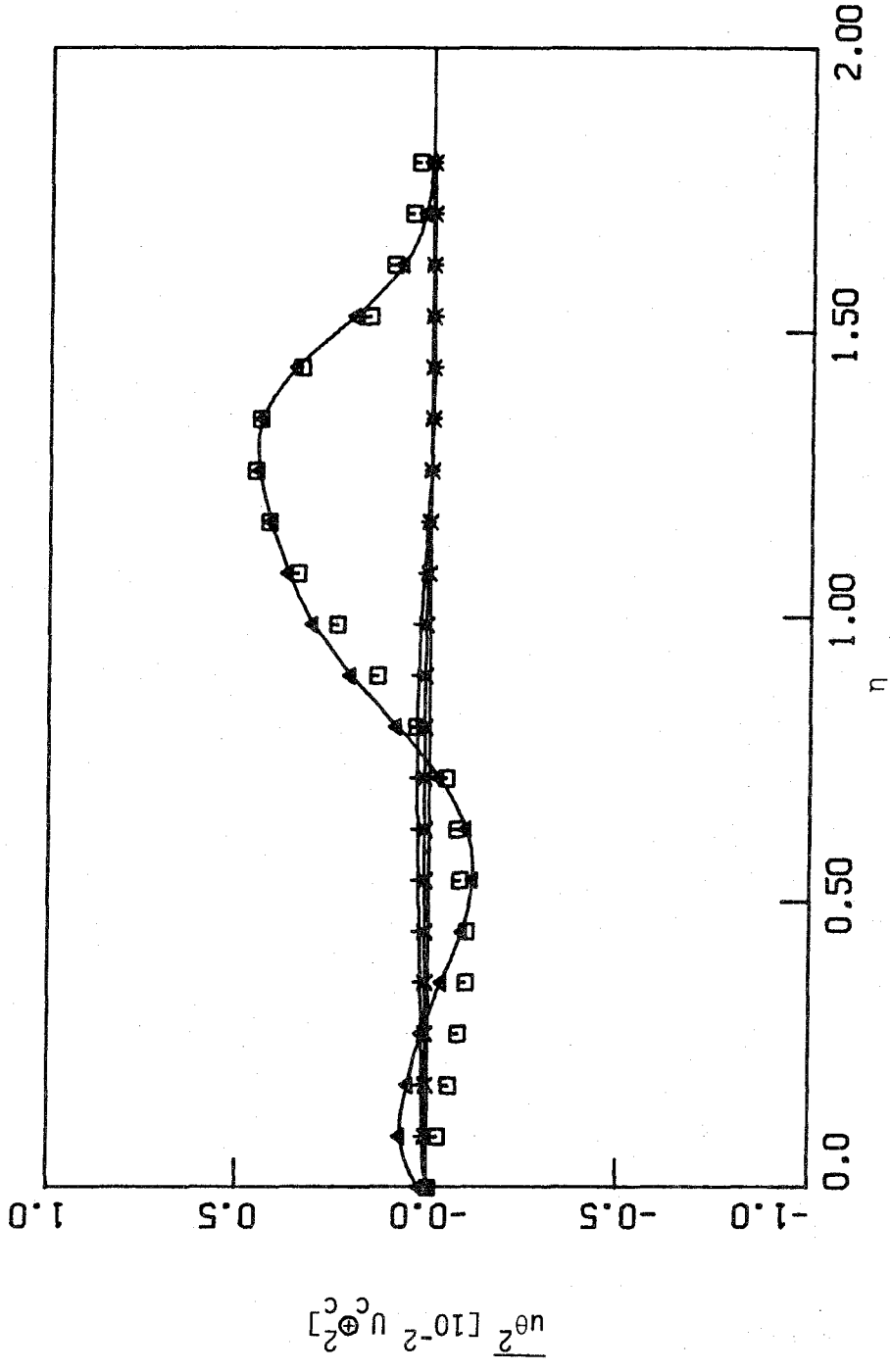
2.00
1.50
1.00
0.50
0.0
η
-1.0
-0.5
-0.0
0.5
1.0
$\overline{u_\theta^2}$ [10^{-2} $u_c \Phi_c^2$]

Fig. 2.5

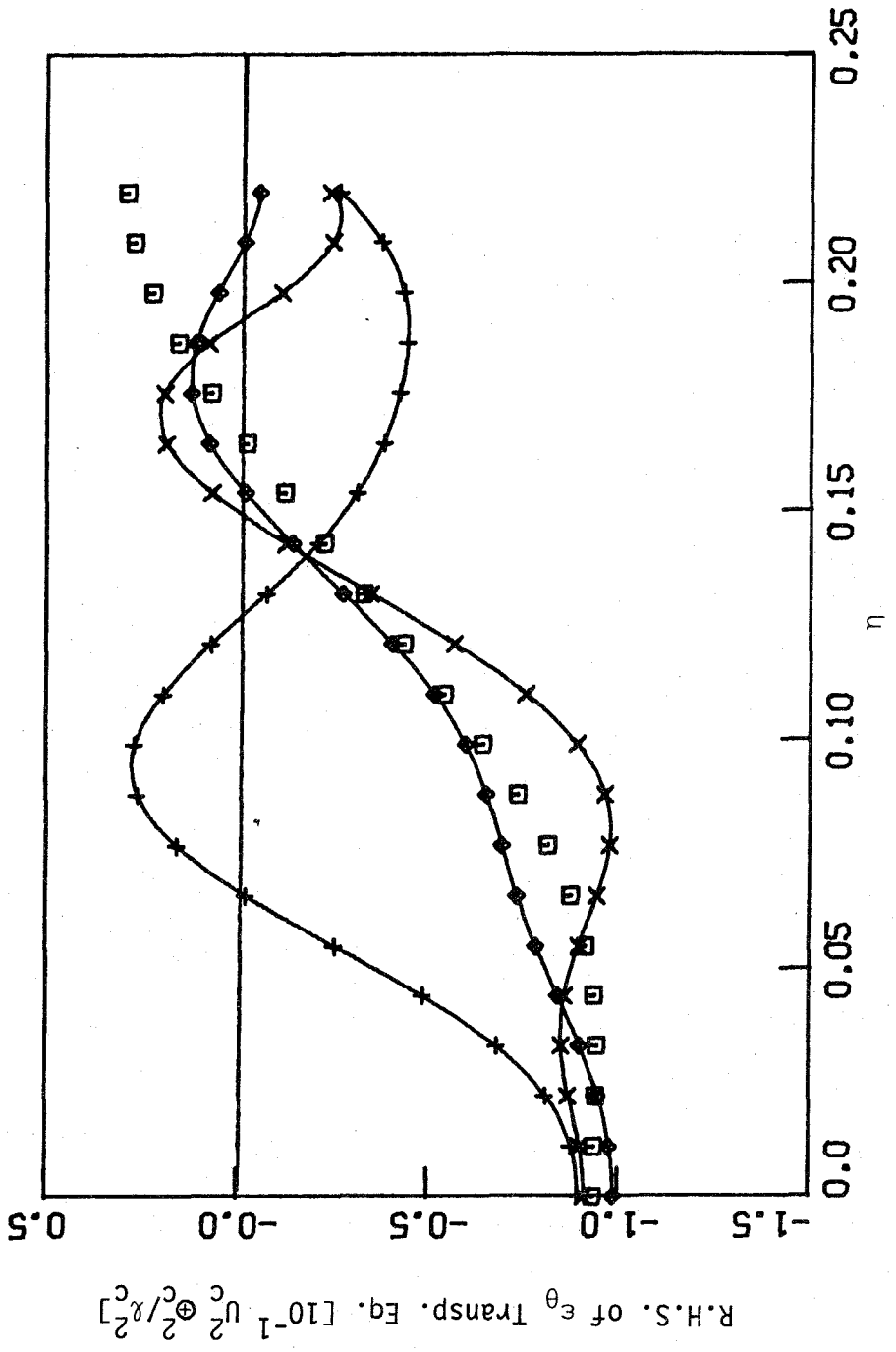
0.25
0.20
0.15
0.10
0.05
0.0
η
-1.5
-1.0
-0.5
-0.0
0.5
R.H.S. of ε_θ Transp. Eq. $[10^{-1}\ U_c^2\ \phi_c^2/\chi_c^2]$

Fig. 3.1

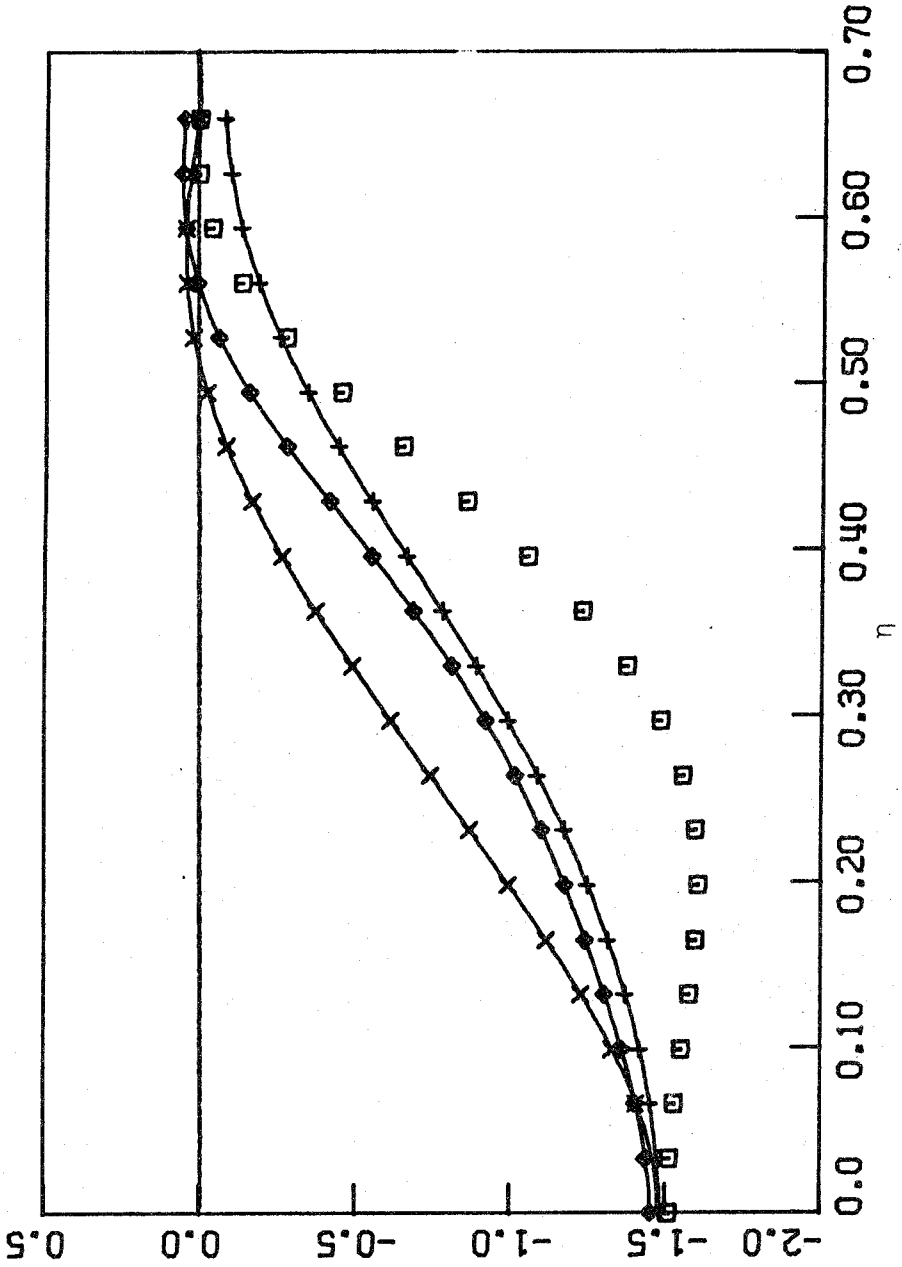
0.0
0.10
0.20
0.30
0.40
0.50
0.60
0.70
η
-2.0
-1.5
-1.0
-0.5
0.0
0.5
R.H.S. of ε_Θ Transp. Eq. $[U_C^2 \Phi_C^2/\lambda_C^2]$

Fig. 3.2

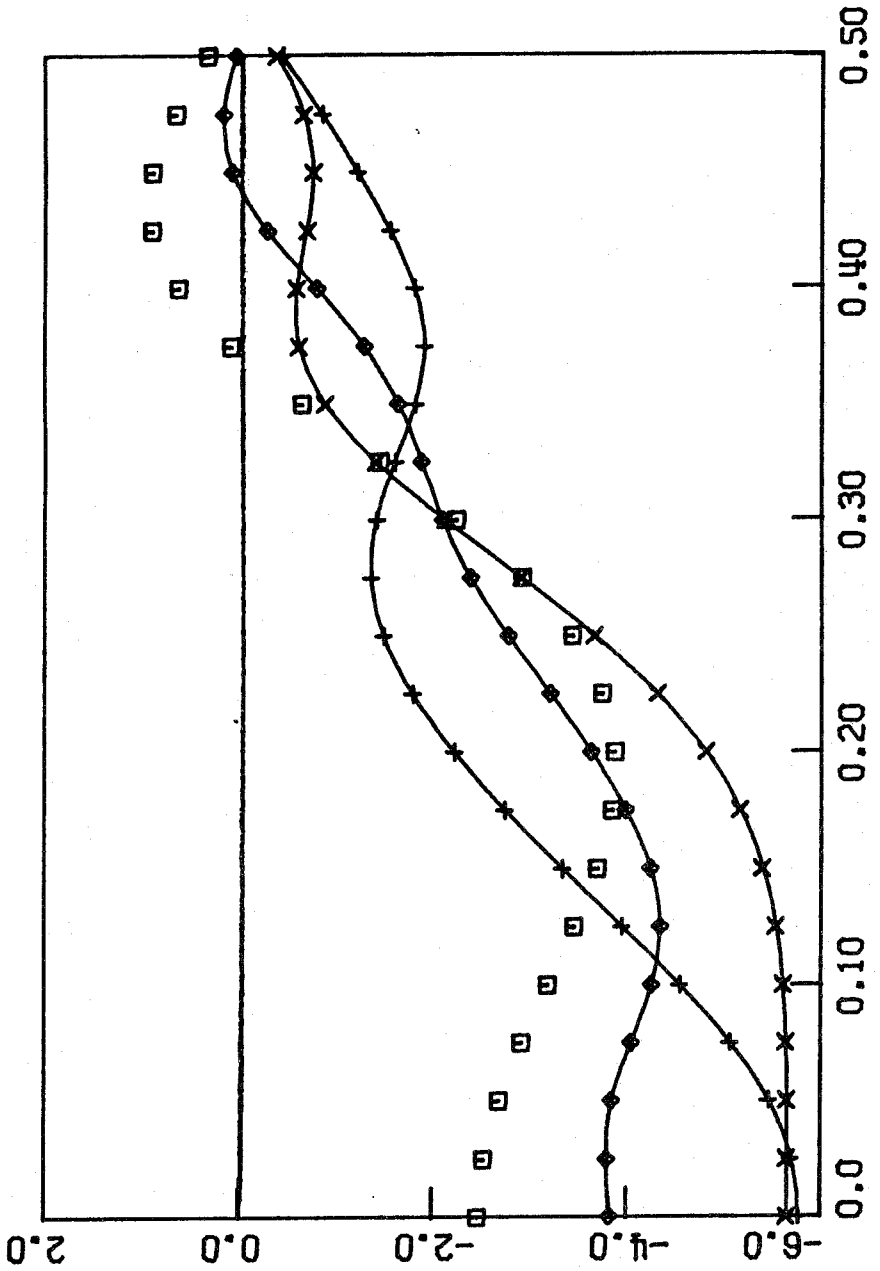
R.H.S. of ε_θ Transp. Eq. $[U_c^2\theta^2/\chi_c^2]$
-6.0
-4.0
-2.0
0.0
2.0
0.0
0.10
0.20
0.30
0.40
0.50
η

Fig. 3.3

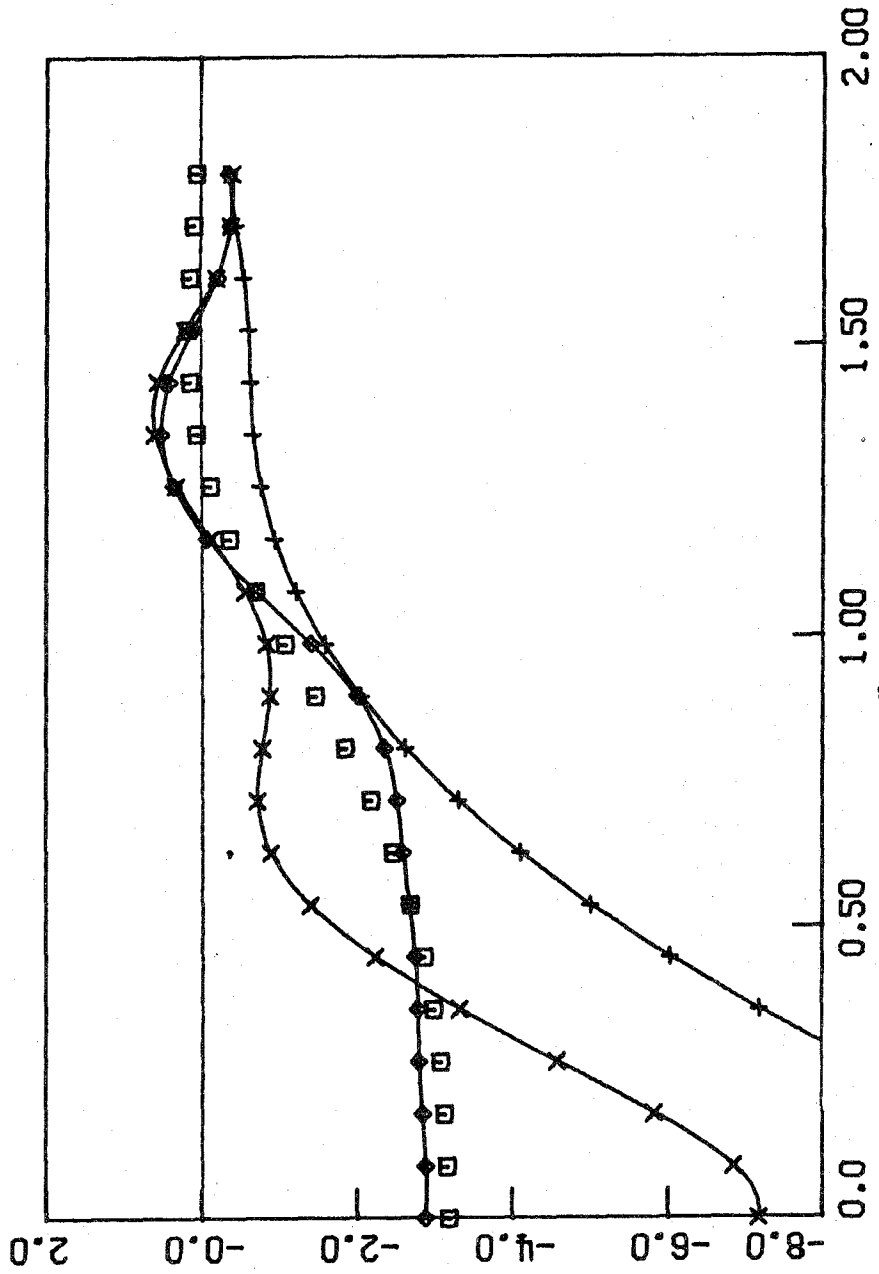
2.00
1.50
1.00
0.50
0.0
η
-8.0
-6.0
-4.0
-2.0
-0.0
2.0
R.H.S. of ε_θ Transp. Eq. $[10^{-3}U_c^2\Theta_c^2/\chi_c^2]$

Fig. 3.4

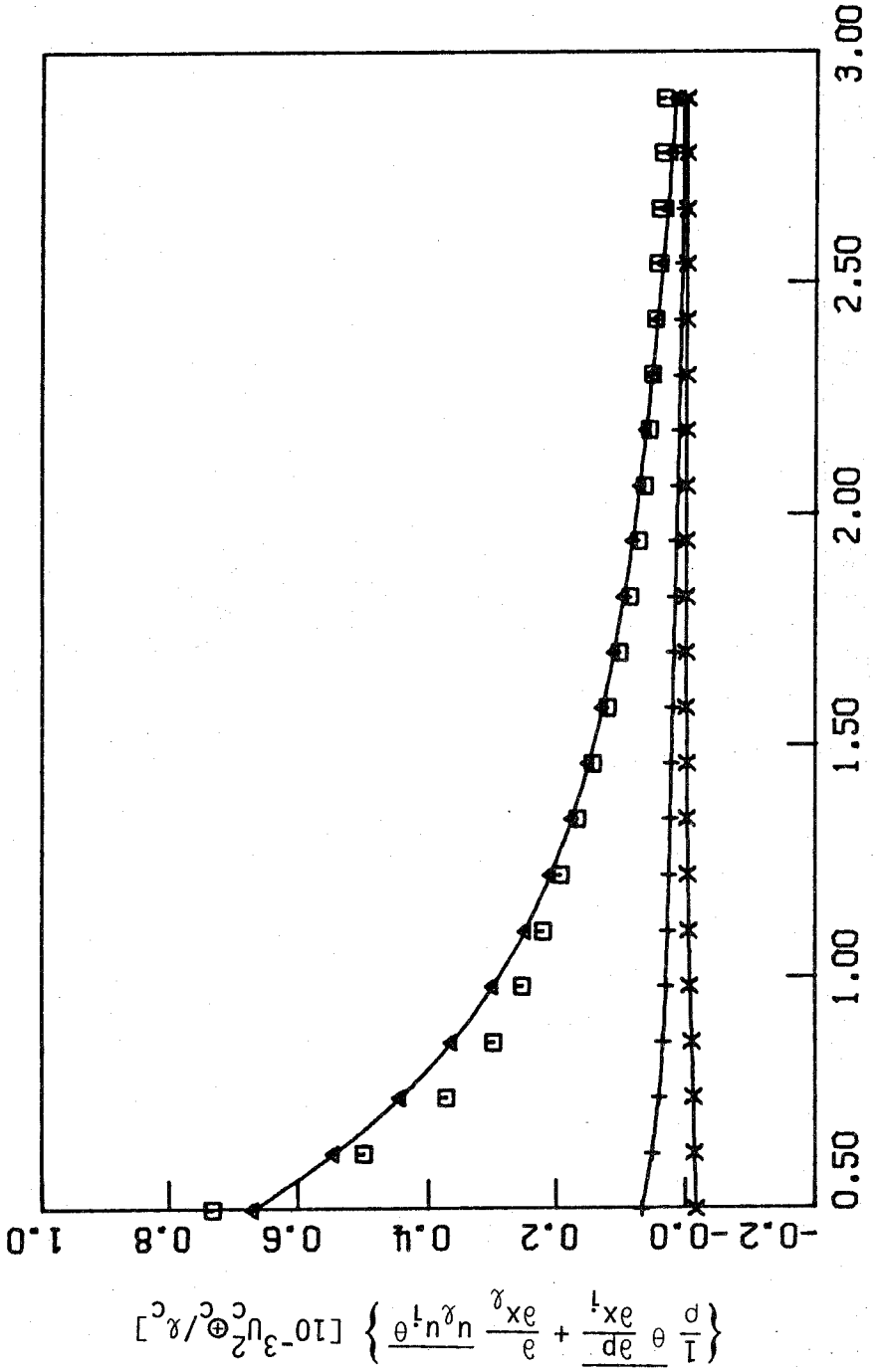
3.00
2.50
2.00
1.50
1.00
0.50
η
-0.2 -0.0 0.2 0.4 0.6 0.8 1.0
$\left\{\frac{1}{\rho}\theta\frac{\partial p}{\partial x_i} + \frac{\partial}{\partial x_\ell}\overline{u_\ell u_i \theta}\right\}\ [10^{-3}U_c^2\Theta_c/\ell_c]$

Fig. 4.1

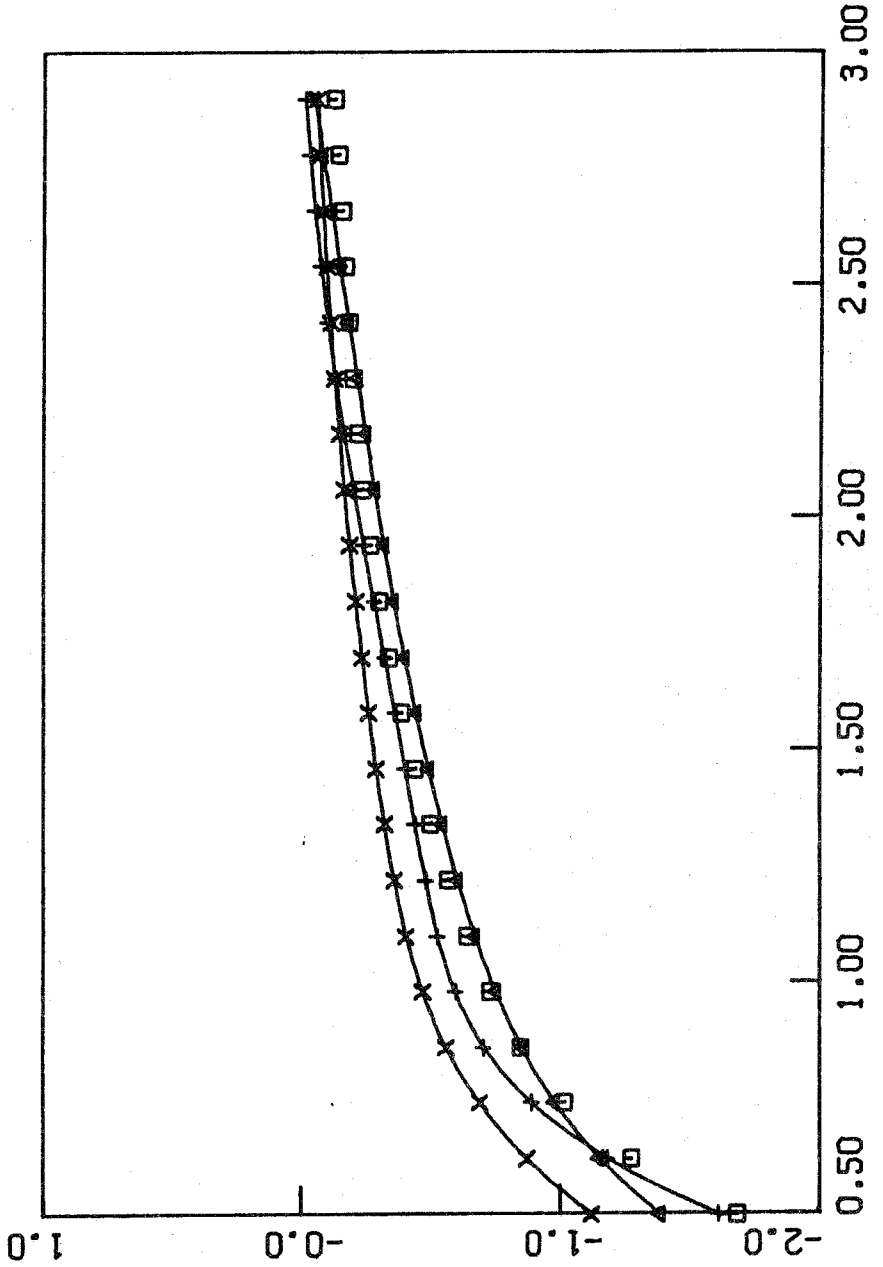
3.00
2.50
2.00
1.50
1.00
0.50
η
-2.0
-1.0
-0.0
1.0
$\left\{\frac{1}{\rho}\,\theta\,\frac{\partial p}{\partial x_i} + \frac{\partial}{\partial x_j}\,\overline{u_i u_j \theta}\right\}\,[10^{-4} U_c^2 \Theta_c/\gamma_c]$

Fig. 4.2

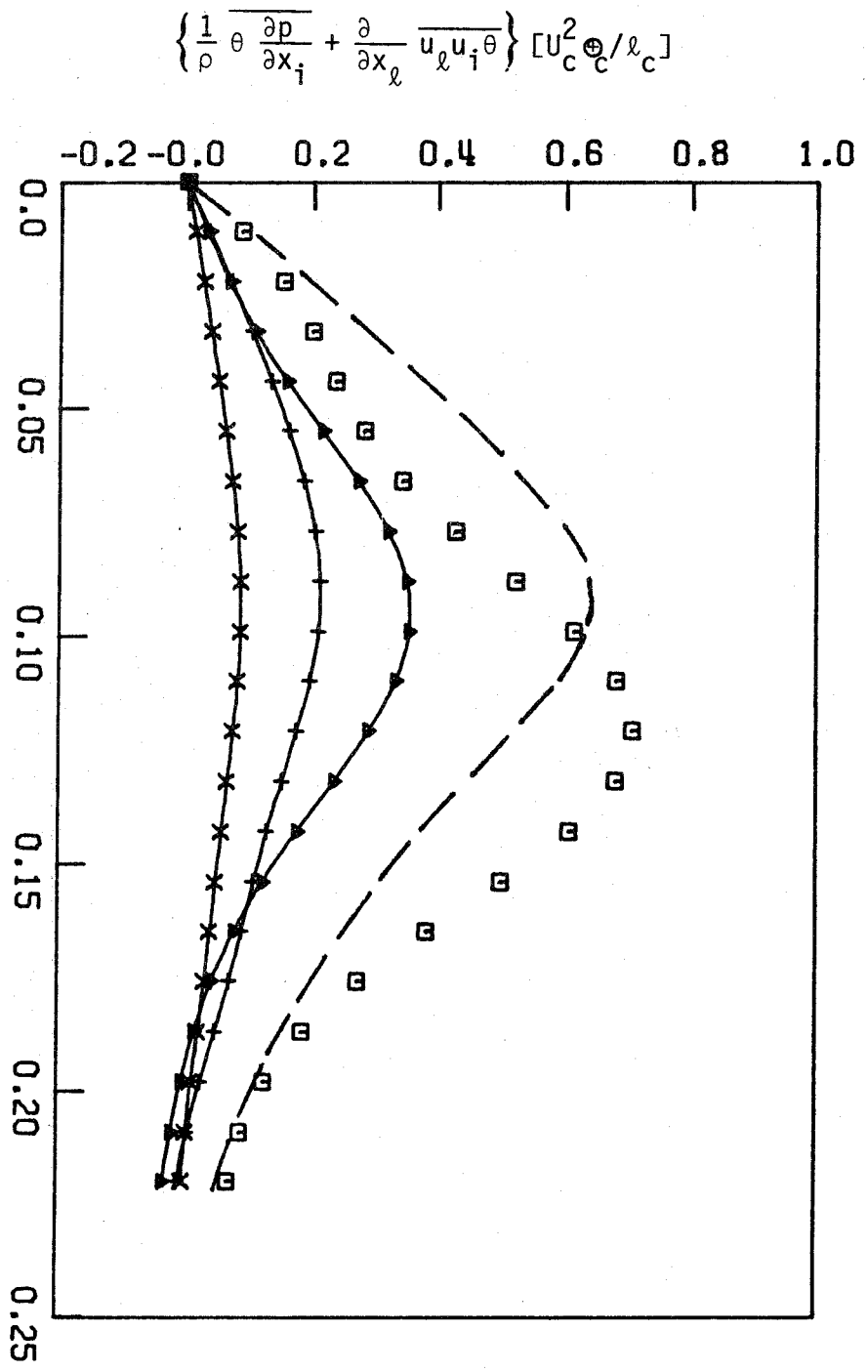
$\left\{\frac{1}{\rho}\,\theta\,\frac{\partial p}{\partial x_i} + \frac{\partial}{\partial x_\ell}\,\overline{u_\ell u_i \theta}\right\}[U_c^2 \Theta_c/\ell_c]$
-0.2 -0.0 0.2 0.4 0.6 0.8 1.0
0.0 0.05 0.10 0.15 0.20 0.25
η

Fig. 4.3

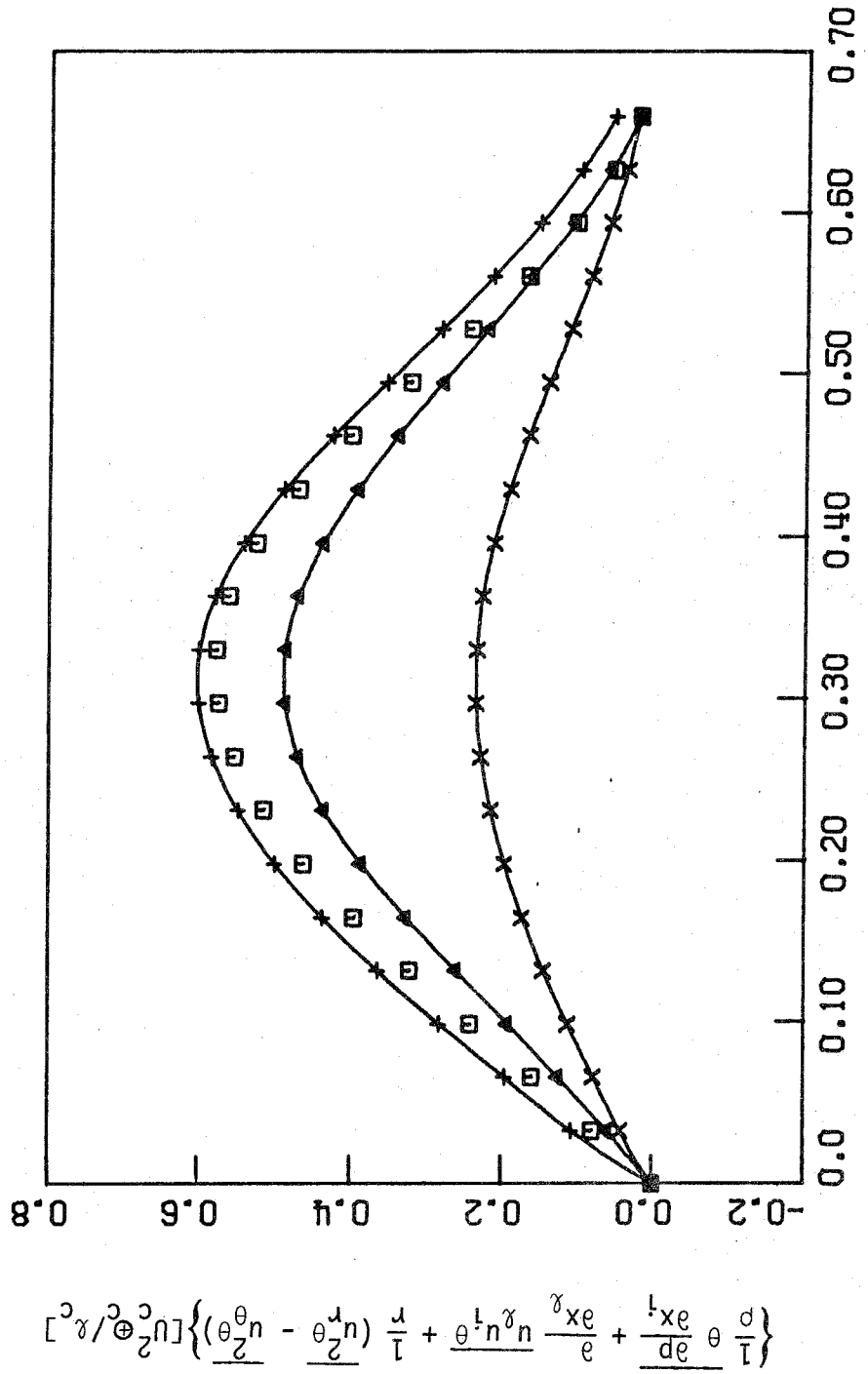

Fig. 4.4

$$\left\{\frac{1}{\rho}\,\theta\,\frac{\partial p}{\partial x_i} + \frac{\partial}{\partial x_j}\,\overline{u_j u_i \theta} + \frac{1}{r}\,(\overline{u_r^2\theta} - \overline{u_\theta^2\theta})\right\}[U_c^2\Theta_c/\gamma_c]$$

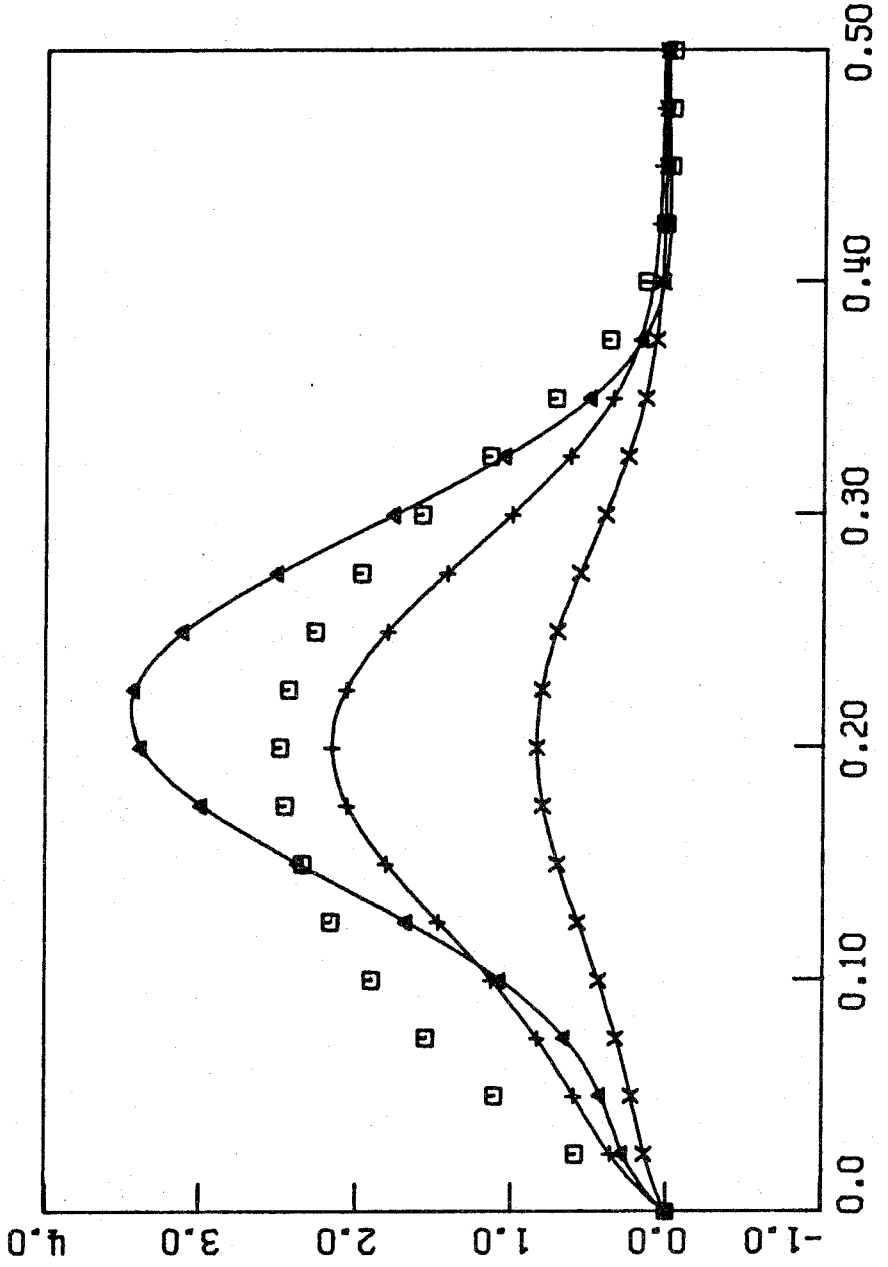
0.0
0.10
0.20
0.30
0.40
0.50
η
-1.0
0.0
1.0
2.0
3.0
4.0
$\left\{\frac{1}{\rho}\theta\frac{\partial\overline{p}}{\partial x_i}+\frac{\partial}{\partial x_j}\overline{u_j u_i\theta}\right\}[U_c^2\Theta_c/\gamma_c]$

Fig. 4.5

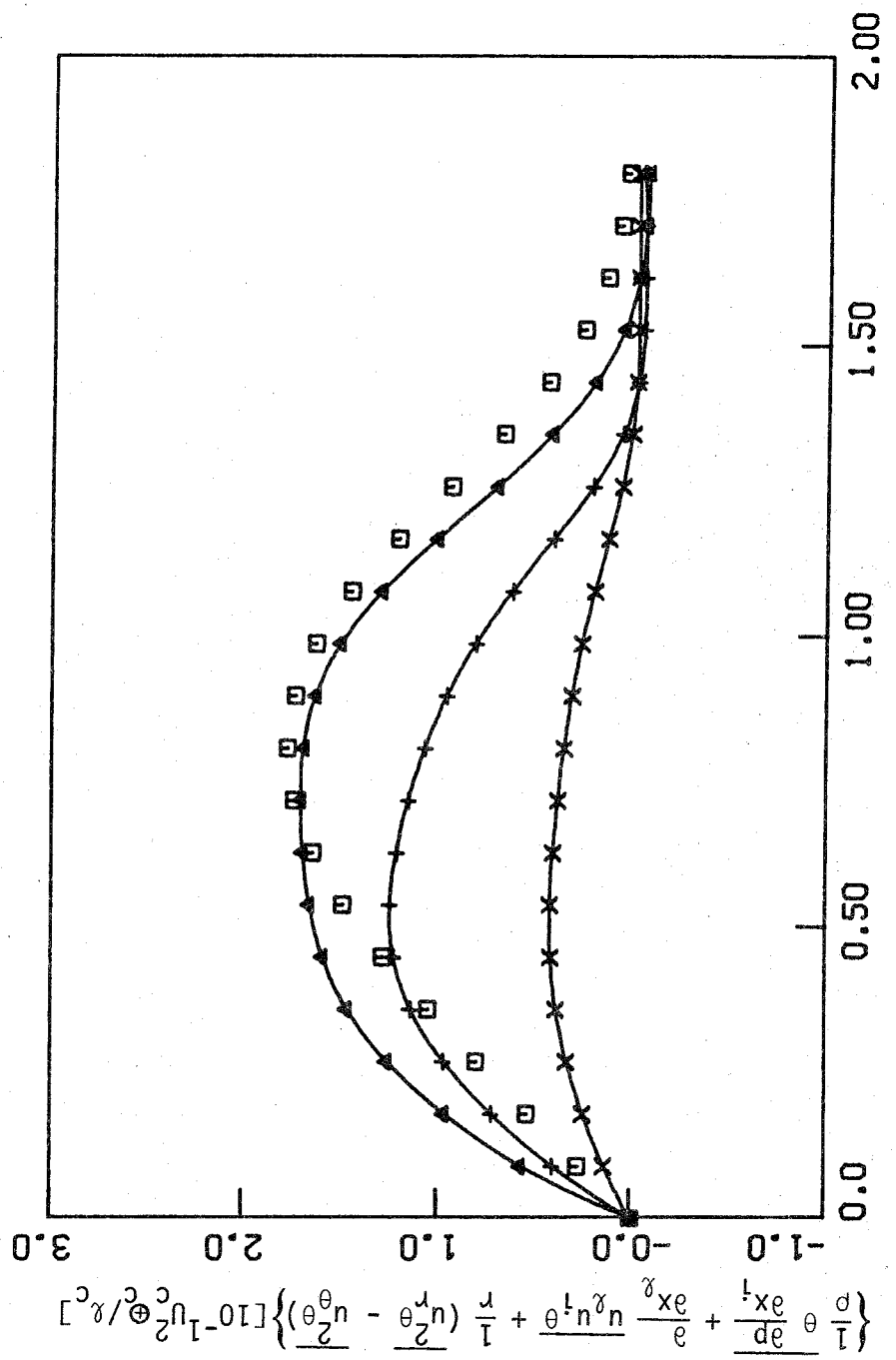
$\left\{\frac{1}{\rho}\,\theta\,\frac{\partial p}{\partial x_i} + \frac{\partial}{\partial x_\ell}\,\overline{u_\ell u_i \theta} + \frac{1}{r}\,(\overline{u_r^2\theta} - \overline{u_\theta^2\theta})\right\}[10^{-1} U_c^2 \Theta_c/\ell_c]$
-1.0
-0.0
1.0
2.0
3.0
0.0
0.50
1.00
1.50
2.00
η

Fig. 4.6

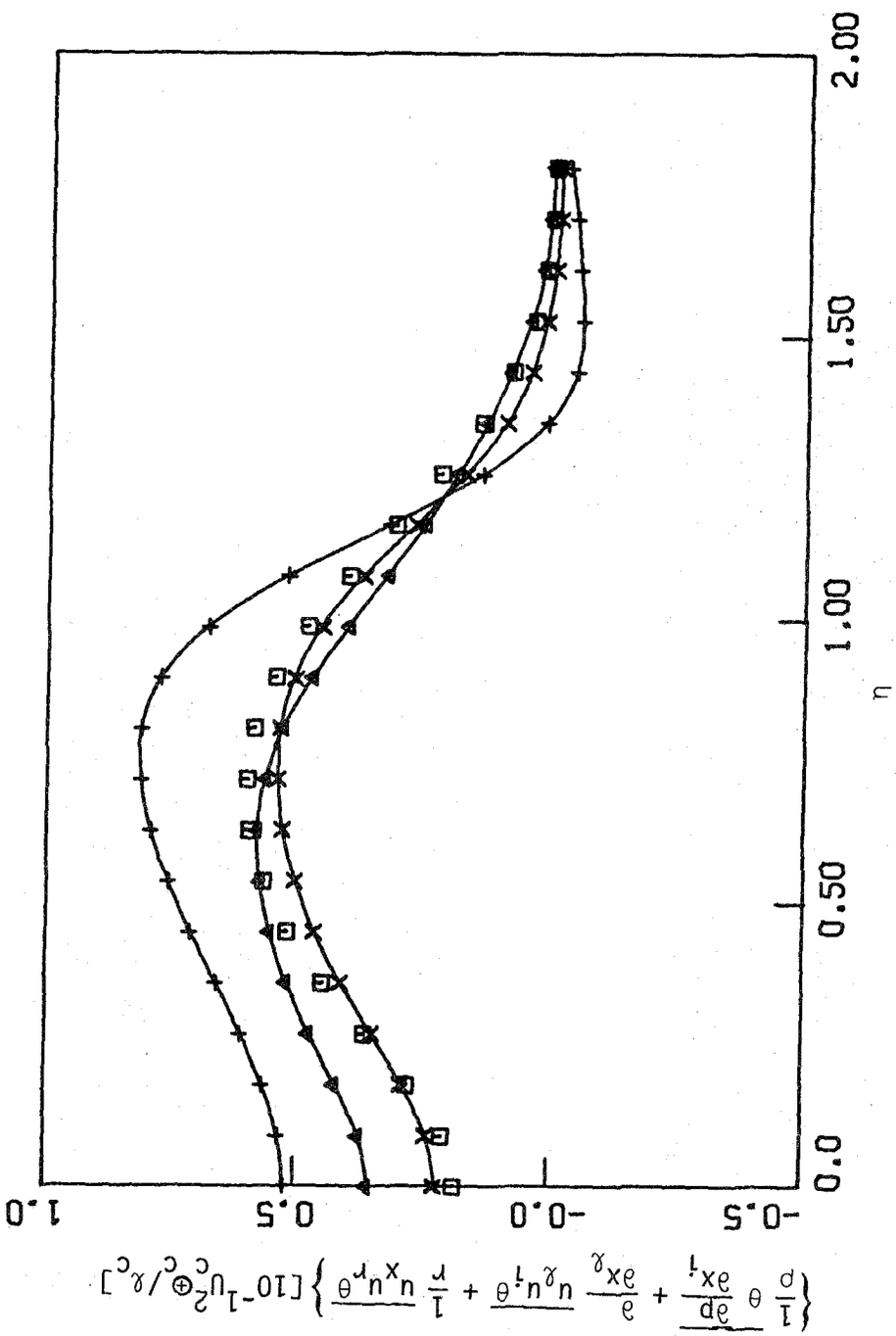
2.00
1.50
1.00
0.50
0.0
η
-0.5
-0.0
0.5
1.0
$\left\{\frac{1}{\rho}\theta\frac{\partial p}{\partial x_i} + \frac{\partial}{\partial x_\ell}\overline{u_\ell u_i\theta} + \frac{1}{r}\overline{u_x u_r\theta}\right\}[10^{-1}U_c^2\Theta_c/\ell_c]$

Fig. 4.7

B. A SEMI-ANALYTICAL MODEL FOR TRIPLE CORRELATIONS IN TURBULENT FLOW

by

S. H. Lee and L. G. Leal

Department of Chemical Engineering
California Institute of Technology
Pasadena, California 91125

Abstract

A semi-analytical method is used to derive models for the triple correlations of fluctuating velocity and temperature in a nonisothermal turbulent flow based upon the exact equations which govern their transport and production processes. In this study, these governing equations are transformed to a set of coupled linear algebraic equations for $\overline{u_i u_j u_k}$, $\overline{u_i u_j}$, $\overline{u_i \theta^2}$ and $\overline{\theta^3}$ by assuming: (1) a quasi-Gaussian structure for the fourth-order moments, (2) slow variations of the mean flow in the streamwise direction, (3) negligible convection of the triple correlations, and (4) certain simple models for the remaining higher-order correlations. A model for the triple correlations can thus be obtained by solving the set of linear algebraic equations.

The model for $\overline{u_i u_j u_k}$ is compared with the following experimetal data for isothermal flows: the asymmetric channel flow of Hanjalic and Launder (1972), the pipe flow of Lawn (1971), the wall jet of Irwin (1973), the two-dimensional mixing layer of Wygnanski and Fiedler (1970), and the round jet of Wygnanski and Fiedler (1969).

We also examine the performance of the models for the velocity-temperature correlations by comparison with experimental data for natural convection heat transfer between two horizontal flat plates, Deardorff and Willis (1967), and for turbulent convection in water over ice, Adrian (1975).

1. Introduction

Second-order methods for modeling of turbulent flows have been developed recently, which show promise for application to various types of flow (cf. Reynolds [1], [2]). In these methods, the transport equations for the second-order moments, i.e. $\overline{u_i u_j}$, $\overline{u_i \theta}$, $\overline{\theta^2}$, etc. are integrated numerically using various models for the unknown higher-order terms in the equations. Considerable research has been done both to propose terms for the necessary models and to develop efficient numerical computational methods for solution of the resulting differential equations (cf. Launder [3], Lumley [4], Daly and Harlow [5], Shir [6], Wyngaard et al. [7], etc.).

Among the several unknown terms in the transport equations for second-order moments in a non-isothermal flow, this paper is concerned only with the triple correlations; namely, $\overline{u_i u_j u_k}$, $\overline{u_i u_j \theta}$, $\overline{u_i \theta^2}$, and $\overline{\theta^3}$. Hanjalic and Launder [8] derived a simple model for the triple velocity correlation from its exact transport equation. Later, Lumley et al. [9] showed that the governing partial differential equations for the triple correlations in nonisothermal turbulence with zero mean motion, could be simplified with various assumptions and approximations to a set of linear first-order algebraic equations. These equations can then be solved directly for the triple correlations, and the result is a model for the triple correlations in terms of second- and lower-order quantities. The proposals of Lumley et al. [9] seem to represent a quite general and systematic approach for model development. Gravitational effects can be analyzed without additional assumptions, and this is very important for the application of turbulence models to meteorological flows or buoyant heat convection.

In the present paper, we adopt Lumley et al.'s [9] approach to develop models for the velocity and temperature triple correlations which can be used in flows with a mean velocity gradient. One consequence of this added generality is that the resulting algebraic equations have a very complicated solution, which cannot be obtained easily by analytical means. We therefore adopt a successive approximation scheme based on a decomposition of the equations into terms which involve the mean strain rate, the mean temperature gradient, or buoyancy effects and others which do not. Finally, the performance of the models which we develop is then evaluated by comparison with experimental data. This was not done by Lumley et al. [9]. The model for the triple velocity correlation was therefore tested with experimental data for isothermal flows, i.e., the asymmetric channel flow of Hanjalic and Launder [10], the pipe flow of Lawn [11], the wall jet of Irwin [12], the two-dimensional mixing layer of Wygnanski and Fiedler [13], and the round jet of Wygnanski and Fiedler [14]. For non-isothermal flow with significant buoyancy, well-documented experimental data are very scarce. Therefore, we compare the model with two simple cases: heat convection between two horizontal plates (Deardorff and Willis [15]) and heat convection in water over ice (Adrian [16]). In these two flows, the diffusion term involving triple correlations contribute substantially to the budget of kinetic energy and thermal variance.

2. Derivation of Equations

2.1 Transport Equations for the Triple Correlations of Velocity and Temperature

We begin with the Navier-Stokes and thermal energy equations, incorporating the usual Boussinesq approximation (cf. Schlichting [17]). If

the instantaneous velocity and temperature fields are decomposed into a mean and a fluctuating part, a sequence of exact equations can be derived for second- and higher-order moments. As is well known, the equations at each order contain higher-order moments and the system can only be closed with a finite number of equations by approximating the highest-order moments as functions of lower-order moments and/or the mean velocity and temperature fields. As indicated in the previous section, our interest is in the so-called second-order approximations in which we retain the transport equations for second-order moments, and attempt to model the unknown higher-order terms which appear in these equations using functions of the second-order correlations and/or the mean velocity and temperature fields. Here, we pursue the approach initially proposed by Lumley et al. [9] for the development of models for the third-order velocity/temperature correlations for non-isothermal turbulent flows with buoyancy. In particular, we attempt to derive the models for third-order moments by direct approximation of the exact transport equations at third-order. These transport equations can be expressed in the form

$$\frac{\partial}{\partial t}\overline{u_i u_j u_k} = - U_l \frac{\partial \overline{u_i u_j u_k}}{\partial x_l} - \left[\frac{\partial U_i}{\partial x_l} \overline{u_j u_k u_l} + \frac{\partial U_j}{\partial x_l} \overline{u_i u_k u_l} + \frac{\partial U_k}{\partial x_l} \overline{u_i u_j u_l} \right]$$

$$- \frac{\partial}{\partial x_l} \overline{u_l u_i u_j u_k} + \overline{u_j u_k} \frac{\partial \overline{u_i u_l}}{\partial x_l} + \overline{u_k u_i} \frac{\partial \overline{u_j u_l}}{\partial x_l} + \overline{u_i u_j} \frac{\partial \overline{u_k u_l}}{\partial x_l}$$

$$- \frac{1}{\rho} \left[\overline{u_j u_k \frac{\partial p}{\partial x_i}} + \overline{u_k u_i \frac{\partial p}{\partial x_j}} + \overline{u_i u_j \frac{\partial p}{\partial x_k}} \right] + \nu \frac{\partial^2 \overline{u_i u_j u_k}}{\partial x_l \partial x_l}$$

$$- 2\nu \left[\overline{u_i \frac{\partial u_j}{\partial x_l} \frac{\partial u_k}{\partial x_l}} + \overline{u_j \frac{\partial u_k}{\partial x_l} \frac{\partial u_i}{\partial x_l}} + \overline{u_k \frac{\partial u_i}{\partial x_l} \frac{\partial u_j}{\partial x_l}} \right]$$

$$- \left[\beta_i \overline{u_j u_k \theta} + \beta_j \overline{u_k u_i \theta} + \beta_k \overline{u_i u_j \theta}\right] \tag{1}$$

$$\frac{\partial}{\partial t}\overline{u_i u_j \theta} = - U_l \frac{\partial}{\partial x_l}\overline{u_i u_j \theta} - \left[\overline{u_j u_l \theta}\frac{\partial U_i}{\partial x_l} + \overline{u_i u_l \theta}\frac{\partial U_j}{\partial x_l} + \overline{u_i u_j u_l}\frac{\partial \oplus}{\partial x_l}\right]$$

$$- \frac{\partial}{\partial x_l}\overline{u_i u_j u_l \theta} + \overline{u_j \theta}\frac{\partial}{\partial x_l}\overline{u_i u_l} + \overline{u_i \theta}\frac{\partial}{\partial x_l}\overline{u_j u_l} + \overline{u_i u_j}\frac{\partial}{\partial x_l}\overline{u_l \theta}$$

$$- \frac{1}{\rho}\left[\overline{u_i \theta \frac{\partial p}{\partial x_j}} + \overline{u_j \theta \frac{\partial p}{\partial x_i}}\right] + \gamma\,\overline{u_i u_j \frac{\partial^2 \theta}{\partial x_l \partial x_l}} + \nu\left[\overline{u_i \theta \frac{\partial^2 u_j}{\partial x_l \partial x_l}}\right.$$

$$\left. + \overline{u_j \theta \frac{\partial^2 u_i}{\partial x_l \partial x_l}}\right] - \left[\beta_i \overline{\theta^2 u_j} + \beta_j \overline{\theta^2 u_i}\right] \tag{2}$$

$$\frac{\partial}{\partial t}\overline{u_i \theta^2} = - U_l \overline{\frac{\partial u_i \theta^2}{\partial x_l}} - \overline{u_i \theta^2}\frac{\partial U_i}{\partial x_l} - 2\frac{\partial \oplus}{\partial x_l}\overline{\theta u_i u_l} - \frac{\partial}{\partial x_l}\overline{\theta^2 u_i u_l}$$

$$+ \overline{\theta^2}\frac{\partial}{\partial x_l}\overline{u_i u_l} + 2\,\overline{\theta u_i}\frac{\partial}{\partial x_l}\overline{u_l \theta} - \frac{1}{\rho}\overline{\theta^2 \frac{\partial p}{\partial x_i}} + \nu\,\overline{\theta^2 \frac{\partial^2 u_i}{\partial x_l \partial x_l}}$$

$$+ 2\gamma\,\overline{\theta u_i \frac{\partial^2 \theta}{\partial x_l \partial x_l}} - \beta_i \overline{\theta^3} \tag{3}$$

$$\frac{\partial \overline{\theta^3}}{\partial t} = - U_l \frac{\partial \overline{\theta^3}}{\partial x_l} - 3\frac{\partial \oplus}{\partial x_l}\overline{u_l \theta^2} - \frac{\partial}{\partial x_l}\overline{u_l \theta^2} - 3\overline{\theta^2}\frac{\partial \overline{u_l \theta}}{\partial x_l}$$

$$+ \gamma \frac{\partial^2 \overline{\theta^3}}{\partial x_l \partial x_l} - 6\gamma\,\overline{\theta \frac{\partial \theta}{\partial x_l}\frac{\partial \theta}{\partial x_l}} \tag{4}$$

where U_i = mean velocity, $\oplus$ = mean temperature

u_i = fluctuating velocity, θ = fluctuating temperature

ν = specific viscosity, γ = thermal diffusivity

and β_i = buoyance vector (thermal expansion rate x gravity) .

The objective of what follows is to approximate the various terms in these equations in such a manner that they are transformed into a set of algebraic equations which can be solved explicitly for the third-order moments directly in terms of second-order moments and mean flow quantities. In order to accomplish this, we consider only steady or very slowly changing flows so that the time derivatives can be neglected in (1) - (4). Furthermore, the convection term (the first term in the right-hand side of equations (1) - (4)) is small in most cases of available experimental results and is also neglected in the present analysis. On the other hand, the terms which involve gradients of the mean velocity and temperature fields are retained (in contrast to the earlier analysis of Lumley et al. [9] which assumed that there was no mean flow). Let us now consider the approximations which will be applied to the higher-order terms of (1) - (4) in order to transform the equations to algebraic equations for the triple correlations.

a. Approximation for the Fourth-Order Velocity-Temperature Moments

Fourth-order moments, such as $\overline{u_i u_j u_k u_l}$, $\overline{u_i u_j u_l \theta}$, $\overline{u_i u_j \theta^2}$ and $\overline{u_i \theta^3}$ have often been modeled in terms of second-order moments by means of a quasi-Gaussian approximation (cf. Monin and Yaglom [18]) and we follow this precedent here. The existence of non-zero third moments is evidence of a non-Gaussian distribution. However, the relaxation time for fourth-

order moments should be considerably smaller than that for third-order moments, and the use of quasi-Gaussian approximation for fourth-order moments in the equation for third-order moments still appears to us to be justified. The same argument was previously made by Lumley et al. [9] who also used the quasi-Gaussian approximation for the fourth-order moments.

b. Approximations for Third-Order Moments Involving Fluctuating Pressure

The correlations in equations (1) - (3) which involve the fluctuating pressure can be modeled directly in terms of the exact solution for fluctuating pressure which was derived originally by Chou [19].

$$\frac{1}{\rho}\,p(\underline{x}) = \frac{1}{2\pi}\iiint \frac{\partial U_m'}{\partial \xi_n}\frac{\partial u_n'}{\partial \xi_m}\frac{1}{r}\,dV - \frac{1}{4\pi}\iiint \frac{\partial^2}{\partial \xi_m \partial \xi_n}\left(\overline{u_m' u_n'} - u_m' u_n'\right)\frac{1}{r}\,dV$$

(I) (II)

$$+ \frac{1}{4\pi}\iiint \beta_1 \frac{\partial \theta'}{\partial \xi_1}\frac{1}{r}\,dV + \frac{1}{4\pi}\frac{1}{\rho}\iint \left\{\frac{1}{r}\frac{\partial p'}{\partial n} - p'\,\frac{\partial}{\partial n}\left(\frac{1}{r}\right)\right\} dS \qquad (5)$$

(III) (IV)

The prime on the various variables indicates that they are variables at $\underline{x} + \underline{\xi} \in V$ or S. The r is $|\underline{\xi}|$ and $\partial/\partial n$ denotes the normal derivative to the surface at $\underline{x} + \underline{\xi} \in S$. Here, the first three terms are volume integrals over the whole fluid domain, while the last term is a surface integral

over the boundaries. This term (IV) can be neglected, in general, for any point in a flow which is not too close to a boundary, since p' at boundary becomes uncorrelated with p when r is large. Furthermore, the characteristic of terms (I) and (III) is different from the term (II) in the sense that the former are linear in fluctuating velocity or temperature, while the latter is quadratic. We denote the sum of (I) and (III) as $p^{(1)}/\rho$ and the term (II) as $p^{(2)}/\rho$. Let us now consider the use of equation (5) for determining models for the pressure correlations in equations (1) - (3).

We begin with the triple correlation of pressure and velocity in equation (1). Utilizing the solution (5) for p and the subsequent decomposition into $p^{(1)}$ and $p^{(2)}$, we can write

$$\frac{1}{\rho}\,\overline{u_i u_j \frac{\partial p^{(1)}}{\partial x_k}} = \frac{1}{2\pi}\frac{\partial U_m}{\partial x_n}\iiint \overline{\frac{\partial u_i u_j u_n'}{\partial \xi_m \partial \xi_k}}\,\frac{1}{r}\,dV + \frac{1}{4\pi}\beta_1 \iiint \overline{\frac{\partial u_i u_j \theta'}{\partial \xi_1 \partial \xi_k}}\,\frac{1}{r}\,dV \qquad (6)$$

$$\frac{1}{\rho}\,\overline{u_i u_j \frac{\partial p^{(2)}}{\partial x_k}} = -\frac{1}{4\pi}\iiint \frac{\partial^3}{\partial \xi_k \partial \xi_m \partial \xi_n}\left(\overline{u_m' u_n'}\;\overline{u_i u_j} - \overline{u_i u_j u_m' u_n'}\right)\frac{1}{r}\,dV \qquad (7)$$

In the derivation of equation (6), it is assumed that the mean velocity field is slowly varying so that $\partial U_m/\partial x_n$ is constant over the correlation length for $\overline{u_i u_j u_k}$ (cf. Rotta [20], [21]). Since the integrals in equation (6) are spatial integrals of the gradients of $\overline{u_i u_j u_n'}$ and $\overline{u_i u_j \theta'}$,

they can be approximated with a linear combination of triple correlations of velocity and temperature.

$$\frac{1}{2\pi}\iiint \frac{\partial^2 \overline{u_i u_j u_n'}}{\partial \xi_m \partial \xi_k}\,\frac{1}{r}\,dV \simeq C_1\delta_{ij}\,\overline{u_m u_n u_k} + C_2(\delta_{im}\,\overline{u_j u_n u_k} + \delta_{jm}\,\overline{u_i u_n u_k}$$

$$+ \delta_{ik}\,\overline{u_j u_n u_m} + \delta_{jk}\,\overline{u_i u_n u_m}) + C_3(\delta_{in}\,\overline{u_j u_m u_k} + \delta_{jn}\,\overline{u_i u_m u_k}$$

$$+ C_4(\delta_{mn}\,\overline{u_i u_j u_k} + \delta_{kn}\,\overline{u_i u_j u_m}) + C_5\,\delta_{mk}\,\overline{u_i u_j u_n} \qquad (8)$$

$$\frac{1}{4\pi}\iiint \frac{\partial^2}{\partial \xi_l \partial \xi_k}\,\overline{u_i u_j \theta'}\,\frac{1}{r}\,dV \simeq D_1\delta_{ij}\,\overline{\theta u_k u_l} + D_2\delta_{kl}\,\overline{\theta u_i u_j}$$

$$+ D_3(\delta_{ik}\,\overline{\theta u_j u_l} + \delta_{jk}\,\overline{\theta u_i u_l} + \delta_{il}\,\overline{\theta u_j u_k} + \delta_{jl}\,\overline{\theta u_i u_k})$$

$$+ D_4\,\delta_{ij}\delta_{kl}\,\overline{\theta u_p u_p} + D_5(\delta_{ik}\delta_{jl} + \delta_{jk}\delta_{il})\,\overline{\theta u_p u_p} \qquad (9)$$

The parameters in equation (8) can be completely determined using the isotropy approximation for two-point correlations (cf. De Karman and Howarth [22]), incompressibility of the fluid, and the tensor symmetries (cf. Launder [3] and Lumley [4]). The parameters in (9) can also be evaluated using these same conditions, plus the additional assumption that $\delta_{ij}\,\overline{\theta u_k u_l}$ is uncorrelated with the left-hand side of (9) since $\overline{\theta u_k u_l}$ does not contain u_i and u_j. In consequence, the model for the triple correlation of velocity and pressure $p^{(1)}$ is as follows:

$$
\begin{aligned}
&-\frac{1}{\rho}\left(\overline{u_j u_k \frac{\partial p^{(1)}}{\partial x_i}} + \overline{u_k u_i \frac{\partial p^{(1)}}{\partial x_j}} + \overline{u_i u_j \frac{\partial p^{(1)}}{\partial x_k}}\right) \\
&\quad \simeq \frac{\partial U_m}{\partial x_n}\left\{\frac{4}{5}\left(\delta_{mk}\,\overline{u_i u_j u_n} + \delta_{mj}\,\overline{u_i u_k u_n} + \delta_{mi}\,\overline{u_j u_k u_n}\right)\right. \\
&\quad \left. -\frac{1}{5}\left(\delta_{nk}\,\overline{u_i u_j u_m} + \delta_{nj}\,\overline{u_i u_j u_m} + \delta_{ni}\,\overline{u_j u_k u_m}\right)\right\} \\
&\quad -\frac{2}{11}\beta_l\left(\delta_{ij}\,\overline{\theta u_k u_l} + \delta_{jk}\,\overline{\theta u_i u_l} + \delta_{ki}\,\overline{\theta u_j u_l}\right) \\
&\quad +\frac{3}{11}\left(\beta_i\,\overline{\theta u_j u_k} + \beta_j\,\overline{\theta u_k u_i} + \beta_k\,\overline{\theta u_i u_j}\right) \\
&\quad +\frac{2}{55}\left\{\delta_{ij}\beta_k + \delta_{jk}\beta_i + \delta_{ki}\beta_j\right\}\overline{\theta u_l u_l}
\end{aligned}
\qquad (10)
$$

It should be reiterated that this model contains no adjustable parameters. Before returning to discuss the expression, equation (7), involving $p^{(2)}$, we may note that the additional correlations associated with $p^{(1)}$ in equations (2) and (3), can be completely determined in a manner which is analogous to that used to obtain (10). Thus, without belaboring the details, we simply note the resulting expressions for the correlations:

$$-\frac{1}{\rho}\left\{\overline{u_i\theta\,\frac{\partial p^{(1)}}{\partial x_j}}+\overline{u_j\theta\,\frac{\partial p^{(1)}}{\partial x_i}}\right\}\simeq\frac{\partial U_m}{\partial x_n}\left\{\frac{4}{5}\left(\delta_{mi}\,\overline{u_nu_j\theta}+\delta_{mj}\,\overline{u_nu_i\theta}\right)\right.$$

$$\left.-\frac{1}{5}\left(\delta_{in}\,\overline{u_ju_m\theta}+\delta_{jn}\,\overline{u_iu_m\theta}\right)\right\}+\frac{3}{10}\left(\beta_i\,\overline{\theta^2u_j}+\beta_j\,\overline{\theta^2u_i}\right)$$

$$-\frac{1}{5}\,\delta_{ij}\beta_l\,\overline{\theta^2u_l} \qquad (11)$$

$$-\frac{1}{\rho}\,\overline{\theta^2\,\frac{\partial p^{(1)}}{\partial x_i}}\simeq\left(\frac{4}{5}\,\frac{\partial U_i}{\partial x_l}-\frac{1}{5}\,\frac{\partial U_l}{\partial x_i}\right)\,\overline{u_l\theta^2}+\frac{1}{3}\,\beta_i\,\overline{\theta^3} \qquad (12)$$

As was the case for the expression (10), these approximations involve no adjustable parameters. Let us now return to the pressure correlations which involve $p^{(2)}$.

The pressure correlations associated with $p^{(2)}$ in equations (1) - (3) are called "return-to-isotropy" terms. Since the triple correlations only become significant when the turbulence is anisotropic, it is plausible to assume that these return-to-isotropy terms will be primarily proportional to the corresponding triple correlations. In contrast, however, equation (7) (or corresponding expressions for the correlations

in equations (2) and (3) which involve $p^{(2)}$ shows that the return-to-isotropy terms can be represented as a volume integral involving a fourth-order moment and a product of two second-order moments. Thus, if a quasi-Gaussian approximation is applied to the fourth-order moment, it is equally plausible to suppose that the return-to-isotropy terms in (1) - (3) can be approximated in terms of products of second-order moments. In the analysis which follows, we combine the intuitive suggestion with that derived from the expression for $p^{(2)}$ and express all of the "return-to-isotropy" pressure correlations as a sum of products of second-order moments and the relevant triple correlation. In contrast to the correlations involving $p^{(1)}$, both types of terms in these models for $p^{(2)}$ will be multiplied by an arbitrary constant which can only be evaluated by comparison with experimental data. Thus, there is no loss of generality in including both types of term at this stage. In order to maintain a maximum degree of simplicity, however, only those products of second-order moments which already appear in the transport equations (1) - (3) were included in the models for the return to isotropy terms. These models are thus

$$-\frac{1}{\rho}\left(\overline{u_j u_k \frac{\partial p^{(2)}}{\partial x_i}} + \overline{u_k u_i \frac{\partial p^{(2)}}{\partial x_j}} + \overline{u_i u_j \frac{\partial p^{(2)}}{\partial x_k}}\right) = \frac{\alpha_1'}{\tau_1}\,\overline{u_i u_j u_k}$$

$$+ \zeta_1'\left(\overline{u_i u_l}\,\frac{\partial \overline{u_j u_k}}{\partial x_l} + \overline{u_j u_l}\,\frac{\partial \overline{u_i u_k}}{\partial x_l} + \overline{u_k u_l}\,\frac{\partial \overline{u_i u_j}}{\partial x_l}\right) \qquad (13)$$

$$-\frac{1}{\rho}\left(\overline{u_i\theta\,\frac{\partial p^{(2)}}{\partial x_j}}+\overline{u_j\,\frac{\partial p^{(2)}}{\partial x_i}}\right)=\frac{\alpha_2'}{\tau_2}\,\overline{u_iu_j\theta}+\zeta_2'\left(\overline{u_iu_1}\,\frac{\partial\overline{u_j\theta}}{\partial x_1}+\overline{u_ju_1}\,\frac{\partial\overline{u_i\theta}}{\partial x_1}+\overline{u_1\theta}\,\frac{\partial}{\partial x_1}\,\overline{u_iu_j}\right) \tag{14}$$

$$-\frac{1}{\rho}\,\overline{\theta^2\,\frac{\partial p^{(2)}}{\partial x_i}}=\frac{\alpha_3'}{\tau_3}\,\overline{u_i\theta^2}+\zeta_3'\left(\overline{u_iu_1}\,\overline{\frac{\partial\theta^2}{\partial x_1}}+2\,\overline{\theta u_1}\,\frac{\partial\overline{u_i\theta}}{\partial x_1}\right) \tag{15}$$

where $\frac{1}{\tau_1}=\frac{\varepsilon}{q^2}$, $\frac{1}{\tau_2}=\left(\frac{\varepsilon}{q^2}\right)^{2/3}\left(\frac{\varepsilon_\theta}{\overline{\theta^2}}\right)^{1/3}$, $\frac{1}{\tau_3}=\left(\frac{\varepsilon}{q^2}\right)^{1/3}\left(\frac{\varepsilon_\theta}{\overline{\theta^2}}\right)^{2/3}$,

$q^2=\overline{u_iu_i}$, $\varepsilon=$ dissipation rate of $\frac{1}{2}q^2$, and

$\varepsilon_\theta=$ dissipation rate of $\overline{\theta^2}$.

We have implicitly assumed in writing these expressions that there are two representative time scales for the evolution of the turbulence microstructure, $\tau_1\equiv q^2/\varepsilon$ for the fluctuating velocity field and $\tau_4=\overline{\theta^2}/\varepsilon_\theta$ for the fluctuating temperature field. Obviously, τ_1 is the relevant time scale for $\overline{u_iu_ju_k}$ while τ_4 is the appropriate time scale for $\overline{\theta^3}$. It is then assumed that the mixed correlations $\overline{u_iu_j\theta}$ and $\overline{u_i\theta^2}$ will have time scales which are intermediate to τ_1 and τ_4. In the present analysis, the intermediate time scales τ_2 and τ_3, corresponding to $\overline{u_iu_j\theta}$ and $\overline{u_i\theta^2}$, are modeled, on intuitive grounds, in terms of τ_1 and τ_4.

C. Models for Molecular Transport Terms

Finally, we turn to models for the molecular transport terms in equations (1) - (4). Using the scaling rule of Tennekes and Lumley [23], the relative magnitudes of these terms can be examined. For instance, $\nu \overline{\frac{\partial^2 u_i u_j u_k}{\partial x_1 \partial x_1}}$ is much smaller than $2\nu\left[\overline{u_i \frac{\partial u_j}{\partial x_1}\frac{\partial u_k}{\partial x_1}} + \overline{u_j \frac{\partial u_k}{\partial x_1}\frac{\partial u_i}{\partial x_1}} + \overline{u_k \frac{\partial u_i}{\partial x_1}\frac{\partial u_j}{\partial x_1}}\right]$ in equation (1) since the length scale for the former term is much larger than that for the latter terms. Thus, we can neglect $\nu \overline{\frac{\partial^2 u_i u_j u_k}{\partial x_1 \partial x_1}}$. We now define ε_{ij} as

$$\varepsilon_{ij} \equiv \nu \frac{\partial u_i}{\partial x_1}\frac{\partial u_j}{\partial x_1}$$

We assume that $\overline{u_j u_k}$ is well correlated with ε_{jk} (cf. Monin and Yaglom [18]),

$$2\nu \overline{u_i \frac{\partial u_j}{\partial x_1}\frac{\partial u_k}{\partial x_1}} = 2\,\overline{u_i \varepsilon_{jk}} \sim 2\,\overline{\varepsilon_{jk}}\;\overline{u_i u_j u_k}/\overline{u_j u_k}$$

$$\sim 2\frac{\varepsilon}{q^2}\overline{u_i u_j u_k} \sim \frac{2}{\tau_1}\overline{u_i u_j u_k}$$

Thus we propose a simple mode for the molecular transport terms in equation (1).

$$\nu \overline{\frac{\partial^2 u_i u_j u_k}{\partial x_1 \partial x_1}} - 2\nu\left[\overline{u_i \frac{\partial u_j}{\partial x_1}\frac{\partial u_k}{\partial x_1}} + \overline{u_j \frac{\partial u_k}{\partial x_1}\frac{\partial u_i}{\partial x_1}} + \overline{u_k \frac{\partial u_i}{\partial x_1}\frac{\partial u_j}{\partial x_1}}\right]$$

$$\sim -\alpha_1'' \frac{1}{\tau_1}\overline{u_i u_j u_k} \qquad (16)$$

Similarly, we can model the molecular transport terms in equations (2) - (4).

$$\gamma\, \overline{u_i u_j \frac{\partial^2 \theta}{\partial x_1 \partial x_1}} + \nu \left(\overline{u_i \theta \frac{\partial^2 u_j}{\partial x_1 \partial x_1}} + \overline{u_j \theta \frac{\partial^2 u_i}{\partial x_1 \partial x_1}} \right) \sim - \alpha_2'' \frac{1}{\tau_2} \overline{u_i u_j \theta} \tag{17}$$

$$\nu\, \overline{\theta^2 \frac{\partial^2 u_i}{\partial x_1 \partial x_1}} + 2\gamma\, \overline{\theta u_i \frac{\partial^2 \theta}{\partial x_1 \partial x_1}} \sim - \alpha_3'' \frac{1}{\tau_3} \overline{u_i \theta^2} \tag{18}$$

$$\gamma\, \overline{\frac{\partial^2 \theta^3}{\partial x_1 \partial x_1}} - 6\gamma\, \overline{\theta \frac{\partial \theta}{\partial x_1} \frac{\partial \theta}{\partial x_1}} \sim - \alpha_4 \frac{1}{\tau_4} \overline{\theta^3} \tag{19}$$

The objective of developing the models listed above is to obtain from the general transport equations (1) - (4) a set of algebraic equations which can be inverted directly in order to obtain models for the third-order moments. Since the arbitrary assumptions and approximations are applied to the fourth-order quantities, rather than directly to ad hoc models for the third-order terms, it is to be hoped that the resulting models for these third-order correlations will be an improvement compared either to existing models, or to models which might be obtained by direct approximation at the third-order level in the case of terms (or physical effects such as buoyancy) that have not been considered in previous modeling studies. In order to obtain the simplified version of equations (1) - (4), we simply introduce the models from the three preceding subsections into these equations, and neglect the time derivative and convection terms (as explained earlier). The result is

$$\frac{\alpha_1}{\tau_1}\overline{u_i u_j u_k} + \frac{2}{5}\left(S_{i1}\overline{u_1 u_j u_k} + S_{j1}\overline{u_1 u_i u_k} + S_{k1}\overline{u_1 u_i u_j}\right)$$

$$+ \frac{2}{11}\beta_1\left(\delta_{ij}\overline{\theta u_k u_1} + \delta_{jk}\overline{\theta u_i u_1} + \delta_{ki}\overline{\theta u_j u_1}\right)$$

$$- \frac{3}{11}\left(\beta_i\overline{\theta u_j u_k} + \beta_j\overline{\theta u_i u_k} + \beta_k\overline{\theta u_i u_j}\right)$$

$$- \frac{2}{55}\left(\delta_{ij}\beta_k + \delta_{jk}\beta_i + \delta_{ki}\beta_j\right)\overline{\theta u_p u_p}$$

$$= -\zeta_1\left\{\overline{u_i u_1}\frac{\partial\overline{u_j u_k}}{\partial x_1} + \overline{u_j u_1}\frac{\partial\overline{u_i u_k}}{\partial x_1} + \overline{u_k u_1}\frac{\partial\overline{u_i u_j}}{\partial x_1}\right\} \qquad (20)$$

$$\frac{\alpha_2}{\tau_2}\overline{u_i u_j\theta} + \frac{2}{5}\left(S_{i1}\overline{u_1 u_j\theta} + S_{j1}\overline{u_1 u_i\theta}\right) + \frac{\partial\textcircled{+}}{\partial x_1}\overline{u_i u_j u_1} + \frac{7}{10}\left(\beta_i\overline{\theta^2 u_j} + \beta_j\overline{\theta^2 u_i}\right)$$

$$+ \frac{1}{5}\delta_{ij}\beta_1\overline{\theta^2 u_1} = -\zeta_2\left(\overline{u_i u_1}\frac{\partial\overline{u_j\theta}}{\partial x_1} + \overline{u_j u_1}\frac{\partial\overline{u_i\theta}}{\partial x_1} + \overline{u_1\theta}\frac{\partial\overline{u_i u_j}}{\partial x_1}\right) \qquad (21)$$

$$\frac{\alpha_3}{\tau_3}\overline{u_i\theta^2} + \frac{2}{5}S_{i1}\overline{u_1\theta^2} + 2\frac{\partial\textcircled{+}}{\partial x_1}\overline{\theta u_i u_1} + \frac{2}{3}\beta_i\overline{\theta^3}$$

$$= -\zeta_3\left(\overline{u_i u_1}\frac{\partial\overline{\theta^2}}{\partial x_1} + 2\,\overline{\theta u_1}\frac{\partial\overline{u_i\theta}}{\partial x_1}\right) \qquad (22)$$

$$\frac{\alpha_4}{\tau_4}\overline{\theta^3} + 3\frac{\partial \oplus}{\partial x_1}\overline{u_1\theta^3} = -3\overline{u_1\theta}\frac{\partial \overline{\theta^2}}{\partial x_1} \tag{23}$$

Here, $S_{ij} \equiv \frac{1}{2}\left(\frac{\partial U_i}{\partial x_j} + \frac{\partial U_j}{\partial x_i}\right)$

2.2 The Matrix Inversion Model

Equations (20) - (23) comprise a set of coupled, linear algebraic equations for the triple correlations, which can be solved to obtain expressions for these quantities in terms of the mean velocity and temperature gradients and second-order moments of the turbulence quantities, all of which appear as coefficients. In consequence, they can be expressed in a simple vector notation.

$$\underline{\underline{A}}\cdot\underline{x} = \underline{f} \tag{24}$$

where $\underline{\underline{A}}$: coefficient matrix for the triple correlations

$\underline{x}$: vector of triple correlations

$$\left\{\overline{u_i u_j u_k},\ \overline{u_i u_j \theta},\ \overline{u_i \theta^2},\ \overline{\theta^3}\right\}$$

$\underline{f}$: vector of the right-hand sides of equations (20) - (23)

The matrix $\underline{\underline{A}}$ is shown in detail for two-dimensional non-isothermal flow in the Appendix A. The form of $\underline{\underline{A}}$ indicates that the triple correlations are related to other triple correlations of the same order in temperature by mean strain rates, to the correlations of one lower order in temperature by gravity, and to the correlations of one higher order in temperature by mean temperature gradients.

A formal solution of the system of equations (24), is simply

$$\underline{x} = \underline{\underline{A}}^{-1} \cdot \underline{f} \quad . \tag{25}$$

However, for the most general three-dimensional flow, the matrix $\underline{\underline{A}}$ is large enough to require a substantial amount of computation time to calculate its inverse. Furthermore, the analytical form of $\underline{\underline{A}}^{-1}$ is too complicated in that case to be presented here. However, examining the matrix $\underline{\underline{A}}$, we notice that it can be divided into two matrices; namely, $\underline{\underline{A}}_1$, a diagonal matrix of terms which do not involve the mean strain rate, and $\underline{\underline{A}}_2$, the remaining matrix.

$$\underline{\underline{A}} = \underline{\underline{A}}_1 + \underline{\underline{A}}_2 \tag{26}$$

This separation implies that triple correlations may be attributed to two separate mechanisms: one part, $\underline{\underline{A}}_1$, represents the production of triple correlations by the small scale turbulent motions, and the other, $\underline{\underline{A}}_2$, represents the production and transport by the mean velocity and temperature gradients and by gravity. When the mean velocity and temperature gradients are not very large, the contribution from $\underline{\underline{A}}_1$ is generally expected to be larger than the contribution from $\underline{\underline{A}}_2$. Moreover, it may be noted that the determinant of $\underline{\underline{A}}_2$ is identically zero for an arbitrary three-dimensional isothermal flow. These two facts suggest that a reasonable approach to the approximating the solution (25) may be to utilize the method of successive approximations in which it is assumed that $\| A_1 \| >> \| A_2 \|$, i.e.

$$\underline{x} \simeq \underline{\underline{A}}_1^{-1} \cdot \underline{f} - \underline{\underline{A}}_1^{-1} \cdot \underline{\underline{A}}_2 \cdot \underline{\underline{A}}_1^{-1} \cdot \underline{f} - \cdots \quad . \tag{27}$$

Let us denote the right-hand side of equations (20), (21), (22) and (23) as $-\zeta_1 f_{ijk}$, $-\zeta_2 g_{ij}$, $-\zeta_3 h_i$, and $-e$, respectively. Then equation (27) can be written as

$$\overline{u_i u_j u_k} \simeq -\frac{\zeta_1}{\alpha_1}\tau_1 f_{ijk} + \frac{2}{5}\frac{\zeta_1}{\alpha_1^2}\tau_1^2(S_{il}f_{ljk} + S_{jl}f_{lik} + S_{kl}f_{lij})$$

$$+ \frac{\zeta_2}{\alpha_1\alpha_2}\tau_1\tau_2\left\{\frac{2}{11}\beta_l(\delta_{ij}g_{kl} + \delta_{jk}g_{il} + \delta_{ki}g_{jl})\right.$$

$$\left. - \frac{3}{11}(\beta_i g_{jk} + \beta_j g_{ki} + \beta_k g_{ij}) - \frac{2}{55}(\delta_{ij}\beta_k + \delta_{jk}\beta_i + \delta_{ki}\beta_j)g_{ll}\right\} \quad (28)$$

$$\overline{u_i u_j \theta} \simeq -\frac{\zeta_2}{\alpha_2}\tau_2 g_{ij} + \frac{2}{5}\frac{\zeta_2}{\alpha_2^2}\tau_2^2(S_{il}g_{lj} + S_{jl}g_{li}) + \frac{\zeta_1}{\alpha_1\alpha_2}\tau_1\tau_2\frac{\partial\oplus}{\partial x_l}f_{ijl}$$

$$+ \frac{\zeta_3}{\alpha_2\alpha_3}\tau_2\tau_3\left\{\frac{7}{10}(\beta_i h_j + \beta_j h_i) + \frac{1}{5}\delta_{ij}\beta_l h_l\right\} \quad (29)$$

$$\overline{u_i\theta^2} \simeq -\frac{\zeta_3}{\alpha_3}\tau_3 h_i + \frac{2}{5}\frac{\zeta_3}{\alpha_3^2}\tau_3^2 S_{il}h_l + \frac{2\zeta_2}{\alpha_2\alpha_3}\tau_2\tau_3\frac{\partial\oplus}{\partial x_l}g_{il}$$

$$+ \frac{2}{3}\frac{1}{\alpha_3\alpha_4}\tau_3\tau_4\beta_i e \quad (30)$$

$$\overline{\theta^3} \simeq -\frac{1}{\alpha_4}\tau_4 e + 3\frac{\zeta_3}{\alpha_3\alpha_4}\tau_3\tau_4\frac{\partial\oplus}{\partial x_l}h_l \quad (31)$$

The parameters $\alpha_1 \sim \alpha_4$ and $\zeta_1 \sim \zeta_3$ which appear in these expressions require evaluation by comparison with experimental data. Indeed, it is this comparison with data and with other models which must serve to verify the usefulness of the general forms (28) - (31) for the various triple correlations.

3. Triple Velocity Correlations for Isothermal Flow

3.1 Review of Previous Models

A model for triple velocity correlations is needed to close the Reynolds stress equation even for isothermal flows, and such models have therefore been widely studied in the recent development of second-order models for turbulent flow calculations. Among the models which have been previously suggested, we note:

The model of Shir [6]

$$\overline{u_i u_j u_k} = - 0.01 \frac{q^4}{\varepsilon} \frac{\partial \overline{u_i u_j}}{\partial x_k} \tag{32}$$

The model of Daly and Harlow [5]

$$\overline{u_i u_j u_k} = - 1.0 \frac{q^2}{\varepsilon} \frac{\partial \overline{u_i u_j}}{\partial x_k} \tag{33}$$

and the model of Hanjalic and Launder [8]

$$\overline{u_i u_j u_k} = - 0.044 \frac{q^2}{\varepsilon} \left(\overline{u_i u_l} \frac{\partial \overline{u_j u_k}}{\partial x_l} + \overline{u_j u_l} \frac{\partial \overline{u_k u_i}}{\partial x_l} + \overline{u_k u_l} \frac{\partial \overline{u_i u_j}}{\partial x_l} \right) \tag{34}$$

More recently, Cormack, Leal and Seinfeld [24] made an extensive study of the triple-velocity correlations and suggested a four-parameter model:

$$\overline{u_i u_j u_k} = - 8.14\cdot10^{-3} \frac{q^4}{\varepsilon} (\delta_{ij}\delta_{kl} + \delta_{ik}\delta_{jl} + \delta_{kj}\delta_{il}) \frac{\partial q^2}{\partial x_l}$$

$$- 1.72\cdot10^{-2} \frac{q^4}{\varepsilon} \left(\frac{\partial a_{ik}}{\partial x_j} + \frac{\partial a_{ij}}{\partial x_k} + \frac{\partial a_{kj}}{\partial x_i}\right)$$

$$- 4.80\cdot10^{-2} \frac{q^2}{\varepsilon} (\delta_{ij}a_{kl} + \delta_{jk}a_{il} + \delta_{ki}a_{jl}) \frac{\partial q^2}{\partial x_l}$$

$$- 1.02\cdot10^{-1} \frac{q^2}{\varepsilon} \left(a_{ij} \frac{\partial a_{kl}}{\partial x_l} + a_{jk} \frac{\partial a_{il}}{\partial x_l} + a_{ki} \frac{\partial a_{jl}}{\partial x_l}\right) \qquad (35)$$

where $a_{ij} = \overline{u_i u_j} - \frac{1}{3} \delta_{ij} q^2$

The models by Shir [6] and Daly and Harlow [5] do not exhibit the same tensorial symmetries as $\overline{u_i u_j u_k}$. Furthermore, the original parameter of the Daly and Harlow model is larger by an order of magnitude than the optimal one, -0.065, found for their model by Cormack [25]. For isothermal flow, there are two parameters, α_1 and ζ_1, to be determined in the model which was derived in the preceding section. From the basic model, equation (20), we obtain

$$\frac{\alpha_1}{\tau_1} \overline{u_i u_j u_k} + \frac{2}{5} (S_{il} \overline{u_l u_j u_k} + S_{jl} \overline{u_l u_i u_k} + S_{kl} \overline{u_l u_i u_j}) = - \zeta_1 f_{ijk} \qquad (36)$$

Alternatively, the linearized model, equation (28), can be simply written as

$$\overline{u_i u_j u_k} \simeq -\frac{\zeta_1}{\alpha_1}\tau_1 f_{ijk} + \frac{2}{5}\frac{\zeta_1}{\alpha_1^2}\tau_1^2 (S_{il}f_{ljk} + S_{jl}f_{lik} + S_{kl}f_{lij}) \qquad (37)$$

It may be noted that the first term in (37) is identical in form with the model of Hanjalic and Launder [8].

Since two experimental data sets for axisymmetric flow are included in our evaluation of the performance of the models, we also derived the transport equation for $\overline{u_i u_j u_k}$ in cylindrical coordinates. The coefficient matrix $\underline{\underline{A}}$ and the models for fourth-order correlations were applied in terms of cylindrical coordinates for the case of axisymmetric flows.

3.2 Experimental Data

We have found five flows which may be used to examine the performance of models for the triple velocity correlations. These are the asymmetric channel flow of Hanjalic and Launder [10], the pipe flow of Lawn [11], the wall jet of Irwin [12], the two-dimensional mixing layer of Wygnanski and Fiedler [12] and the round jet of Wygnanski and Fiedler [14]. Although there are no well-documented experimental data for three-dimensional flow, the flows listed above do provide a diverse basis for the examination of models. Two flows are axisymmetric and the other flows are two-dimensional. Hence, there occur only six non-zero triple correlations, namely, $\overline{u^3}$, $\overline{v^3}$, $\overline{u^2 v}$, $\overline{uv^2}$, $\overline{uw^2}$, and $\overline{vw^2}$. Here, u, v and w represent u_x, u_y and u_z in

Cartesian coordinates and u_z, u_r and u_ϕ in cylindrical coordinates, respectively.

As $\overline{uw^2}$ in the asymmetric channel flow and $\overline{vw^2}$ in the pipe flow are not reported in the references, it is necessary to estimate their values for comparison with the models. Since the small scale turbulence tends to be isotropic, we assume $\overline{uw^2} \sim \overline{uv^2}$ in the asymmetric channel flow. This assumption is supported by examination of the measurements of the mixing layer and wall jet in the region of strong mean strain rate. Laufer's [26] early work on pipe flow showed that $\overline{vw^2}/(\overline{w^4})^{\frac{1}{2}}(\overline{v^2})^{\frac{1}{2}} \sim \frac{1}{2}\,\overline{v^3}/(\overline{v^4})^{\frac{1}{2}}(\overline{v^2})^{\frac{1}{2}}$. If the flattening factor for w is similar to that for v, $\overline{vw^2}$ can be evaluated from the measured variables.

$$\overline{vw^2} \simeq \frac{1}{2}\,\frac{\overline{w^2}}{\overline{v^2}}\,\overline{v^3}$$

With the two exceptions which were just mentioned, all the other nonzero correlations were directly measured in the experiments. It should be noted, however, that the presentation of the triple velocity self-correlation function is ambiguous in the original paper of Wygnanski and Fiedler [14] for the round jet. The correlation $\overline{u^3}$ is <u>not</u> given in their figure 27. However, $\overline{w^3}$, which should be zero for the axisymmetric flow, is shown to be identical with $\overline{v^3}$. It appears to us that the symbol $\overline{w^3}$ has been used inadvertently in place of $\overline{u^3}$ in figure 27, and we adopt the assumption $\overline{u^3} \sim \overline{v^3}$ for approximate comparison of Wygnanski and Fiedler's data with the models.

3.3 Parameter Estimation

The basic model (36) and the linear model (37) have two parameters α_1 and ζ_1 to be evaluated with experimental data. We optimized these two parameters to yield the minimal standard deviation of experimental data from the models. The experimental data were fitted with smooth curves in order to obtain consistent values of variables and their derivatives. The total range of the appropriate independent variable was discretized into 40 grid intervals for each data set. All terms were evaluated at node points by interpolation or smooth curve representation of experimental data. Furthermore, the data were normalized with their root-mean-square values to ensure that all the data sets of various experiments had comparable weight in the determination of the parameters of the models.

For the basic model (36), we employed a search method to obtain the optimal values of α_1 and ζ_1. The parameters in the linear model (37) were determined by a least-squares method. The results, in terms of α_1 ζ_1 and the standard deviation of the model from experimental data, are given in Table 1, together with the same (or similar) results from other models. The numerical results show different optimal values of the parameters in equations (36) and (37). The linear model gives less deviation from the experimental data than the basic model. However, it should be noted that the values of α_1 and ζ_1 calculated by equation (36) are more general since the linear model is only an approximate form of the basic model.

As previously mentioned, the first term in equation (37) corresponds to Hanjalic and Launder's [8] model. From the comparison of their model

and our model, equation (37), it is apparent that the second term in equation (37) (i.e. the term with mean strain rate) can be partly represented by adjusting the parameter $\frac{\zeta_1}{\alpha_1}$ for the flows examined in this paper. The two-parameter linear model and the models of previous authors, with optimized parameters, are compared with a number of data sets for the triple velocity correlation in figures 1.1 - 5.6. The models of Shir [6] and Daly and Harlow [5] are not properly symmetric in the indices. Hence, we arbitrarily chose the combination of indices for each flow to obtain the best representation of experimental data. From its inherent characteristics, the model of Shir predicts that $\overline{u^3}$ and $\overline{uw^2}$ are identically zero for the flows with negligible change along stream lines (see figure 1.1, 1.5, 2.1, and 2.5).

The model of Cormack, Leal and Seinfeld [25] apparently has more flexibility due to its four adjustable parameters than the other models. It shows an especially good representation of $\overline{u^3}$ for the asymmetric channel flow, the pipe flow and the wall jet.

For the round jet, all the models do a relatively poor job of representing the experimental data. In particular, the triple correlations calculated by the models decrease too rapidly in the radial direction. Moreover, it is rather disappointing that most of the models, including our two-term model, yield the negative values for $\overline{u_z u_r^2}$ and $\overline{u_z u_\phi^2}$ around the center line, whereas the experimental data always remain positive. It may be speculated that significant terms for round jet may be neglected in the process of the simplification of the models. As more extensive data are not available for examination of the approximations involved in the modeling, our efforts to construct more sophisticated models are limited at present.

4. Nonisothermal Flow with Buoyancy Effects

One of the advantages of the generalized modeling approach which we have adopted is that gravitational effects can be included without further assumptions or approximations. Hence, this section is concerned with the application of the model to flows with significant buoyancy. Unfortunately, there are no well-documented experimental data for the flows with buoyancy except for a few unidirectional flows with heat convection. Due to this lack of diversified data, it is difficult to evaluate the optimal values of α_2, α_3, α_4, ζ_2, and ζ_3 in equations (21) - (23). The best we can do is to estimate their values, recognizing that they should be carefully re-examined after the accumulation of reliable triple correlation data.

First, we assume ζ_2 and ζ_3 are unity. The optimal value of ζ_1 for $\overline{u_i u_j u_k}$ is 1.19 as calculated from the basic model. Moreover, the parameter associated with $\overline{\theta^3}$ is unity. We thus presume the parameters, ζ_2 and ζ_3 are close to unity since the transport equations for $\overline{u_i u_j \theta}$ and $\overline{u_i \theta^2}$ have characteristics intermediate to those for $\overline{u_i u_j u_k}$ and $\overline{\theta^3}$. The triple correlations with α_1, α_2 and α_3 in equations (16), (17) and (18) are contributed from the correlations with $p^{(2)}$ and the molecular transport. Given this similar characteristic of the transport equations for $\overline{u_i u_j u_k}$, $\overline{u_i u_j \theta}$ and $\overline{u_i \theta^2}$, we conjecture that $\frac{\zeta_1}{\alpha_1} \simeq \frac{\zeta_2}{\alpha_2} \simeq \frac{\zeta_3}{\alpha_3}$. The optimal value of α_1 from the basic model is 21.6. For the molecular transport term for $\overline{\theta^3}$, Lumley et al. [9] neglected $\gamma \overline{\frac{\partial^2 \theta^3}{\partial x_1 \partial x_1}}$ by the consideration of characteristic length scales. In addition, they assumed $\overline{\theta^2}$ and ε_θ are well correlated. Consequently, they proposed

$$\gamma \frac{\partial^2 \overline{\theta^3}}{\partial x_1 \partial x_1} - 6\gamma \overline{\theta \frac{\partial \theta}{\partial x_1} \frac{\partial \theta}{\partial x_1}} \sim - 6 \frac{\overline{\theta^3}}{\overline{\theta^2}} \varepsilon_\theta$$

If Lumley et al.'s model is adopted, α_4 in equation (31) becomes six. Based upon these assumptions and approximations, the parameters which will be used for the following calculations are

$$\alpha_1 = 21.6, \quad \alpha_2 = 18.3, \quad \alpha_3 = 18.3, \quad \alpha_4 = 6$$

$$\zeta_1 = 1.18, \quad \zeta_2 = 1., \text{ and } \zeta_3 = 1 .$$

We now compare the model with the coefficients as estimated above with the experimental data for the heat convection between two plates due to Deardorff and Willis [15], and for the turbulent convection in water over ice due to Adrian [16]. For these flows, there is no comprehensible occurrence of mean velocity, and the equation (24) yields a very simple form.

$$\begin{bmatrix} \frac{\alpha_1}{\tau_1} & -\frac{21}{55}\beta_2 & & \\ \frac{\partial +}{\partial x_2} & \frac{\alpha_2}{\tau_2} & \frac{8}{5}\beta_2 & \\ & 2\frac{\partial \oplus}{\partial x_2} & \frac{\alpha_3}{\tau_3} & \frac{2}{3}\beta_2 \\ & & 3\frac{\partial \oplus}{\partial x_2} & \frac{\alpha_4}{\tau_4} \end{bmatrix} \cdot \begin{bmatrix} \overline{v^3} \\ \overline{v^2\theta} \\ \overline{v\theta^2} \\ \overline{\theta^3} \end{bmatrix} = \begin{bmatrix} f_{222} \\ g_{22} \\ h_2 \\ e \end{bmatrix} \qquad (38)$$

In the former experiment, only $\overline{v\theta^2}$ was measured at three Rayleigh numbers: 6.3×10^5, 2.5×10^6, and 1.0×10^7. The basic model, equation (25),

and the linear model, equation (27), are compared with experimental data in figure 6.3. The other triple correlations calculated by the models are depicted in figures 6.1, 6.2 and 6.4. In the region apart from the wall, the diagonal terms of $\underline{\underline{A}}$ are important since the mean temperature gradient is small. However, near the wall at the top, there is a thermal boundary layer in which the gradient of mean temperature profile is very large. Therefore, the matrix $\underline{\underline{A}}$ is dominated by the off-diagonal components rather than the diagonal components. Between these two different regions, there exists a region where the determinant of $\underline{\underline{A}}$ becomes extremely small, thus yielding sudden increases in the calculated triple correlations from the model. Obviously, we cannot expect that the model will be valid in the boundary layer due to the various assumptions which are made in the development of the model. However, as shown in figure 6.3, the model quite reasonably represents the experimental data for the region far from the wall.

In the turbulent convection in water over ice which was studied by Adrian [16], the dissipation rates of kinetic energy and thermal variance were not reported. In addition, the kinetic energy data were also left out of Adrian's paper. In order to get a quantitative comparison with the model, it was necessary to adopt plausible assumptions and estimate the missing data. In particular, we assumed $\overline{u^2} \simeq \overline{v^2} \simeq \overline{w^2}$ and $\frac{\varepsilon_\theta}{\overline{\theta^2}} \simeq \frac{\varepsilon}{q^2}$. The ε_θ was calculated by difference from the $\overline{\theta^2}$ transport equation.

In this flow, the mean temperature increases rapidly near the ice, is then almost constant across the body of the fluid, and finally exhibits a steep temperature increase near the free surface. It is difficult to precisely evaluate the gradient of mean temperature from experimental data

in the region where it remains almost constant. Moreover, it is also difficult to accurately calculate ε_θ in the vicinity of the free surface due to the steep gradient of $\overline{v\theta^2}$. Nevertheless, the model is compared with the experimental data for $\overline{v\theta^2}$ and $\overline{\theta^3}$ in figures 7.1 and 7.2. The calculated forms for $\overline{v^3}$ and $\overline{v^2\theta}$ are not reported in the belief that the assumptions, $\frac{\varepsilon_\theta}{\overline{\theta^2}} \simeq \frac{\varepsilon}{q^2}$ and $\overline{u^2} \simeq \overline{v^2} \simeq \overline{w^2}$ are likely to affect these two terms most strongly so that they may not be reliable.

In spite of all of the difficulty in obtaining experimental data, the matrix inversion model shows essentially correct profiles for $\overline{v\theta^2}$ and $\overline{\theta^3}$. Near the free surface, there are abrupt variations of triple correlations in the region where the dominance of the matrix $\underline{\underline{A}}$ transits from diagonal terms to off-diagonal terms. This feature is well confirmed by the experimental results, and provides strong support for the validity of the matrix inversion model, even considering the uncertainties in estimating the missing experimental data.

5. Conclusions

A model for triple correlations in a general non-isothermal flow was derived from their transport equations. As triple correlations are linearly related in the model, they can be easily calculated by matrix inversion. For flows with dominant diagonal terms in the matrix of coefficients, we proposed a first-order linearized model, which eliminates the matrix inversion computation. The advantage of the model is that the whole family of triple correlations of temperature and velocity can be simultaneously modeled. In addition, the gravitational effects are automatically taken into account.

We extensively compared the model which we obtained by this matrix inversion scheme with the experimental data for triple velocity correlations in isothermal flows, including asymmetric channel flow, pipe flow, wall jet, two-dimensional mixing layer, and round jet. It was found that the model represents the experimental data for the round jet relatively poorly. Although any model should be invariant to changes in the coordinate system, it is still probable that an important term for axisymmetric flow may be neglected in the process of the construction of a simple model. Overall, the model shows a reasonable representation for all flows. The term with mean strain rate did not significantly improve the model, although the magnitude of the generation term is comparable with any other term in the transport equation when the mean velocity is rapidly changing. This indicates that the term with mean strain rate can be partly represented by adjusting the parameter of the first term of the model, equation (32).

There are scarcely any well-documented experimental data for non-isothermal flows with buoyancy effects. We calculated triple correlations for heat convection between two plates and for convection in water over ice. The model shows abrupt changes in the triple correlations, namely $\overline{v\theta^2}$ and $\overline{\theta^3}$, near the thermal boundary layer at the free surface, and these are well confirmed by the experiment of Adrian [16]. For the heat convection between two plates, the model fails near the solid wall, as expected, since the wall effects were not included in the derivation of the model. Nevertheless, the calculations for $\overline{v\theta^2}$ exhibit at least the correct qualitative dependence on Rayleigh number.

In conclusion, the matrix inversion model has shown a promising broad applicability to various flows. We believe that the model has the potential of correct prediction for complicated nonisothermal turbulent flows with buoyancy effects, as well as for simple isothermal flows.

References

1. Reynolds, W. C., "Recent Advances in the Computation of Turbulent Flows," Advances in Chemical Engineering, Vol. 9, 1974, pp. 193-246.
2. Reynolds, W. C., "Computation of Turbulent Flows," Annual Review of Fluid Mechanics, 1976, pp. 183-208.
3. Launder, B. E., "Progress in Modeling of Turbulent Transport," Lecture Series, No. 76, von Karman Inst., Belgium, 1975.
4. Lumley, J. L., "Prediction Methods for Turbulent Flows," Lecture Series, No. 76, von Karman Inst., Belgium, 1975.
5. Daly, B. J., and Harlow, F. H., "Transport Equations in Turbulence," Phys. Fluids, Vol. 13, 1970, pp. 2634.
6. Shir, C. C., "A Preliminary Numerical Study of Atmospheric Turbulent Flows in the Idealized Planetary Boundary Layer," J. Atmos. Sci., Vol. 30, 1973, pp. 1327-1339.
7. Wyngaard, J. C., Cote, O. R., and Rao, K. S., "Modeling the Atmospheric Boundary Layer," Adv. in Geophysics, 18A, 1974, pp. 193-211.
8. Hanjalic, K. and Launder, B. E., "A Reynolds Stress Model of Turbulence and Its Application to Thin Shear Flows," J. Fluid Mech., Vol. 52, 1972, pp. 609-638.
9. Lumley, J. I., Zeman, O. and Siess, J., "The Influence of Buoyancy on Turbulent Transport," J. Fluid Mech., Vol. 84, 1976, pp. 581.
10. Hanjalic, K. and Launder, B. E., "Fully Developed Asymmetric Flows in a Plane Channel," J. Fluid Mech., Vol. 51, 1972, pp. 301-335.
11. Lawn, C. J., "The Determination of the Rate of Dissipation in Turbulent Pipe Flow," J. Fluid Mech., Vol. 48, 1971, pp. 477-505.

12. Irwin, H. P. A. H., "Measurements in a Self-Preserving Plane Wall-Jet in a Positive Pressure Gradient," J. Fluid Mech., Vol. 61, 1973, pp. 33-63.

13. Wygnanski, I. and Fiedler, H. E., "The Two-Dimensional Mixing Region," J. Fluid Mech., Vol. 41, 1970, pp. 327-361.

14. Wygnanski, I. and Fiedler, H. E., "Some Measurements in the Self-Preservation Jet," J. Fluid Mech., Vol. 38, 1969, pp. 577-612.

15. Deardorff, J. W. and Willis, G. E., "Investigation of Turbulent Thermal Convection between Two Horizontal Plates," J. Fluid Mech., Vol. 28, 1967, pp. 675-704.

16. Adrian, R. J., "Turbulent Convection in Water over Ice," J. Fluid Mech., Vol. 69, 1975, pp. 753-781.

17. Schlichting, H., Boundary Layer Theory, McGraw-Hill, 1968

18. Monin, A. S. and Yaglom, A. M., Statistical Fluid Mechanics, Vols. 1 and 2, MIT Press, Cambridge, 1971.

19. Chou, P. Y., "On Velocity Correlations and the Solutions of the Equations of Turbulent Fluctuations," Quart. of App. Math., Vol. 3, 1945, pp. 38-54

20. Rotta, J., "Statistiche Theorie nichthomogener Turbulenz, 1 Mitteilung," Zeitschrift fur Physik, Bd. 129, 1951, pp. 547-572.

21. Rotta, J., "Statistiche Theorie nichthomogener Turbulenz, 1 Mitteilung," Zeitschrift fur Physik, Bd. 131, 1951, pp. 51-77.

22. De Karman, T. and Horwarth, I., "On the Statistical Theory of Isotropic Turbulence," Proc. Roy. Soc. London, 164A, 1938, pp. 192-215.

23. Tennekes, H. and Lumley, J. I., A First Course in Turbulence, MIT Press, Cambridge, 1972.

24. Cormack, D. E., Leal, L. G., and Seinfeld, J. H., "An Evaluation of Mean Reynolds Stress Turbulence Models: The Triple Velocity Correlation," J. Fluids Eng., Trans ASME, Ser. I., Vol. 100, 1978, pp. 47-

25. Cormack, D. E., PhD Dissertation, California Institute of Technology, 1975.

26. Laufer, J., "The Structure of Turbulence in Fully Developed Pipe Flow," N.A.C.A. Rep. No. 1174, 1955.

APPENDIX A: Matrix $\underline{\underline{A}}$ for two-dimensional non-isothermal flow (the gravity is in x_2-direction).

$t_1 + 3a$		$3c$						$\frac{6}{11}\beta_2$				
	$t_1 + 3b$		$3c$			$\frac{-6}{55}\beta_2$	$\frac{-21}{55}\beta_2$		$\frac{-6}{55}\beta_2$			
c		$t_1 + 2a + b$	$2c$			$\frac{-17}{55}\beta_2$	$\frac{8}{55}\beta_2$		$\frac{-2}{55}\beta_2$			
	c	$2c$	$t_1 + a + 2b$					$\frac{-4}{11}\beta_2$				
				$t_1 + a$	c			$\frac{2}{11}\beta_2$				
				c	$t_1 + b$	$\frac{-2}{55}\beta_2$	$\frac{8}{55}\beta_2$		$\frac{-17}{55}\beta_2$			
T_1		T_2				$t_2 + 2a$		$2c$			$\frac{1}{5}\beta_2$	
	T_2		T_1				$t_2 + 2b$	$2c$			$\frac{8}{5}\beta_2$	
		T_1	T_2			c	c	$t_2 + a + b$		$\frac{7}{10}\beta_2$		
				T_1	T_2				t_2		$\frac{1}{5}\beta_2$	
						$2T_1$	$2T_2$			$t_3 + a$	c	
							$2T_2$	$2T_1$		c	$t_3 + b$	$\frac{2}{3}\beta_2$
										$3T_1$	$3T_2$	t_4

Here, the order of variables = $\left\{\overline{u^3},\ \overline{v^3},\ \overline{u^2v},\ \overline{uv^2},\ \overline{uw^2},\ \overline{vw^2}\right\}, \left\{\overline{u^2\theta},\ \overline{v^2\theta},\ \overline{uv\theta},\ \overline{w^2\theta}\right\}, \left\{\overline{u\theta^2},\ \overline{v\theta^2}\right\}, \left\{\overline{\theta^3}\right\}$

$t_1 = \frac{\alpha_1}{\tau_1}$, $t_2 = \frac{\alpha_2}{\tau_2}$, $t_3 = \frac{\alpha_3}{\tau_3}$, $t_4 = \frac{\alpha_4}{\tau_4}$, $a = \frac{2}{5}S_{11}$, $b = \frac{2}{5}S_{22}$, $c = \frac{2}{5}S_{12}$, $T_1 = \frac{\partial\Theta}{\partial x}$, and $T_2 = \frac{\partial\Theta}{\partial y}$.

Table 1. Comparison of Models for Triple Velocity Correlations

Model	Parameter (Optimized Parameter)	Standard[1] Deviation
Hanjalic and Launder [8]	-0.044 (-0.0581)	0.749 (0.731)
Shir [6]	-0.01 (-0.0162)	0.945 (0.935)
Daly and Harlow [5]	-0.65[2] (-0.157)	0.825 (0.716)
Cormack, Leal and Seinfeld [24]	-0.00814, -0.0172, -0.0480, -0.102 (-0.00702, -0.00534, -0.0480, -0.072)	0.583 (0.514)
Equation (37)	-0.0332[3], 0.00361[4]	0.663
Equation (36)	-0.0331[3], 0.00055[4]	0.703

[1]Defined as $\sqrt{\frac{\Sigma(\hat{x}_i - x_i)^2}{N}}$.

$\hat{x}_1$: from Model; x_i: from experimental results.

[2]Optimized value by Cormack [25].

[3]$-\zeta_1/\alpha_1$ in equation (32).

[4]$\frac{2}{5}\zeta_1/\alpha_1^2$ in equation (32).

Figure Captions

1) Figures 1.1 - 5.6: ——— The model of equation (37).

— — — The model of Hanjalic and Launder [8].

— - — The model of Daly and Harlow [5].

— — — The model of Shir [6].

— — — — The model of Cormack, Leal and Seinfeld [24].

++++++ Smooth curve representation of experimental data (cf. section 3.2 for Fig. 1.5 and 2.6).

Figures 1.1 - 1.6: Asymmetric channel flow (Hanjalic and Launder [10]).

Figures 2.1 - 2.6: Pipe flow (Lawn [11]).

Figures 3.1 - 3.6: Wall jet (Irwin [12]).

Figures 4.1 - 4.6: Two-dimensional mixing layer (Wygnanski and Fiedler [13]).

Figures 5.1 - 5.6: Round jet (Wygnanski and Fiedler [14]).

The parameters of the models were optimized for the whole five flows. η : similarity variable.

2) Figures 6.1 - 7.2: ——— The basic model, equation (25).

------ The linear model, equation (27).

o,Δ,+ Experimental data.

Figures 6.1 - 6.6: Heat convection between two plates (Deardorf and Willis [15]).

Figures 7.1 - 7.2: Heat convection in water over ice (Adrian [16]).

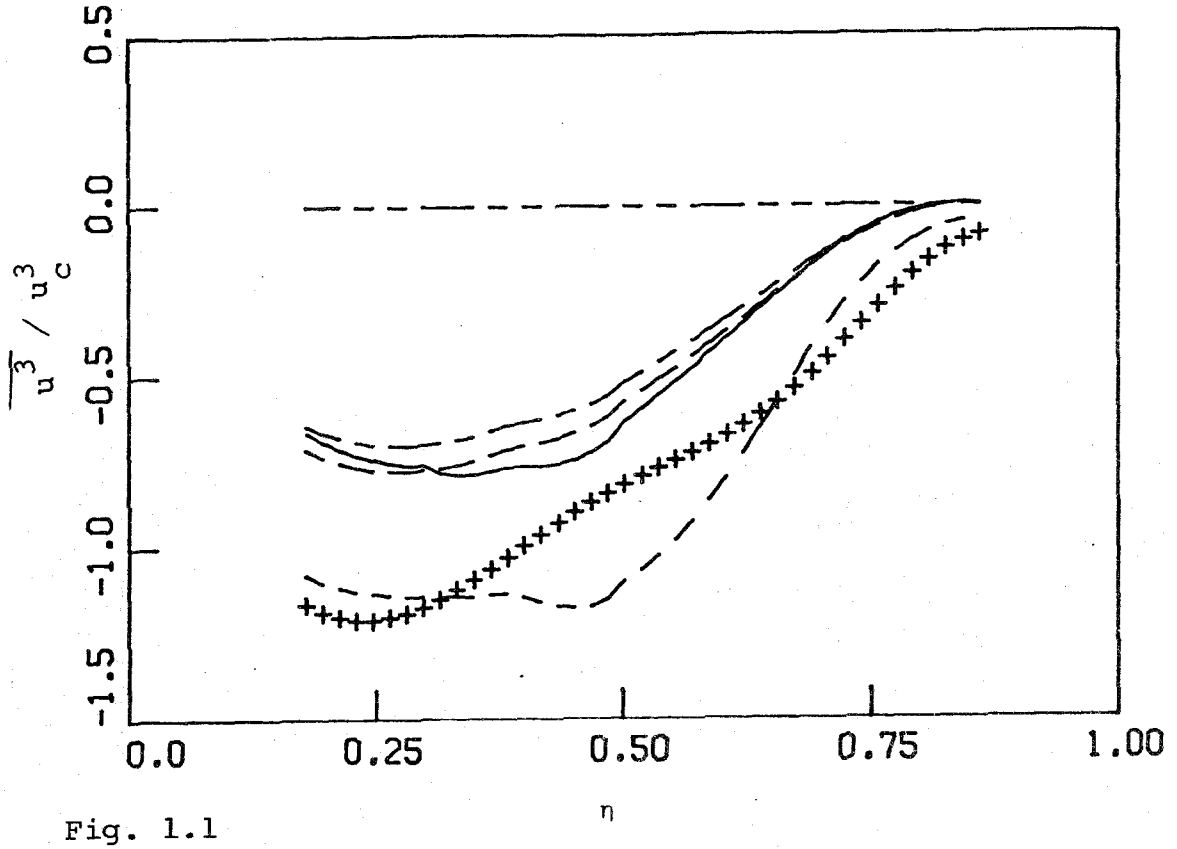
0.5
0.0
-0.5
-1.0
-1.5
$\overline{u^3} / u_c^3$
0.0
0.25
0.50
0.75
1.00
η

Fig. 1.1

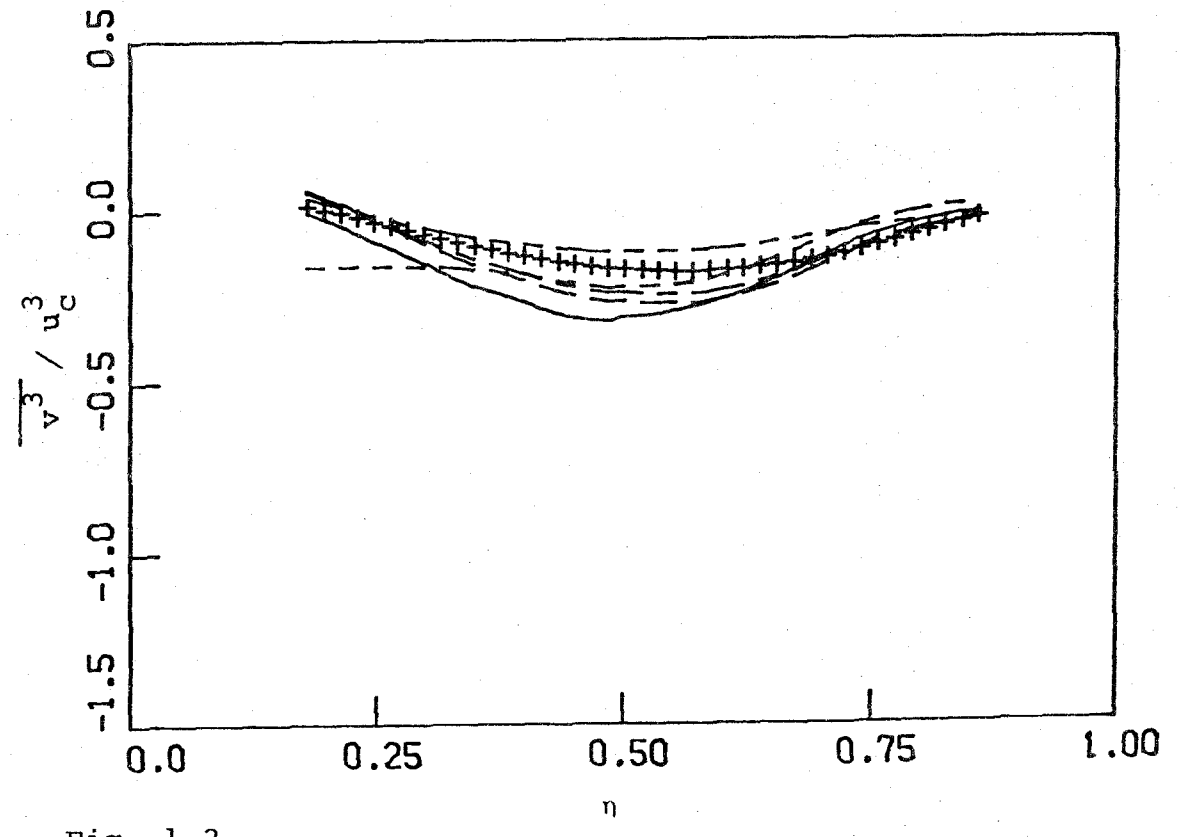
0.5
0.0
-0.5
-1.0
-1.5
$\overline{v^3} / u_c^3$
0.0
0.25
0.50
0.75
1.00
η

Fig. 1.2

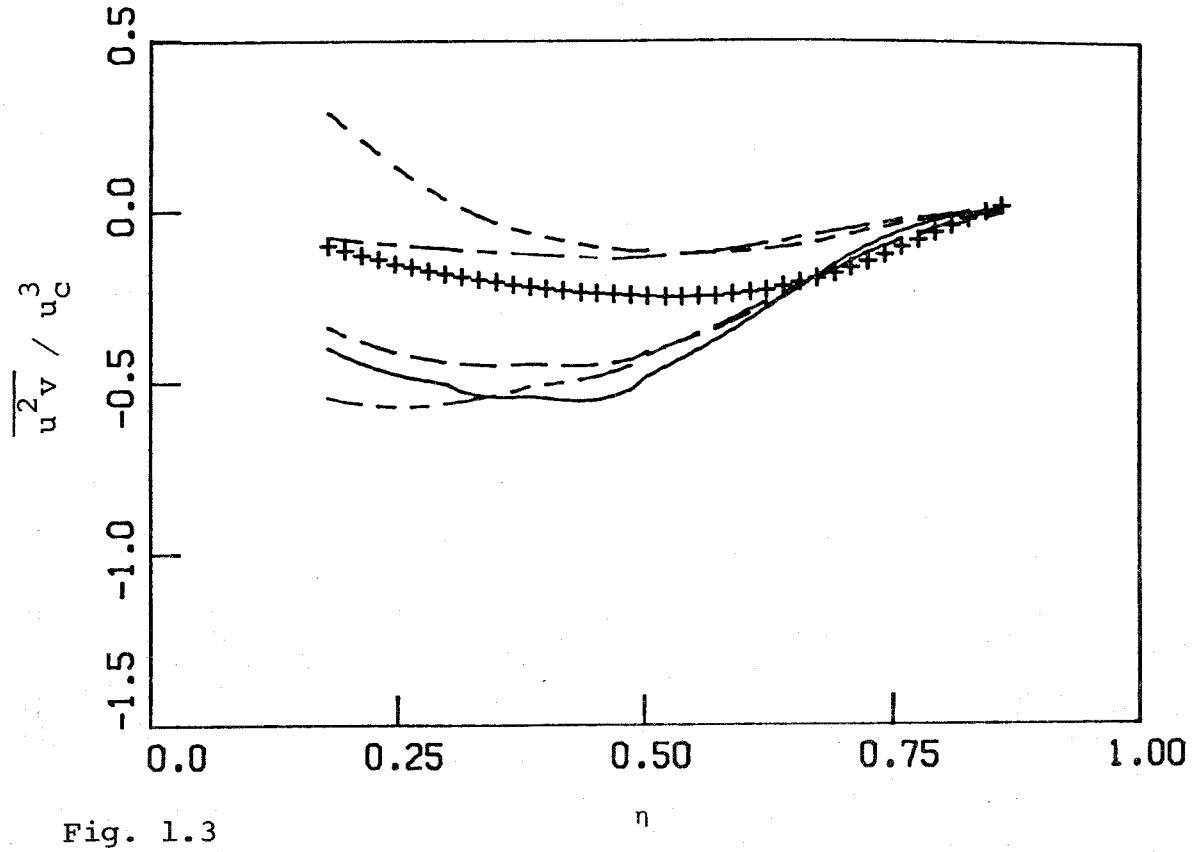
0.5
0.0
-0.5
-1.0
-1.5
$\overline{u^2v}$ / u_c^3
0.0
0.25
0.50
0.75
1.00
η

Fig. 1.3

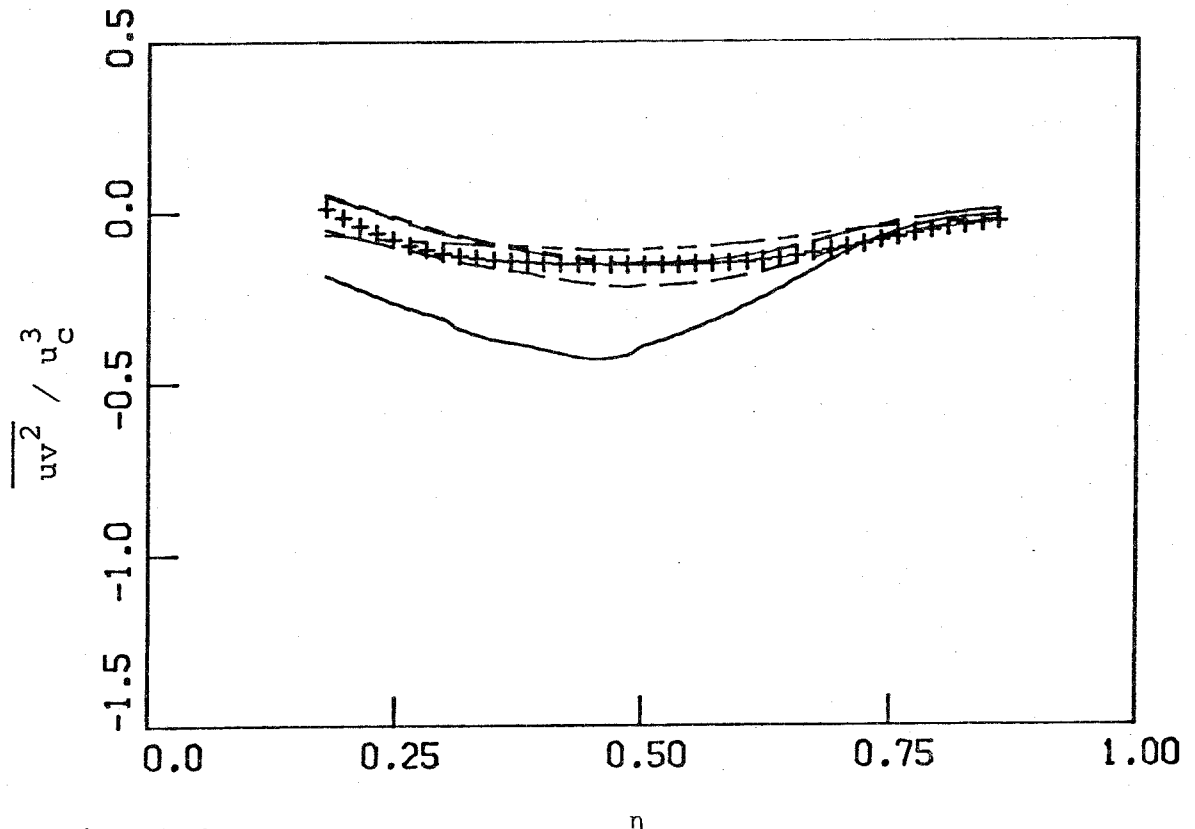
0.5
0.0
-0.5
-1.0
-1.5
$\overline{uv^2}$ / u_c^3
0.0
0.25
0.50
0.75
1.00
η

Fig. 1.4

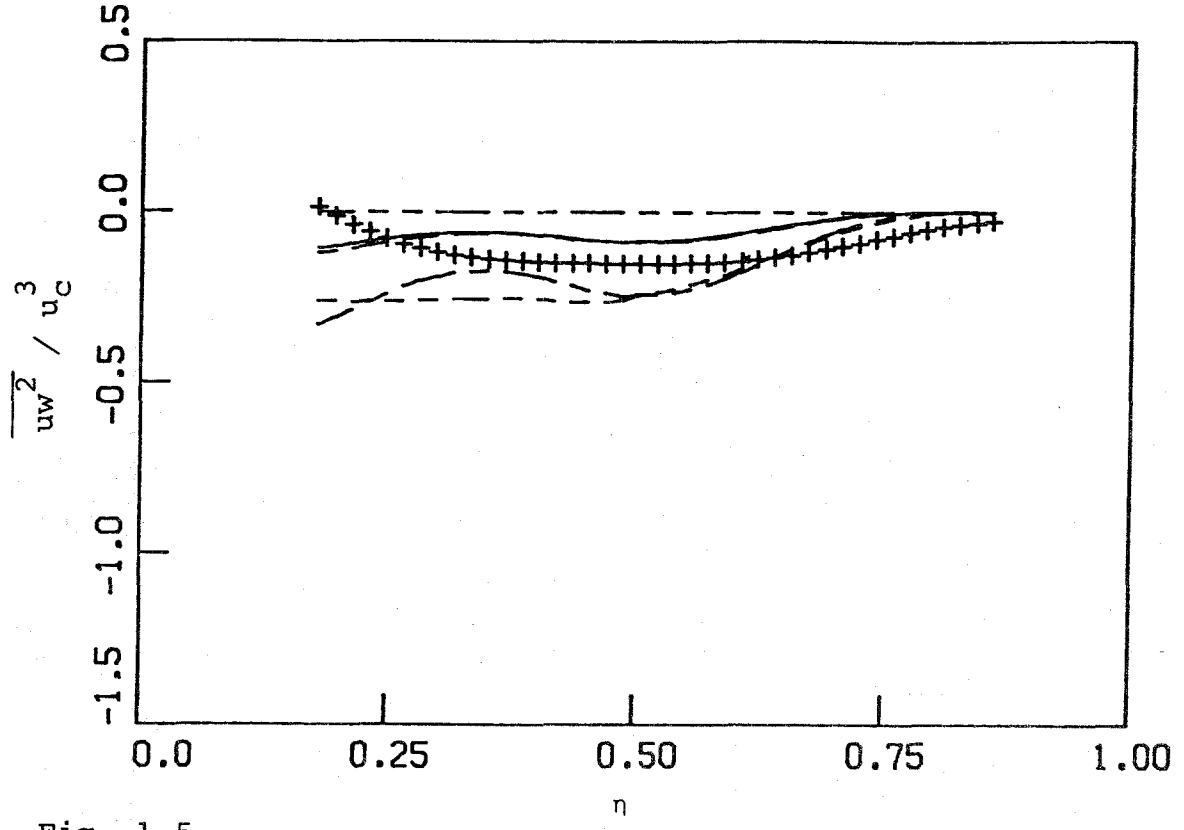
0.5
0.0
-0.5
-1.0
-1.5
$\overline{uw^2} / u_c^3$
0.0
0.25
0.50
0.75
1.00
η

Fig. 1.5

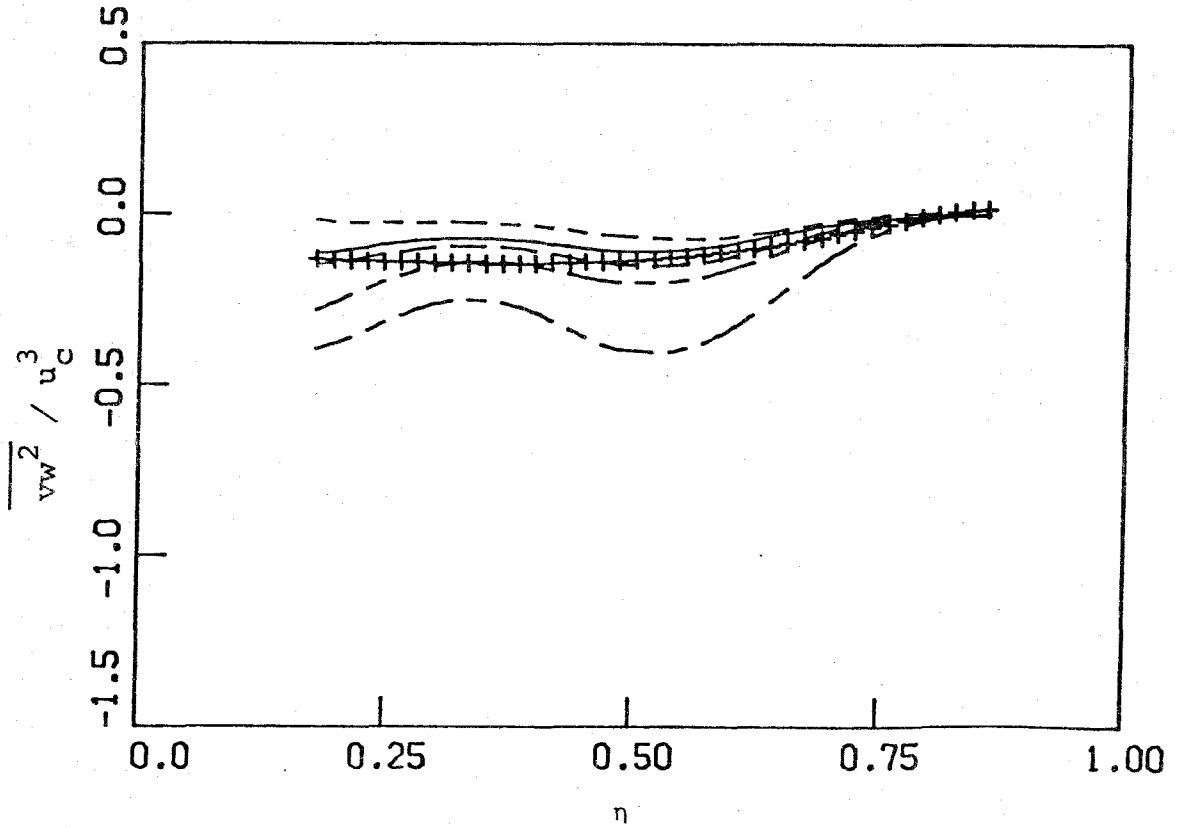
0.5
0.0
-0.5
-1.0
-1.5
$\overline{vw^2} / u_c^3$
0.0
0.25
0.50
0.75
1.00
η

Fig. 1.6

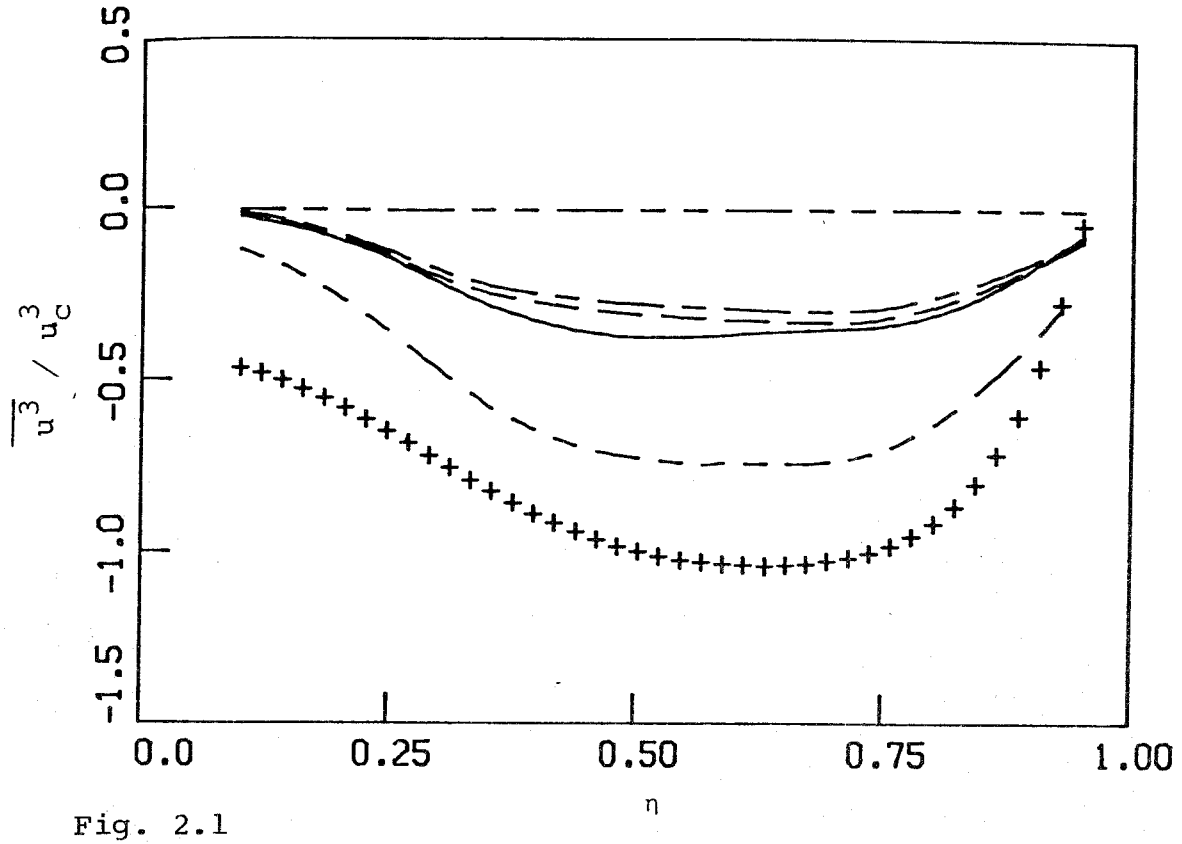
0.5
0.0
-0.5
-1.0
-1.5
$\overline{u^3} / u_c^3$
0.0
0.25
0.50
0.75
1.00
η

Fig. 2.1

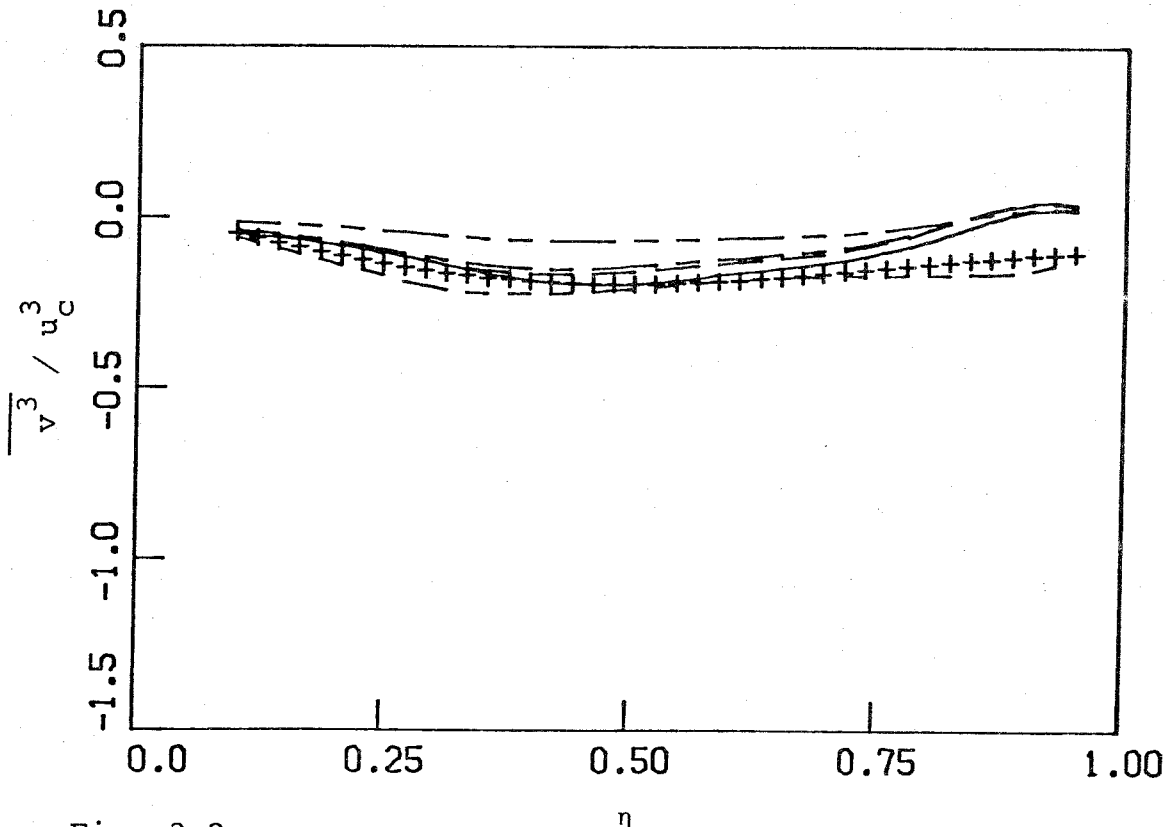
0.5
0.0
-0.5
-1.0
-1.5
$\overline{v^3} / u_c^3$
0.0
0.25
0.50
0.75
1.00
η

Fig. 2.2

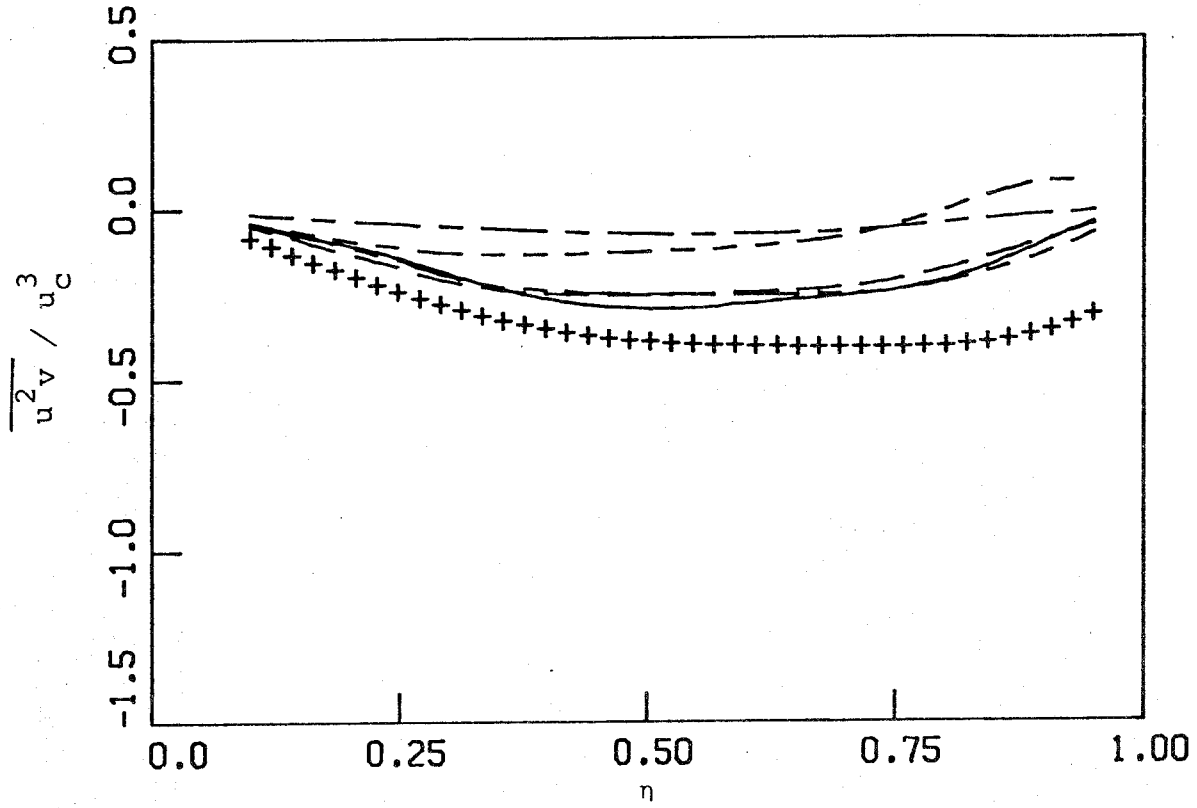
0.5
0.0
-0.5
-1.0
-1.5
$\overline{u^2 v} / u_c^3$
0.0
0.25
0.50
0.75
1.00
η

Fig. 2.3

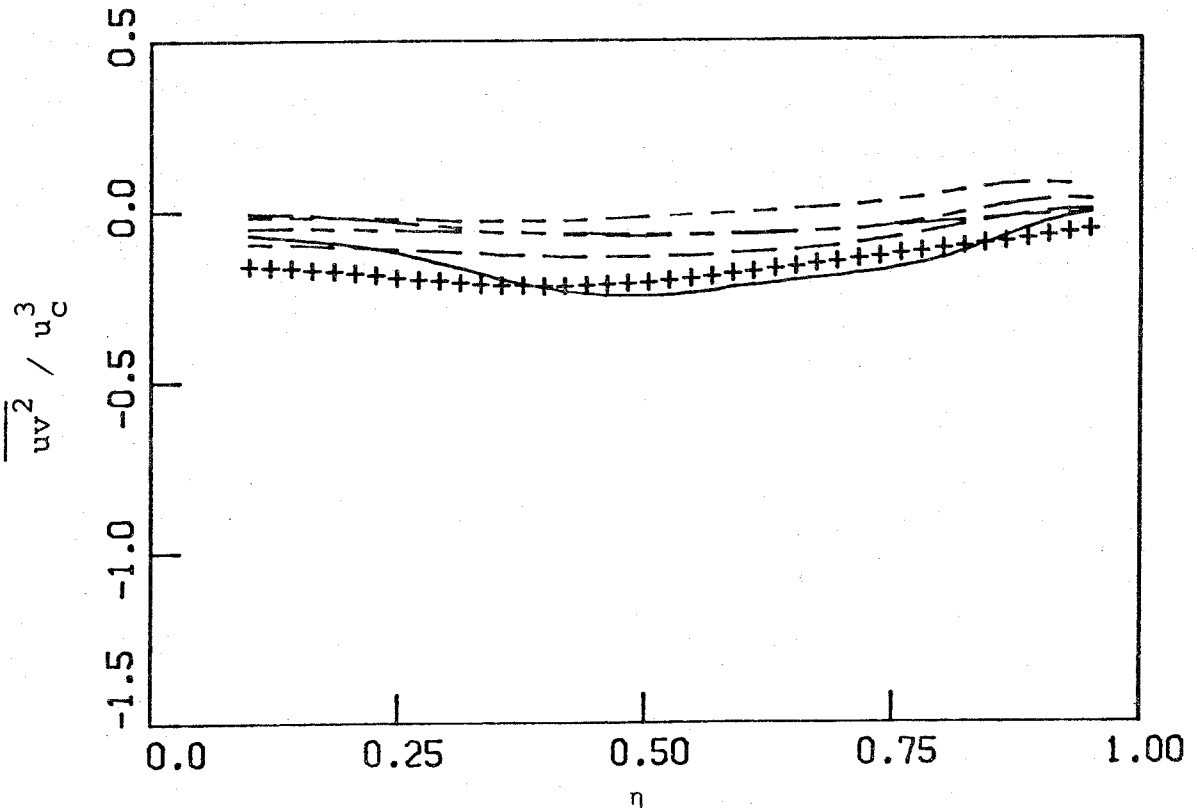
0.5
0.0
-0.5
-1.0
-1.5
$\overline{uv^2} / u_c^3$
0.0
0.25
0.50
0.75
1.00
η

Fig. 2.4

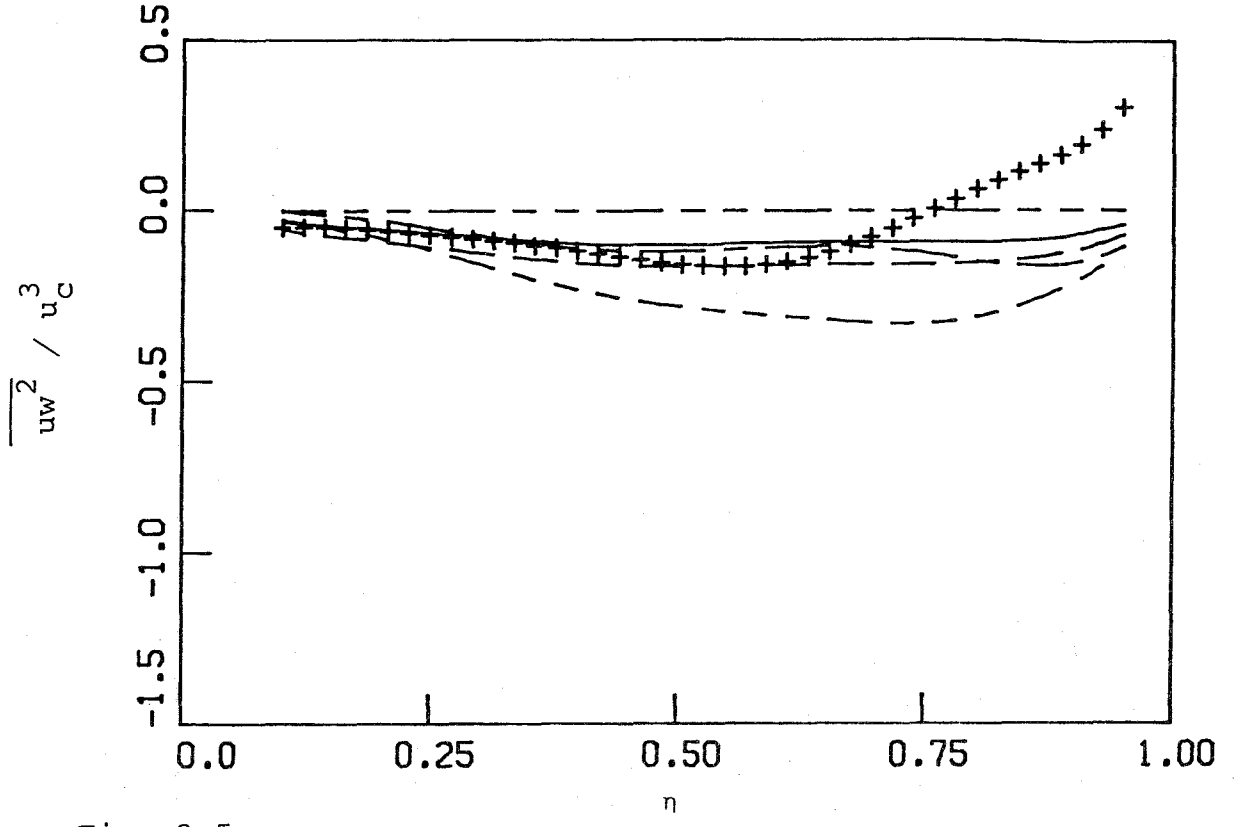
0.5
0.0
-0.5
-1.0
-1.5
$\overline{uw}^2 / u_c^3$
0.0
0.25
0.50
0.75
1.00
η

Fig. 2.5

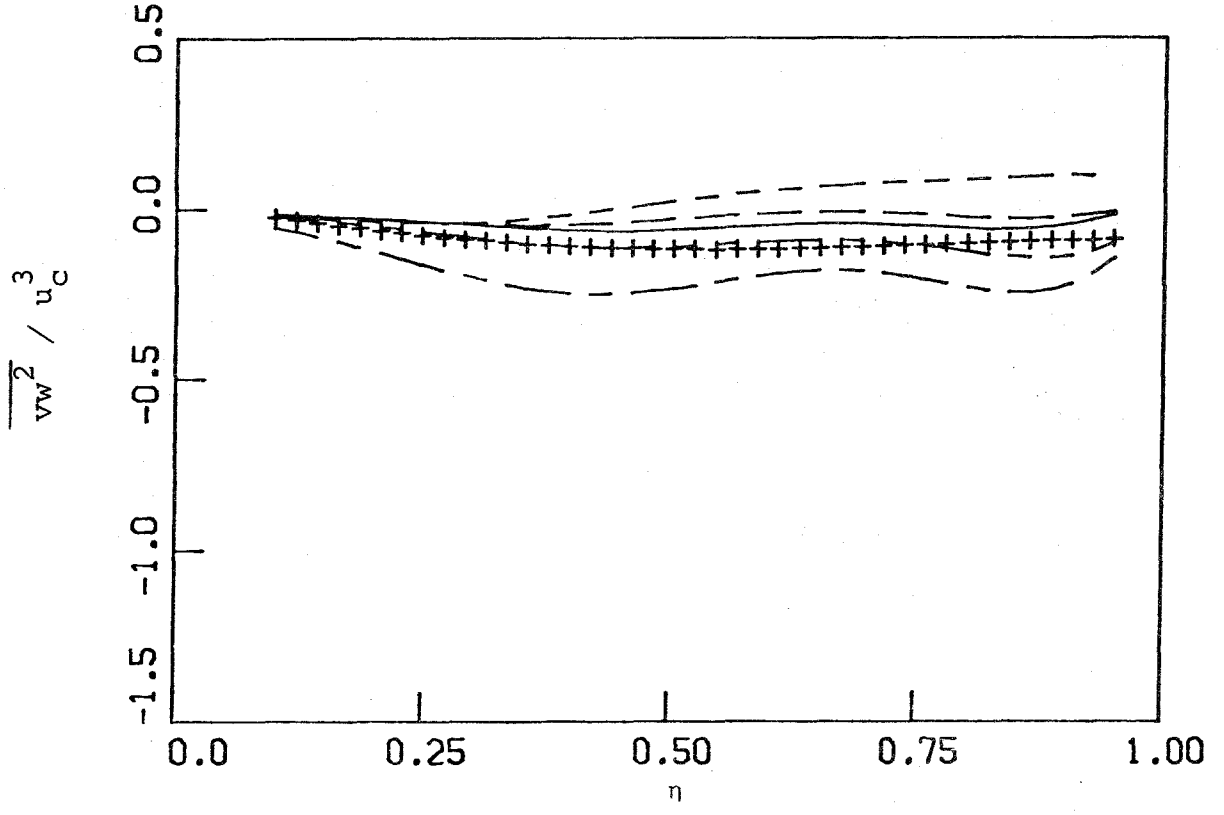
0.5
0.0
-0.5
-1.0
-1.5
$\overline{vw}^2 / u_c^3$
0.0
0.25
0.50
0.75
1.00
η

Fig. 2.6

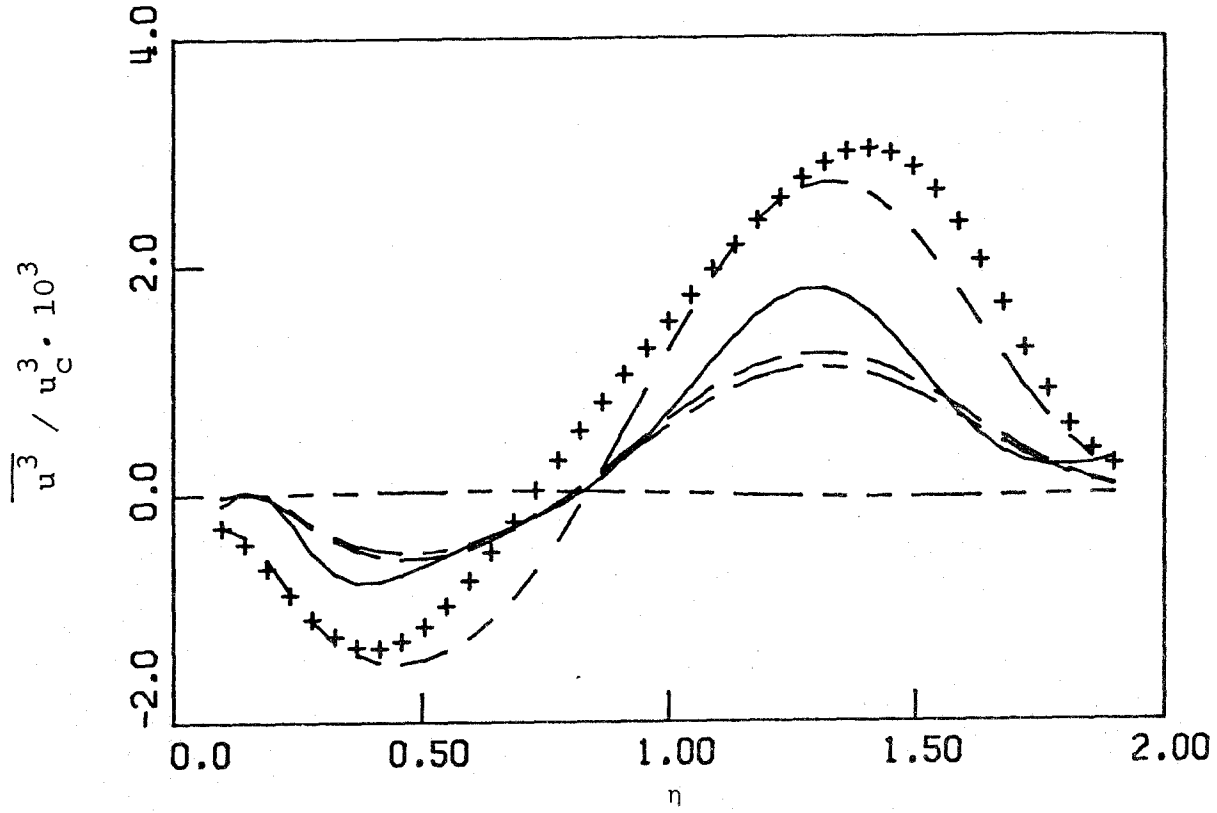
4.0
2.0
0.0
-2.0
0.0
0.50
1.00
1.50
2.00
η
$\overline{u^3} / u_c^3 \cdot 10^3$

Fig. 3.1

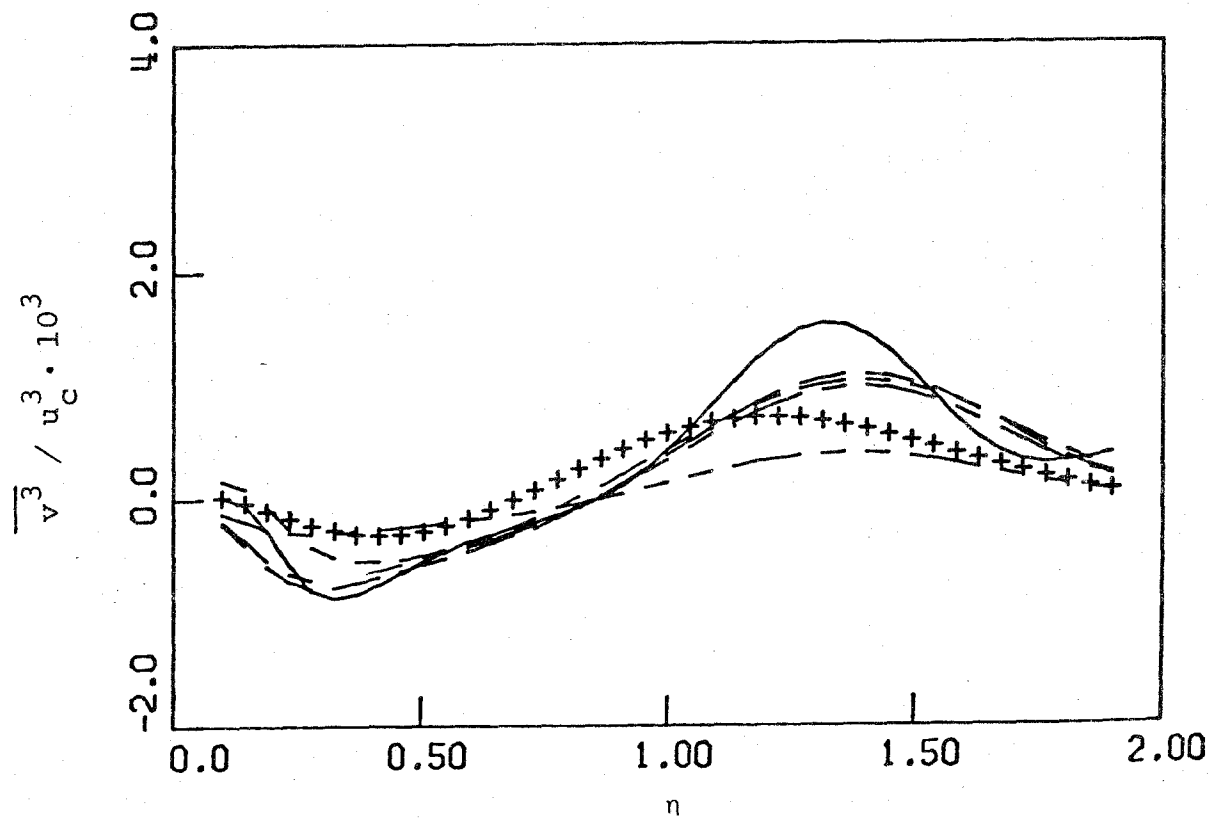
4.0
2.0
0.0
-2.0
0.0
0.50
1.00
1.50
2.00
η
$\overline{v^3} / u_c^3 \cdot 10^3$

Fig. 3.2

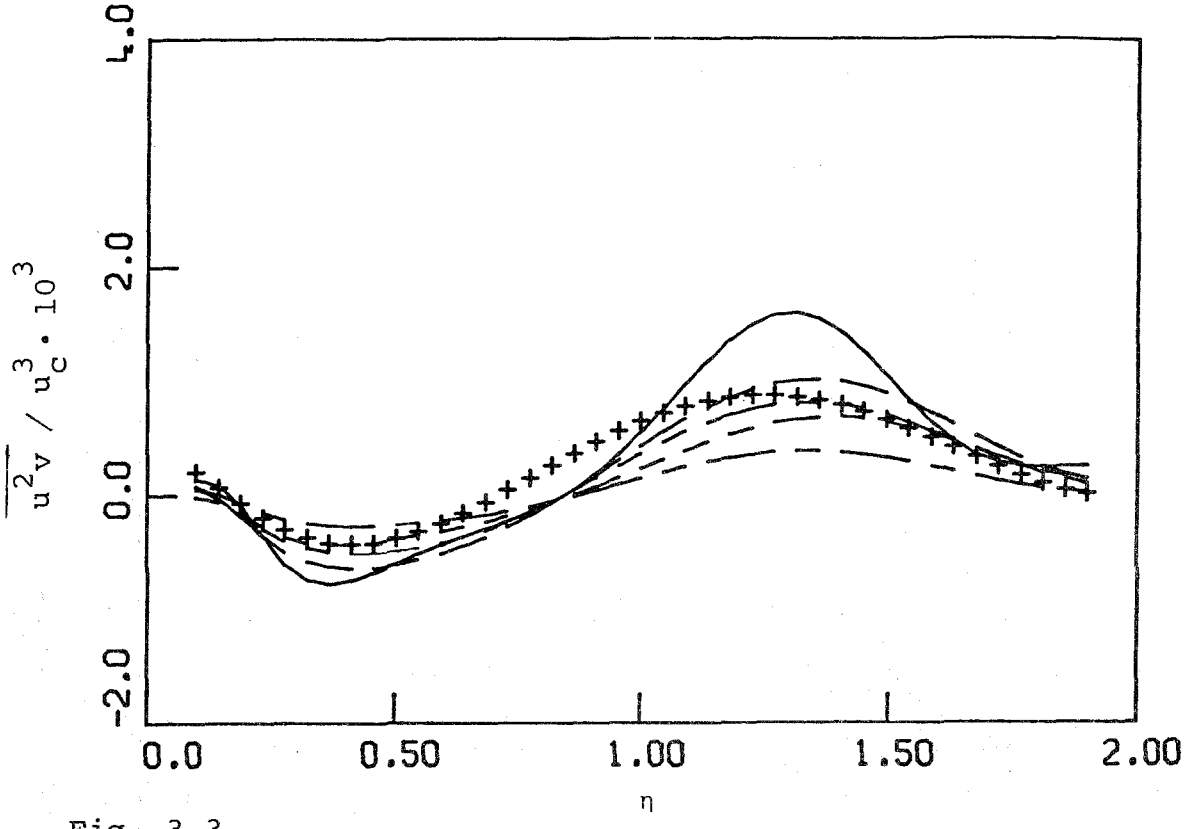
4.0
2.0
0.0
-2.0
$\overline{u^2v}$ / $u_c^3 \cdot 10^3$
0.0
0.50
1.00
1.50
2.00
η

Fig. 3.3

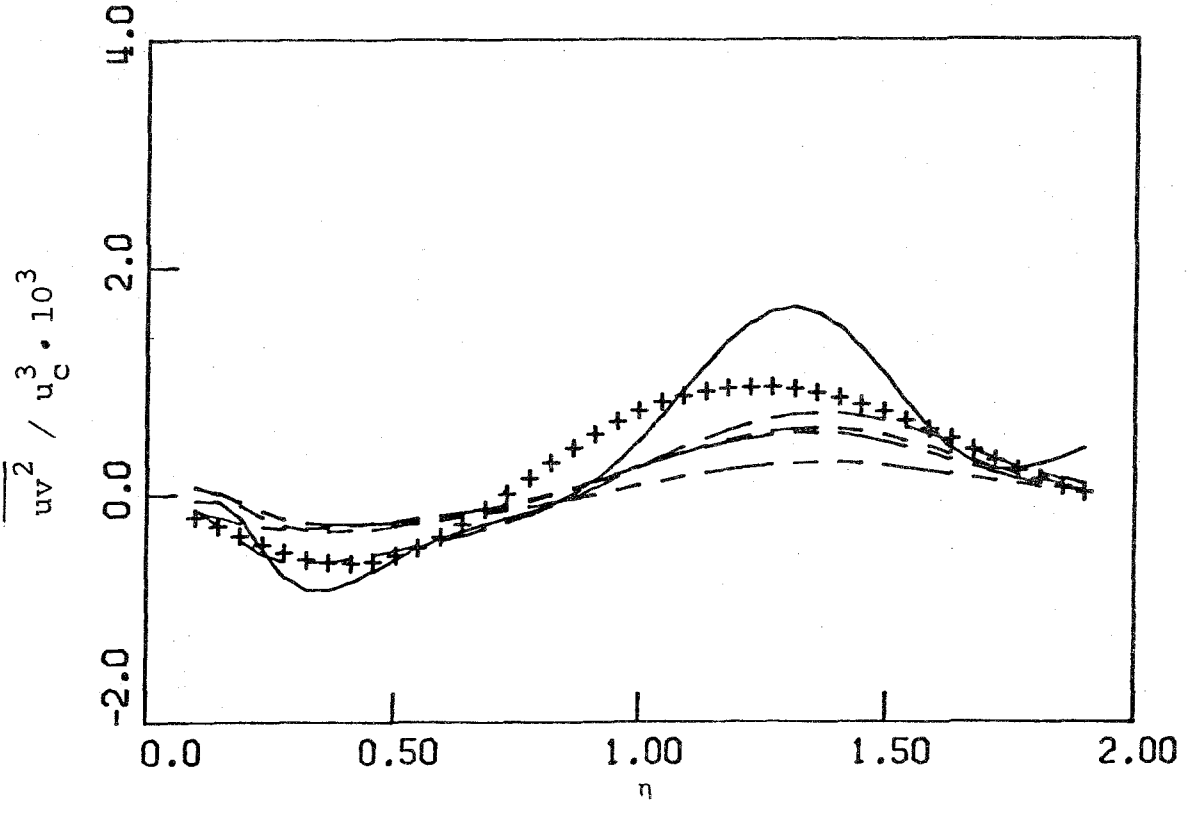
4.0
2.0
0.0
-2.0
$\overline{uv^2}$ / $u_c^3 \cdot 10^3$
0.0
0.50
1.00
1.50
2.00
η

Fig. 3.4

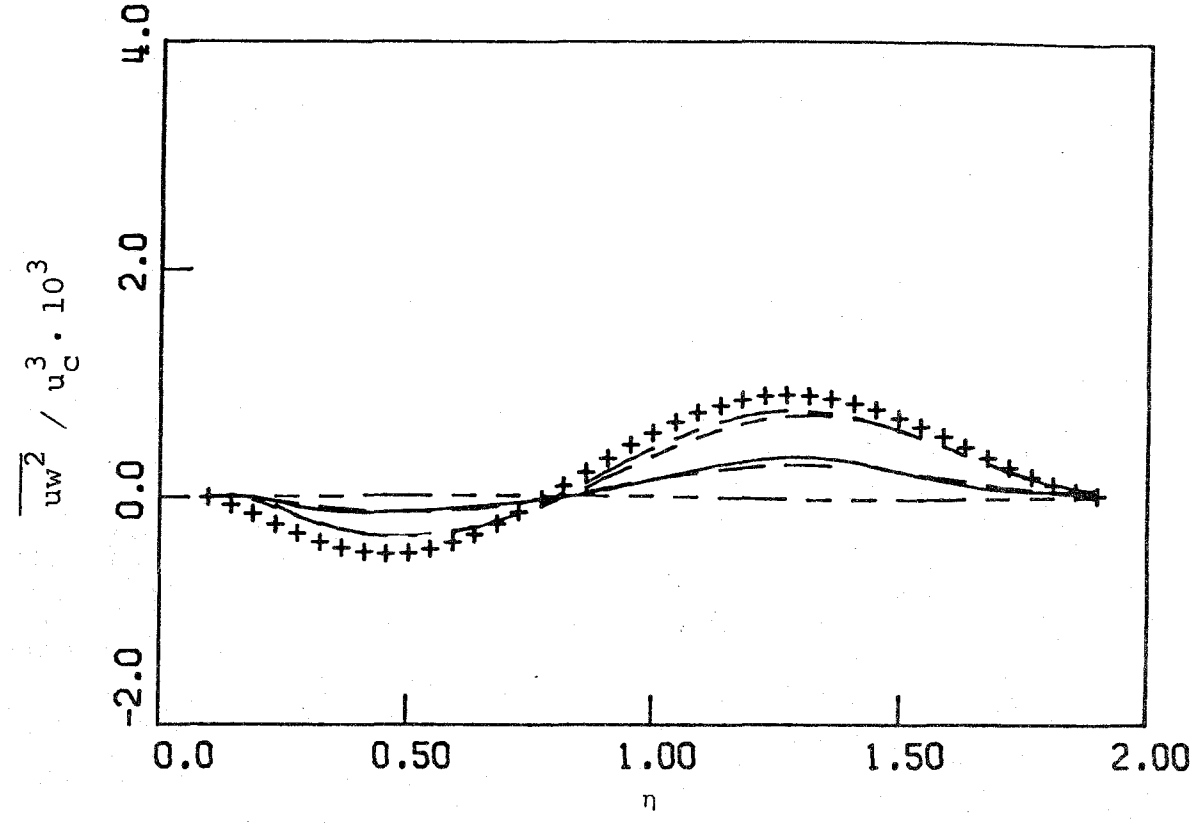
4.0
2.0
0.0
-2.0
$\overline{uw}^2 / u_c^3 \cdot 10^3$
0.0
0.50
1.00
1.50
2.00
η

Fig. 3.5

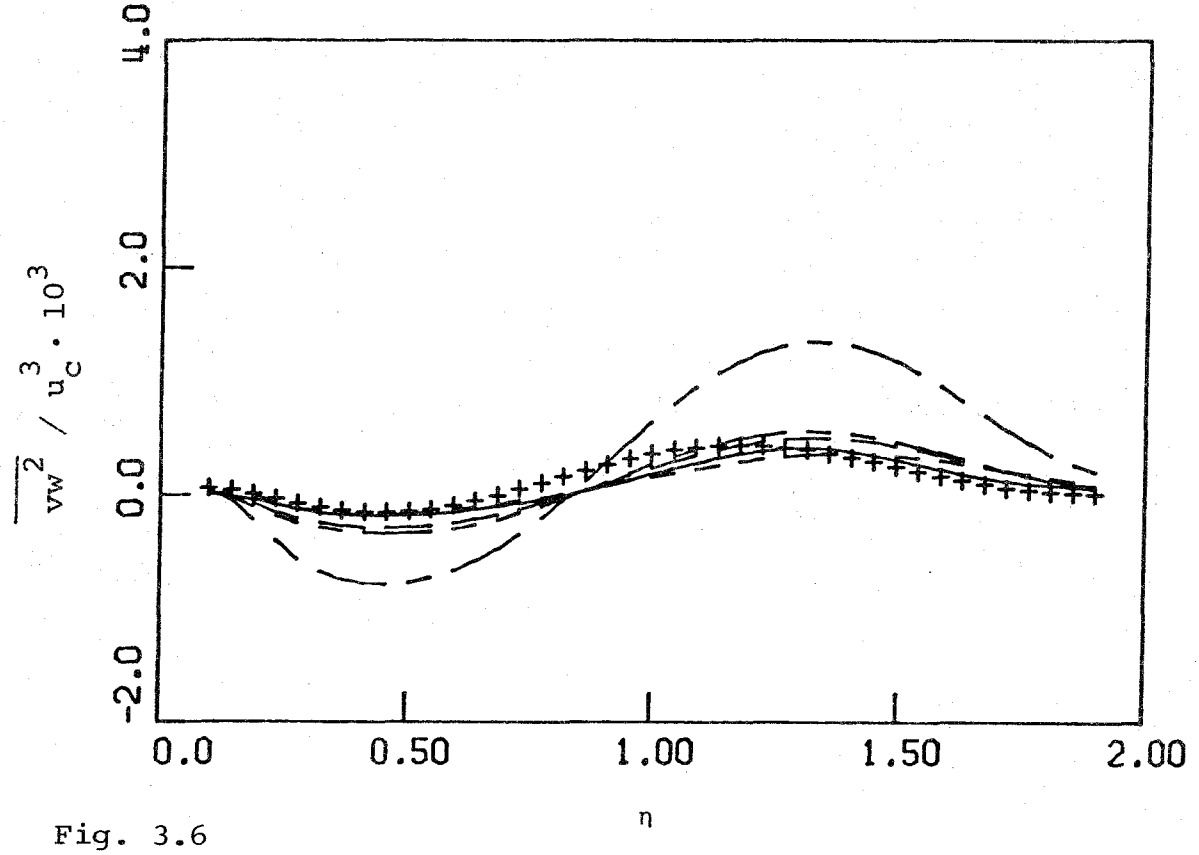
4.0
2.0
0.0
-2.0
$\overline{vw}^2 / u_c^3 \cdot 10^3$
0.0
0.50
1.00
1.50
2.00
η

Fig. 3.6

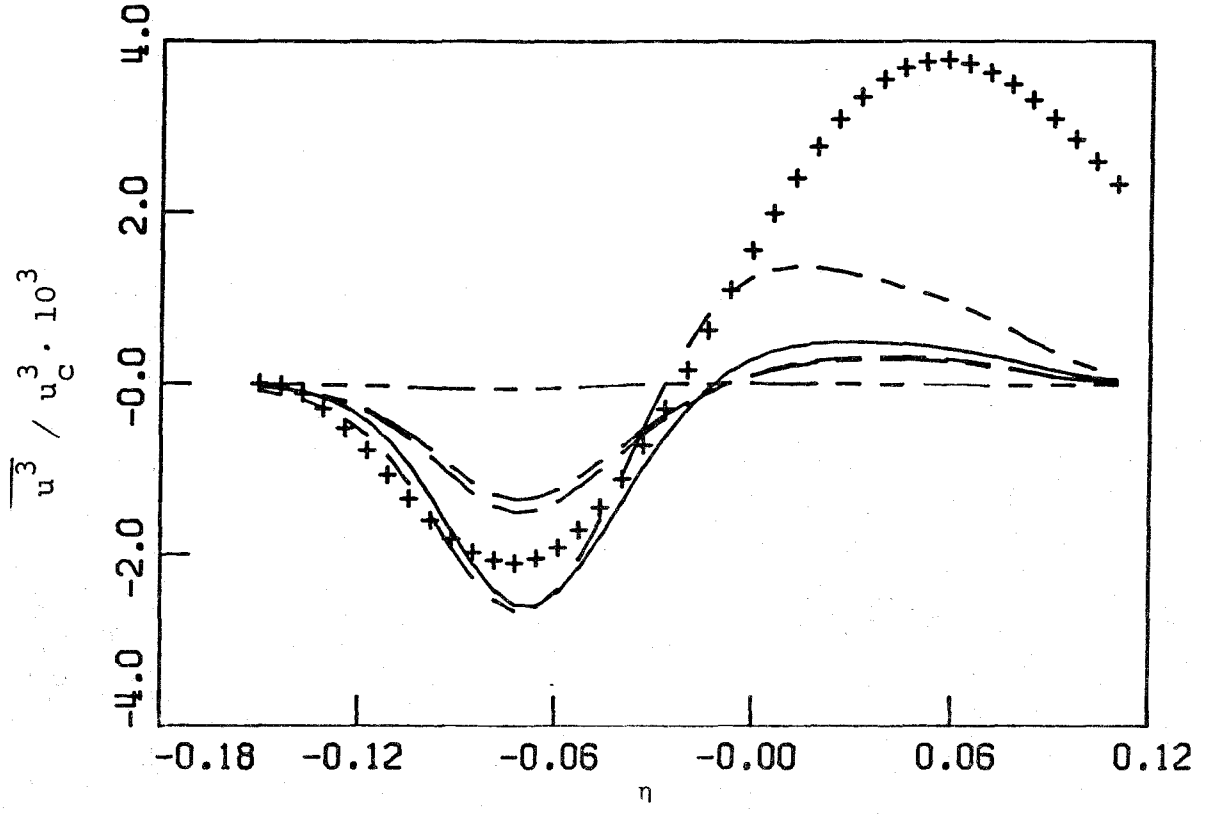
4.0
2.0
-0.0
-2.0
-4.0
$\overline{u^3} / u_c^3 \cdot 10^3$
-0.18
-0.12
-0.06
-0.00
0.06
0.12
η

Fig. 4.1

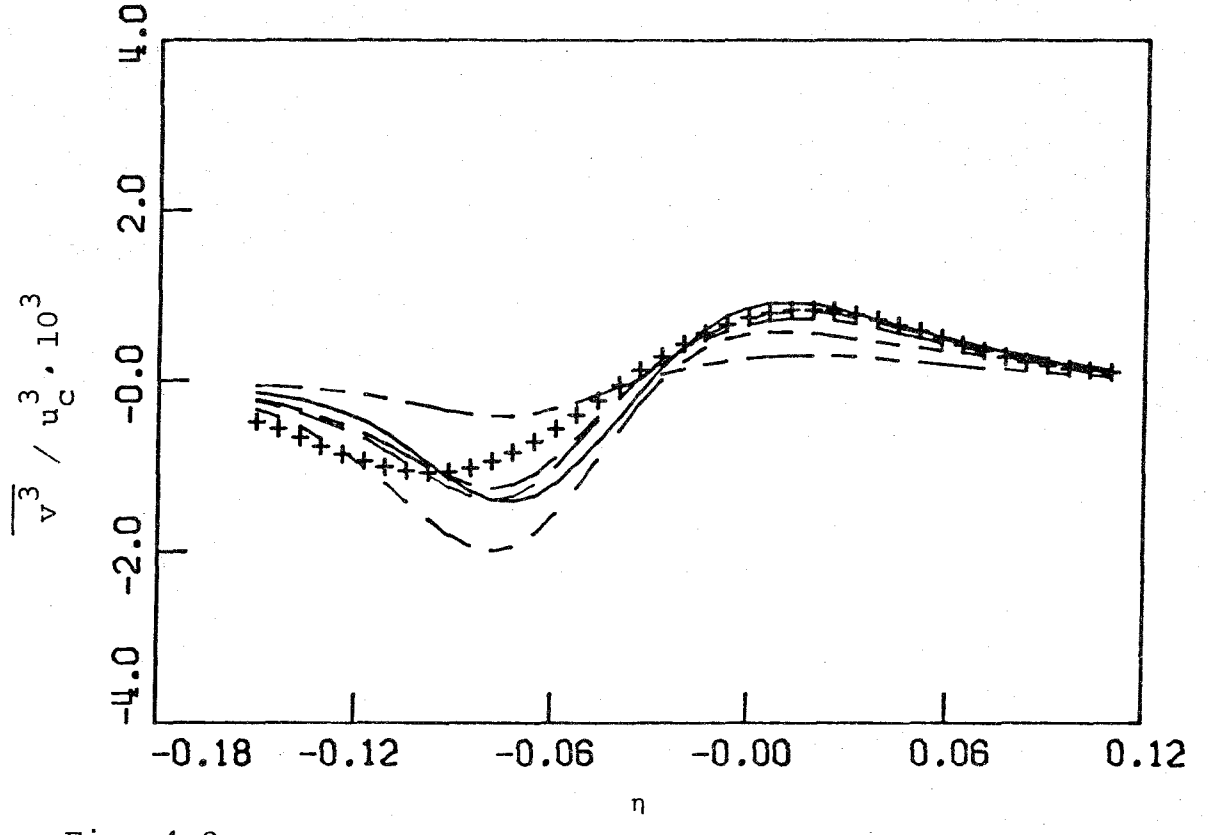
4.0
2.0
-0.0
-2.0
-4.0
$\overline{v^3} / u_c^3 \cdot 10^3$
-0.18
-0.12
-0.06
-0.00
0.06
0.12
η

Fig. 4.2

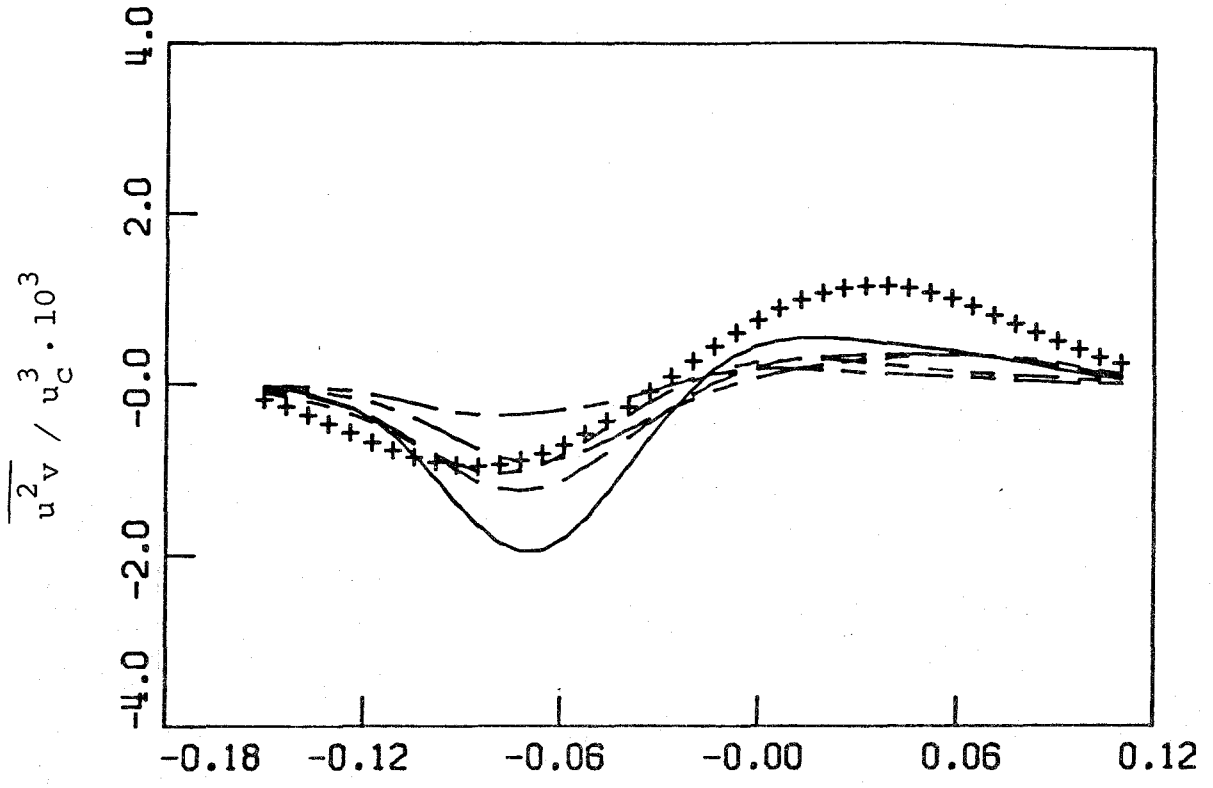
4.0
2.0
-0.0
-2.0
-4.0
-0.18
-0.12
-0.06
-0.00
0.06
0.12
η

Fig. 4.3

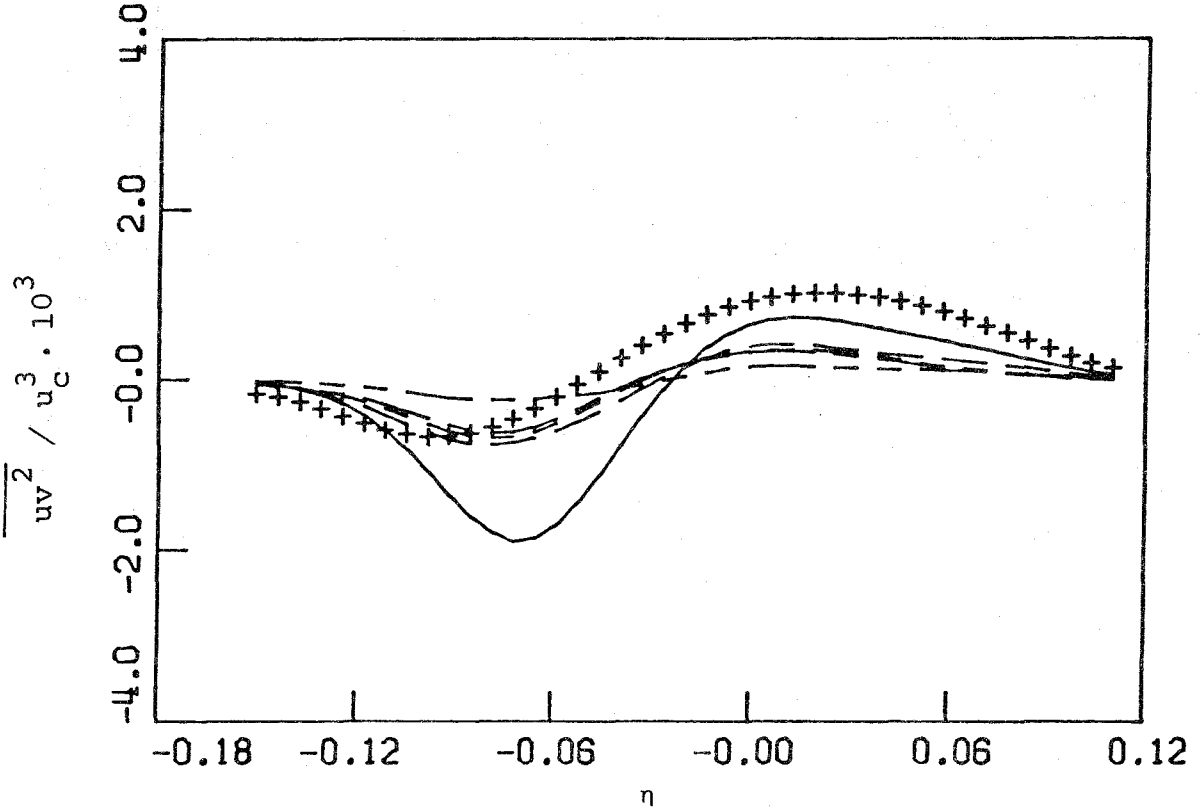
4.0
2.0
-0.0
-2.0
-4.0
-0.18
-0.12
-0.06
-0.00
0.06
0.12
η

Fig. 4.4

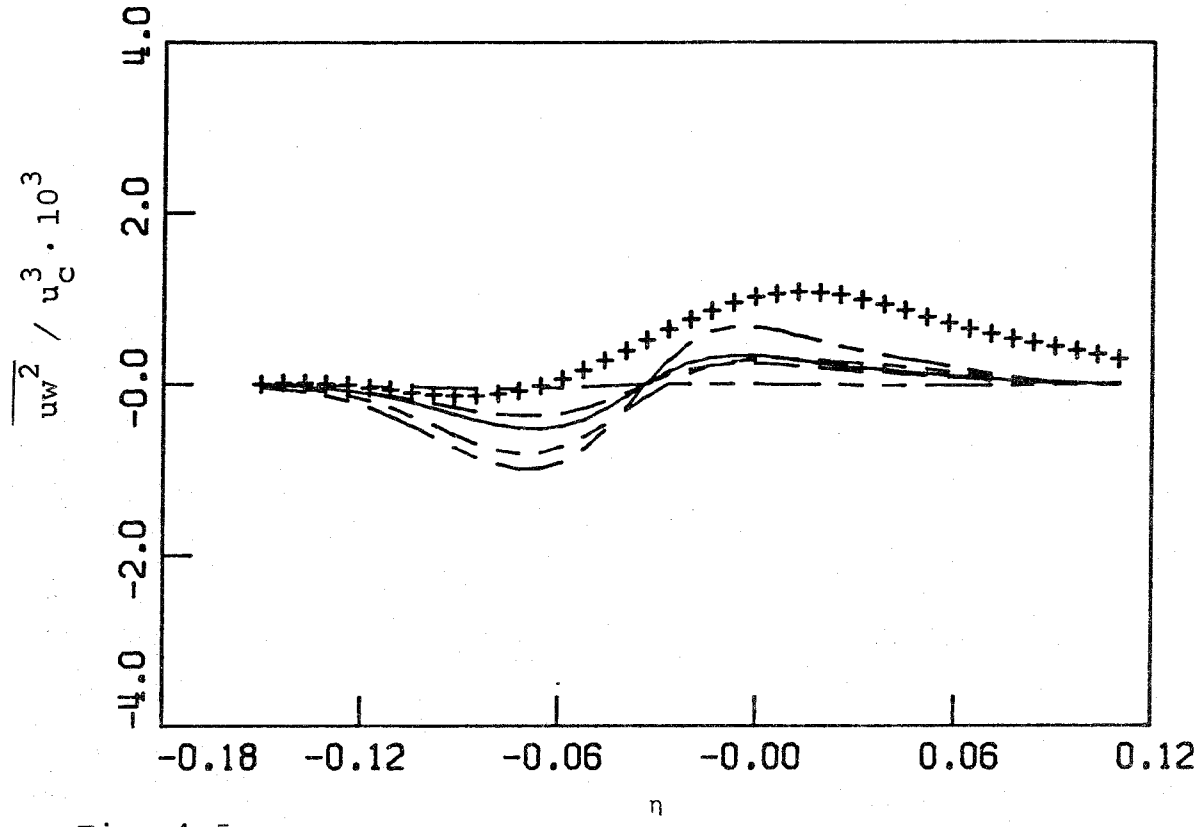
4.0
2.0
-0.0
-2.0
-4.0
-0.18
-0.12
-0.06
-0.00
0.06
0.12
η
$\overline{uw}^2 / u_c^3 \cdot 10^3$

Fig. 4.5

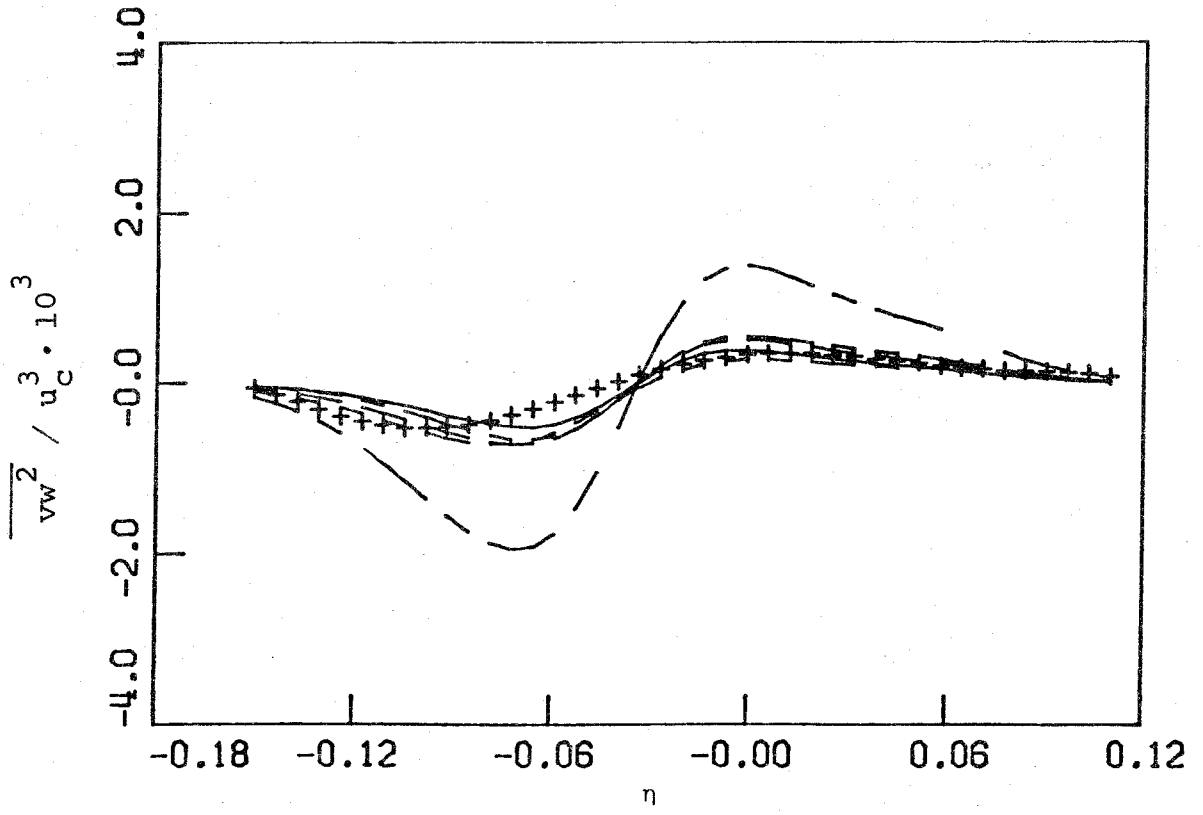
4.0
2.0
-0.0
-2.0
-4.0
-0.18
-0.12
-0.06
-0.00
0.06
0.12
η
$\overline{vw}^2 / u_c^3 \cdot 10^3$

Fig. 4.6

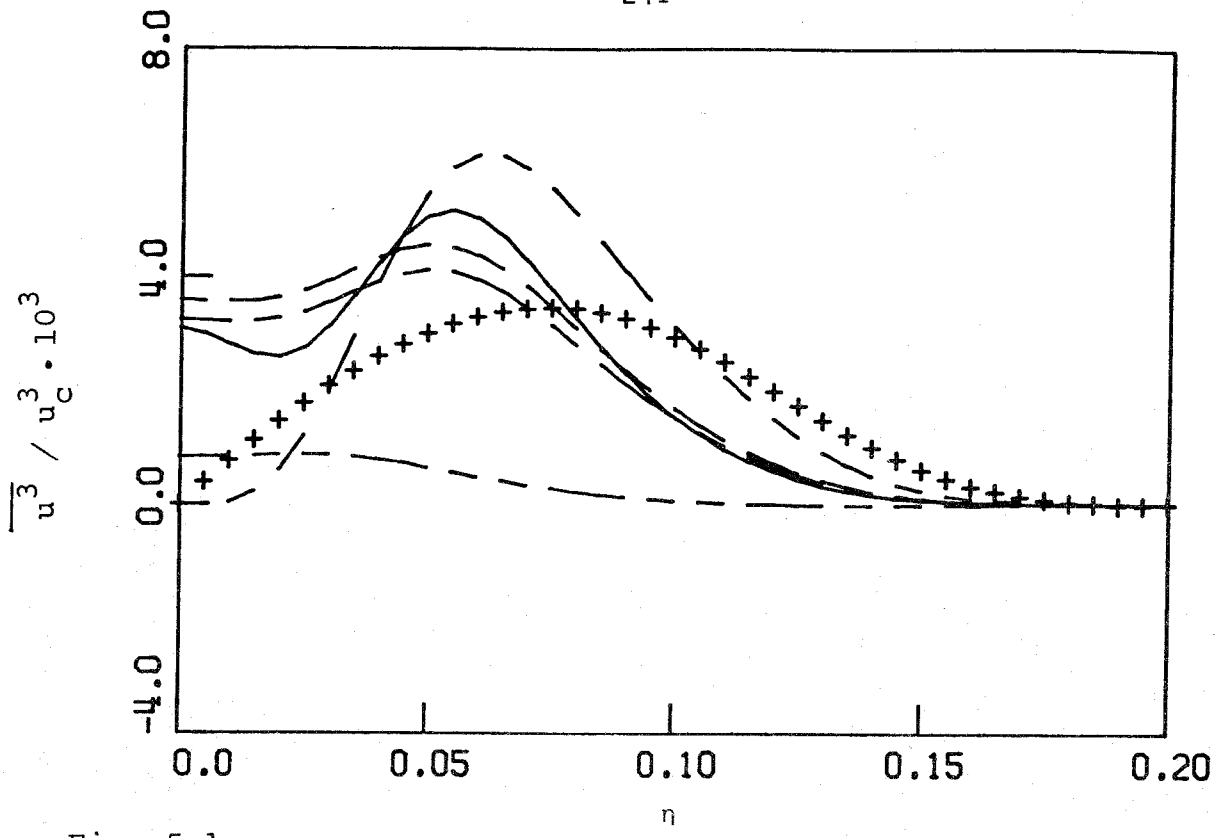
8.0
4.0
0.0
-4.0
0.0
0.05
0.10
0.15
0.20
η
$\overline{u^3} / u_c^3 \cdot 10^3$

Fig. 5.1

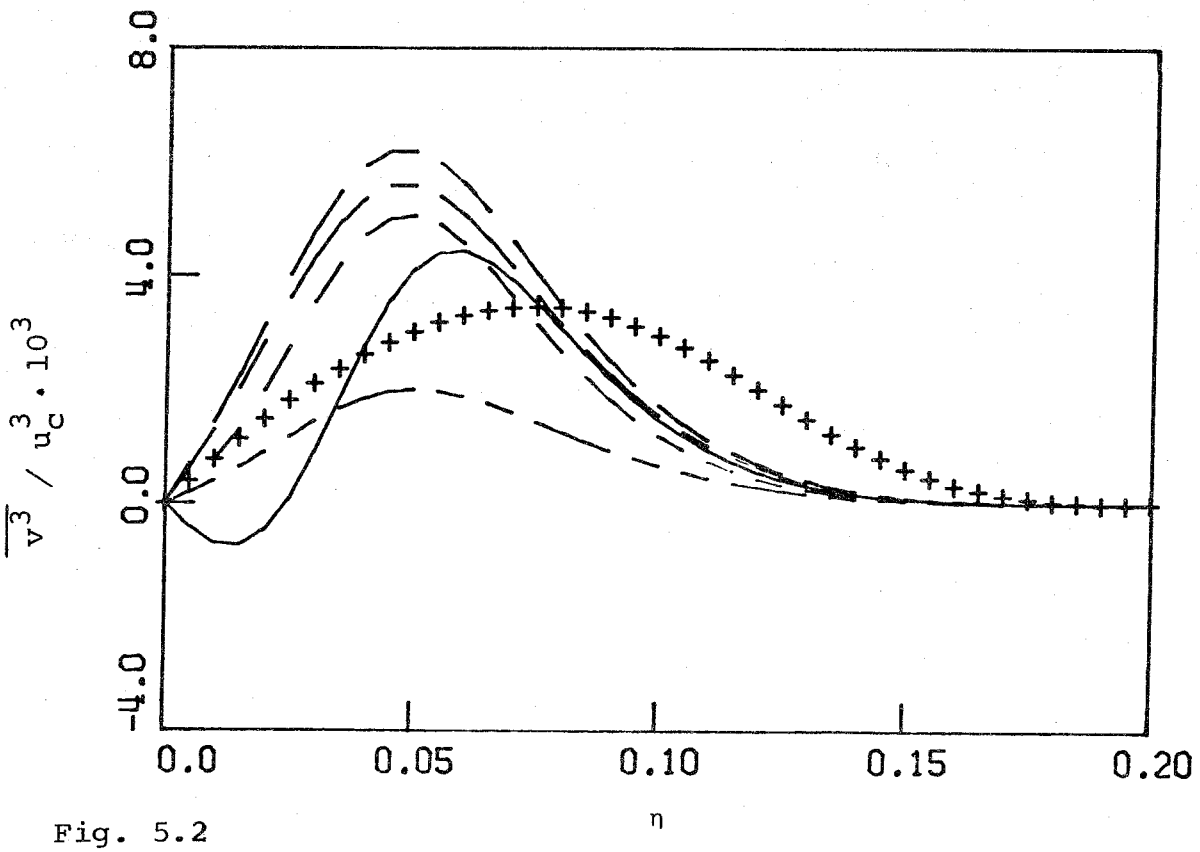
8.0
4.0
0.0
-4.0
0.0
0.05
0.10
0.15
0.20
η
$\overline{v^3} / u_c^3 \cdot 10^3$

Fig. 5.2

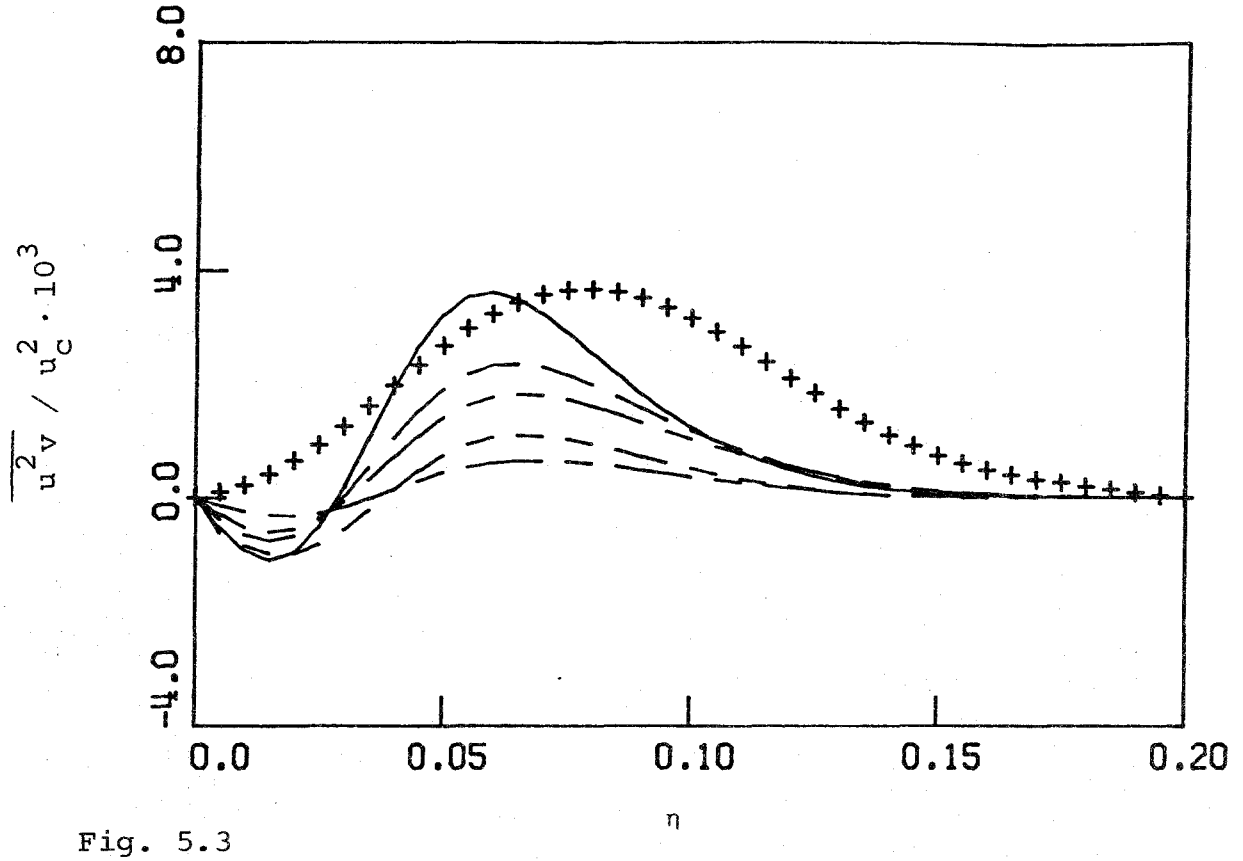
8.0
4.0
0.0
-4.0
0.0
0.05
0.10
0.15
0.20
η
$\overline{u^2 v} / u_c^2 \cdot 10^3$

Fig. 5.3

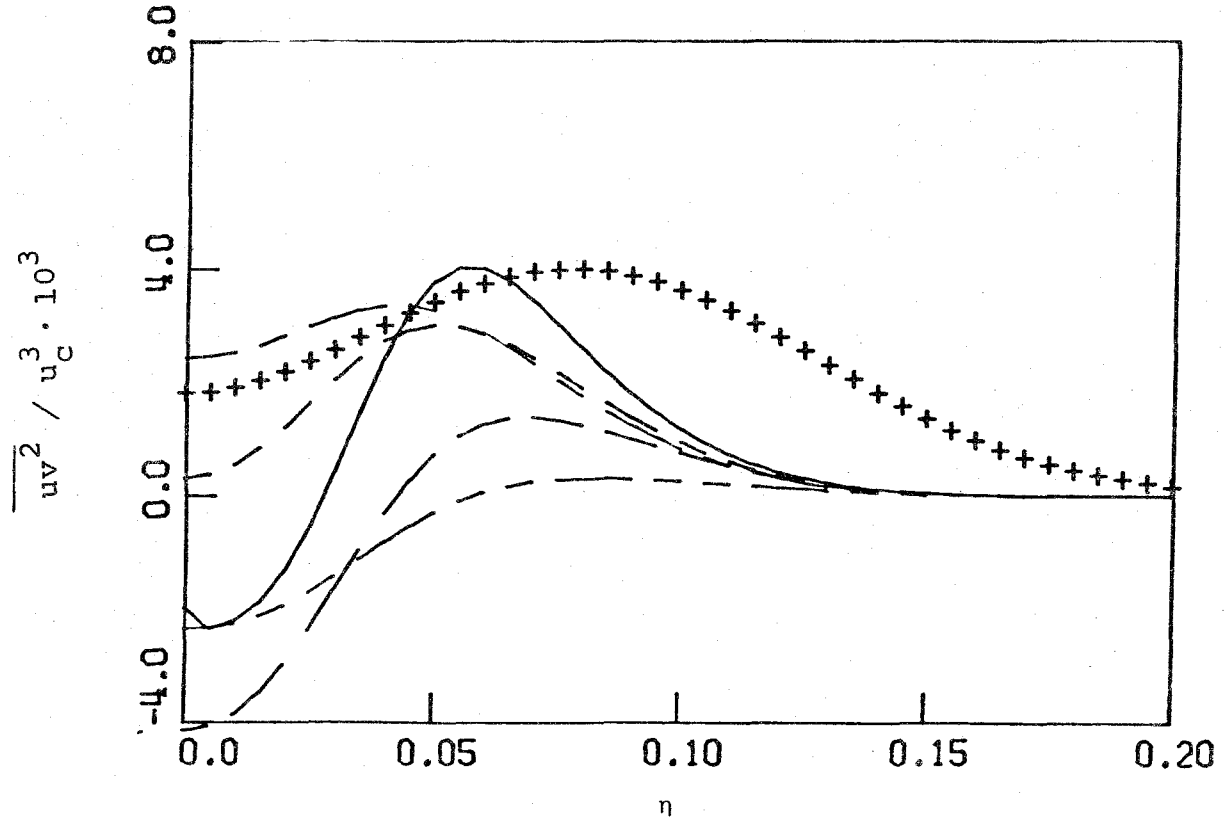
8.0
4.0
0.0
-4.0
0.0
0.05
0.10
0.15
0.20
η
$\overline{uv^2} / u_c^3 \cdot 10^3$

Fig. 5.4

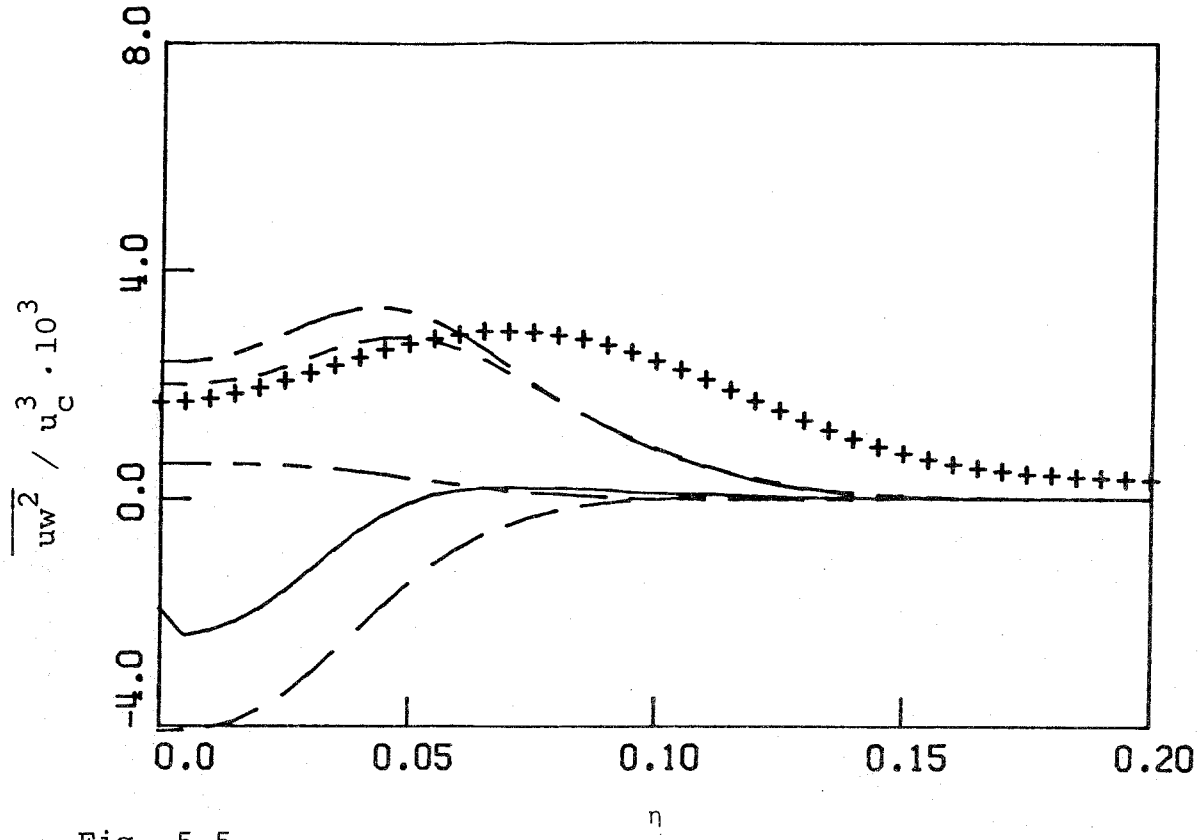
8.0
4.0
0.0
-4.0
0.0
0.05
0.10
0.15
0.20
η
$\overline{uw^2} / u_c^3 \cdot 10^3$

Fig. 5.5

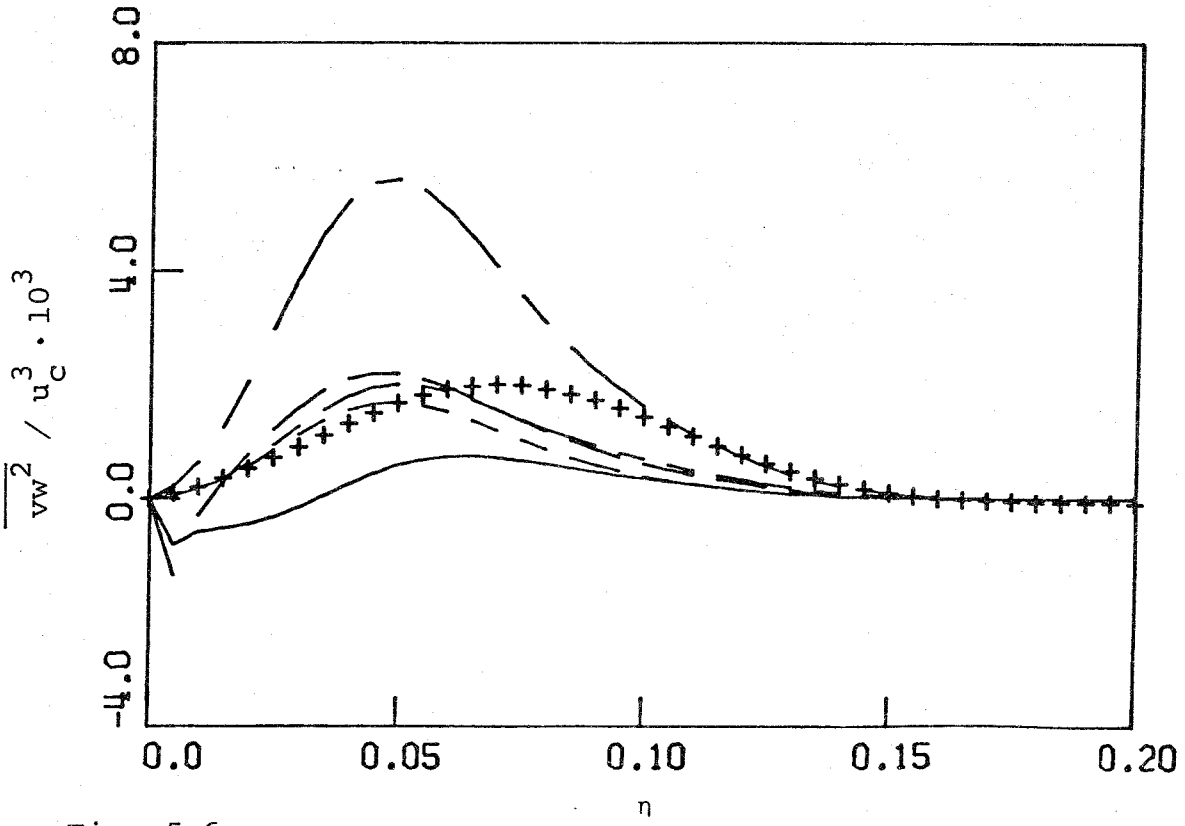
8.0
4.0
0.0
-4.0
0.0
0.05
0.10
0.15
0.20
η
$\overline{vw^2} / u_c^3 \cdot 10^3$

Fig. 5.6

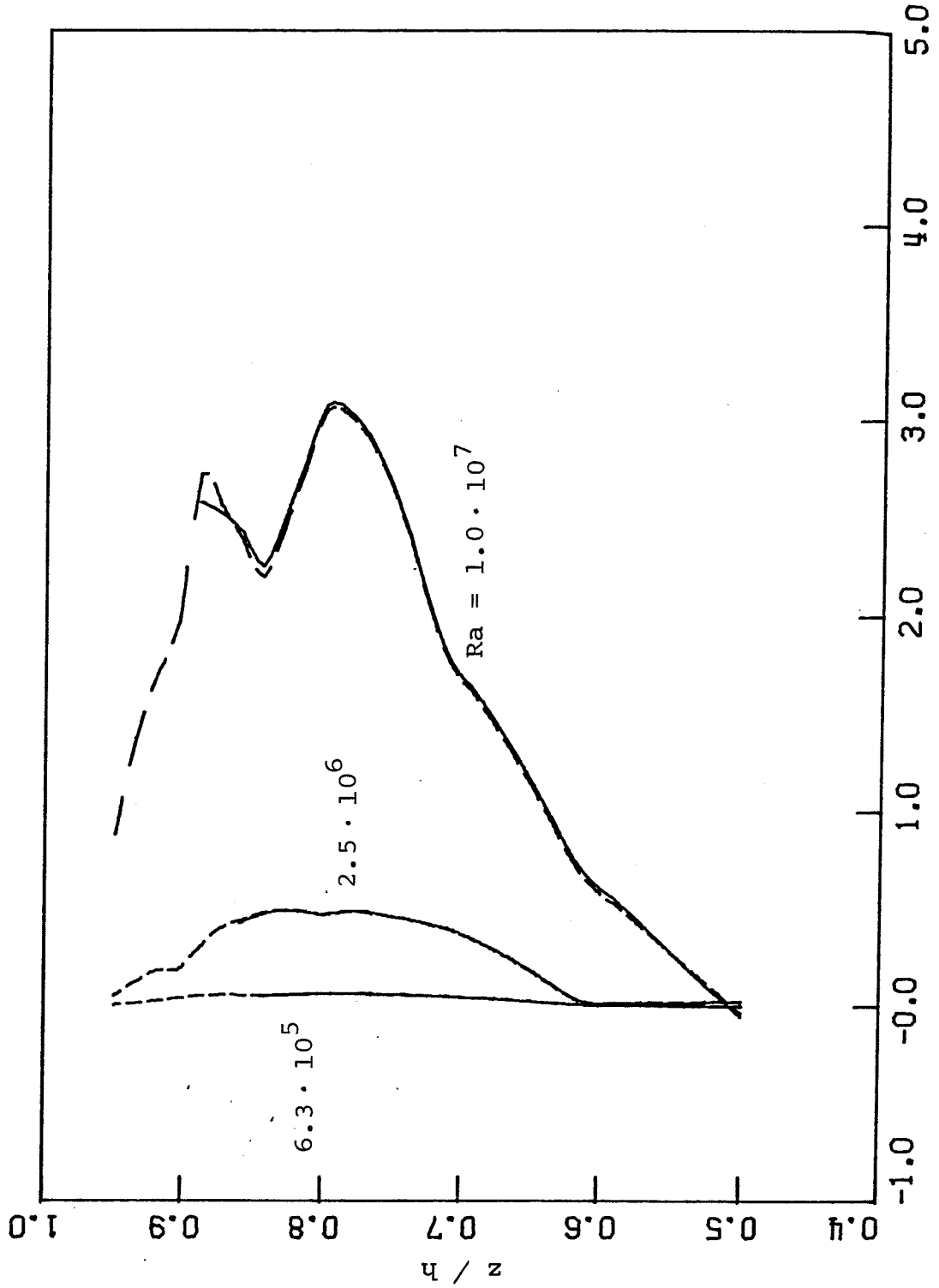
Ra = 1.0 · 10^7
2.5 · 10^6
6.3 · 10^5
z / h
0.4
0.5
0.6
0.7
0.8
0.9
1.0
-1.0
-0.0
1.0
2.0
3.0
4.0
5.0
v^3 / u_c^3 · 10^7

Fig. 6.1

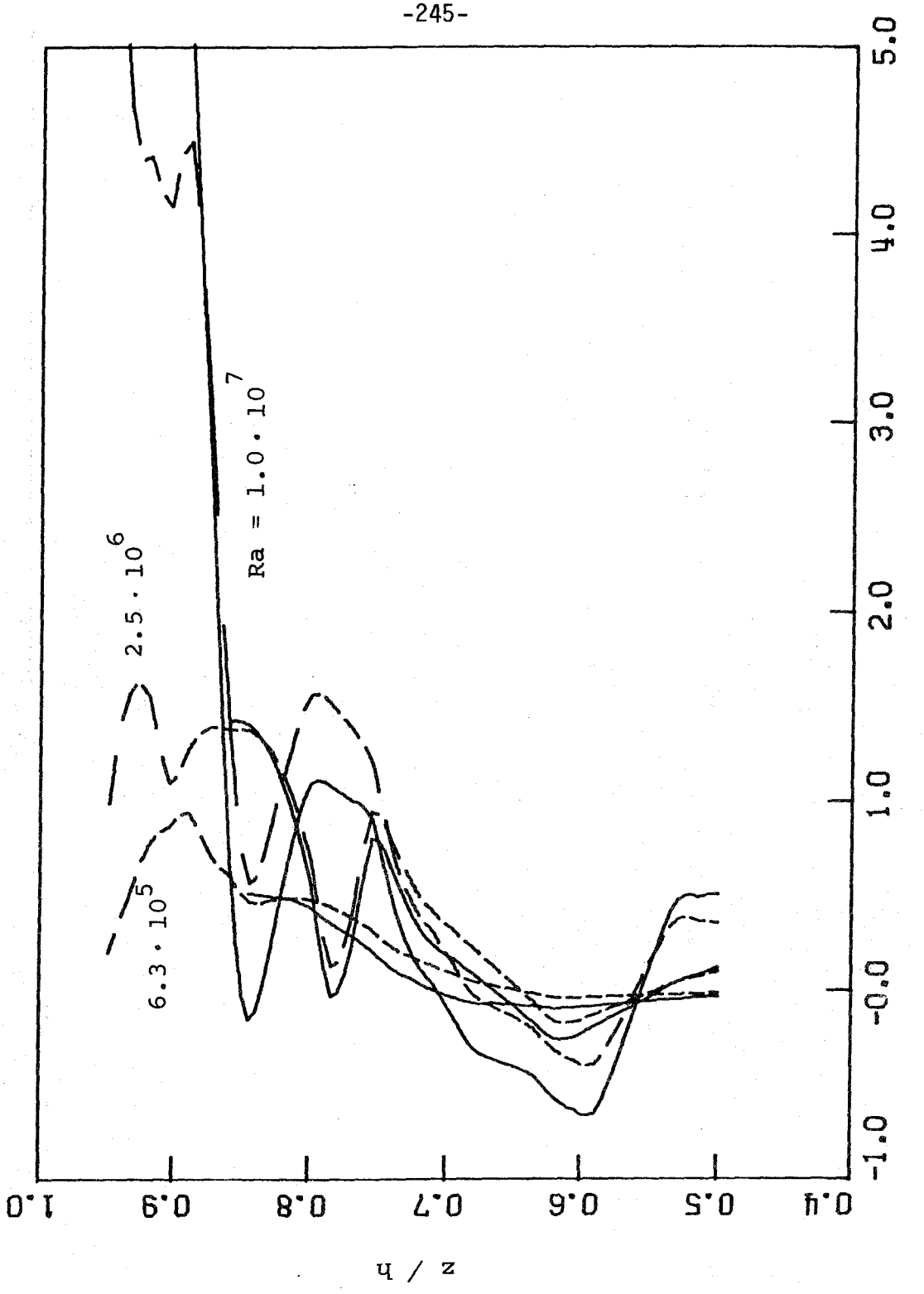
Ra = 1.0 · 10^7
2.5 · 10^6
6.3 · 10^5
5.0
4.0
3.0
2.0
1.0
-0.0
-1.0
0.4
0.5
0.6
0.7
0.8
0.9
1.0
z / h
$\overline{v^{2}\theta}$ / $u_c^2 T_c \cdot 10^3$

Fig. 6.2

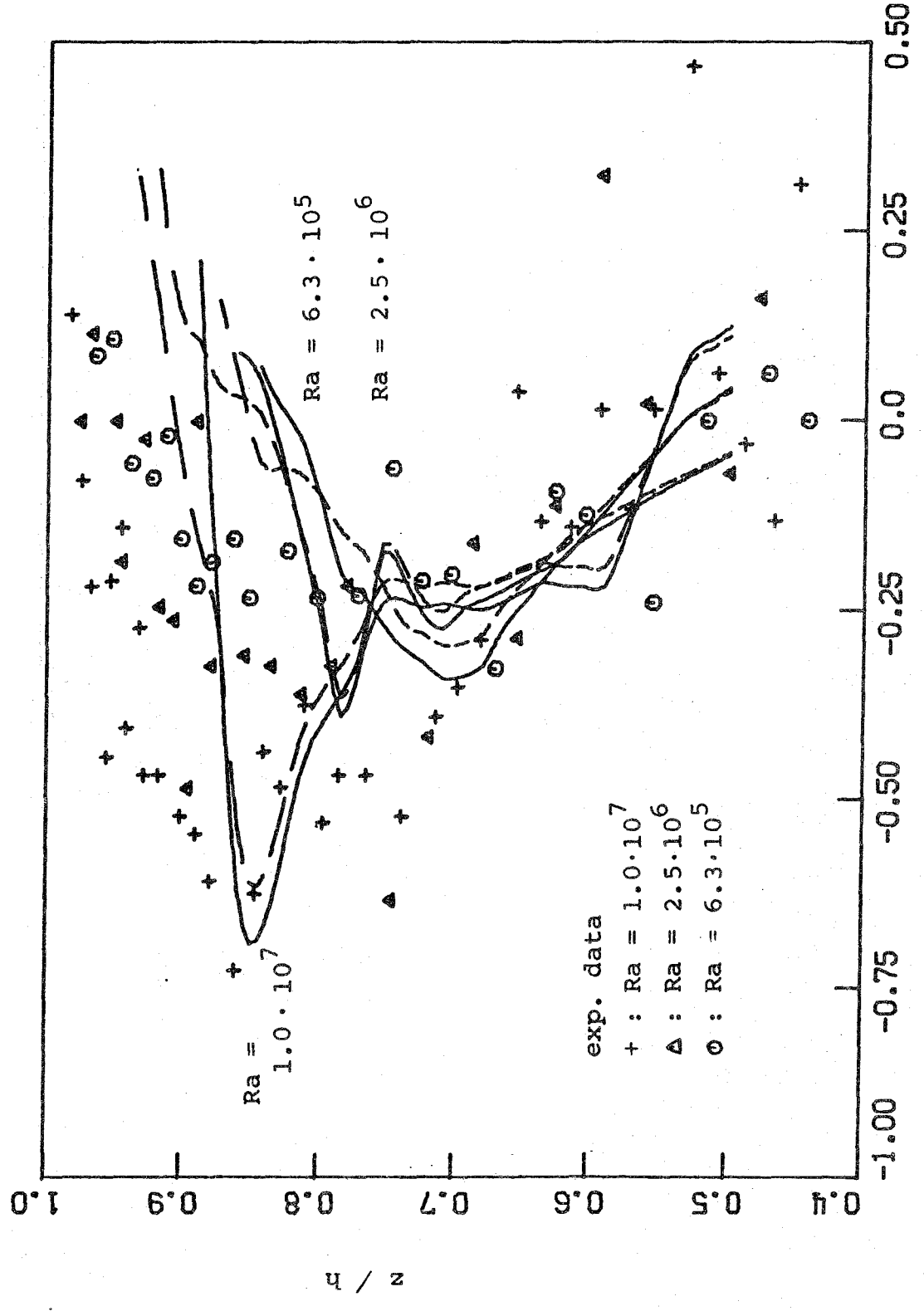
Ra = 1.0 · 10^7
Ra = 6.3 · 10^5
Ra = 2.5 · 10^6
exp. data
+ : Ra = 1.0·10^7
Δ : Ra = 2.5·10^6
o : Ra = 6.3·10^5
0.50
0.25
0.0
-0.25
-0.50
-0.75
-1.00
0.4
0.5
0.6
0.7
0.8
0.9
1.0
z / h
$\overline{v\theta^2} / u_c T_c^2$

Fig. 6.3

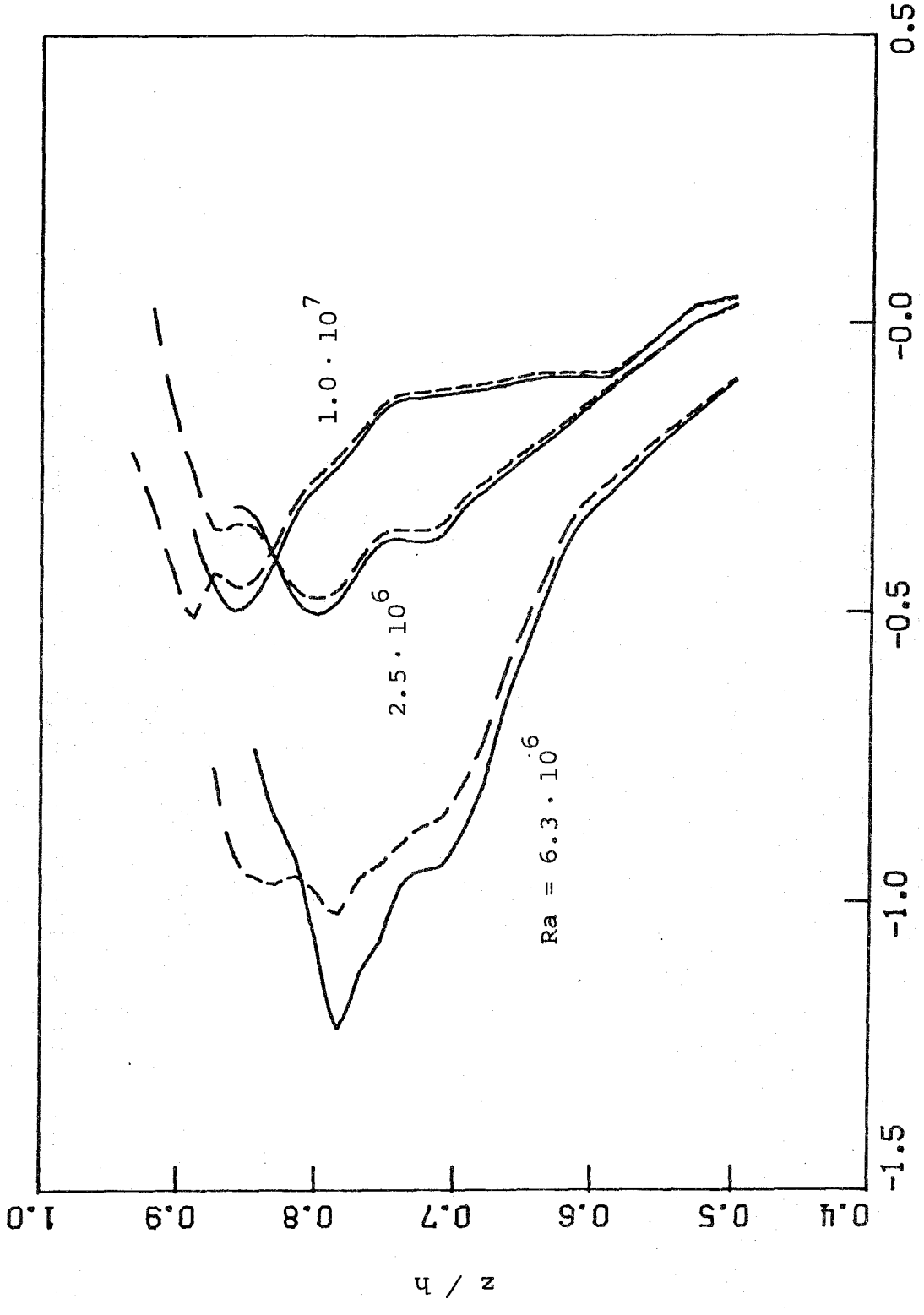
0.5
-0.0
-0.5
-1.0
-1.5
$\overline{\theta^3} / T_c^3 \cdot 10^3$
0.4
0.5
0.6
0.7
0.8
0.9
1.0
z / h
$1.0 \cdot 10^7$
$2.5 \cdot 10^6$
$Ra = 6.3 \cdot 10^6$

Fig. 6.4

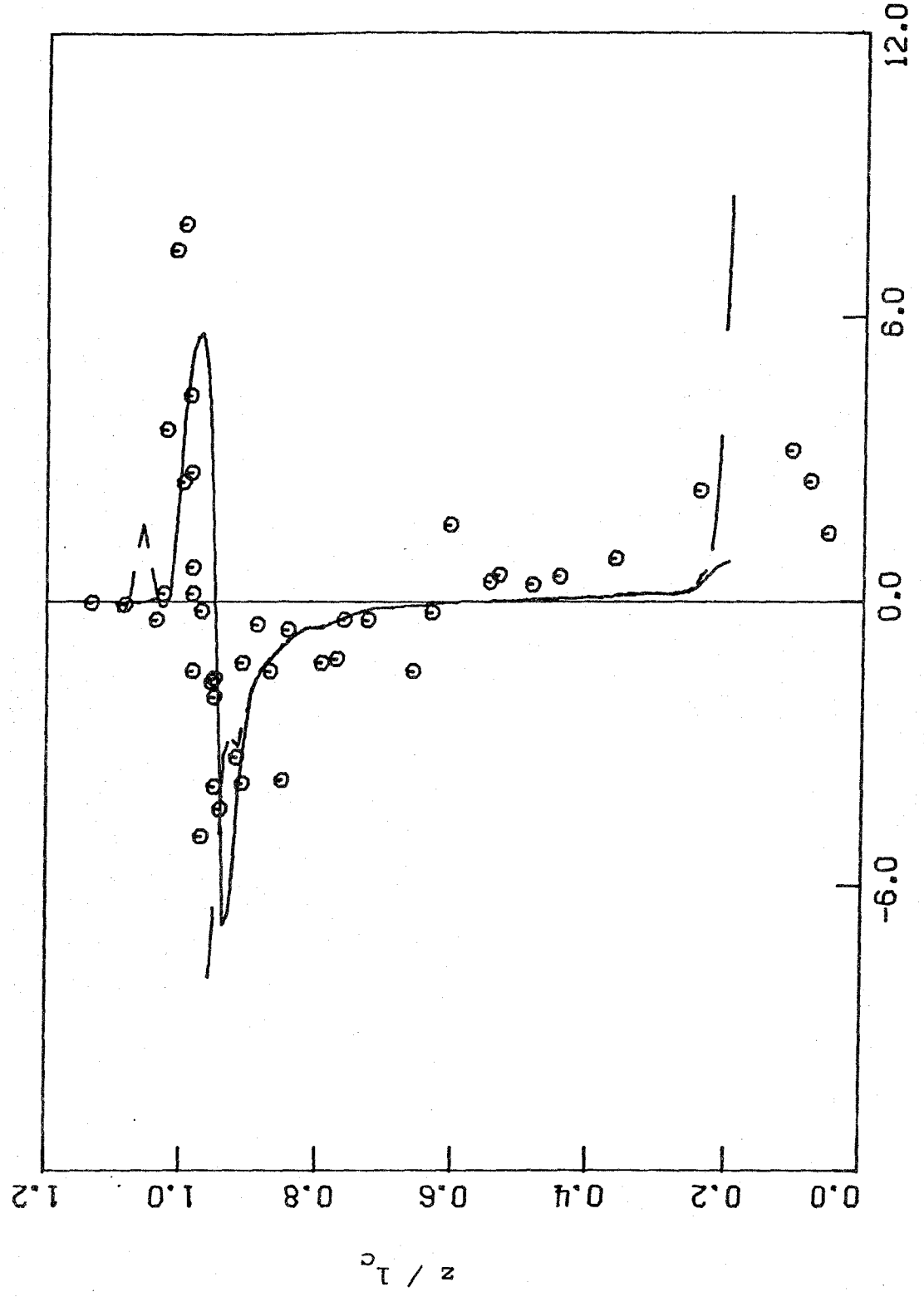

Fig. 7.1

4.0
2.0
0.0
-2.0
-4.0
0.0
0.2
0.4
0.6
0.8
1.0
1.2
z / l_c
$\overline{\theta^3} / (\overline{\theta^2})^{3/2}$

Fig. 7.2